Dynamics-based Recognition Mechanism of dsRBD-dsRNA interaction

A Thesis

Submitted in Partial Fulfillment of Requirements for the Award of Degree of

Doctor of Philosophy

By

Harshad Paithankar

20143299

IISER PUNE

Indian Institute of Science, Education, and Research, Pune

2019

भारतीय विज्ञान शिक्षा एवं अनुसंधान संस्थान पुणे
INDIAN INSTITUTE OF SCIENCE EDUCATION AND RESEARCH PUNE

डॉ. होमी भाभा मार्ग, पुणे 411008, महाराष्ट्र, भारत | Dr. Homi Bhabha Road, Pune 411008, Maharashtra, India
T +91 20 2590 8001   **W** www.iiserpune.ac.in

Jeetender Chugh, Ph.D.
Assistant Professor,
Department of Chemistry & Department of Biology
Indian Institute of Science Education & Research (IISER),
Homi Bhabha Road, Pashan, Pune 411008, India
E-mail: cjeet@iiserpune.ac.in
Phone: +91-20-25908121, +91-8378979667

Certificate

I certify that the thesis entitled **"Dynamics-based Recognition Mechanism of dsRBD-dsRNA interaction"** presented by **Mr. Harshad Paithankar** represents his/her original work which was carried out by him at IISER, Pune under my guidance and supervision during the period from 01st January, 2014 to 22nd August, 2019. The work presented here or any part of it has not been included in any other thesis submitted previously for the award of any degree or diploma from any other University or institutions. I further certify that the above statements made by him in regard to his thesis are correct to the best of my knowledge.

Date: 20|12|2019   (Supervisor: Dr. Jeetender Chugh)
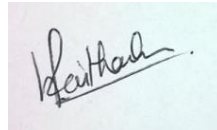
DECLARATION

I declare that this written submission represents my idea in my own words and where others´ ideas have been included; I have adequately cited and referenced the original sources. I also declare that I have adhered to all principles of academic honesty and integrity and have not misrepresented or fabricated or falsified any idea/data/fact/source in my submission. I understand that violation of the above will be cause for disciplinary action by the Institute and can also evoke penal action from the sources which have thus not been properly cited or from whom proper permission has not been taken when needed.

Place: **Pune**

Date: 18/12/2019 **Mr. Harshad Paithankar**

Acknowledgments

Synopsis

Dynamics-based recognition mechanism of dsRBD-dsRNA interaction

Name: Mr. Harshad Paithankar.

Registration No.: 20143299.

Thesis Supervisor: Dr. Jeetender Chugh.

Department: Department of Chemistry, IISER, Pune.

Chapter 1: Introduction

The broad range of cellular activities – ranging from cell-growth, development, to death – involves interaction between double-stranded RNAs (dsRNAs) and dsRNA-binding domains (dsRBDs)[1,2]. The dsRBDs have a well-defined structural fold of α-β-β-β-α, where two α-helices are packed against three antiparallel β-strands[1,2]. The dsRBDs from multiple proteins with this common fold are known to interact with A-form helical dsRNAs via minor-major-minor grooves spanning a length of about 12 base-pairs[3]. However, the dsRNAs in the cellular matrix can have imperfections in their duplex structures like internal loop or bulge that lead to change in their topology[4]. In the cellular environment, these dsRNAs with assortment of topologies are recognized by a handful of dsRBDs. The dsRBDs are present as modular units in proteins like TRBP (TAR RNA-binding protein), ADAR (Adenosine deaminase acting on RNA), and Staufen, and are involved in RNAi[2], RNA editing[5], RNA transport[6], respectively. Recent reports have shown that dsRBDs slides along the length of the dsRNAs having different secondary structures in an ATP-independent manner[7,8]. These observations lead to the broader question that is "how do dsRBDs target a versatile range of dsRNA topologies?". We hypothesized that conformational dynamics in the dsRBDs might play a role in the above-mentioned dsRBD-dsRNA interactions. In this thesis, two dsRBDs from two different species – TRBP2-dsRBD1 from *Homo sapiens* and dADAR-dsRBD1 from *Drosophila melanogaster* – were employed to study their interaction with dsRNAs. TRBP has three dsRBD domains which it uses to target dsRNA (with dsRBD1 and dsRBD2) and bind to Dicer – an endonuclease (with dsRBD3) – so that Dicer can act on target dsRNA sites[9]. Previous studies have shown that dsRBD1 and dsRBD2 of TRBP can interact with various dsRNAs with and without helical imperfections[10,11]. However, the mechanism of recognition of these dsRNAs by dsRBDs is still unclear.

Another protein used in the thesis is dADAR, which contains two N-terminal dsRBDs that allow binding to dsRNAs, and a deaminase domain at C-terminus that targets dsRNAs to carry out A-to-I editing post-transcriptionally[12]. Similar to TRBP, studies have shown that dADAR can interact with dsRNAs non-specifically[12] as opposed to structure and sequence-specific interactions reported for

ADAR2 in humans[13,14], thus creating ambiguity about the recognition of the dsRNAs by dsRBD of ADAR. The known dsRNA binding partner of TRBP – precursor of miR-16-1[11] – is an RNA for which interaction with other dsRBDs like that of Dicer[15], Drosha and DGCR8[16] has been reported. Thus, the duplex of this miRNA – miR-16-1:miR-16-1* – was employed to explore the recognition of dsRNAs by dsRBDs.

Chapter 2: Methods

In order to enhance the structural understanding of the dsRBD-dsRNA interactions, we have used various biophysical techniques for characterizing dsRBDs in the absence and presence of their substrates. These techniques include Size-exclusion chromatography coupled with Multi-Angle Light Scattering (SEC-MALS) detection, Circular Dichroism (CD), Isothermal Titration Calorimetry (ITC) and NMR spectroscopy. While on one hand, SEC-MALS, CD, and ITC give information on the global characteristics of the protein, NMR gives atomic level information. Along with the structural characterization of proteins, the motions at multiple timescales from ps to seconds or slower can also be probed by NMR. The two timescales particularly important from the functional viewpoint are ps-ns and μs-ms timescale. The detailed information about the NMR experiments that allow to characterize motions at these two timescales have been specifically discussed in detail in this chapter.

Chapter 3: Protein purification and Resonance assignment

A primary step in the characterization of the protein structure and dynamics by NMR is the assignment of the resonances that represent various nuclei in the protein chain. For this, an isotopically enriched (^{13}C and/or ^{15}N) protein was over-expressed in a bacterial expression system and purified by various chromatographic steps. The purified sample was then subjected to a set of experiments called triple-resonance experiments and ^{15}N-edited-TOCSY-HSQC. These experiments allow to get the resonance assignments for N, H^N, C_α, and C′ of the protein backbone and C_β of the sidechain. The ^{15}N-edited-TOCSY-HSQC also allows to get few other side-chain protons of the amino acids. By using this approach, we have successfully assigned resonances for TRBP2-dsRBD1 protein. These resonances helped us to calculate the structure of the protein, which showed an additional helix α_0 present at the N-terminus of the dsRBD1 structural fold[17]. A comparison of the dsRBD core with the previously reported crystal structure showed a good match between the two structures. We also transferred the resonance assignment of dADAR-dsRBD1 from the previously reported assignment[12].

Chapter 4: Characterization of intrinsic dynamics of dsRBDs

Preliminary information about the thermal stabilities of the two dsRBDs were extracted from CD-based melting studies which showed similar thermal stability of the two proteins. The characterization of ps-ns timescale dynamics by NMR showed that the two dsRBDs exhibit different dynamics profile. The TRBP2-dsRBD1 was found to be more flexible as compared to dADAR-

dsRBD1. Interestingly, analysis of the ps-ns dynamics data for both the proteins suggested the presence of slower μs-ms timescale motions that are spread across the protein chain. This motional timescale is relevant for the ligand-binding interactions of the proteins. Further characterization of motions in this timescale by relaxation dispersion method showed that they exhibit a similar profile in two proteins. The RNA binding residues and a few allosteric residues exhibited motions at faster μs timescale with $k_{ex} > 50000$ s^{-1}. Many of the residues in both the proteins showed presence of motions with $k_{ex} < 5000$ s^{-1}. The presence of such dynamics at multiple sites directed us to conclude that the dsRBDs exist as an ensemble of conformations in their native state. This partly supported our hypothesis of the presence of conformational dynamics of dsRBDs and excited us to further explore the effect of the substrate dsRNAs on these motions.

Chapter 5: Effect of dsRNA substrates on dsRBD dynamics

To study the effect of different dsRNA topologies on dsRBD-dsRNA interaction, three mutant RNAs were designed from the miR-16-1 RNA duplex. The 3D structure of these four RNA duplexes were modeled using SimRNA program which showed different topologies adapted by the four RNAs. ITC-based binding studies of four RNAs with each of the dsRBD pointed that though the interaction between the dsRBD and dsRNA is an enthalpically driven process, the binding modes of dsRBDs vary in dsRNA shape-dependent manner. This observation was further corroborated with the distinct line-broadening pattern observed for four different dsRNAs when titrated in TRBP2-dsRBD1 and probed by ^{1}H-^{15}N HSQC experiment. The analysis of line-broadening observed in HSQC and the limited site-specific nuclear spin relaxation parameters (R_1, R_2, and [^{1}H]-^{15}N-NOE) obtained suggested that interaction might involve intermediate exchange timescale process between apo- and RNA-bound state of the protein and diffusion of dsRBD along dsRNA as reported earlier[8]. Further characterization of motions in the dsRNA-bound state using a short RNA duplex revealed that high-frequency motions (at μs timescale) present in apo-dsRBDs are quenched in the bound state, while it is induced in few other residues. Interestingly these residues are in close spatial proximity to the residues that show quenched dynamics and thus can be viewed as the relay of dynamics to the neighboring residues during dsRBD-dsRNA interaction. This supports the second part of our hypothesis that the inherent conformational dynamics in dsRBDs makes it adaptable to interact with substrate dsRNAs.

Chapter 6: Conclusion

Based on the studies carried out in the apo-state of the protein, we observe that irrespective of the origin of the dsRBD, their aggregation behavior, and the site-specific ps-ns timescale motions; dsRBDs exhibit similar dynamic behavior at μs-ms timescale. More specifically, the RNA-binding residues and few allosteric residues exhibit motions at fast μs timescale indicated by $k_{ex} > 50000$ s^{-1}. Further ITC and NMR based studies also showed that the mode of interaction between dsRBD and dsRNA varied in shape-dependent fashion and might involve intermediate timescale motions. The characterization of

dynamics in the bound state of the protein and its comparison with dynamics in the apo-state helped us to conclude that the fast μs timescale dynamics is transferred to the nearby residues in the bound state. The ability to transfer dynamics in order to interact with the substrate makes dsRBDs adaptable, which is necessary for its interaction with dsRNAs of different topologies. Thus, we conclude that the conformational dynamics in dsRBDs allow them to recognize the dsRNAs in a shape-dependent manner.

References

1   G. Masliah, P. Barraud and F. H.-T. Allain, RNA recognition by double-stranded RNA binding domains: a matter of shape and sequence, *Cell. Mol. Life Sci.*, 2013, **70**, 1875–1895.

2   B. Tian, P. C. Bevilacqua, A. Diegelman-Parente and M. B. Mathews, The double-stranded-RNA-binding motif: Interference and much more, *Nat. Rev. Mol. Cell Biol.*, 2004, **5**, 1013–1023.

3   I. Fierro-Monti and M. B. Mathews, Proteins binding to duplexed RNA: one motif, multiple functions, *Trends Biochem. Sci.*, 2000, **25**, 241–246.

4   M. H. Bailor, X. Sun and H. M. Al-Hashimi, Topology links RNA secondary structure with global conformation, dynamics, and adaptation, *Science (80-.).*, 2010, **327**, 202–206.

5   O. M. Stephens, B. L. Haudenschild and P. A. Beal, The binding selectivity of ADAR2's dsRBMs contributes to RNA-editing selectivity, *Chem. Biol.*, 2004, **11**, 1239–1250.

6   X. Wang, X. Xu, Z. Ma, Y. Huo, Z. Xiao, Y. Li and Y. Wang, Dynamic mechanisms for pre-miRNA binding and export by Exportin-5, *RNA*, 2011, **17**, 1511–1528.

7   H. R. Koh, M. A. Kidwell, K. Ragunathan, J. A. Doudna and S. Myong, ATP-independent diffusion of double-stranded RNA binding proteins, *Proc. Natl. Acad. Sci. U. S. A.*, 2013, **110**, 151–156.

8   X. Wang, L. Vukovic, H. R. Koh, K. Schulten and S. Myong, Dynamic profiling of double-stranded RNA binding proteins, *Nucleic Acids Res.*, 2015, **43**, 7566–7576.

9   S. M. Daniels and a. Gatignol, The Multiple Functions of TRBP, at the Hub of Cell Responses to Viruses, Stress, and Cancer, *Microbiol. Mol. Biol. Rev.*, 2012, **76**, 652–666.

10   C. L. Noland and J. A. Doudna, Multiple sensors ensure guide strand selection in human RNAi pathways., *RNA*, 2013, **19**, 639–648.

11   R. Acevedo, N. Orench-Rivera, K. A. Quarles and S. A. Showalter, Helical defects in MicroRNA influence protein binding by TAR RNA binding protein, *PLoS One*, 2015, **10**, e0116749.

12   P. Barraud, B. S. E. Heale, M. A. O'Connell and F. H. T. Allain, Solution structure of the N-terminal dsRBD of Drosophila ADAR and interaction studies with RNA, *Biochimie*, 2012, **94**, 1499–1509.

13   R. Stefl, F. C. Oberstrass, J. L. Hood, M. Jourdan, M. Zimmermann, L. Skrisovska, C. Maris, L. Peng, C. Hofr, R. B. Emeson and F. H. T. Allain, The solution structure of the ADAR2 dsRBM-RNA complex reveals a sequence-specific readout of the minor groove, *Cell*, 2010, **143**, 225–237.

14   R. Stefl, M. Xu, L. Skrisovska, R. B. Emeson and F. H. T. Allain, Structure and specific RNA binding of ADAR2 double-stranded RNA binding motifs, *Structure*, 2006, **14**, 345–355.

15   C. Wostenberg, J. W. Lary, D. Sahu, R. Acevedo, K. A. Quarles, J. L. Cole and S. A. Showalter, The role of human Dicer-dsRBD in processing small regulatory RNAs, *PLoS One*, 2012, **7**, e51829.

16   C. Wostenberg, K. A. Quarles and S. A. Showalter, Dynamic origins of differential RNA binding function in two dsRBDs from the miRNA 'Microprocessor' complex, *Biochemistry*, 2010, **49**, 10728–10736.

17   G. Masliah, C. Maris, S. L. König, M. Yulikov, F. Aeschimann, A. L. Malinowska, J. Mabille, J. Weiler, A. Holla, J. Hunziker, N. Meisner-Kober, B. Schuler, G. Jeschke and F. H. Allain, Structural basis of siRNA recognition by TRBP double-stranded RNA binding domains, *EMBO J.*, 2018, e97089.

List of Publications

1   H. Paithankar, P. V. Jadhav, A. S. Naglekar, S. Sharma, and J. Chugh, 1H, 13C and 15N resonance assignment of domain 1 of trans-activation response element (TAR) RNA binding protein isoform 1 (TRBP2) and its comparison with that of isoform 2 (TRBP1), *Biomol. NMR Assign.*, 2018, **12**, 189–194.

2   H. Paithankar, and J. Chugh, Characterization of conformational dynamics at microsecond timescale in the RNA-binding regions of dsRNA-binding domains, *bioRxiv*, 2019, 797449. (**Manuscript submitted**).

3   H. Paithankar, and J. Chugh, Role of protein dynamics in enthalpy-driven recognition of topologically distinct dsRNAs by dsRBDs, *bioRxiv*, 2019, 862326. (**Manuscript submitted**).

Table of Content

Abbreviations

°C	Degree Celcius
Å	Angstrom
aa	Amino acid
ADAR	Adenosine deaminase acting on RNA
ATP	Adenosine triphosphate
BMRB	Biological Magnetic Resonance Bank
bp	Base-pair
BSA	Bovine Serum Albumin
cal, kcal	Calorie, kilo-calorie
CARA	Computer Aided Resonance Assignment
CD	Circular Dichroism
CPMG	Carr-Purcell-Meiboom-Gill
CSA	Chemical Shift Anisotropy
CSP	Chemical Shift Perturbation
D_2O	Deuterium oxide
DGCR8	Di-George syndrome Critical Region 8
DNA	Deoxy-ribonucleic acid
dsRBD	Double-stranded RNA-Binding Domain
dsRNA	Double-stranded RNA
DSS	4,4-dimethyl-4silapentane-1-sulphonic acid
DTT	Dithiothreitol
EDTA	Ethylene diamine tetraacetic acid
HARD	Heteronuclear Adiabatic Relaxation dispersion
hr	Hour
HS	Hyperbolic Secant
HSQC	Heteronuclear Single Quantum Coherence
Hz, kHz, MHz	Hertz, kilo-Hertz, mega-Hertz
IPTG	Isopropyl-β-D-1-thiogalactopyranoside
ITC	Isothermal Titration Calorimetry
K	Kelvin
kDa	Kilo-Dalton
M, mM, μM	Mole, milli-mole, micro-mole
MALS	Multi-Angle Light Scattering

MBP	Maltose Binding Protein
miRNA, miR	microRNA
ml, µl	Milli-liter, micro-liter
NaCl	Sodium chloride
NDB	Nucleic acid Data Bank
nm	Nano-meter
NMR	Nuclear Magnetic Resonance
NOE	Nuclear Overhauser Effect
nt	nucleotide
OD	Optical Density
PDB	Protein Data Bank
PKR	Protein kinase R
ppm	Parts per million
RD	Relaxation Dispersion
RISC	RNA Induced Silencing Complex
RMSD	Root-Mean-Square-Deviation
RNA	Ribonucleic acid
RNAi	RNA interference
s, ms, µs, ps, ns	Second, milli-second, micro-second, pico-second, nano-second
SDS-PAGE	Sodium dodecyl sulfate - Polyacryl Amide Gel Electrophoresis
SEC	Size Exclusion Chromatography
siRNA	Small interfering RNA
TEV	Tobacco Etch Virus
TOCSY	Total correlation Spectroscopy
TRBP	Trans Activation Response RNA Binding Protein
TSP	Total Soluble Protein

List of Figures

List of Tables

Chapter 1 Introduction

1.1. Protein-RNA interactions

RNA performs a broad range of vital cellular functions. They serve as information carriers[1], form part of ribosome[2], exhibit catalytic activities[3,4], involved in gene regulation[5,6], etc. Most of these functions involve the interaction of RNAs with proteins. For example, the genetic information contained in DNA is transcribed to RNA assisted by RNA polymerase[7,8], the ribosome contains tRNA molecules bound to aminoacyl-tRNA synthetase that are responsible for the translation of information encoded in the mRNA[9,10], etc.. Another example of protein-RNA interaction involves the processing of RNAs by ribonucleases that form the ribonucleoprotein complex (RNP)[11]. These complexes are involved in gene regulation, antiviral defense, immune response, etc. The formation of the correct complex is governed by the different types of interactions between the amino acids of the protein and the nucleobases or ribose sugar or phosphodiester backbone of the RNA that include hydrogen bonding, electrostatic, stacking interactions, etc. Any irregularities in these interactions can lead to dysfunction of the complex and can lead to diseases such as cancer[12], cardiovascular dysfunction[13], neurodegenerative diseases[14], to name a few. Regardless of the large number functionally significant protein-RNA interactions known, the molecular mechanisms of interactions between the RNA and the protein are poorly understood[15–19]. An important aspect of understanding these mechanisms involves the characterization of these interactions at structural, kinetic, and thermodynamic levels.

Seconadry structures of RNA
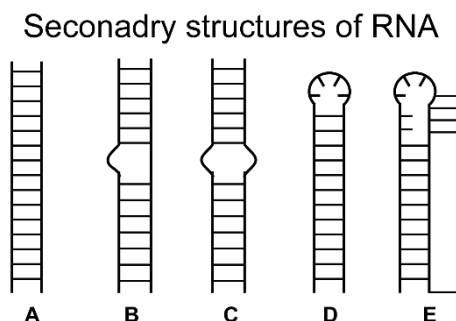
Figure 1.1: Some Examples of Secondary structures of RNA: (**A**) double-stranded RNA, (**B**) Bulge, (**C**) Internal-loop, (**D**) Hairpin and (**E**) Pseudoknot

RNA molecules can fold into a variety of secondary and tertiary structures that are formed due to the various type of base-pairing interactions between the nucleobases. The base-pairing in RNA can vary from most commonly observed Watson-Crick pairs to others like Hoogsteen, Wobble, reverse Watson-Crick, reverse Hoogsteen, etc[20,21]. Proteins can recognize RNAs by interacting with a single-stranded RNA and/or secondary and tertiary structures like an RNA duplex, duplex with internal bulge or mismatch, stem-loop structures, quadruplexes, etc (Figure 1.1). The basis of recognition of these different RNA structures by proteins involves the direct or the solvent-mediated contacts between protein and the RNA[22]. The simplest of these RNA structures is the double-stranded (ds) RNA which plays a vital role in many biological processes. RNAs like, tRNA, mRNA, precursors of small

regulatory RNA (miRNA or siRNA) also contain segments that are double-stranded. The segments of the protein chain known to interact with these double-stranded RNAs or RNA segments are termed as double-stranded RNA-binding domains (dsRBD).

1.2.   *Double-stranded RNA-Binding Domain*

The double-stranded RNA-Binding Domain (dsRBD) was first reported by sequence similarity studies as a conserved domain among three different proteins namely, Staufen protein in *Drosophila*, RNA-Binding Protein A (Xlrbpa) in *Xenopus leavis*, and human TAR RNA-Binding Protein (TRBP)[23]. Later, dsRBDs have been identified in several prokaryotic, eukaryotic, and viral proteins[24,25]. These dsRBDs are critical factors for cellular functions that involve RNA interference[25], -localization[26,27], -export[28,29], -editing[30], -splicing[31] etc. Ivo Fierro-Monti and Michael B. Mathews have reported nine different protein families that contain one or more dsRBDs in a protein chain and are distributed in different organisms[24]. The arrangement of multiple dsRBDs in a protein may serve to enhance the binding affinity of the protein. For example, the second dsRBD of PKR has a limited binding affinity, but the affinity of the protein is enhanced due to the cooperative effect of the first dsRBD[32]. A typical dsRBD is about 65-70 amino acid long with conserved dsRNA-binding residues. The sequence comparison among different dsRBDs has shown strong sequence conservation of > 40 % in the last one-third sequence at the C-terminus of the domain while the N-terminal one-third region shows relatively weaker sequence conservation[24,33]. The dsRBDs with conserved RNA-binding residues are grouped as type-I dsRBDs. Some of the dsRBDs having more divergent sequences are reported to show weaker binding affinity (than type-I dsRBDs) and have been categorized as type-II dsRBDs[33].

The characterization of the three-dimensional structure of the dsRBDs, initially reported for *E. coli* RNase III dsRBDs and *Drosophila* Staufen dsRBD3 by solution NMR, showed an α_1-β_1-β_2-β_3-α_2 fold where two α-helices are packed against three antiparallel β-strands[34,35]. Though the structures of many dsRBDs have been reported in absence of RNA, mere 22 structures of dsRBDs in presence of substrates are available (data as on December 2019) in the protein data bank (https://www.rcsb.org/)[36,37] and nucleic acid database (http://ndbserver.rutgers.edu/)[38,39]. It has been concluded from the analysis of these structures that the typical arrangement of the secondary structures not only helps dsRBD in maintaining the tertiary structural contacts but also in dsRNA binding[33]. The hydrophobic core, formed by the aliphatic residues, has been reported for almost all the secondary structures and the aromatic sidechains that are typically present in the β-strands and have been shown to contribute to the stability of the protein tertiary structure[33]. Some of the dsRBDs have been reported to show some structural variation or extended secondary structures. For example, the mammalian ADAR2 dsRBDs contain a shorter loop connecting α_1 helix and β_1 strand[40]. This loop helps in the alignment of the secondary structures in dsRBD to maintain the structural fold of the dsRBD. Though no particular effect on RNA-

binding has been observed for this protein, a study on Yeast RNase III (Rnt1p) has shown that the mutation in this region can lead to loss of RNA-binding activity[41].

Another variation in the structure of dsRBDs can be in the form of an extension of the secondary structural elements. The first extension was reported in Yeast RNase II (Rnt1p) that contains an additional α-helix at the C-terminus[42]. Though this helix has not been reported to interact with dsRNA directly, it has been reported to aid in RNA-binding by helping in proper positioning α1 helix for RNA recognition. A recent study on human dihydrouridine synthase-2 dsRBD has shown that it contains N- and C-terminal extensions[43]. Out of these, the N-terminal extension has been reported to show extended contacts for interaction with t-RNA like substrate while residues in both N- and C-terminal have been reported to contribute to the hydrophobic core of the dsRBD thus stabilizing the tertiary structure[43,44].
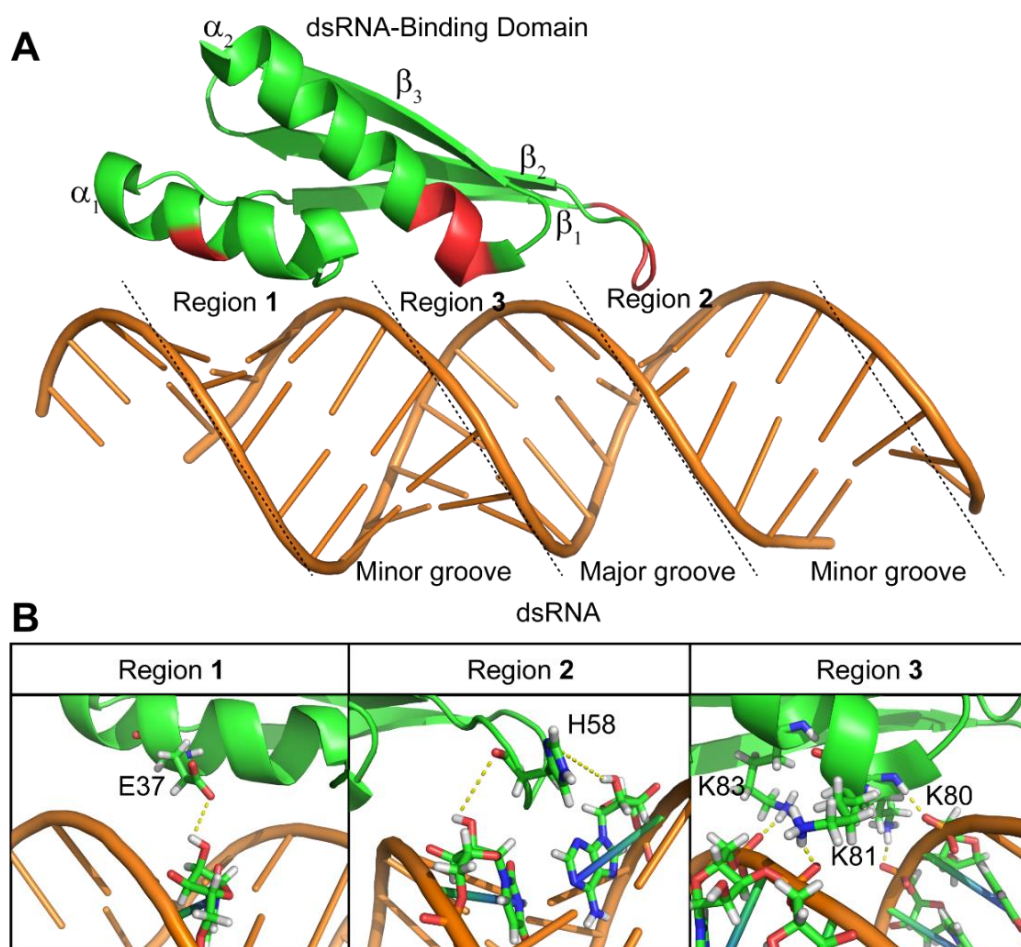
Figure 1.2: The interaction interface between dsRNA and dsRNA-Binding domain 1 of TRBP (PDB ID: 5N8M)[45]. (**A**) The dsRNA-binding domain (dsRBD - shown in green) shows a well-defined structural fold of α_1-β_1-β_2-β_3-α_2 specific to dsRBD. The dsRNA-binding residues of the dsRBD are clustered in three regions (marked in red color) in α_1-helix (Region 1), in the β_1-β_2 loop (Region 2) and at N-terminal of α_2-helix (Region 3). The conserved RNA-binding residues (marked in (**B**)) in the three RNA-binding regions interact with the ribose sugar and phosphodiester (shown in stick representation in (**B**)) backbone in the minor-major-minor groove of the dsRNA (shown in orange).

Although dsRBDs can have such structural variations, the RNA-binding residues are mostly conserved among type-I dsRBDs. The interactions between a dsRBD and a dsRNA is known to occur

via three distinct regions in the dsRBD[25,33], that mainly involve: (1) E residue in the middle of α_1 helix; (2) GPxH motif in the loop connecting β_1-β_2 sheets; and (3) KKxAK motif at N-terminus of α_2 helix (Figure 1.2). dsRNAs typically adopt A-form helical structure and the dsRBDs interact with the dsRNA from one of the faces of this A-form helix covering consecutive minor-major-minor groove that spans a length of about 12 base-pairs. Region 1 and region 2 has been shown to interact with the two minor grooves via extensive interaction with the 2′-OH of the ribose sugar. In region 1, a hydrogen bond is formed between the carboxylic group of the glutamate and the 2′-OH of the ribose sugar of the RNA. In region 2, the carbonyl group of histidine present in the peptide backbone interacts with 2′-OH of the one strand of the dsRNA, while the imidazole ring stacks on the ribose ring and shows hydrogen bonding interactions with the 2′-OH of the previous ribose on another strand of the dsRNA. The region 3 interacts with both the strands across the major groove of the A-form helix of the RNA where the amino group of each of the lysine contacts the non-bridging oxygen of the phosphodiester backbone of the dsRNA. From the three lysines, the first and the third lysine have been shown to interact with one of the strands whereas the second lysine gets directed towards the other strand of the dsRNA. Along with these well-conserved interactions, few other interactions in a specific dsRBD can be observed at the interface of the two molecules.

Since the commonly observed interactions at the dsRBD-dsRNA surface involve contacts with the backbone of the A-form helical dsRNA, these interactions are known to be structure-specific rather than sequence-specific[25,33]. However, it has been shown that the dsRBDs can bind to the dsRNAs with some imperfections in the A-form helical structure like internal loops or mismatches[46,47]. These imperfections in the dsRNAs can alter the A-form helical structure (by altering the Eular angles[48]) and thus can change the spread of the minor-major-minor grooves that interacts with the dsRBDs. These imperfections in the double-stranded regions of RNA leading to different RNA topologies can affect the interaction between a dsRBD and a dsRNA. Though some structural studies of the interactions of dsRBDs – like Staufen-dsRBD3[27], Rnt1p-dsRBD[49], ADAR2-dsRBD1[50], hDUS-dsRBD[43] – with dsRNAs deviating from the A-form helical dsRNA structures have been reported, the mechanism of interaction of dsRBDs with these topologically different dsRNAs with or without helical imperfections still remains unexplored. Therefore, in order to understand the mechanism of interaction of dsRBD and to study the effect of these helical imperfections on the interactions, this thesis has employed two model dsRBDs, namely TRBP2-dsRBD1 from *Homo sapiens* and ADAR-dsRBD1 from *Drosophila melanogaster*, involved in microRNA biogenesis pathway.

1.3.   *microRNAs and microRNA biogenesis pathway*

MicroRNAs (miRNAs) are small non-coding single-stranded RNAs of ~20-24 nt in length and are responsible for cellular processes like post-transcriptional gene regulation, immune response, antiviral response, etc[51,52]. They are the principal components of the RNAi pathway where they bind to

the mRNAs and induce or suppress the expression levels of the target gene or cause mRNA degradation[53]. Dysregulated miRNA levels have been reported in various diseases and thus they can be used as a marker that indicates a disturbance in the normal physiological state of an organism[13,54–57] and can serve as indicators for disease diagnosis. In order to understand the physiological or pathophysiological role of these miRNAs, it is necessary to study the processes which are involved in their synthesis.
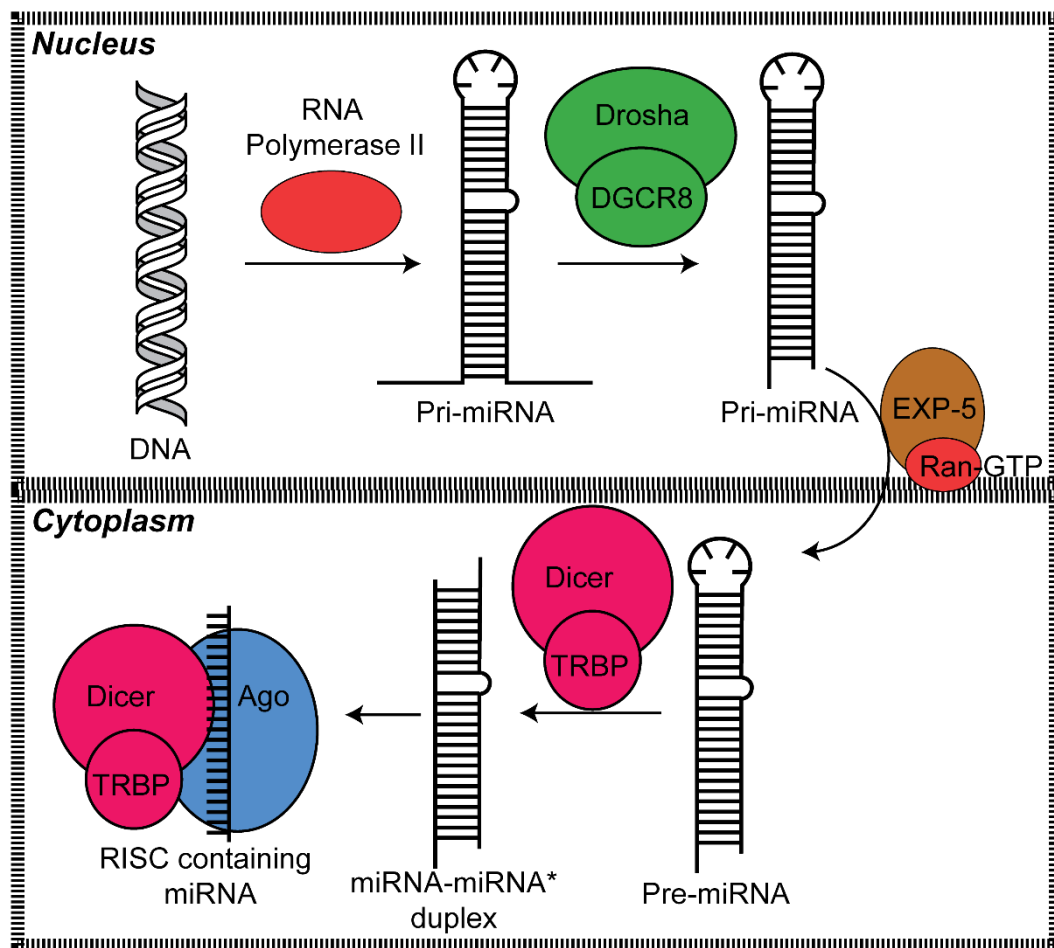
Figure 1.3: An overview of the canonical microRNA biogenesis pathway. The process starts with the generation of pri-miRNA that is transcribed from the miRNA gene. This pri-miRNA is processed by microprocessor complex containing Drosha and DGCR8 proteins to a shorter hairpin RNAs (pre-miRNA). The pre-miRNA is then transported by the nuclear export factor Exportin-5 (EXP-5) to the cytoplasm. In the cytoplasm, the pre-miRNA is further processed to ~22 bp duplex RNA by an RNase III enzyme Dicer with the help of TRBP. One of the strands of this duplex (miRNA) is transferred to the effector protein complex (RISC) which then acts for gene regulation. The other strand (miRNA*) is often degraded.

The canonical process of miRNA biogenesis is a two-step process (Figure 1.3), that starts with the transcription of the miRNA genes, located either in the intron or exons of the protein-coding genes or in the intergenic regions of the genome, primarily by RNA polymerase-II[58–60]. The primary transcripts called pri-miRNAs contain hairpin structures with or without the internal loops and bulges and are recognized and processed by microprocessor complex in the nucleus[61–63]. This complex contains an endonuclease Drosha – an RNase III enzyme – and a protein cofactor DGCR8 (Di-George Syndrome Critical Region 8) – a dsRNA-Binding Protein – that cleaves the pri-miRNA near dsRNA-ssRNA

junction at the base of the hairpin to a shorter (~60-70 nt long) hairpin precursor miRNA (pre-miRNA). Once generated, the pre-miRNAs, which often contain 3′-overhang, are exported by nuclear export protein Exportin-5 with the associated events involving RanGTP hydrolysis[28,29]. In the cytoplasm, the pre-miRNAs are processed by another RNaseIII enzyme Dicer to ~22 bp long RNA duplex (miRNA:miRNA*) and the process is aided by a dsRNA-Binding protein TRBP (TAR RNA-Binding Protein)[64–66]. This ribonucleoprotein complex is called the RNA Induced Silencing Complex (RISC) Loading Complex (RLC). From the duplex RNA, one of the strands termed as guide strand act as miRNA and the other strand called the passenger strand is often degraded. The guide strand is selectively transferred to effector complex (RISC), which contains the Argonaute (Ago) protein along with Dicer and TRBP, and the process of the transfer is assisted by TRBP that helps in the guide strand selection based on the thermodynamic stability of the two strands[67]. The mature miRNA in the RISC is then involved in the gene regulation activities.

Various proteins are involved in spatial and temporal regulation of the miRNA biogenesis[52,68,69]. They act at the transcriptional level, or at processing by RNase III enzymes (Drosha or Dicer) in the nucleus, by RNA editing or by RNA decay, etc. For example, proteins like SMAD[69,70], p53[52,70], ADAR[71–73] regulate the processing of pri-miRNA by the Drosha-DGCR8 complex. Further, PACT[74,75], ADAR[71–73], MAPK ERK[76,77], Lin-28[78,79] are some of the examples of proteins that regulate the cytoplasmic processing of the pre-miRNAs. The synthesis of miRNA involves interactions of RNAs – that are mostly present in the form of stem-loop structures – with the proteins involved in the biogenesis pathway (Drosha, DGCR8, Dicer, TRBP) and other regulatory proteins like ADAR, PACT contains one or more dsRBDs[80–82]. Therefore, studying the interactions of these domains and RNAs are important for a detailed understanding of the biogenesis pathway.

1.4. *Interactions between dsRBDs and dsRNAs along the miRNA biogenesis pathway*

It has been shown that the absence or presence of the double-stranded RNA-binding proteins affect the functioning of other proteins like RNase III enzymes Dicer[67,83] or Drosha[63,84,85]. Therefore, the interaction of the dsRBDs with dsRNAs is one of the major regulators of the miRNA biogenesis pathway. There are about 48860 miRNAs known till date,[86–88] most of which are produced from the canonical miRNA biogenesis pathway from their precursors. These precursors may have one or more helical perturbations like mismatch or bulge in the stem-loop structure (in the pri-miRNA and the pre-miRNA) or the dsRNA (in the miRNA:miRNA* duplex), and the dsRBDs need to interact with all of these topologically different dsRNAs. Thus, it would be interesting to understand the molecular mechanism of recognition of multiple substrate RNAs of different topologies by a single dsRBD. Further, it will be exciting to explore whether the dsRBDs from different proteins have similar mechanisms of interaction or they differ from each other.

Such detailed information can be extracted from the structural and dynamical characterization of dsRBDs from various proteins in the presence and absence of their substrates. As mentioned before, there are only 22 structures of dsRBD complexed with dsRNAs are available (till December 2019) in PDB and NDB and thus the generalizable conclusion cannot be made from these structures[36–39]. Further NMR-based studies have shown that the interaction between dsRNA and dsRBD of Dicer involves dynamical component as indicated by line-broadening of NMR peaks[81]. Also, recently fluorescence-based studies have shown that dsRBDs of TRBP slide along the length of dsRNA and such sliding is responsible for the accurate processing by the catalytic protein partner Dicer[47]. Another report has shown that such sliding is a property of dsRNA-Binding Proteins containing multiple dsRBDs as it is observed in four different proteins – ADAR1, ADAR2, Staufen1, and TRBP[46]. There are only a few studies which report on the atomic-level characterization of motions in dsRBDs by NMR spectroscopy and show that dsRBDs in DRB4 in *Arabidopsis thaliana*[89], in Rnt1p of *S. cerevisiae*[41], in Protein Kinase R[32], Drosha[80] and DGCR8[80] in humans possess intrinsic dynamics, which governs its interaction with substrate RNAs.

This thesis has focused on studies of two dsRBDs as model systems – one being from TRBP (TAR RNA-Binding protein), part of canonical miRNA biogenesis pathway; and the other from ADAR (Adenosine Deaminase Acting on RNA), one of the regulatory protein of miRNA biogenesis – to enhance the understanding of the dsRBD-dsRNA interaction. The two proteins are from two different species – TRBP from humans and ADAR from *Drosophila* – to understand and reflect the evolutionary differences, if any.

1.5. *TAR RNA-Binding Protein (TRBP)*

Trans-Activation Response (TAR) RNA-Binding Protein (TRBP) is a dsRNA-binding protein involved in various biological processes. It was first identified as a protein partner for HIV TAR RNA element[90]. The protein was later reported to be involved in the RNAi pathway, canonical miRNA biogenesis pathway, stress response, viral replication, cell growth, and cancer[91].

TRBP is expressed in two isoforms, TRBP1 and TRBP2, due to differential splicing of the mRNA transcribed from the same *Trbp2* gene[92,93]. TRBP2 differs from TRBP1 by 21 amino acids that are present at the N-terminus of TRBP2 (Figure 1.4), however, the structural and functional differences between the two isoforms have still not been explored. A report by Daniels *et al.* has suggested that these additional 21 amino acids might be responsible for cellular localization of the TRBP2[94]. Both the isoforms of TRBP contain three dsRBDs arranged in a modular fashion, of which two N-terminal dsRBDs are involved in protein-RNA interaction[82] while dsRBD3 is involved in protein-protein interaction[95]. All the three dsRBDs have α_1-β_1-β_2-β_3-α_2 fold – a canonical structural feature of all dsRBDs[64,82].
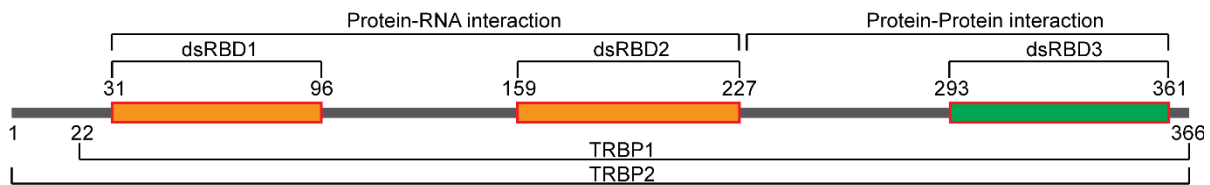
Figure 1.4: Domain organization of TRBP isoforms (TRBP1 and TRBP2) and functional role of Domains.

Being a part of the miRNA biogenesis pathway, TRBP has been known to interact with a wide range of topologically distinct miRNA precursors. It encounters RNA precursors at two distinct stages in cytoplasmic processing[67]. Firstly, it interacts with pre-miRNA and allows its positioning on Dicer and ensures accurate processing by Dicer to generate RNA duplexes[94,96]. Secondly, it interacts with the RNA duplexes, generated by Dicer, to assist selective transport of the guide strand to the Argonaute protein, which acts as mature miRNA in RISC[83,97]. Reports by Noland *et al.*, Daniels *et al.*, and Lee *et al.* have independently shown that TRBP is an indispensable cofactor for Dicer processing and helps it to accurately process pre-miRNAs (60-70 nt long stem-loop structures) to duplex RNAs (22-23 base pairs) during microRNA biogenesis[83,94,98]. About ~1881 precursor microRNAs (pre-miRNAs) are known, most of which are targeted by TRBP containing RNA induced silencing complex (RISC) loading complex for the processing. The stem part of pre-miRNAs may or may not be a perfect duplex and often has imperfections, like base-pair mismatches or bulges in the A-form helix. Such imperfections perturb the A-form helical structure of the molecule and create an assortment of topologies defined by the Euler angles[48]. A study by Yamashita *et al.* has shown that the interaction of dsRNA with TRBP-dsRBDs does not perturb the structure of the protein[82]. Also, a report by Acevedo *et al.* has reported that this interaction does not lead to the bending of RNA[99] as has been reported for DNA-protein interactions[100,101].

Since the interaction between the dsRBD and the dsRNA does not perturb the structure of either of the partner, it is intriguing to understand how dsRBDs of TRBP interact with the miRNA precursors with an assortment of topologies. Reports by Koh *et al.*, have shown that the RNA processing by Dicer gets affected by the diffusion of the TRBP-dsRBDs along the length of the RNA[47] and the perturbations in the helical structure[46,102]. Furthermore, they have shown that the fraction of TRBP involved in the diffusion process is dependent on the structure of dsRNA[47]. A perfect duplex RNA shows a major fraction involved in the diffusion while as the points of imperfections in the duplex are increased it leads to a reduction in the diffusive fraction of TRBP. Fareh *et al.* have recently reported two binding events[103] at TRBP:dsRNA interactions: (i) a short binding mode involving entry of RNA to Dicer-TRBP complex; and (ii) a long binding mode involving cleavage competent state of the complex. These reports suggest the involvement of dynamics at the dsRBD-dsRNA interface responsible for the interaction between the two; however, till date the details of the mechanism of interaction remain unexplored.

1.6.   *Adenosine Deaminase acting on RNA (ADAR)*

Adenosine Deaminase acting on RNA (ADAR) are a group of proteins involved in editing dsRNA substrates where they catalyze the conversion of Adenosine to Inosine by deamination reaction (Figure 1.5)[104]. Inosine is read as guanine by the translational machinery and thus leads to a change in the triplet code and the resultant protein sequence.
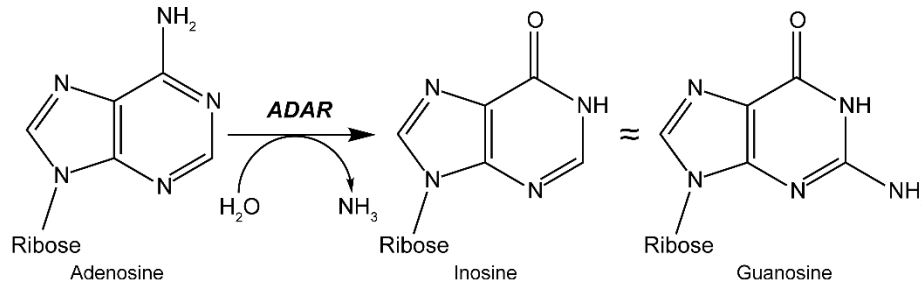
Figure 1.5: Adenosine to Inosine conversion by Adenosine Deaminase acting on RNA (ADAR).

ADAR is known to mainly affect the RNA transcripts that get translated to proteins involved in electrical and chemical neurotransmission[104]. ADAR is also known to alter the dsRNAs which enter into the RNAi pathway and regulate gene expression[71,105]. The edited RNA may inhibit the action of microprocessor complex or RISC loading complex or may interact with other mRNAs and thus affect gene expression. In humans, ADAR exists in three isoforms – ADAR1, ADAR2, and ADAR3, where all three proteins contain two dsRBDs. However, *Drosophila melanogaster* has only one ADAR protein (represented as dADAR in this thesis hereafter) homologous to ADAR2 in humans with two dsRBDs at N-terminus and one deaminase domain at C-terminus (as shown in Figure 1.6). The interaction of ADAR2 with dsRNA has been reported to be sequence-specific, wherein dsRBD1 of ADAR2 has been shown to bind to an RNA with G-X9-A sequence and dsRBD2 has been shown to bind to G-X8-A sequence[50]. However, an article by Eggington and coworkers has shown that the specificity of ADAR is exhibited mainly by the catalytic domain of the protein[106] and de-amination can occur in the absence of dsRBDs at the N-terminus of the deaminase domain[107]. Barraud *et al.* have also shown that dsRBD of dADAR interacts with dsRNAs with minimal sequence-preference and thus create uncertainty about the sequence specificity of the dsRBDs of ADAR family of protein[108]. This protein may also involve dynamic interactions as reported for other dsRBDs; however, the characterization of dynamics has not been reported.
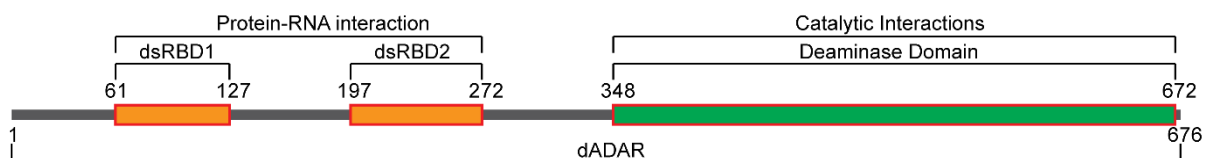
Figure 1.6: Domain Organization of ADAR protein from *Drosophila melanogaster* and the functional role of its domains.

With this background, we proposed that the characterization of the dynamics of dsRBD of TRBP and ADAR (as model systems) will enhance our understanding of the dsRBD-dsRNA interactions. The characterization needs to be performed in the absence and presence of a substrate RNA to distinguish the inherent dynamics of the dsRBDs from those in the RNA-bound state. Among various miRNA sequences available from the database, we proposed to use miR-16-1 (Figure 1.7) as the target RNA substrate for the above-mentioned study as this has been reported in the literature to interact with the dsRBDs of Drosha[80], DGCR8[80], Dicer[81], and TRBP[109].

1.7. *miRNA-16-1*

miR-16 is one of the miRNAs of miRNA-15 family that has been extensively investigated for its biological functions. This miRNA is known to be deleted in many chronic lymphocytic leukemias[110] and downregulated in malignancies like glioma[111], prostate cancer[112], etc. It is also known to regulate the function of vascular smooth muscle cells (VSMC)[113] and act as a tumor suppressor in Gastric cancer[114].
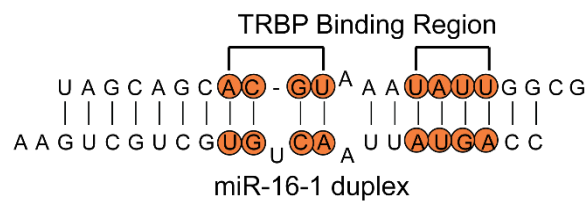
Figure 1.7: Secondary structure of the duplex of miR-16-1 showing probable TRBP binding residues (marked in orange)[115].

The precursor miRNA sequence of this miRNA is available in the miRBase registry (http://www.mirbase.org/)[86–88,116] with accession number MI0000070. The secondary structure of miR-16-1 duplex shows that it contains one mismatch and one bulge in the probable TRBP binding sites[115] (Figure 1.7). It has previously been reported by studies involving DNA-substitution in siRNA that the base-pair 9 to 12 and 15 to 18 are involved in binding of RNA to TRBP[115]. Thus, apart from being a known binder of TRBP, it can also serve as an informative substrate to study the effect of structural perturbations (mismatch and bulge) in the A-form helix of RNA duplex on dsRBD-dsRNA interactions. Though a report by Takahashi *et al.* have predicted the TRBP binding site on dsRNA[115], there are multiple studies reporting multiple dsRBDs binding to a dsRNA[80,81,109,117]. Also, Acevedo *et al.* have shown that stoichiometry of the interaction of TRBP-dsRBD12 and miR-16-1 duplex is more than one which supports multiple dsRBDs interacting with a dsRNA[109]. These multiple dsRBD binding also supports the non-sequence specific interaction of dsRBDs that spans 10-12 bp on a dsRNA that can have longer length[25,33,109]. Interactions of Dicer-dsRBD with pre-miR-16-1 and with pre-siRNA have shown that it is unable to discriminate between various dsRNA substrates, but interacts with them with nearly similar affinities[81]. A report by Acevedo *et al.* has also shown interactions of TRBP-dsRBD12 with miR-16-1 precursors where the binding with pre-miRNA as well as with its product

(miRNA:miRNA* duplex) after Dicer cleavage is shown to have similar binding affinities[109] as observed for Dicer-dsRBD[81]. Further, they report that the imperfections like mismatch or bulge in the A-form helix affect the binding affinity of TRBP-dsRBD12[109]. With this background, we have used miR-16-1 duplex as a model dsRNA in this thesis, to enhance the structural understanding of dsRBD-dsRNA interactions and also to study the effect of the helical imperfections on these interactions.

1.8.   Scope of the Thesis

This work carried out in this thesis will add to the current knowledge of the dsRBD-dsRNA interaction and will explore the mechanism of interaction between dsRBD and dsRNA. The investigations carried out in this thesis have used NMR spectroscopy as a primary tool for the characterization of the structure and dynamics of the dsRBDs in the free and substrate-bound state. Chapter 2 discusses the basic features and applications of the different biophysical techniques used in the later chapters. Chapter 3 discusses the resonance assignment of the dsRBDs, which is the primary step to the structure and dynamics characterization of the proteins by NMR spectroscopy. Chapter 4 discusses the intrinsic dynamics of the two dsRBDs at a ps-ns timescale that contributes to the internal residue level flexibility of the protein and μs-ms timescale motions that are responsible for catalytic interactions, ligand-binding and -release, allosteric effects, etc. Chapter 5 discusses the effect of the dsRNA with and without helical imperfections on dsRBDs based on the biophysical characterization of the binding events and then will focus on the mechanism of interaction of dsRBD and dsRNA via characterization of the dynamics of the dsRBDs in dsRNA-bound state. We hypothesize that the results of these studies will allow us to understand the role of dynamics in the dsRBDs recognition of dsRNAs of different shapes; and how these adapt to a suitable conformation to be able to bind to the substrate due to the inherent adaptability in the dsRBD fold.

1.9.   References

1   M. N. Win and C. D. Smolke, RNA as a versatile and powerful platform for engineering genetic regulatory tools, *Biotechnol. Genet. Eng. Rev.*, 2007, **24**, 311–346.

2   P. B. Moore, The three-dimensional structure of the ribosome and its components, *Annu. Rev. Biophys. Biomol. Struct.*, 1998, **27**, 35–58.

3   W. G. Scott and A. Klug, Ribozymes: Structure and mechanism in RNA catalysis, *Trends Biochem. Sci.*, 1996, **21**, 220–224.

4   T. M. Tarasow and B. E. Eaton, Dressed for success: Realizing the catalytic potential of RNA, *Biopolymers*, 1998, **48**, 29–37.

5   H. Siomi and M. C. Siomi, Posttranscriptional Regulation of MicroRNA Biogenesis in Animals, *Mol. Cell*, 2010, **38**, 323–332.

6   K. Shruti, K. Shrey and R. Vibha, Micro RNAs: Tiny sequences with enormous potential,

Biochem. Biophys. Res. Commun., 2011, **407**, 445–449.

7   J. Gelles and R. Landick, RNA polymerase as a molecular motor, *Cell*, 1998, **93**, 13–16.

8   A. Polyakov, E. Severinova and S. A. Darst, Three-dimensional structure of E. coil core RNA polymerase: Promoter binding and elongation conformations of the enzyme, *Cell*, 1995, **83**, 365–373.

9   D. Moras, Aminoacyl-tRNA synthetases, *Curr. Opin. Struct. Biol.*, 1992, **2**, 138–142.

10   V. Rajendran, P. Kalita, H. Shukla, A. Kumar and T. Tripathi, Aminoacyl-tRNA synthetases: Structure, function, and drug discovery, *Int. J. Biol. Macromol.*, 2018, **111**, 400–414.

11   A. W. Nicholson, Ribonuclease III mechanisms of double-stranded RNA cleavage, *Wiley Interdiscip. Rev. RNA*, 2014, **5**, 31–48.

12   B. Kechavarzi and S. C. Janga, Dissecting the expression landscape of RNA-binding proteins in human cancers, *Genome Biol.*, 2014, **15**, 1–16.

13   D. Quiat and E. N. Olson, Review series MicroRNAs in cardiovascular disease : from pathogenesis to prevention and treatment, *J. Clin. Invest.*, 2013, **123**, 11–18.

14   J. Shi, Regulatory networks between neurotrophins and miRNAs in brain diseases and cancers, *Acta Pharmacol. Sin.*, 2015, **36**, 149–157.

15   Kathleen B Hall, RNA–protein interactions, *Curr. Opin. Struct. Biol.*, 2002, **12**, 283–288.

16   K. Nagai, RNA-protein interactions, *Curr. Opin. Struct. Biol.*, 1992, **2**, 131–137.

17   G. Varani, RNA - Protein Intermolecular Recognition, *Acc. Chem. Res.*, 1997, **30**, 189–195.

18   D. E. Draper, Themes in RNA-Protein Recognition, *J. Mol. Biol.*, 1999, **293**, 255–270.

19   D. E. Draper, Protein-RNA Recognition, *Annu. Rev. Biochem.*, 1995, **64**, 593–620.

20   T. R. Cech, The RNA worlds in context, *Cold Spring Harb. Perspect. Biol.*, 2012, **4**, 1–5.

21   J. Rosenbaum and M. Ward, The non-Watson-Crick base pairs and their associated isostericity matrices, *Nucleic Acids Res.*, 2002, **30**, 3497–3531.

22   J. M. Fox, M. Zhao, M. J. Fink, K. Kang and G. M. Whitesides, The Molecular Origin of Enthalpy/Entropy Compensation in Biomolecular Recognition, *Annu. Rev. Biophys.*, 2018, **47**, 223–250.

23   D. S. T. Johnston, N. H. Brown, J. G. Gallt and M. Jantscht, A conserved double-stranded RNA-binding domain, *Proc Natl Acad Sci U S A*, 1992, **89**, 10979–10983.

24   I. Fierro-Monti and M. B. Mathews, Proteins binding to duplexed RNA: one motif, multiple functions, *Trends Biochem. Sci.*, 2000, **25**, 241–246.

25   B. Tian, P. C. Bevilacqua, A. Diegelman-Parente and M. B. Mathews, The double-stranded-RNA-binding motif: Interference and much more, *Nat. Rev. Mol. Cell Biol.*, 2004, **5**, 1013–1023.

26   S. Heber, I. Gáspár, J.-N. Tants, J. Günther, S. M. F. Moya, R. Janowski, A. Ephrussi, M. Sattler and D. Niessing, Staufen2-mediated RNA recognition and localization requires combinatorial action of multiple domains, *Nat. Commun.*, 2019, **10**, 1659.

27   A. Ramos, S. Grunert, J. Adams, D. R. Micklem, M. R. Proctor, S. Freund, M. Bycroft, D. St Johnston and G. Varani, RNA recognition by a Staufen double-stranded RNA-binding domain, *EMBO J*, 2000, **19**, 997–1009.

28   X. Wang, X. Xu, Z. Ma, Y. Huo, Z. Xiao, Y. Li and Y. Wang, Dynamic mechanisms for pre-miRNA binding and export by Exportin-5, *RNA*, 2011, **17**, 1511–1528.

29   C. Okada, E. Yamashita, S. J. Lee, S. Shibata, J. Katahira, A. Nakagawa, Y. Yoneda and T. Tsukihara, A high-Resolution structure of the pre-microrna nuclear export machinery, *Science (80-.).*, 2009, **326**, 1275–1279.

30   B. L. Bass, RNA Editing by Adenosine Deaminases That Act on RNA, *Annu. Rev. Biochem.*, 2007, **71**, 817–846.

31   Y. Fu, X. Zhao, Z. Li, J. Wei and Y. Tian, Splicing variants of ADAR2 and ADAR2-mediated RNA editing in glioma, *Oncol. Lett.*, 2016, **12**, 788–792.

32   S. Nanduri, F. Rahman, B. R. G. Williams and J. Qin, A dynamically tuned double-stranded RNA binding mechanism for the activation of antiviral kinase PKR, *EMBO J.*, 2000, **19**, 5567–5574.

33   G. Masliah, P. Barraud and F. H.-T. Allain, RNA recognition by double-stranded RNA binding domains: a matter of shape and sequence, *Cell. Mol. Life Sci.*, 2013, **70**, 1875–1895.

34   A. Kharrat, M. J. Macias, T. J. Gibson, M. Nilges and A. Pastore, Structure of the dsRNA binding domain of E. coli RNase III., *EMBO J.*, 1995, **14**, 3572–3584.

35   M. Bycroft, S. Grünert, A. G. Murzin, M. Proctor and D. St Johnston, NMR solution structure of a dsRNA binding domain from Drosophila staufen protein reveals homology to the N-terminal domain of ribosomal protein S5., *EMBO J.*, 1995, **14**, 3563–3571.

36   H. M. Berman, J. Westbrook, Z. Feng, G. Gilliland, T. N. Bhat, H. Weissig, I. N. Shindyalov and P. E. Bourne, The Protein Data Bank, *Nucleic Acids Res*, 2000, **28**, 235–242.

37   S. K. Burley, H. M. Berman, C. Bhikadiya, C. Bi, L. Chen, L. Di Costanzo, C. Christie, K. Dalenberg, J. M. Duarte, S. Dutta, Z. Feng, S. Ghosh, D. S. Goodsell, R. K. Green, V. Guranovic, D. Guzenko, B. P. Hudson, T. Kalro, Y. Liang, R. Lowe, H. Namkoong, E. Peisach, I. Periskova, A. Prlic, C. Randle, A. Rose, P. Rose, R. Sala, M. Sekharan, C. Shao, L. Tan, Y. P. Tao, Y. Valasatava, M. Voigt, J. Westbrook, J. Woo, H. Yang, J. Young, M. Zhuravleva and C. Zardecki, RCSB Protein Data Bank: biological macromolecular structures enabling research and education in fundamental biology, biomedicine, biotechnology and energy, *Nucleic Acids Res*, 2019, **47**, D464–D474.

38   H. M. Berman, W. K. Olson, D. L. Beveridge, J. Westbrook, A. Gelbin, T. Demeny, S. H. Hsieh, A. R. Srinivasan and B. Schneider, The nucleic acid database. A comprehensive relational database of three-dimensional structures of nucleic acids, *Biophys. J.*, 1992, **63**, 751–759.

39   B. Coimbatore Narayanan, J. Westbrook, S. Ghosh, A. I. Petrov, B. Sweeney, C. L. Zirbel, N. B. Leontis and H. M. Berman, The Nucleic Acid Database: new features and capabilities,

Nucleic Acids Res., 2013, **42**, D114–D122.

40   R. Stefl, M. Xu, L. Skrisovska, R. B. Emeson and F. H. T. Allain, Structure and specific RNA binding of ADAR2 double-stranded RNA binding motifs, *Structure*, 2006, **14**, 345–355.

41   E. Hartman, Z. Wang, Q. Zhang, K. Roy, G. Chanfreau and J. Feigon, Intrinsic Dynamics of an Extended Hydrophobic Core in the S . cerevisiae RNase III dsRBD Contributes to Recognition of Specific RNA Binding Sites, *J. Mol. Biol.*, 2013, **425**, 546–562.

42   N. Leulliot, S. Quevillon-Cheruel, M. Graille, H. Van Tilbeurgh, T. C. Leeper, K. S. Godin, T. E. Edwards, S. T. L. Sigurdsson, N. Rozenkrants, R. J. Nagel, M. Ares and G. Varani, A new α-helical extension promotes RNA binding by the dsRBD of Rnt1p RNAse III, *EMBO J.*, 2004, **23**, 2468–2477.

43   C. Bou-Nader, P. Barraud, L. Pecqueur, J. Pérez, C. Velours, W. Shepard, M. Fontecave, C. Tisné and D. Hamdane, Molecular basis for transfer RNA recognition by the double-stranded RNA-binding domain of human dihydrouridine synthase 2, *Nucleic Acids Res.*, 2019, **47**, 3117–3126.

44   C. Bou-Nader, L. Pecqueur, P. Barraud, M. Fontecave, C. Tisné, S. Sacquin-Mora and D. Hamdane, Conformational Stability Adaptation of a Double-Stranded RNA-Binding Domain to Transfer RNA Ligand, *Biochemistry*, 2019, **58**, 2463–2473.

45   G. Masliah, C. Maris, S. L. König, M. Yulikov, F. Aeschimann, A. L. Malinowska, J. Mabille, J. Weiler, A. Holla, J. Hunziker, N. Meisner-Kober, B. Schuler, G. Jeschke and F. H. Allain, Structural basis of siRNA recognition by TRBP double-stranded RNA binding domains, *EMBO J.*, 2018, e97089.

46   X. Wang, L. Vukovic, H. R. Koh, K. Schulten and S. Myong, Dynamic profiling of double-stranded RNA binding proteins, *Nucleic Acids Res.*, 2015, **43**, 7566–7576.

47   H. R. Koh, M. A. Kidwell, K. Ragunathan, J. A. Doudna and S. Myong, ATP-independent diffusion of double-stranded RNA binding proteins, *Proc. Natl. Acad. Sci. U. S. A.*, 2013, **110**, 151–156.

48   M. H. Bailor, X. Sun and H. M. Al-Hashimi, Topology links RNA secondary structure with global conformation, dynamics, and adaptation, *Science (80-.).*, 2010, **327**, 202–206.

49   H. Wu, A. Henras, G. Chanfreau and J. Feigon, Structural basis for recognition of the AGNN tetraloop RNA fold by the double-stranded RNA-binding domain of Rnt1p RNase III, *Proc. Natl. Acad. Sci. U. S. A.*, 2004, **101**, 8307 LP – 8312.

50   R. Stefl, F. C. Oberstrass, J. L. Hood, M. Jourdan, M. Zimmermann, L. Skrisovska, C. Maris, L. Peng, C. Hofr, R. B. Emeson and F. H. T. Allain, The solution structure of the ADAR2 dsRBM-RNA complex reveals a sequence-specific readout of the minor groove, *Cell*, 2010, **143**, 225–237.

51   V. N. Kim, J. Han and M. C. Siomi, Biogenesis of small RNAs in animals, *Nat. Rev. Mol. Cell Biol.*, 2009, **10**, 126–139.

52 M. Ha and V. N. Kim, Regulation of microRNA biogenesis., *Nat. Rev. Mol. Cell Biol.*, 2014, **15**, 509–24.

53 P. D. Zamore, RNA interference: Listening to the sound of silence, *Nat. Struct. Biol.*, 2001, **8**, 746–750.

54 W. W., K. E.J. and T. L.-H., MicroRNAs in learning, memory, and neurological diseases, *Learn. Mem.*, 2012, **19**, 359–368.

55 S. Pfeffer and O. Voinnet, Viruses, microRNAs and cancer, *Oncogene*, 2006, **25**, 6211–6219.

56 G. A. Calin and C. M. Croce, MicroRNA-cancer connection: The beginning of a new tale, *Cancer Res.*, 2006, **66**, 7390–7394.

57 A. Caroli, M. T. Cardillo, R. Galea and L. M. Biasucci, Potential therapeutic role of microRNAs in ischemic heart disease, *J. Cardiol.*, 2013, **61**, 315–320.

58 Y. Lee, M. Kim, J. Han, K. H. Yeom, S. Lee, S. H. Baek and V. N. Kim, MicroRNA genes are transcribed by RNA polymerase II, *EMBO J.*, 2004, **23**, 4051–4060.

59 V. N. Kim and J. W. Nam, Genomics of microRNA, *Trends Genet.*, 2006, **22**, 165–173.

60 S. L. Clarke, M. R. Davis and R. Sunkar, in *MicroRNAs as Tools in Biopharmaceutical Production*, ed. N. Barron, Springer S., 2012, pp. 1–124.

61 Y. Lee, C. Ahn, J. Han, H. Choi, J. Kim, J. Yim, J. Lee, P. Provost, O. Ra˚dmark, Sunyoung Kim and V. N. Kim, The nuclear RNase III Drosha initiates microRNA processing, *Nature*, 2003, **425**, 415–419.

62 J. Han, Y. Lee, K. H. Yeom, J. W. Nam, I. Heo, J. K. Rhee, S. Y. Sohn, Y. Cho, B. T. Zhang and V. N. Kim, Molecular Basis for the Recognition of Primary microRNAs by the Drosha-DGCR8 Complex, *Cell*, 2006, **125**, 887–901.

63 C. Landbouwcatalogus, The Drosha–DGCR8 complex in primary microRNA processing, *Genes Dev.*, 2004, **18**, 3016–3027.

64 R. C. Wilson, A. Tambe, M. A. Kidwell, C. L. Noland, C. P. Schneider and J. A. Doudna, Dicer-TRBP complex formation ensures accurate mammalian MicroRNA biogenesis, *Mol. Cell*, 2015, **57**, 397–408.

65 P. W. Lau, K. Z. Guiley, N. De, C. S. Potter, B. Carragher and I. J. MacRae, The molecular architecture of human Dicer, *Nat. Struct. Mol. Biol.*, 2012, **19**, 436–440.

66 H.-W. Wang, C. Noland, B. Siridechadilok, D. W. Taylor, E. Ma, K. Felderer, J. A. Doudna and E. Nogales, Structural insights into RNA processing by the human RISC-loading complex., *Nat. Struct. Mol. Biol.*, 2009, **16**, 1148–1153.

67 C. L. Noland, E. Ma and J. A. Doudna, siRNA Repositioning for Guide Strand Selection by Human Dicer Complexes, *Mol. Cell*, 2011, **43**, 110–121.

68 J. Lee, Z. Li, R. Brower-Sinning and B. John, Regulatory circuit of human microRNA biogenesis, *PLoS Comput. Biol.*, 2007, **3**, 721–732.

69 B. N. Davis and A. Hata, Regulation of MicroRNA Biogenesis: A miRiad of mechanisms, *Cell*

Commun. Signal., 2009, **7**, 1–22.

70   H. I. Suzuki and K. Miyazono, Emerging complexity of microRNA generation cascades, *J. Biochem.*, 2011, **149**, 15–25.

71   K. Nishikura, Editor meets silencer: Crosstalk between RNA editing and RNA interference, *Nat. Rev. Mol. Cell Biol.*, 2006, **7**, 919–931.

72   K. SW and B. BL, The role of RNA editing by ADARs in RNAi, *Mol. Cell*, 2002, **10**, 809–817.

73   D. G. West, ADAR Editing Wobbles the MicroRNA World, *ACS Chem. Biol.*, 2010, **2**, 1–9.

74   Y. Lee, I. Hur, S. Y. Park, Y. K. Kim, R. S. Mi and V. N. Kim, The role of PACT in the RNA silencing pathway, *EMBO J.*, 2006, **25**, 522–532.

75   E. Koscianska, J. Starega-Roslan and W. J. Krzyzosiak, The role of dicer protein partners in the processing of microRNA precursors, *PLoS One*, 2011, **6**, e28548.

76   Z. Paroo, X. Ye, S. Chen and Q. Liu, Phosphorylation of the Human MicroRNA-Generating Complex Mediates MAPK/Erk Signaling, *Cell*, 2009, **139**, 112–122.

77   K. M. Herbert, G. Pimienta, S. J. DeGregorio, A. Alexandrov and J. A. Steitz, Phosphorylation of DGCR8 Increases Its Intracellular Stability and Induces a Progrowth miRNA Profile, *Cell Rep.*, 2013, **5**, 1070–1081.

78   T. Treiber, N. Treiber, U. Plessmann, S. Harlander, J. L. Daiß, N. Eichner, G. Lehmann, K. Schall, H. Urlaub and G. Meister, A Compendium of RNA-Binding Proteins that Regulate MicroRNA Biogenesis, *Mol. Cell*, 2017, **66**, 270–284.

79   I. Heo, C. Joo, Y.-K. Kim, M. Ha, M.-J. Yoon, J. Cho, K.-H. Yeom, J. Han and V. N. Kim, TUT4 in Concert with Lin28 Suppresses MicroRNA Biogenesis through Pre-MicroRNA Uridylation, *Cell*, 2009, **138**, 696–708.

80   C. Wostenberg, K. A. Quarles and S. A. Showalter, Dynamic origins of differential RNA binding function in two dsRBDs from the miRNA 'Microprocessor' complex, *Biochemistry*, 2010, **49**, 10728–10736.

81   C. Wostenberg, J. W. Lary, D. Sahu, R. Acevedo, K. A. Quarles, J. L. Cole and S. A. Showalter, The role of human Dicer-dsRBD in processing small regulatory RNAs, *PLoS One*, 2012, **7**, e51829.

82   S. Yamashita, T. Nagata, M. Kawazoe, C. Takemoto, T. Kigawa, P. Güntert, N. Kobayashi, T. Terada, M. Shirouzu, M. Wakiyama, Y. Muto and S. Yokoyama, Structures of the first and second double-stranded RNA-binding domains of human TAR RNA-binding protein, *Protein Sci.*, 2011, **20**, 118–130.

83   C. L. Noland and J. A. Doudna, Multiple sensors ensure guide strand selection in human RNAi pathways., *RNA*, 2013, **19**, 639–648.

84   M. Faller, D. Toso, M. Matsunaga, I. Atanasov, R. Senturia, Y. Chen, Z. H. Zhou and G. Feng, DGCR8 recognizes primary transcripts of microRNAs through highly cooperative binding and formation of higher-order structures, *RNA*, 2010, **16**, 1570–1583.

85   K. A. Quarles, D. Chadalavada and S. A. Showalter, Deformability in the cleavage site of primary microRNA is not sensed by the double-stranded RNA binding domains in the microprocessor component DGCR8, *Proteins Struct. Funct. Bioinforma.*, 2015, **83**, 1165–1179.

86   S. Griffiths-Jones, The microRNA Registry, *Nucleic Acids Res.*, 2004, **32**, D109–D111.

87   S. Griffiths-Jones, R. J. Grocock, S. van Dongen, A. Bateman and A. J. Enright, miRBase: microRNA sequences, targets and gene nomenclature, *Nucleic Acids Res.*, 2006, **34**, D140–D144.

88   A. Kozomara, M. Birgaoanu and S. Griffiths-Jones, miRBase: from microRNA sequences to function, *Nucleic Acids Res.*, 2018, **47**, D155–D162.

89   S. C. Chiliveri, R. Aute, U. Rai and M. V. Deshmukh, DRB4 dsRBD1 drives dsRNA recognition in Arabidopsis thaliana tasi/siRNA pathway, *Nucleic Acids Res.*, 2017, **45**, 8551–8563.

90   A. Gatignol, A. Buckler-White, B. Berkhout and K. T. Jeang, Characterization of a human TAR RNA-binding protein that activates the HIV-1 LTR, *Science (80-.).*, 1991, **251**, 1597–1600.

91   S. M. Daniels and a. Gatignol, The Multiple Functions of TRBP, at the Hub of Cell Responses to Viruses, Stress, and Cancer, *Microbiol. Mol. Biol. Rev.*, 2012, **76**, 652–666.

92   S. Bannwarth, L. Talakoub, F. Letourneur, M. Duarte, D. F. Purcell, J. Hiscott and A. Gatignol, Organization of the Human tarbp2 Gene Reveals Two Promoters That Are Repressed in an Astrocytic Cell Line, *J. Biol. Chem.*, 2001, **276**, 48803–48813.

93   M. Duarte, K. Graham, A. Daher, P.-L. Battisti, S. Bannwarth, E. Segeral, K.-T. Jeang and A. Gatignol, Characterization of TRBP1 and TRBP2, *J. Biomed. Sci.*, 2000, **7**, 494–506.

94   S. M. Daniels, C. E. Melendez-Peña, R. J. Scarborough, A. Daher, H. S. Christensen, M. El Far, D. F. J. Purcell, S. Lainé, A. Gatignol, C. E. Melendez-Pena, R. J. Scarborough, A. Daher, H. S. Christensen, M. El Far, D. F. J. Purcell, S. Laine and A. Gatignol, Characterization of the TRBP domain required for Dicer interaction and function in RNA interference, *BMC Mol. Biol.*, 2009, **10**, 38.

95   G. Laraki, G. Clerzius, A. Daher, C. Melendez-Peña, S. Daniels and A. Gatignol, Interactions between the double-stranded RNA-binding proteins TRBP and PACT define the Medipal domain that mediates protein-protein interactions, *RNA Biol.*, 2008, **5**, 92–103.

96   L. Jaskiewicz and M. Zavolan, Dicer partners expand the repertoire of miRNA targets, *Genome Biol.*, 2012, **13**, 179.

97   M. P. Perron and P. Provost, Protein interactions and complexes in human microRNA biogenesis and function., *Front. Biosci.*, 2010, **13**, 2537–47.

98   H. Y. Lee and J. A. Doudna, TRBP alters human precursor microRNA processing in vitro, *RNA*, 2012, **18**, 2012–2019.

99   R. Acevedo, D. Evans, K. A. Penrod and S. A. Showalter, Binding by TRBP-dsRBD2 Does Not Induce Bending of Double-Stranded RNA, *Biophysj*, 2016, **110**, 2610–2617.

100   G. Parkinson, C. Wilson, A. Gunasekera, Y. W. Ebright, R. E. Ebright and H. M. Berman,

Structure of the CAP-DNA Complex at 2.5 Å Resolution: A Complete Picture of the Protein-DNA Interface, *J. Mol. Biol.*, 1996, **260**, 395–408.

101 Y. Kim, J. H. Geiger, S. Hahn and P. B. Sigler, Crystal structure of a yeast TBP/TATA-box complex, *Nature*, 1993, **365**, 512–520.

102 H. R. Koh, M. A. Kidwell, J. Doudna and S. Myong, RNA scanning of a molecular machine with a built-in ruler, *J. Am. Chem. Soc.*, 2017, **139**, 262–268.

103 M. Fareh, K. H. Yeom, A. C. Haagsma, S. Chauhan, I. Heo and C. Joo, TRBP ensures efficient Dicer processing of precursor microRNA in RNA-crowded environments, *Nat. Commun.*, 2016, **7**, 1–11.

104 Y. A. Savva, L. E. Rieder and R. A. Reenan, The ADAR protein family, *Genome Biol.*, 2012, **13**, 252.

105 K. Nishikura, Functions and Regulation of RNA Editing by ADAR Deaminases, *Annu. Rev. Biochem.*, 2010, **79**, 321–349.

106 J. M. Eggington, T. Greene and B. L. Bass, Predicting sites of ADAR editing in double-stranded RNA, *Nat. Commun.*, 2011, **2**, 319.

107 G. Tang, siRNA and miRNA: An insight into RISCs, *Trends Biochem. Sci.*, 2005, **30**, 106–114.

108 P. Barraud, B. S. E. Heale, M. A. O'Connell and F. H. T. Allain, Solution structure of the N-terminal dsRBD of Drosophila ADAR and interaction studies with RNA, *Biochimie*, 2012, **94**, 1499–1509.

109 R. Acevedo, N. Orench-Rivera, K. A. Quarles and S. A. Showalter, Helical defects in MicroRNA influence protein binding by TAR RNA binding protein, *PLoS One*, 2015, **10**, e0116749.

110 D. Zhao, Y. Zhang and L. Song, MiR-16-1 Targeted Silences Far Upstream Element Binding Protein 1 to Advance the Chemosensitivity to Adriamycin in Gastric Cancer, *Pathol. Oncol. Res.*, 2018, **24**, 483–488.

111 X. Li, N. Ling, Y. Bai, W. Dong, G. Z. Hui, D. Liu, J. Zhao and J. Hu, MiR-16-1 Plays a Role in Reducing Migration and Invasion of Glioma Cells, *Anat. Rec.*, 2013, **296**, 427–432.

112 D. Bonci, V. Coppola, M. Musumeci, A. Addario, R. Giuffrida, L. Memeo, L. D'Urso, A. Pagliuca, M. Biffoni, C. Labbaye, M. Bartucci, G. Muto, C. Peschle and R. De Maria, The miR-15a-miR-16-1 cluster controls prostate cancer by targeting multiple oncogenic activities, *Nat. Med.*, 2008, **14**, 1271–1277.

113 Q. Gu, G. Zhao, Y. Wang, B. Xu and J. Yue, Silencing miR-16 Expression Promotes Angiotensin II Stimulated Vascular Smooth Muscle Cell Growth, *Cell Dev. Biol.*, 2017, **06**, 1–7.

114 T. Wang, J. Hou, Z. Li, Z. Zheng, J. Wei, D. Song, T. Hu, Q. Wu, J. Y. Yang and J. C. Cai, miR-15a-3p and miR-16-1-3p negatively regulate twist1 to repress gastric cancer cell invasion and metastasis, *Int. J. Biol. Sci.*, 2017, **13**, 122–134.

115   T. Takahashi, S. Zenno, O. Ishibashi, T. Takizawa, K. Saigo and K. Ui-Tei, Interactions between the non-seed region of siRNA and RNA-binding RLC/RISC proteins, Ago and TRBP, in mammalian cells, *Nucleic Acids Res.*, 2014, **42**, 5256–5269.

116   S. Griffiths-Jones, H. K. Saini, S. van Dongen and A. J. Enright, miRBase: tools for microRNA genomics, *Nucleic Acids Res*, 2008, **36**, D154-8.

117   M. P. M. H. Benoit, L. Imbert, A. Palencia, J. Pérard, C. Ebel, J. Boisbouvier and M. J. Plevin, The RNA-binding region of human TRBP interacts with microRNA precursors through two independent domains, *Nucleic Acids Res.*, 2013, **41**, 4241–4252.

Chapter 2 Biophysical Techniques

2.1.   Introduction

Proteins are complex molecules, wherein permutation and combination of 20 different amino acids in the primary sequence lead to a variety of three-dimensional structures, making their characterization a difficult task. However, it is necessary to characterize proteins to understand their structure-function relationship. Different biophysical techniques have been developed to provide a detailed understanding into the structural and dynamic properties of proteins and protein-ligand complexes. In order to enhance the current structure and dynamic information of dsRBDs and their interaction(s) with dsRNAs, the different biophysical techniques that have been used in this thesis are reviewed in the following sections.

2.2.   Size Exclusion Chromatography (SEC) – Multi-Angle Light Scattering (MALS)

For the biophysical characterization of the proteins and other biomolecules, it is necessary that they need to be studied in their native form (as monomers, oligomers, aggregates, etc.). Biophysical studies in non-native form adversely affect the interpretation of their structure and dynamic properties along with ligand-binding or functional properties. For the characterization of the structure and dynamics in proteins by NMR, it is necessary that the homogeneity of the protein sample needs to be tested. This can be done by using Size Exclusion Chromatography (SEC) coupled with Multi-Angle Light Scattering (MALS) detection[1]. This technique has been used to determine the absolute molecular mass of the molecules – monomers as well as oligomers or aggregates – in the solution[2,3].
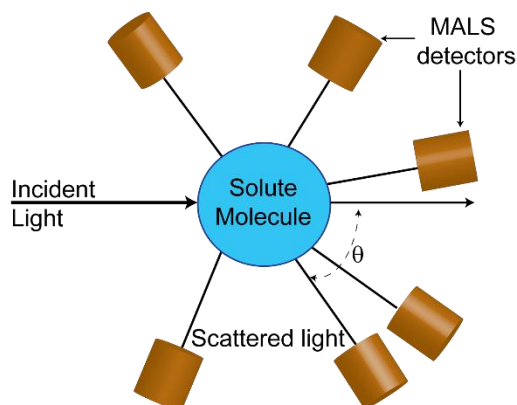
Figure 2.1: Light scattered by the solute is detected by MALS detector at various angles

During SEC-MALS analysis of a protein solution, the species in the solution are first separated based on their molecular size by SEC. Size-separated molecules in the sample enter into inline three detector system UV, differential refractive index (dRI), and MALS[3,4]. The UV and dRI detectors help to measure the concentration of the protein by measuring the absorbance at 280 nm and by recording the change in the refractive index that occurs due to the differences in solute concentration, respectively. Since the determination of concentration by UV depends on the calculation of the theoretical extinction

coefficient, which can get affected by the tertiary structure of the molecule, dRI detectors become a preferred choice. dRI is a universal detector that measures concentration of biological samples based on the change in the refractive index of the solution. The MALS detector measures the intensity of light scattered at different angles (as shown in Figure 2.1). This intensity changes due to scattering with respect to the intensity of the incident light, called as Rayleigh Ratio ($R(\theta)$) at scattering angle θ, is used to calculate the molecular mass by using Equation 2.1 and 2.2[4–6]:

$$M = \frac{R(0)}{Kc\left(\frac{dn}{dc}\right)^2} \tag{2.1}$$

$$K = \frac{4\pi^2 n^2}{\lambda_0^4 N_A}\left(\frac{dn}{dc}\right)^2 \tag{2.2}$$

where, M is the molecular mass of the solute, $R(0)$ is the relay ratio at scattering angle of zero obtained from the $R(\theta)$ determined by MALS detector, K is the system constant, c is the concentration determined by UV or dRI detector and (dn/dc) is the refractive index increment in the solution due to solute, n is the solvent refractive index and λ_0 is the vacuum wavelength of the incident light, N_A is the Avogadro's Number. Thus, MALS provides a direct readout of the molecular weight of each species separated by the SEC, without any need of a reference material or calibration curve. Additionally, MALS detection provides information about the radius of gyration of the molecule and thus can support to interpret about the size and shape of the molecule in the solution. Since dsRBDs have been reported to form oligomers[7–10], SEC-MALS measurements will serve as a basis for the detection of the oligomeric species of dsRBDs, if any, present in the solution. Though the technique is very useful in identifying the soluble oligomers in the sample, it has a few disadvantages[11]: (1) The SEC technique separates molecules based on their size, thus different molecules of same size cannot be distinguished; (2) MALS detector requires long equilibration time as particles from SEC columns can interfere in the light scattering signal of the detector; (3) the injection volume of the sample also influences the separation ability of SEC columns and thus high concentrations are required from small sized proteins relative to the larger proteins; (4) SEC-MALS analysis can be applied to a suitably resolved peaks only, which depends on the resolution of the SEC columns – the oligomers that are exceed the column resolution range might elute during void volume and cannot be characterized ; (5) the oligomeric species being larger in size have higher light scattering and thus can create errors in the calculated mass of that species.

2.3.   *Circular Dichroism*

Circular Dichroism (CD) is a type of absorption spectroscopy that relies on the difference in the absorption of the left (A_L) and right (A_R) circularly polarized light by the molecule with chiral center or placed in a chiral environment. When there is differential absorption of the left and/or right circularly polarized light, it results in an elliptically polarized light (Figure 2.2(A)). This differential absorption is referred to as Circular Dichroism (CD)[12]. The CD signal is expressed as the difference in these

absorption signals ($\Delta A = A_L - A_R$) or in terms of ellipticity ($\theta = \tan^{-1}(b/a)$) where b and a indicate the minor and major axis of the ellipse (Figure 2.2(A)). Proteins contain many chiral centers and chromophores and thus they show differential absorption of the circularly polarized light resulting in the CD signal[13]. The far-UV CD spectrum in between 190-250 nm, which originates because of the differential absorption by the peptide bond, is used for the analysis of the secondary structure content[13–15]. The signature peaks for (1) an α-helical structure are observed as a strong maximum near 190 nm and double minima at 208 nm and 222 nm; (2) the β-sheet as a maximum near 195 nm and a minimum near 217 nm; and (3) random coil as a minimum near 200 nm. Typical spectra representing the secondary structural features of the proteins have been illustrated in Figure 2.2(B)[16]. The CD spectrum in the near UV region from 250-350 nm originates from the sidechains of the aromatic residues like tryptophan, tyrosine, phenyl-alanine, and from disulfide bonds and thus signal in this region reflects the tertiary structural features of the protein[13]. Any change in the conformation of protein either due to unfolding, ligand binding, or pH change, etc., be it in the tertiary structure or in the secondary structure, is reflected by the changes in the CD spectrum of the protein in the respective wavelength range.
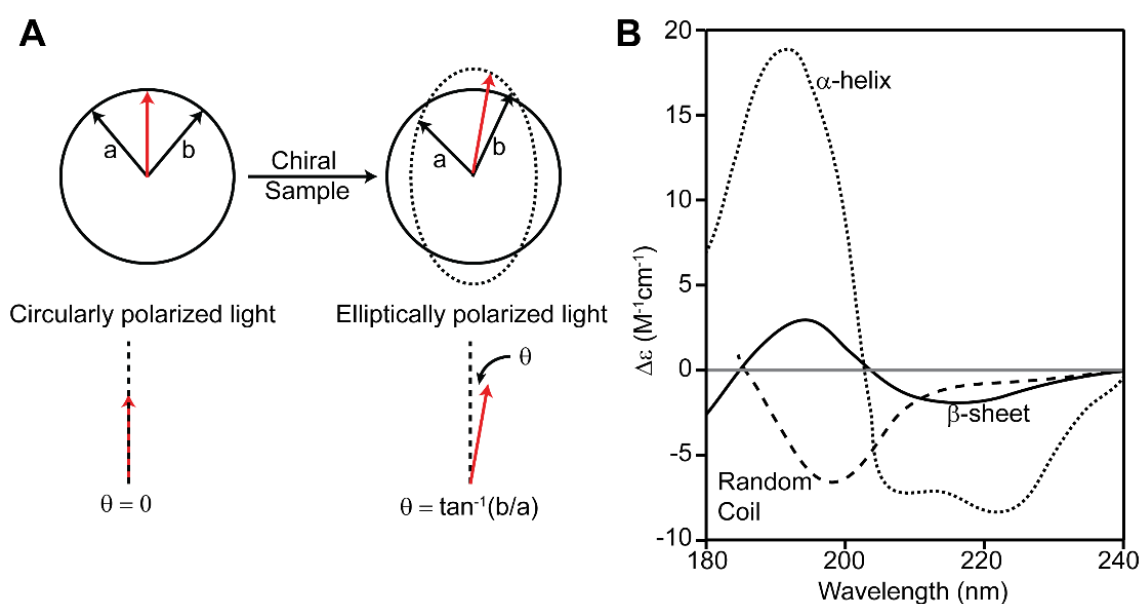
Figure 2.2: (**A**) Origin of CD signal: a and b are the components of left and right circularly polarized light. The resultant of the two components is shown by red arrow which makes an angle θ which is recorded as CD signal (Adapted from Kelly and Pric. *Current Protein and Peptide Science,* 2000, Vol. 1, No. 4). (**B**) Typical CD spectra of the secondary structures in the proteins α-helix (dotted line), β-sheet (dashed line), and random coil (solid line) (Adapted from Ruggeri et al. *Current Pharmaceutical Design,* 2016, Vol. 22, No. 26).

Far-UV CD spectroscopy is commonly used to monitor the thermal stability of a protein by measuring CD signal as a function of temperature. For example, the unfolding of the protein from a well-defined structural fold to a random coil leads to a change in the CD signal. As a simple case, the transition can be assumed to be between a folded (*f*) and an unfolded state (*u*). During the transition, fraction folded (α) at each temperature can be calculated as in Equation 2.3:

$$\alpha = \frac{S_{obs} - S_U}{S_F - S_U} \qquad\qquad (2.3)$$

where, S_{obs}, S_F and S_{UF} are the CD signal at a fixed wavelength at observed temperature, for completely folded protein and for completely unfolded protein, respectively.

If the unfolding is reversible, then the thermodynamics of the unfolding event can be calculated by using the Gibbs-Helmholtz equation (Equation 2.4-2.6):

$$\Delta G = \Delta H(1 - T/T_M) - \Delta C_P((1 - T/T_M) + Tln(T/T_M) \qquad\qquad (2.4)$$

$$K = exp(-\Delta G/RT) \qquad\qquad (2.5)$$

$$\alpha = K/(1 + K) \qquad\qquad (2.6)$$

where ΔG is the free energy (cal.mol^{-1}) of the unfolding at temperature T (Kelvin), ΔH is the change in enthalpy during unfolding (cal.mol^{-1}), ΔCp is the heat capacity at constant pressure (cal.K^{-1}.mol^{-1}), T_M is the melting temperature (Kelvin), K is the equilibrium constant of folding at temperature T and R is the gas constant (1.98 cal.K^{-1}.mol^{-1}). Even if the unfolding is irreversible, the CD signal as a function of temperature can give information about the thermal stability of the protein. The T_M and/or the slope of the transition helps to have insights into the relative stability when, for example, mutations are carried out in the protein. In the current study, CD spectroscopy has been used as a tool for identification of the thermal stability of the dsRBDs and has been helpful in providing an overview of the conformational entropy the dsRBDs may have to interact with target dsRNAs.

2.4. *Isothermal Titration calorimetry*

Isothermal titration calorimetry (ITC) is a powerful technique used to study the thermodynamics of interaction of biomolecules like protein, nucleic acids among each other and with the small molecules like drugs[17–19]. Any binding interaction between two molecules is associated with a net change in the total energy of the system as absorption (endothermic processes) or release (exothermic processes) of heat with the surroundings. For protein-RNA interaction studies, other techniques like Spectroscopy or Surface Plasmon Resonance (SPR) can also be used to determine the thermodynamics of the interactions; however, ITC is unique as it provides direct measure of heat change during binding[20]. In addition, ITC is a sensitive and non-destructive technique and does not require any modification or immobilization of the samples[17].

In ITC experiments, titrations are carried out by gradually adding one binding partner (or ligand) from a syringe in to the sample cell containing a solution of the other binding partner, and the heat change is measured as the amount of external energy required to maintain the sample and the reference cell at a fixed temperature. This change is monitored until all of the binding partner is saturated and a constant change resulting from the dilution of the ligand is observed and is plotted as a function of time. The area under the curve for each of the peaks represents the heat change associated

with the binding interaction upon addition of the ligand and is proportional to the enthalpy of the interaction. The resultant plot is an isotherm of the enthalpy of interaction against the molar ratio of the two binding partners[18,21] (Figure 2.3).
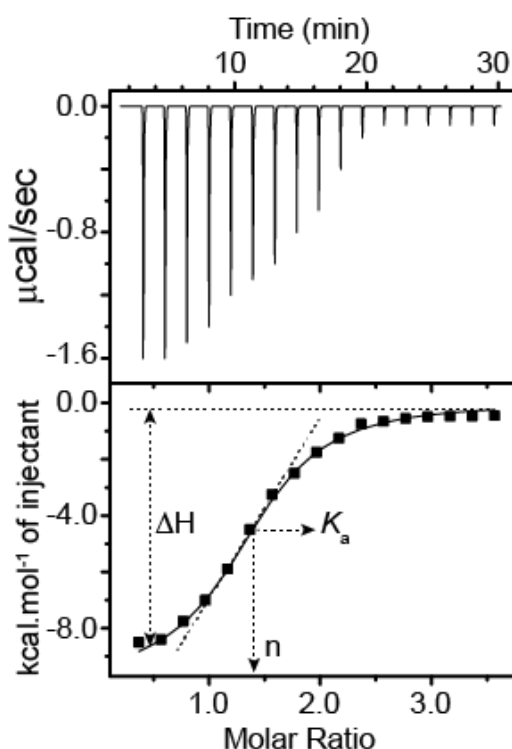
Figure 2.3: Typical ITC titration profile. The upper panel is the plot of energy required to maintain sample and reference cells at the same temperature after each addition of ligand. The lower panel depicts the heat of binding calculated by peak integration from the upper panel plotted against molar ratio of the two binding partners.

The fitting of the isotherm to various binding models[22,23] allows estimation of the binding stoichiometry – n as the inflection point; association constant – K_a as the slope of the curve; and binding enthalpy – ΔH as the amplitude of heat change, respectively. Since the titrations are carried out isothermally, the free energy change associated with the binding can be calculated from the association constant. The free energy of binding along with the enthalpy change determined from the titration serves as a measure to calculate the entropy change. The association constant and the free energy change of binding indicates the affinity of the ligand to its binding partner, while the enthalpy and entropy contribution of each process represents the physical process involved in binding like conformational change, hydrogen bonding or van der Waal interactions etc[17]. The enthalpy-entropy contribution also suggests the probable mechanism of the binding of the two molecules[20]. Though the technique has wide applicability, it requires that the titrant and the titrate must be in the same buffer. Also, as the heat evolved in a titration depends on the concentration of the interacting species, this may require large amount of sample for the optimization of the titration in the range to get the isotherm that can correctly define the mechanism of binding between the interacting molecules. In the current study, the ITC titrations of dsRBDs with dsRNAs have been performed to explore the mechanism of interactions at the thermodynamic level.

2.5. *NMR Spectroscopy*

Nuclear Magnetic Resonance (NMR) spectroscopy is a well-known biophysical technique used to explore the structure and dynamics in biomolecules at the atomic level. Though the structure of proteins can give information on their function, proteins have intrinsic flexibility at multiple timescales, which might also serve as a critical factor for their functions. Nevertheless, the structure of the protein can be determined by biophysical techniques like X-ray Crystallography or Cryo-Electron-Microscopy; NMR spectroscopy has an advantage that it can also give information about the dynamics in proteins. NMR is unique in quantifying protein dynamics as: (1) it can quantify motions occurring at picoseconds to seconds or slower; (2) it can probe dynamics using various NMR active nuclei simultaneously without the need of any external probe; and (3) the dynamics can be quantified in equilibrium conditions without any perturbations required. In order to study the structure or dynamics in proteins by NMR, it is labeled with ^{15}N and/or ^{13}C NMR active nuclei mostly by using recombinant DNA technology. This labeling scheme provides uniformly labeled protein when overexpressed in a suitable expression system – bacterial system being most commonly used – by using ^{13}C-D(+)-glucose as a sole source of carbon and/or ^{15}N-ammonium chloride as a sole source of nitrogen in the bacterial growth medium. The overexpressed protein is then purified in the desired state using various chemical and/or chromatographic methods.
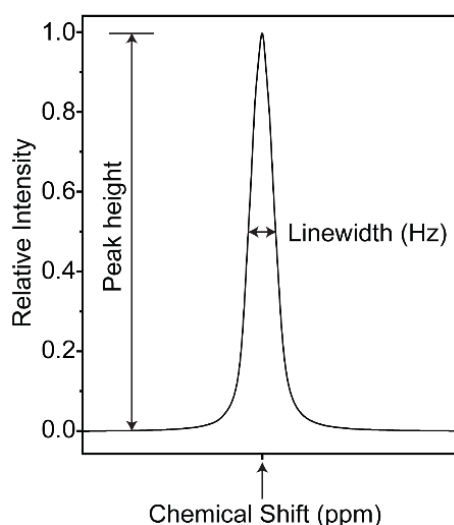
Figure 2.4: Primary NMR observables: (1) Chemical shift which reports on the local chemical environment, (2) Linewidth measured at peak width measured at half height reports on local dynamics, and (3) Intensity, measured as peak height or volume reports on the population of the spins in the local environment defined by chemical shift.

The structural and dynamics information of a nucleus under investigation by NMR is contained in the form of three fundamental observables[24,25]: (1) chemical shift (or frequency), (2) linewidth and (3) intensity of the NMR signal (Figure 2.4). The chemical shift, δ, of an NMR peak depends on the local chemical environment of the nucleus in the molecule under study. The linewidth, λ, is determined as width of the peak at half height and depends on the relaxation profile of the nuclear spin and informs about the dynamic properties of the nucleus in the solution. The intensity, I, of the peak is expressed in

terms of peak height, integral, or volume and reports on the number of spins in the local chemical environment defined by the chemical shift of the peak.

2.5.1. Resonance Assignment and structure calculations

In order to determine the structure or to characterize the dynamics in proteins, a preliminary requirement is to have the resonance assignment, that is to identify which NMR peak corresponds to which atom in the protein chain. These resonance frequencies, expressed in terms of chemical shift in NMR, contain information of the local chemical environment of the nucleus. Coupling interactions between the NMR active nuclei present in the ^{15}N and/or ^{15}N-^{13}C labeled protein chain are used to assign the chemical shifts of each nucleus. The chemical shift information that can be collected from NMR experiments is divided in two sets – backbone resonances (that include chemical shifts of H^N, N, H_α, C_α, C′) and side-chain resonances (for example, chemical shifts of C_β, H_β, C_γ, H_γ, etc)[26,27]. Generally, backbone resonances are sufficient to assign the resonances in the HSQC spectrum to the amino acids in the protein chain. However, determination of type of amino acid may require information of some of the side-chain nuclei. It is also shown that backbone chemical shifts can also suffice to calculate the structure of the protein[28,29]. The resonance assignment for protein starts with the recording of the ^{1}H-^{15}N heteronuclear single quantum correlation (HSQC) spectrum which is a map of all the backbone amide resonances. This spectrum contains peaks (in the form of contours) corresponding to every amide N-H in the protein chain. For example, if there are 100 non-proline amino acids – as N involved in the peptide bond of proline lacks a H^N – in the protein, then we can expect 100 peaks in the HSQC spectrum. In addition, the side-chain -NH_2 of amino acids (Asn, Gln, Arg, Lys) also show peaks in the HSQC spectrum and can be easily identified as they appear as doublets with two ^{1}H-chemical shifts for a single ^{15}N-chemical shift. Just having an HSQC spectrum with these peaks does not provide information on which peak represents which amino acid, and it is necessary to collect additional resonance information. For the backbone resonance assignment, a set of triple resonance experiments which include, CBCANH, CBCA(CO)NH, HNCA, HN(CO)CA, HNCO, and HN(CA)CO can be recorded[26,27,30,31]. These experiments give information on chemical shift(s) of the additional nucleus (nuclei) in the protein in additional dimension – mostly carbon in case of triple resonance experiments – coupled to backbone N-H of the amino acid represented by a peak in the ^{1}H-^{15}N HSQC. These experiments allow transfer of magnetization from one nuclear spin to another via through-bond (scalar) coupling interactions between the NMR active nuclei in the amino acid chain. The nuclei in the amino acids that are detected via these coupling interactions are shown in Figure 2.5(A). For example, in case of CBCANH experiment, we get correlations between C_α, C_β, N^H, and H^N. In CBCANH experiment, every peak in the ^{1}H-^{15}N-HSQC spectrum can be correlated to four additional peaks in the ^{13}C-dimension – two from self $C_{\alpha,i}$ and $C_{\beta,i}$ and two from previous $C_{\alpha,i-1}$ and $C_{\beta,i-1}$ (Figure 2.5(B)) and has been represented as strips as shown in Figure 2.5(D). This experiment is complemented by another experiment CBCA(CO)NH where peaks only from the previous residue i.e. $C_{\alpha,i-1}$ and $C_{\beta,i-1}$ are observed (Figure 2.5(C)), thus allowing distinction

between the two sets of peaks in the CBCANH spectrum. The distinction between C_α and C_β can be done based on the phase of the peak as they appear in opposite phases in the spectrum. In addition, the self-peaks appear more intense than the peaks for the previous residue as one bond intra-residue coupling ($N-C_\alpha$) is stronger than the two bond inter-residue coupling ($N-C'-C_\alpha$). By aligning the C_α and C_β peaks in ^{13}C-dimension of CBCANH, after identifying the self and the previous peaks, it is possible to get the sequential connections between the peaks to assign resonances in the HSQC spectrum. An example of the sequential connectivities in the CBCANH spectrum is shown in Figure 2.5(d).
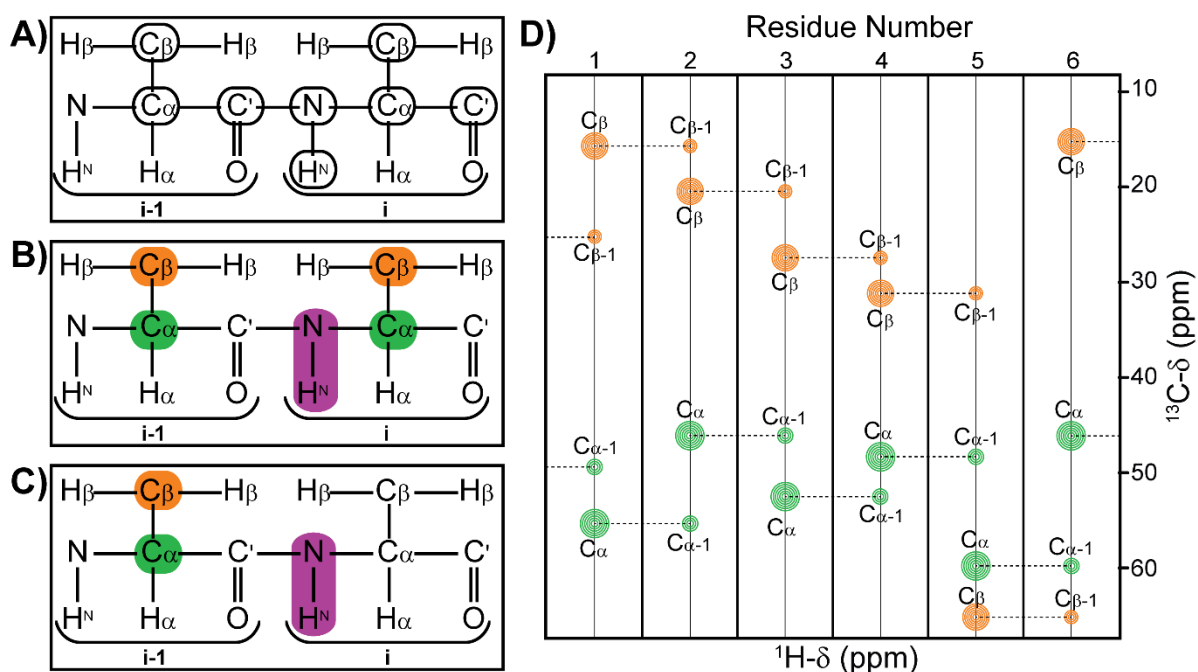
Figure 2.5: Resonance assignment in proteins. (**A**) Nuclei in the amino-acid chain coupled through scalar coupling used for getting sequential connectivities in various triple resonance experiments. Connectivities observed have been marked in colour in (**B**) a CBCANH spectrum and (**C**) a CBCA(CO)NH experiment. Atoms for which peaks are observed in the ^1H-^{15}N HSQC are marked in purple and carbon (^{13}C) atoms that are correlated to the NH peak are represented by green box for C_α and orange for C_β. (**D**) A representation of the correlations observed in the CBCANH experiments allowing sequential walk along the protein chain. Colours represent C_α and C_β as marked in the spectral connectivities of CBCANH experiment (Figure(**B**)). Bigger circles represent higher intensity of peaks due to stronger one-bond coupling between N_i and $C\alpha_i$ and smaller circles represent lower intensity peaks due to weaker two-bond coupling between N_i and $C\alpha_{i-1}$ in the CBCANH spectrum.

Table 2.1: Correlations observed in ^{13}C-dimension for every NH peak in HSQC in triple resonance experiments.

Experiment	Peaks in ^{13}C-Dimension
HNCA	$C\alpha_i$, $C\alpha_{i-1}$
HN(CO)CA	$C\alpha_{i-1}$
CBCANH	$C\alpha_i$, $C\alpha_{i-1}$, $C\beta_i$, $C\beta_{i-1}$
CBCA(CO)NH	$C\alpha_{i-1}$, $C\beta_{i-1}$
HNCO	C'_{i-1}
HN(CA)CO	C'_i, C'_{i-1}

All triple resonance experiments show peaks corresponding to a different set of carbons in ^{13}C-dimension for every peak in the ^{1}H-^{15}N-correlation plane. The correlations observed ^{13}C-dimension in various experiments have been listed in Table 2.1.

The ^{1}H-^{15}N-TOCSY-HSQC experiment, recorded on a ^{15}N labeled sample, is used to identify the type of the residue. TOCSY experiment gives a correlation among the protons of the same spin system or amino acid. Since every residue in the protein chain represents a spin system, it shows a typical pattern of TOCSY correlation representative of the type of the amino acid. In the ^{1}H-^{15}N-TOCSY-HSQC experiment, every peak in the HSQC or the amide resonance is correlated to the spin system of the residue it represents. Since all the amino acids have a defined pattern of these TOCSY correlations, it helps to identify which type of amino acid is represented by the HSQC peak. Thus, having information from these triple resonance experiments and the ^{1}H-^{15}N-TOCSY-HSQC can help to identify and confirm the assignment for each peak in the ^{1}H-^{15}N-HSQC. These methods are widely applicable to the structural analysis of the proteins of ~20 kDa in size; proteins with higher molecular mass may require deuteration of the protein during synthesis or use of modified techniques like TROSY based experiments for the resonance assignments[26,32].

The chemical shifts obtained from the NMR analysis are highly sensitive to the local environment of each spin and can aid in extracting information about secondary structure and hydrogen bonding interactions between different residues. Shen *et al.* have reported a robust protocol in the Chemical shift (CS)-Rosetta program to generate the protein structure from the incomplete resonance assignment[28,29,33–35]. The program is available at the Biological Magnetic Resonance Bank at https://csrosetta.bmrb.wisc.edu/csrosetta/submit. The protocol uses chemical shifts at two stages for model generation: (1) fragment selection with sequence similarity and the structural data deposited in the Protein Data Bank; and (2) re-scoring of the all-atom models generated by fragment assembly with energy minimization by *ab initio* protein structure prediction by Rosetta method. It has been shown that this protocol is sufficient to generate structural models comparable with the models generated from the all-atom resonance assignments along with the distance restrains[29,34]. The calculated structures from CS-Rosetta can then be validated at a range of available programs like MOLPROBITY[36] (http://molprobity.biochem.duke.edu/), Protein Structure Validation Software (PSVS) suite[37] (http://psvs.nesg.org/), ProCheck[38] (https://www.ebi.ac.uk/thornton-srv/software/PROCHECK/), etc.

2.5.2. *Protein dynamics*

Dynamics in proteins leads to spatial and/or temporal changes in the local/global changes in the protein structure. Thus, the native structure of the protein may not correctly represent its active conformation that is responsible for its function. These changes, reflected by the flexibility at atomic level at multiple timescales, are important to understand its functions. Most experiments used to study

the dynamics in proteins by NMR spectroscopy are based on the relaxation behavior of the nuclear spins of NMR active nuclei like ^{15}N, ^{13}C, and ^{1}H/ ^{2}H. While ^{15}N-relaxation-based experiments are widely used to study backbone dynamics in proteins, the ^{13}C and ^{2}H relaxation experiments are important probes for characterization of the side-chain dynamics. The different dynamic processes in proteins occur at different timescales and they can be probed by a vast variety of NMR experiments[24,39–43]. Each of the experiments is able to detect dynamics occurring in different timescale window (Figure 2.6). The most commonly studied dynamic timescale in proteins involve ps-ns timescale and μs-ms timescale because of their sensitivity towards functionally relevant processes. The local motions in the proteins like bond vibration, side-chain rotation, as well as loop motions or molecular tumbling are characterized by ps-ns timescale dynamics while the μs-ms timescale dynamics represent slower motions responsible for conformational changes resulting from ligand binding or release, catalytic or allosteric interactions, protein folding, etc. The dynamics information at ps-ns and μs-ms timescales are obtained by nuclear spin relaxation, relaxation dispersion methods, residual dipolar couplings, etc. We have used nuclear spin relaxation and relaxation dispersion methods to probe the dynamics and these two methods are discussed in more detail below.
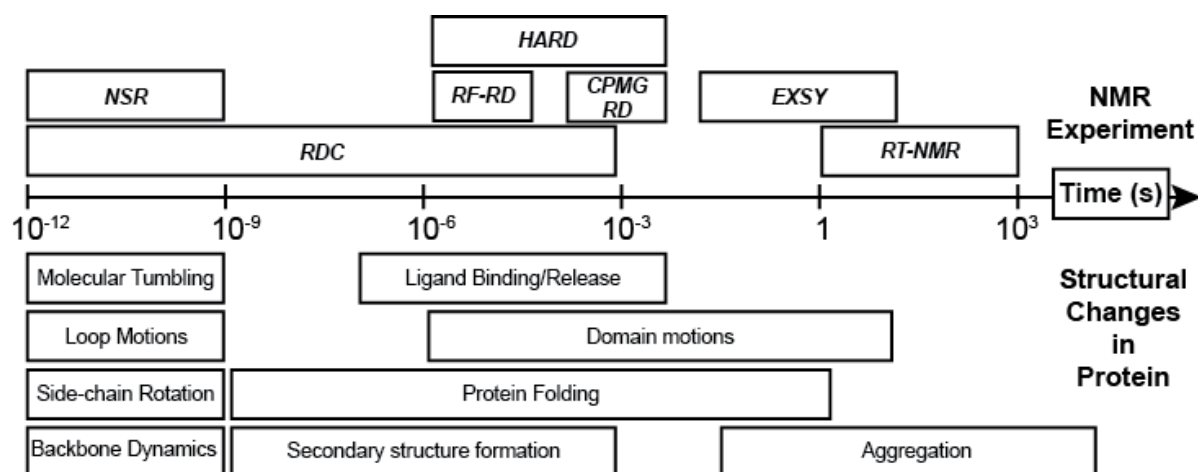
Figure 2.6: Range of NMR experiments that probe dynamics in proteins responsible for various structural changes occurring at different timescales. These include (1) Nuclear Spin Relaxation (NSR), (2) Residual Dipolar Coupling (RDC), (3) Heteronuclear Adiabatic Relaxation Dispersion (HARD), (4) Rotating Frame Relaxation Dispersion (RF-RD), (5) Carr-Purcell-Meiboom-Gill Relaxation Dispersion (CPMG RD), (6) Exchange Spectroscopy (EXSY), (7) Real Time NMR (RT-NMR).

2.5.2.1. ps-ns dynamics in proteins revealed by Nuclear Spin Relaxation method

Picosecond to nanosecond timescale motions involve bond vibration, loop motion, side-chain rotation, molecular tumbling etc[42,44–47]. The nuclear spins excited by application of the radio frequency pulses relax to the equilibrium state by three principle mechanisms that are linked to ps-ns motions: (1) Chemical shift anisotropy (CSA), (2) Dipolar Coupling, and (3) Quadrupolar interactions[24,26]. These motions can be characterized by using nuclear spin relaxation experiments that measure site-specific parameters: (1) Longitudinal relaxation rates, R_1, (2) Transverse relaxation rates R_2, and (3)

heteronuclear nuclear overhauser effects (*het*NOE). Longitudinal relaxation (R_1) refers to the process where excited spins relax to thermal equilibrium by transferring their energy to the environment. It is determined by the inversion recovery experiment where the magnetization is first inverted and then allowed to relax for a defined delay period followed by detection in the transverse plane. The rate of decay of the signal indicates the R_1 relaxation rate. Transverse relaxation rates (R_2) dictate the irreversible loss of coherence in the transverse plane in the ensemble of spins. These R_2 rates are determined by flipping the magnetization to transverse plane and then allowing to diffuse for variable delay period followed by detection. *het*NOE measures the perturbations in through-space magnetization transfer between different types of nuclei (typically a ^{1}H and a ^{15}N or ^{13}C) coupled via dipolar interactions. It is calculated as a ratio of the signal intensity with and without saturation of the magnetization transfer between the two coupled nuclei. Though these parameters can be determined directly, they provide limited information for dynamics characterization. Typically, a plot of these values along the protein chain helps to identify the residues or regions of inconsistent dynamic behavior. If the protein is internally rigid and tumbles isotropically, then these parameters have parallel values for each residue and the residues with inconsistent dynamics deviate from the average values of these parameters. These relaxation parameters are a function of rotational correlation time (τ_c) and frequency of motions (ω) and can vary (as shown in Figure 2.7)[48,49].
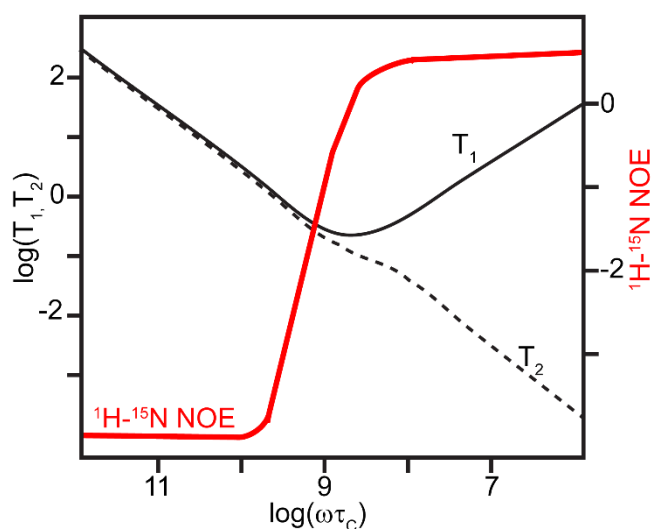
Figure 2.7: Plot of log(T_1, T_2) and ^{1}H-^{15}N NOE against log($\omega\tau_C$) for ^{15}N-nuclear spin relaxation (Adapted from Lewis E. Kay, Dennis A. Torchia, and Ad Bax, *Biochemistry,* Vol. 28, No. 23, 1989)

The quantification of the ps-ns timescale motions from these observables is achieved by using a time-dependent rotational correlation function C(t), or a spectral-density function J(ω), for each bond vector. The correlation function describes the probability that a bond-vector is found in an orientation relative to the permanent magnetic field at time t=0 and a later time t. The actual form of the correlation function depends on the nature of the molecular motions involved. For example, in a simple case of random isotropic rotations of a molecule without internal motion, the correlation function follows

exponential decay C(t) = exp(t/τ_m), where τ_m is the molecular rotational time. Fourier transform of the correlation function is the spectral density function J(ω) that remodels this information in terms of probabilities of motions at a frequency ω. The relation between the spectral density function J(ω) and the measured site-specific relaxation parameters (R_1, R_2, and *het*NOE) are given by equations (2.7-2.9)[50]:

$$R_1(X) = \frac{d^2}{4} [J(\omega_H - \omega_X) + 3J(\omega_X) + 6J(\omega_H + \omega_X)] + c^2 J(\omega_X) \qquad (2.7)$$

$$R_2(X) = \frac{d^2}{8} [4J(0) + J(\omega_H - \omega_X) + 3J(\omega_X) + 6J(\omega_H) + 6J(\omega_H + \omega_X)] + \frac{c^2}{6} [4J(0) + 3J(\omega_X)] + R_{ex} \qquad (2.8)$$

$$het\text{NOE} = 1 + \frac{d^2}{4R_1} \frac{\gamma_H}{\gamma_X} [6J(\omega_H + \omega_X) - J(\omega_H - \omega_X)] \qquad (2.9)$$

where X = ^{13}C or ^{15}N nucleus attached to a ^{1}H nucleus, ω_x is the Larmor frequency of the nucleus X, d = ($\mu_0 h \gamma_H \gamma_X / 8\pi^2$)($r_{HX}^{-3}$) is the dipolar interaction between H and X directly attached with the distance between them r_{HX}, μ_0 is the permeability of free space, h is the Planck's constant, γ_H and γ_X are the gyromagnetic ratio for H and X, c = ($\Delta\sigma_X/\sqrt{3}$) with $\Delta\sigma_X$ is the CSA of the X nucleus.

The term R_{ex} in equation 2.8 describes the contribution of the chemical exchange to the R_2 rate. As it can be noted that each of the relaxation parameters (R_1, R_2, and *het*NOE) are functions of multiple frequencies ω of motion as well as J(0) which depends on the inhomogeneity in the static magnetic field. Simultaneous fitting of the observed relaxation rates (R_1 and R_2) and the *het*NOE values to these equations allows to determine the spectral density at the respective motional frequencies. To improve accuracy in the extracted fitting parameters, the data is collected at multiple magnetic fields. The spectral density approach[51] to describe the ps-ns motions in proteins – a technique pioneered by Peng and Wagner – allows to extract site-specific information about the motions at a range of frequencies. However, the approach has no assumption to assess the global motions in the proteins. Also, this approach does not provide information about the amplitude of motions. Though spectral densities provide limited information about the ps-ns motions, they can be translated to model-free parameters described by the Lipari-Szabo model-free approach[52–54].

The model-free approach assumes that the internal motions of the residues are independent and faster than the global motions of the protein. As the name suggests, the approach assumes no structural model to describe the motion. It describes motions using four distinct types of parameters[24,26,43,47]: (1) rotational diffusion tensor *D*, which is a combination of three terms D_{xx}, D_{yy}, and D_{zz} which represent the rate of molecular rotation about x-, y-, and z-axis, respectively. This is also defined in terms of rotational correlation time (τ_c); (2) the effective correlation time (τ_e) for every N-H bond vector that represents timescale of motion of a N-H bond vector; (3) site-specific order parameter (S^2) which is a measure of the amplitude of motion of the N-H bond vector; and (4) an R_{ex} value that is the indicator of the chemical exchange broadening which contributes to R_2 rates due to µs-ms timescale motions. The

approach was further extended by Clore *et al.* for interpretation of more complex dynamics with motions on two independent internal timescales[55]: (1) at faster ps timescale defined by S^2_f (amplitude of motion) and τ_f (timescale of motion) and (2) slower motions at ns timescale but faster than the global tumbling of the molecule defined by S^2_s (amplitude of motion) and τ_s (timescale of motion).

The order parameter (S^2) brings in the most from the model-free analysis. It represents the amplitude of motion of the N-H bond vector in a cone with semi-angle θ, such that $S^2 = [(1/2)\,(\cos θ)\,(1+\cos θ)]^2$. The larger the cone angle represents higher flexibility with S^2 value close to 0. The rigid residues show motions within smaller cone and have S^2 values close to 1. Empirically, the value of S^2 calculated from ^{15}N-relaxation experiments for a residue in the structured region are more than 0.8 while for loops and turns they range from 0.5 to 0.8[24], however, with increased flexibility the values close to 0 can be observed. A plot of S^2 against residue number helps to identify the deviation in the S^2 value from the average that represents the residue having higher flexibility at ps-ns timescale than the rest of the structured areas of the protein. Further changes in the S^2 upon ligand binding or changes in the environmental conditions is an indicator of the conformational plasticity of the molecule. Other model-free parameters also deliver valuable information about the ps-ns timescale motion. The correlation times (τ_e, τ_f, τ_s) directly give the timescale of the motions for every nuclear spin studied, while the D value is an indicator of hydrodynamic properties of the molecule suggestive of the overall shape of the molecule. The R_{ex} value represents the contribution of the µs-ms timescale dynamics in the detected spin relaxation parameters. These motions can be studied in more detail by the relaxation dispersion experiments. In the current study, the nuclear spin relaxation experiments of the dsRBDs allow to study the local motions at ps-ns dynamics that give information on the conformational entropy of the dsRBDs. Further, it will also give insights into the effect of dsRNAs of different shapes on the internal flexibility of the dsRBDs. Though the model-free approach is a method of choice, the method is applicable only when the protein structure is predetermined. For a multi-domain protein, the approach may not be applicable to all residues, as all of them may not be represented by the same global diffusion model and may have different dynamics based on the physiochemical phenomenon they are involved in.

2.5.2.2. µs-ms dynamics in proteins revealed by Relaxation Dispersion method

µs-ms timescale motions result from the dynamical fluctuations in the residue(s) in the protein or segment(s) of a protein that leads to changes in the conformation. These conformational changes may result from protein folding-unfolding events, ligand binding or release processes, domain motions, etc[39,56–58]. These dynamic processes are commonly defined as chemical exchange[39,59] of the spin between at least two distinct states, A and B with resonance frequency of the two states being ω_A and ω_B, respectively; with k_1 as the forward rate constant for A to B conversion and k_{-1} as the reverse rate constant (Figure 2.8). The intensity of the two peaks representing the two states is proportional to the population of the two states (p_A and p_B) and the exchange rates between the two states. Thus, the

chemical exchange process between these states directly remodels the fundamental observables in NMR. The appearance of the peak pattern depends on the relative magnitude of the exchange rate defined as $k_{ex} = k_1 + k_{-1}$ and the resonance frequency difference between the two states $\Delta\omega = |\omega_A - \omega_B|$ as shown in Figure 2.8.
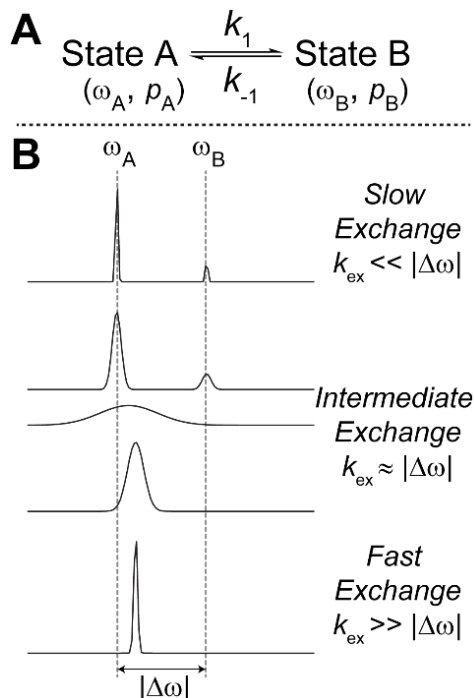
Figure 2.8: Effect of chemical exchange on primary NMR observables. (**A**) Description of the Chemical exchange process between two states, A and B, can be given by the forward and reverse rate constants, k_1 and k_{-1}, and resonance frequency (indicated by chemical shift in NMR) of two states and the population of the two states. (**B**) The pattern of the peak depends on the relative magnitude of the $k_{ex} = k_1 + k_{-1}$ and the $\Delta\omega$ and are categorized in three exchange timescale regimes. The peaks are simulated assuming that the $p_A = 80\%$ and $p_B = 20\%$.

When in the slow exchange regime ($k_{ex} < |\Delta\omega|$), the two states can be distinguished and two separate signals can be obtained and thus two states can be directly characterized from fundamental NMR observables. However, when the exchange is in the intermediate or fast exchange regime ($k_{ex} \geq |\Delta\omega|$), the NMR peak observed is a population-averaged signal from the two states. Dynamics in this time frame are characterized in terms of the exchange contribution, R_{ex}, to the transverse relaxation rate – as detected in model-free analysis – as:

$$R_{2,eff} = R_2^0 + R_{ex} \tag{2.10}$$

where, $R_{2,eff}$ and R_2^0 represent the effective and the intrinsic transverse relaxation rates, respectively for the observed spin. Two commonly used approaches for characterization of these dynamics include Carr-Purcell-Maiboom-Gill (CPMG) relaxation dispersion technique and Rotating frame relaxation dispersion that monitors motions mainly on slower ms timescale and faster µs timescale, respectively. Both the relaxation dispersion methods allow suppression of the exchange term creating a dispersion in the measured R_2 values that help to characterize the exchange process by extracting the population of

the two states (p_A and p_B) and the difference in the two chemical shifts ($\Delta\omega$) along with the exchange rate k_{ex}.

Constant time CPMG (Carr-Purcell-Maiboom-Gill) relaxation dispersion experiment[60] is the most often used experiment for characterization of slow dynamics in slow ms regime. The experiment is simply based on the concept that dephasing of the spins can be refocused by using a Spin-Echo scheme (τ - 180° - τ). In absence of any exchange, if spins exist in two distinct states, their evolution results in two distinct peaks at their respective chemical shifts. However, if the spins are in the chemical exchange between two states during chemical shift evolution, the exchange between the states leads to dephasing of the signal and thus results in line broadening. The Spin-Echo block helps to refocus the magnetization during evolution. As the frequency of the application of 180° pulses – CPMG frequency ($\nu_{CPMG} = 1/4\tau$) – is increased compared to k_{ex}, it results in better refocusing of the magnetization. Thus, it suppresses the dephasing/exchange between the two states. The change in the line broadening is detected by calculating effective transverse relaxation. In CPMG relaxation dispersion experiment, series of HSQC spectra are recorded with an increasing number of spin-echo blocks applied during fixed relaxation time (T_{relax}) – thus increasing the frequency of CPMG blocks applied – and the effective relaxation rates can be determined by equation 2.11:

$$R_{2eff\,(\nu_{CPMG})} = -\frac{1}{T_{relax}} \ln\left(\frac{I_{\nu,CPMG}}{I_0}\right) \tag{2.11}$$

where I_0 indicates the intensity of the peak in the absence of CPMG block applied and $I\nu_{CPMG}$ indicates the intensity of the peak in the presence of CPMG block with frequency applied. The relation between the amount of refocusing defined by the effective relaxation rate ($R_{2,eff}$) and the CPMG frequency (ν_{CPMG}) allows to extract the dynamics parameters describing exchange event[40,58,61–64]. For a two-site exchange process in fast exchange limit ($k_{ex} \gg |\Delta\omega|$), the relation between $R_{2,eff}$ and ν_{CPMG} is commonly defined by Carver-Richards equation[61] as:

$$R_{2eff} = R_2 + \left(\frac{\varphi_{ex}}{k_{ex}}\right)\left(1 - \frac{4\nu_{CPMG}}{k_{ex}} \tanh\left\{\frac{k_{ex}}{4\nu_{CPMG}}\right\}\right) \tag{2.12}$$

where, R_2 is the intrinsic relaxation rate of each proton, $\varphi_{ex} = p_A p_B \Delta\omega^2$ is the exchange contribution to the effective relaxation rate, k_{ex} is the timescale of the exchange event, $\Delta\omega$ is the chemical shift difference between two states in exchange and p_A, p_B are the populations of the two states. Fitting of the relaxation dispersion data can show best fit by multiple sets of model parameters. In order to retrieve accurate exchange parameters, the number of observables are increased by recording data at multiple static magnetic fields. Experimentally, CPMG relaxation dispersion is limited to probe exchange processes occurring at 0.3-10 ms timescale due to the limit of applied CPMG frequency and the intrinsic relaxation properties of the protein. The lower limit of the CPMG frequency can be set with a single spin-echo applied during CPMG block. For proteins, this limit is around 25 Hz as the transverse magnetization for the proteins will decay before a total CPMG time of 20-50 ms[24,26]. The upper limit of

CPMG frequency is set around 1200 Hz by the hardware limitation, as fast pulsing with much shorter τ delay can lead to probe and sample heating[24].

Another method of detecting chemical exchange is by Rotating frame ($R_{1\rho}$) relaxation dispersion experiment[65,66] is used to study events occurring at a timescale of 20-100 μs. This method uses either on-resonance or off-resonance radio-frequency (RF) pulses to spin-lock the magnetization in the rotating frame during evolutions. These pulses can produce effective filed strengths from 1000 to 50000 Hz. The strength of spin-lock for each nucleus depends on the three primary parameters of the RF pulse (1) carrier frequency, ω_{RF}, (2) amplitude, ω_1, and (3) phase, φ. The nuclei that are affected by the applied spin-lock pulse also depend on the resonance offset $\Omega = \omega_0 - \omega_{RF}$, where ω_0 is the Larmor frequency of a particular nucleus. The relaxation rate ($R_{1\rho}$) in the rotating frame is defined as (Equation 2.13):

$$R_{1\rho} = R_1 \cos^2 \theta + R_2 \sin^2 \theta + \frac{\varphi_{ex} k_{ex}}{k_{ex}^2 + \omega_e^2} \sin^2 \theta \qquad (2.13)$$

where, R_1 and R_2 represent laboratory frame longitudinal and transverse relaxation rates, and θ is the tilt angle ($\theta = \tan^{-1}(\omega_1/\Omega)$) of the effective spin-locking field $\omega_e = (\omega_1^2 + \Omega^2)^{1/2}$. The application of spin-lock pulses with varying field strengths by varying carrier frequency and amplitude of the pulse. This allows suppression of the exchange between the two states to different extent with variable field strength and thus creates a dispersion in the observed $R_{1\rho}$ rates. Since the effective field can be varied by varying the offset, the measurements at multiple static magnetic fields are not required as required in the $R_{1\rho}$ RD. Though this poses an advantage, the variation in the effective field with offset demands the collection of relaxation data with multiple offsets for a spin-lock field-strength. Further to get the dispersion, multiple of such field-strengths need to be applied. This thus increases the total data recording time. Further, for ^{15}N spectral widths as large as 40 ppm for backbone amides of proteins, on-resonance data needs to be recorded at multiple offsets to keep the tilt angle close to 90 degrees. A slight deviation in the tilt angle from 90 degrees creates large phase errors in the spectrum away from the offset values limiting the number of analyzable peaks in a given offset data.

In the current study, a modified version of $R_{1\rho}$ type relaxation dispersion experiments called Heteronuclear Adiabatic Relaxation Dispersion (HARD) was used[67,68]. This experiment uses hyperbolic secant family (HSn, where n = stretching factor) adiabatic pulses that allow spin-locking of the magnetization in the rotating frame[69–71]. The method has an advantage that the applied spin-lock fields can cover the whole range of spectral width that ^{15}N-spins in proteins spans and thus avoids the need of collection of data at multiple offsets or ω_{RF} as required in conventional $R_{1\rho}$ type experiment. The applied RF field strength is varied by modification in phase and amplitude of the pulse – by changing the stretching factor (n). Both longitudinal ($R_{1\rho}$) and transverse ($R_{2\rho}$) relaxation rates in the rotating frame are determined for each spin by recording HSQC spectra with increasing relaxation delays in terms of a number of adiabatic pulses applied. The method uses five adiabatic pulses (HS1, HS2, HS4, HS6, and

HS8) and the relaxation rates for each of the pulse are calculated which indicate dispersion when plotted against HS pulse stretching factor. The magnetic field strength increases with increase in the stretching factor and results in increase in $R_{1\rho}$ rate and decrease in $R_{2\rho}$ rate. These rates along with the R_1 rates are used for determining exchange parameters – k_{ex}, p_A or p_B and $\Delta\omega$ – from computational approach, geometric approximation approach[72] by data fitting in Bloch-McConnell equation for two site exchange model. In general, the evolution of magnetization (N) of a nuclear spin (a) under the influence of radiofrequency pulse is defined by phenomenological Bloch equations in as (Equation 2.14):

$$\frac{d}{dt}\begin{bmatrix} N_{ax} \\ N_{ay} \\ N_{az} \end{bmatrix} = \begin{bmatrix} -R_2 & -\Omega_a & 0 \\ \Omega_a & -R_2 & -\omega_1 \\ 0 & \omega_1 & -R_1 \end{bmatrix}\begin{bmatrix} N_{ax} \\ N_{ay} \\ N_{az} \end{bmatrix} + R_1\begin{bmatrix} 0 \\ 0 \\ N_{a0} \end{bmatrix}$$

(2.14)

where R_1 and R_2 are the longitudinal and transverse relaxation rates, ω_1 is the amplitude of the radiofrequency pulse, and Ω_a is the resonance offset. The term N_{aj} is the component of nuclear magnetization of spin (a) in x-, y-, and z-direction respectively. In the presence of exchange, the magnetization is affected due to the exchange phenomenon and the Bloch-McConnel equation that define the evolution is modified as (Equation 2.15):

$$\text{State A} \underset{k_b}{\overset{k_a}{\rightleftharpoons}} \text{State B}$$

$$\frac{d}{dt}\begin{bmatrix} N_{ax} \\ N_{bx} \\ N_{ay} \\ N_{by} \\ N_{az} \\ N_{bz} \end{bmatrix} = \begin{bmatrix} -k_a-R_2 & k_b & -\delta_a & 0 & \omega_1 & 0 \\ k_a & -k_b-R_2 & 0 & -\delta_b & 0 & \omega_1 \\ \delta_a & 0 & -k_a-R_2 & k_b & 0 & 0 \\ 0 & \delta_b & k_a & -k_b-R_2 & 0 & 0 \\ -\omega_1 & 0 & 0 & 0 & -k_a-R_1 & k_b \\ 0 & -\omega_1 & 0 & 0 & k_a & -k_b-R_1 \end{bmatrix}\begin{bmatrix} N_{ax} \\ N_{bx} \\ N_{ay} \\ N_{by} \\ N_{az} \\ N_{bz} \end{bmatrix} + R_1\begin{bmatrix} 0 \\ 0 \\ 0 \\ 0 \\ N_{a0} \\ N_{b0} \end{bmatrix}$$

(2.15)

The parameters (k_a and k_b) the forward and reverse reaction rates, (δ_a and δ_b) the resonance offset of state A and B with respect to radiofrequency pulse, (ω_1) the amplitude of the radiofrequency pulse, and (R_1 and R_2) the longitudinal and transverse relaxation rates describe the system undergoing exchange. The term N_{ij} is the nuclear magnetization where $i = a, b$ defines state A or B, and $j = x, y, z$ defines components of magnetization in x-, y-, and z-direction respectively. The geometric approximation method helps to construct solution surfaces for the above equation by assuming $R_{1\rho}$ and $R_{2\rho}$ rates as a linear combination of functions of R_1, R_2, and R_{ex} for the defined set of dynamic parameters (k_{ex}, p_A, $\Delta\omega$, and offset). A rigorous grid search through these solution surfaces by the Monte Carlo method allows to determine the exchange parameters best fit to the observed dispersion in $R_{1\rho}$ and $R_{2\rho}$ rates. This method has been suggested to be able to probe motions over a much wider range of 10 μs – 10 ms. Though the method shows better applicability than the typical CPMG-RD or $R_{1\rho}$ type experiments, at the current stage, the method cannot be used for global analysis, where the residues

involved in a specific catalytic process may have similar exchange rates. Also the method needs further developments in order to accommodate the exchange models with exchange between more than two states.

Relaxation dispersion experiments for the dsRBDs in absence of substrate RNA will allow to study the internal conformational dynamics at μs-ms timescale. Further, relaxation dispersion experiments on dsRBDs in presence of dsRNAs will permit to probe the interaction surface of dsRBD at the dsRBD-dsRNA interface, which in turn will help to study the perturbation in the inherent conformational dynamics of the dsRBD due to the substrate dsRNAs.

2.6.   *References*

1   T. B. Acton, R. Xiao, S. Anderson, J. Aramini, W. A. Buchwald, C. Ciccosanti, K. Conover, J. Everett, K. Hamilton, Y. J. Huang, H. Janjua, G. Kornhaber, J. Lau, D. Y. Lee, G. Liu, M. Maglaqui, L. Ma, L. Mao, D. Patel, P. Rossi, S. Sahdev, R. Shastry, G. V. T. Swapna, Y. Tang, S. Tong, D. Wang, H. Wang, L. Zhao and G. T. Montelione, in *Methods in Enzymology*, ed. L. C. B. T.-M. in E. Kuo, Academic Press, 2011, vol. 493, pp. 21–60.

2   E. Folta-Stogniew and K. R. Williams, Determination of molecular masses of proteins in solution: Implementation of an HPLC size exclusion chromatography and laser light scattering service in a core laboratory, *J. Biomol. Tech.*, 1999, **10**, 51–63.

3   E. Folta-Stogniew, in *New and Emerging Proteomic Techniques. Methods in Molecular Biology*, eds. D. Nedelkov and R. W. Nelson, Humana Press, Totowa, NJ, 2006, pp. 97–112.

4   P. J. Wyatt, Light scattering and the absolute characterization of macromolecules, *Anal. Chim. Acta*, 1993, **272**, 1–40.

5   B. H. Zimm, Molecular theory of the scattering of light in fluids, *J. Chem. Phys.*, 1945, **13**, 141–145.

6   E. Sahin and C. J. Roberts, in *Therapeutic Proteins: Methods and Protocols, Methods in Molecular Biology*, eds. V. Voynov and J. A. Caravella, Springer Science+Business Media, 2012, vol. 899, p. 4999.

7   E. G. Hitti, N. B. Sallacz, V. K. Schoft and M. F. Jantsch, Oligomerization activity of a double-stranded RNA-binding domain, *FEBS Lett.*, 2004, **574**, 25–30.

8   A. Heyam, C. E. Coupland, C. Dégut, R. A. Haley, N. J. Baxter, L. Jakob, P. M. Aguiar, G. Meister, M. P. Williamson, D. Lagos and M. J. Plevin, Conserved asymmetry underpins homodimerization of Dicer-Associated double-stranded RNA-binding proteins, *Nucleic Acids Res.*, 2017, **45**, 12577–12584.

9   A. Daher, M. Longuet, D. Dorin, F. Bois, E. Segeral, S. Bannwarth, P. L. Battisti, D. F. Purcell, R. Benarous, C. Vaquero, E. F. Meurs and A. Gatignol, Two Dimerization Domains in the Trans-activation Response RNA-binding Protein (TRBP) Individually Reverse the Protein Kinase R Inhibition of HIV-1 Long Terminal Repeat Expression, *J. Biol. Chem.*, 2001, **276**, 33899–33905.

10   L. Valente and K. Nishikura, RNA binding-independent dimerization of adenosine deaminases acting on RNA and dominant negative effects of nonfunctional subunits on dimer functions, *J. Biol. Chem.*, 2007, **282**, 16054–16061.

11   H. Amartely, O. Avraham, A. Friedler, O. Livnah and M. Lebendiker, Coupling Multi Angle Light Scattering to Ion Exchange chromatography (IEX-MALS) for protein characterization, 2018, 1–9.

12   B. Banerjee, G. Misra and M. T. Ashraf, in *Data Processing Handbook for Complex Biological Data Sources*, Elsevier Inc., 2019, pp. 21–30.

13   S. Kelly and N. Price, The Use of Circular Dichroism in the Investigation of Protein Structure and Function, *Curr. Protein Pept. Sci.*, 2005, **1**, 349–384.

14   W. C. Johnson, Secondary Structure of Proteins through Circular Dichroism Spectroscopy, *Annu. Rev. Biophys. Biophys. Chem.*, 1988, **17**, 145–166.

15   N. J. Greenfield, Using circular dichroism collected as a function of temperature to determine the thermodynamics of protein unfolding and binding interactions, *Nat. Protoc.*, 2006, **1**, 2527–2535.

16   F. S. Ruggeri, J. Habchi, A. Cerreta and G. Dietler, AFM-Based Single Molecule Techniques: Unraveling the Amyloid Pathogenic Species, *Curr. Pharm. Des.*, 2016, **22**, 3950–3970.

17   Y. Liang, Applications of isothermal titration calorimetry in protein science, *Acta Biochim. Biophys. Sin. (Shanghai).*, 2008, **40**, 565–576.

18   O. Callies and A. Hernández Daranas, Application of isothermal titration calorimetry as a tool to study natural product interactions, *Nat. Prod. Rep.*, 2016, **33**, 881–904.

19   A. L. Feig, Applications of Isothermal Titration Calorimetry in RNA Biochemistry and Biophysics, *Biopolymers*, 2007, **87**, 293–301.

20   X. Du, Y. Li, Y. L. Xia, S. M. Ai, J. Liang, P. Sang, X. L. Ji and S. Q. Liu, Insights into protein–ligand interactions: Mechanisms, models, and methods, *Int. J. Mol. Sci.*, 2016, **17**, 1–34.

21   A. L. B. T.-M. in E. Feig, in *Methods in Enzymology*, ed. Daniel Herschlag, Academic Press, 2009, vol. 468, pp. 409–422.

22   E. Freire, O. L. Mayorga and M. Straume, Isothermal Titration, *Anal. Chem.*, 1990, **62**, 950A-959A.

23   M. W. Freyer and E. A. Lewis, Isothermal Titration Calorimetry: Experimental Design, Data Analysis, and Probing Macromolecule/Ligand Binding and Kinetic Interactions, *Methods Cell Biol.*, 2008, **84**, 79–113.

24   I. R. Kleckner and M. P. Foster, An introduction to NMR-based approaches for measuring protein dynamics, *Biochim. Biophys. Acta - Proteins Proteomics*, 2011, **1814**, 942–968.

25   K. Teilum, M. B. A. Kunze, S. Erlendsson and B. B. Kragelund, (S)Pinning down protein interactions by NMR, *Protein Sci.*, 2017, **26**, 436–451.

26   G. S. Rule and T. K. Hitchens, *Fundamentals of Protein NMR Spectroscopy. Focus on Structural Biology*, Springer Netherlands, 2006, vol. 53.

27   J. Cavanagh, *Protein NMR spectroscopy : principles and practice*, Academic Press, Amsterdam ; Boston, 2nd edn., 2007.

28   Y. Shen, O. Lange, F. Delaglio, P. Rossi, J. M. Aramini, G. Liu, A. Eletsky, Y. Wu, K. K. Singarapu, A. Lemak, A. Ignatchenko, C. H. Arrowsmith, T. Szyperski, G. T. Montelione, D. Baker and A. Bax, Consistent blind protein structure generation from NMR chemical shift data, *Proc. Natl. Acad. Sci. U. S. A.*, 2008, **105**, 4685–4690.

29   Y. Shen, R. Vernon, D. Baker and A. Bax, De novo protein structure generation from incomplete chemical shift assignments, *J. Biomol. NMR*, 2009, **43**, 63–78.

30   L. E. Kay, The evolution of solution state NMR pulse sequences through the 'eyes' of triple-resonance spectroscopy, *J. Magn. Reson.*, 2019, 1–7.

31   L. E. Kay, M. Ikura, R. Tschudin and A. Bax, Three-dimensional triple-resonance NMR spectroscopy of isotopically enriched proteins, *J. Magn. Reson.*, 1990, **89**, 496–514.

32   J. Cavanagh, W. J. Fairbrother, A. G. Palmer, M. Rance and N. J. Skelton, in *Protein NMR Spectroscopy (Second Edition)*, eds. J. Cavanagh, W. J. Fairbrother, A. G. Palmer, M. Rance and N. J. Skelton, Academic Press, Burlington, 2007, pp. 533–678.

33   P. M. Bowers, C. E. M. Strauss and D. Baker, De novo protein structure determination using sparse NMR data, *J. Biomol. NMR*, 2000, **18**, 311–318.

34   Y. Shen, P. N. Bryan, Y. He, J. Orban, D. Baker and A. Bax, De novo structure generation using chemical shifts for proteins with high-sequence identity but different folds, *Protein Sci.*, 2010, **19**, 349–356.

35   O. F. Lange, P. Rossi, N. G. Sgourakis, Y. Song, H. W. Lee, J. M. Aramini, A. Ertekin, R. Xiao, T. B. Acton, G. T. Montelione and D. Baker, Determination of solution structures of proteins up to 40 kDa using CS-Rosetta with sparse NMR data from deuterated samples, *Proc. Natl. Acad. Sci. U. S. A.*, 2012, **109**, 10873–10878.

36   I. W. Davis, A. Leaver-Fay, V. B. Chen, J. N. Block, G. J. Kapral, X. Wang, L. W. Murray, W. B. Arendall, J. Snoeyink, J. S. Richardson and D. C. Richardson, MolProbity: All-atom contacts and structure validation for proteins and nucleic acids, *Nucleic Acids Res.*, 2007, **35**, 375–383.

37   H. N. B. Moseley, G. Sahota and G. T. Montelione, Assignment validation software suite for the evaluation and presentation of protein resonance assignment data, *J. Biomol. NMR*, 2004, **28**, 341–355.

38   R. A. Laskowski, J. A. C. Rullmann, M. W. MacArthur, R. Kaptein and J. M. Thornton, AQUA and PROCHECK-NMR: Programs for checking the quality of protein structures solved by NMR, *J. Biomol. NMR*, 1996, **8**, 477–486.

39   F.-A. Chao and R. A. Byrd, Protein dynamics revealed by NMR relaxation methods, *Emerg. Top. Life Sci.*, 2018, **2**, 93–105.

40   M. Kovermann, P. Rogne and M. Wolf-Watz, Protein dynamics and function from solution state NMR spectroscopy, *Q. Rev. Biophys.*, 2016, **49**, e6.

41   C. Göbl and N. Tjandra, Application of solution NMR spectroscopy to study protein dynamics, *Entropy*, 2012, **14**, 581–598.

42   J. G. Kempf and J. P. Loria, Protein dynamics from solution NMR, *Cell Biochem. Biophys.*, 2002, **37**, 187–211.

43   A. G. Palmer, NMR characterization of the dynamics of biomacromolecules, *Chem. Rev.*, 2004, **104**, 3623–3640.

44   S. C. Sahu, A. K. Bhuyan, A. Majumdar and J. B. Udgaonkar, Backbone dynamics of barstar: A 15 N NMR relaxation study, *Proteins Struct. Funct. Genet.*, 2000, **41**, 460–474.

45   S. Morin and S. M. Gagné, NMR dynamics of PSE-4 β-lactamase: An interplay of ps-ns order and μs-ms motions in the active site, *Biophys. J.*, 2009, **96**, 4681–4691.

46   T. I. Igumenova, K. K. Frederick and A. J. Wand, Characterization of the fast dynamics of protein amino acid side chains using NMR relaxation in solution, *Chem. Rev.*, 2006, **106**, 1672–1699.

47   V. A. Jarymowycz and M. J. Stone, Fast time scale dynamics of protein backbones: NMR relaxation methods, applications, and functional consequences, *Chem. Rev.*, 2006, **106**, 1624–

1671.

48   L. E. Kay, D. A. Torchia and A. Bax, Backbone Dynamics of Proteins As Studied by 15N Inverse Detected Heteronuclear NMR Spectroscopy: Application to Staphylococcal Nuclease, *Biochemistry*, 1989, **28**, 8972–8979.

49   N. Bloembergen, E. M. Purcell and R. V. Pound, Relaxation Effects in Nuclear Magnetic Resonance Absorption, *Phys. Rev.*, 1948, **73**, 679.

50   J. G. Kempf and J. P. Loria, Protein dynamics from solution NMR: theory and applications, *Cell Biochem Biophys*, 2003, **37**, 187–211.

51   J. W. Peng and G. Wagner, Mapping of the Spectral Densities of N-H Bond Motions in Eglin C Using Heteronuclear Relaxation Experiments, *Biochemistry*, 1992, **31**, 8571–8586.

52   G. Lipari and A. Szabo, Model-Free Approach to the Interpretation of Nuclear Magnetic-Resonance Relaxation in Macromolecules .2. Analysis of Experimental Results, *J. Am. Chem. Soc.*, 1982, **104**, 4559–4570.

53   G. Lipari and A. Szabo, Model-Free Approach to the Interpretation of Nuclear Magnetic-Resonance Relaxation in Macromolecules .1. Theory and Range of Validity, *J. Am. Chem. Soc.*, 1982, **104**, 4546–4559.

54   G. Lipari and A. Szabo, Analysis of Nmr Relaxation Data on Macromolecules Using the Model-Free Approach, *Biophys. J.*, 1982, **37**, A380–A380.

55   G. M. Clore, A. Szabo, A. Bax, L. E. Kay, P. C. Driscoll and A. M. Gronenborn, Deviations from the simple two-parameter model-free approach to the interpretation of nitrogen-15 nuclear magnetic relaxation of proteins, *J. Am. Chem. Soc.*, 1990, **112**, 4989–4991.

56   D. D. Boehr, D. McElheny, H. J. Dyson and P. E. Wright, The Dynamic Energy Landscape of Dihydrofolate Reductase Catalysis, *Science (80-.).*, 2006, **313**, 1638 LP – 1642.

57   J. P. Loria, R. B. Berlow and E. D. Watt, Characterization of enzyme motions by solution NMR relaxation dispersion, *Acc. Chem. Res.*, 2008, **41**, 214–221.

58   D. F. Hansen, P. Vallurupalli, P. Lundström, P. Neudecker and L. E. Kay, Probing chemical shifts of invisible states of proteins with relaxation dispersion NMR spectroscopy: How well can we do?, *J. Am. Chem. Soc.*, 2008, **130**, 2667–2675.

59   A. G. Palmer, Chemical exchange in biomacromolecules: Past, present, and future, *J. Magn. Reson.*, 2014, **241**, 3–17.

60   M. Tollinger, N. R. Skrynnikov, F. A. Mulder, J. D. Forman-Kay and L. E. Kay, Slow dynamics

in folded and unfolded states of an SH3 domain, *J Am Chem Soc*, 2001, **123**, 11341–11352.

61   J. P. Carver and R. E. Richards, A general two-site solution for the chemical exchange produced dependence of T2 upon the carr-Purcell pulse separation, *J. Magn. Reson.*, 1972, **6**, 89–105.

62   P. Vallurupalli, G. Bouvignies and L. E. Kay, Increasing the exchange time-scale that can be probed by CPMG relaxation dispersion NMR, *J. Phys. Chem. B*, 2011, **115**, 14891–14900.

63   A. J. Baldwin and L. E. Kay, An R1ρ expression for a spin in chemical exchange between two sites with unequal transverse relaxation rates, *J. Biomol. NMR*, 2013, **55**, 211–218.

64   A. J. Baldwin, An exact solution for R2,eff in CPMG experiments in the case of two site chemical exchange, *J. Magn. Reson.*, 2014, **244**, 114–124.

65   A. G. Palmer and F. Massi, Characterization of the dynamics of biomacromolecules using rotating-frame spin relaxation NMR spectroscopy, *Chem. Rev.*, 2006, **106**, 1700–1719.

66   T. Szyperski, P. Luginbühl, G. Otting, P. Güntert and K. Wüthrich, Protein dynamics studied by rotating frame 15N spin relaxation times, *J. Biomol. NMR*, 1993, **3**, 151–164.

67   S. Mangia, N. J. Traaseth, G. Veglia, M. Garwood and S. Michaeli, Probing slow protein dynamics by adiabatic R(1rho) and R(2rho) NMR experiments, *J Am Chem Soc*, 2010, **132**, 9979–9981.

68   N. J. Traaseth, F. A. Chao, L. R. Masterson, S. Mangia, M. Garwood, S. Michaeli, B. Seelig and G. Veglia, Heteronuclear Adiabatic Relaxation Dispersion (HARD) for quantitative analysis of conformational dynamics in proteins, *J Magn Reson*, 2012, **219**, 75–82.

69   S. Mangia, T. Liimatainen, M. Garwood and S. Michaeli, Rotating frame relaxation during adiabatic pulses vs. conventional spin lock: simulations and experimental results at 4 T, *Magn Reson Imaging*, 2009, **27**, 1074–1087.

70   A. Tannús and M. Garwood, Adiabatic pulses, *NMR Biomed.*, 1998, **10**, 423–434.

71   S. Michaeli, D. J. Sorce and M. Garwood, $T_{2\rho}$ and $T_{1\rho}$ adiabatic relaxations and contrasts, *Curr. Anal. Chem.*, 2008, **4**, 8–25.

72   F. A. Chao and R. A. Byrd, Geometric Approximation: A New Computational Approach To Characterize Protein Dynamics from NMR Adiabatic Relaxation Dispersion Experiments, *J Am Chem Soc*, 2016, **138**, 7337–7345.

Chapter 3 Protein Purification and Resonance Assignment

3.1. Introduction

NMR spectroscopy is a well-known biophysical technique used to explore the structure and dynamics of proteins at the atomic level. A pre-requisite for this characterization is to have the resonance assignment of the protein, which is achieved by triple-resonance NMR experiments[1,2] as discussed in section 2.5.1 using protein samples, isotopically enriched with NMR active ^{15}N and/or ^{13}C nuclei. These experiments help us to obtain the sequential connectivities along the protein chain via correlations of every N-H peak in the ^{1}H-^{15}N-HSQC spectrum to the carbon resonances in the self and previous residue in the amino acid chain in the spectra from the triple-resonance experiments. A double-resonance experiment ^{1}H-^{15}N-TOCSY-HSQC is recorded to identify the type of amino acid, where a unique pattern of TOCSY correlation for every amino acid can be observed in the third dimension for every N-H correlation in the HSQC. The backbone chemical shifts (H^{N}, N, C′, C_{α}, H_{α}) obtained from these experiments help us to determine the structure of the protein using the CS-rosetta[3] web server (https://csrosetta.bmrb.wisc.edu/csrosetta/submit) available at Biological Magnetic Resonance Bank[4] (BMRB). The model protein structures generated from the submitted NMR chemical shift data further need to be validated in order to ensure the best fit for the geometrical constraints.

3.2. Materials and Methods

3.2.1. Resonance Assignment for TRBP2-dsRBD1

3.2.1.1. Protein expression and Purification

The plasmid (pSV272-TRBP2-dsRBD1) containing the cDNA for TRBP2-dsRBD1 (received from Prof. Jennifer Doudna, University of California, Berkeley, USA as a gift) was transformed into bacterial cells *E. coli* strain BL21(DE3) for protein expression. Briefly, the cells were allowed to multiply in 20 ml of LB broth containing 50 µg/ml of Kanamycin overnight at 37°C. The culture was then transferred to 1 liter of LB broth containing the antibiotic and was further allowed to grow till OD_{600} ~1.0 was obtained. This plasmid system upon induction with Isopropyl-β-D-thiogalactoside (IPTG) overexpresses TRBP2-dsRBD1 as His_6-MBP-TEV-TRBP2-dsRBD1 recombinant protein. The His_6 tag enables the purification of overexpressed protein by the Ni-NTA affinity chromatography. The Maltose binding protein (MBP) tag has been known to improve the solubility of the protein[5,6]. The Tobacco Etch Virus (TEV) cleavage site after the MBP tag helps to remove the tag from the protein of interest (TRBP2-dsRBD1).

The expression of TRBP2-dsRBD1 protein was optimized with respect to IPTG concentration (0.1 mM, 0.5 mM, 1.0 mM), induction temperature (16°C, 28°C and 37°C) and time of induction (2 hours -16 hours) to get the maximum yield of protein. Post-standardization, induction was performed with optimized 1 mM IPTG wherein cells were allowed to overexpress protein at 28°C for 8 hours.

After 8 hrs, cells were harvested by centrifugation at 8000xg for 20 min at 4°C. The cell pellet thus obtained was resuspended in Lysis buffer (20 mM Tris-HCl, 500 mM NaCl, 10 mM Imidazole, 10% glycerol, 1 mM DTT), pH 7.5. The cells were lysed by incubating with 1 % Triton-X 100, and 100 µl of Lysozyme (20 mg/ml; Sigma Aldrich) for 20 min. This is followed by cycles of sonication by ultrasonic sonicator (Vibra Cell VCX-130, Sonics & Materials Inc., USA) to ensure complete cell lysis and to fragment the nucleic acids released during lysis. The sonication was performed with cell suspension in ice using a 6 mm microprobe with a sonication cycle of 10 sec ON, 10 sec OFF at an amplitude of 70 %. The lysate was then centrifuged at 32000 x g at 4°C for 30 min and the supernatant (further referred to as total soluble protein - TSP) was collected. The TSP was then circulated from the Ni-sepharose column (HisTrap column, 5ml, GE healthcare). The column was washed with wash buffer (pH 7.5), containing 30 mM Imidazole. The tagged protein was then eluted using Elution buffer (pH 7.5) containing 300 mM Imidazole. This purified protein was exchanged with TEV cleavage buffer (20 mM Tris-HCl, 25 mM NaCl, 10 % glycerol, 1 mM DTT), pH 7.5. The concentration of TEV required for the cleavage was optimized by adding TEV to the purified tagged protein in TEV protease:protein ratio of 1:30, 1:100, 1:500, 1:1000 and 1:5000 and incubated at 4°C with end to end rotation for 16 hours. The concentration of TEVprotease optimal to remove the fusion tag by was in the ratio of 1:100 to the protein for 16 hours at 4°C with end to end rotation. The His$_6$-MBP tag was separated from the cleaved protein by passing through a fresh Ni-sepharose column (HisTrap column, 5ml, GE healthcare) and the protein without tag was collected by washing column with Gel filtration buffer (20 mM Tris-HCl, 500 mM NaCl, 10 % glycerol, 1 mM DTT), pH 7.5. The protein was concentrated and passed through the size-exclusion chromatographic column (Sephacryl S100 HR 16/60, GE healthcare) to ensure > 95 % purity of the protein. The purified protein TRBP2-dsRBD1 thus obtained was finally exchanged with NMR buffer (10 mM Sodium Phosphate, 100 mM NaCl, 1 mM EDTA, 1 mM DTT), pH 6.4 for all NMR experiments. The purified protein has amino acid sequence as:

```
             10         20         30         40         50         60
GGA  MSEEEQGSGT TTGCGLPSIE QMLAANPGKT PISLLQEYGT RIGKTPVYDL LKAEGQAHQP

             70         80         90        100        105
     NFTFRVTVGD TSCTGQGPSK KAAKHKAAEV ALKHLKGGSM LEPAL
```

where GGA at the N-terminus (Underlined in the sequence above) of the protein are non-native residues left after cleavage by TEV protease.

3.2.1.2. Preparation of isotopically labeled protein sample

^{15}N-TRBP2-dsRBD1 sample was prepared by using ^{15}N-NH$_4$Cl (Sigma-Aldrich) as the sole source of nitrogen in minimal media used for cell growth. The composition of the minimal media used is as mentioned in Table 3.1. The sample containing ^{13}C-^{15}N-TRBP2-dsRBD1 was prepared with ^{13}C-D(+)-glucose (Cambridge Isotope Laboratories) as the sole source of carbon along with ^{15}N-NH$_4$Cl as

the sole source of nitrogen in minimal media. The expression and purification protocol remains the same for the labeled proteins as optimized for the unlabeled protein sample.

Table 3.1: Composition of Minimal Media for labeled protein overexpression.

Ingredient	Volume required for 1 L of Medium
5x Minimal salt solution (30 g/L Na_2HPO_4, 15 g/L KH_2PO_4, 2.5 g/L NaCl, 1 g/L NH_4Cl) pH 7.4	200 ml
20 %w/v D-(+)-Glucose	20 ml
1 M $MgCl_2$	1 ml
1 M $CaCl_2$	100 µl
1.5 %w/v Casein Hydrolysate	120 ml
Water	to 1liter

3.2.1.3. NMR Experimental data collection

All the NMR data were recorded on Bruker AVANCE III HD 600MHz NMR spectrometer. All the samples for NMR studies were exchanged in NMR buffer (10 mM sodium phosphate, 100 mM NaCl, 1 mM EDTA, and 1 mM DTT), pH 6.4 for data collection. All the experiments were performed at 25 °C unless mentioned otherwise. A standard set of triple-resonance NMR experiments, HNCA, HN(CO)CA, CBCANH, CBCA(CO)NH, HNCO, and HN(CA)CO along with ^{1}H-^{15}N-TOCSY-HSQC experiment, were recorded to get the backbone chemical shift assignment of the protein. The experimental parameters used for the collection of NMR data for resonance assignments have been listed in Table 3.2. The spectra collected were referenced with respect to DSS directly in ^{1}H-dimension and indirectly in ^{15}N and ^{13}C dimension[7,8] using a sample of DSS in NMR buffer, pH 6.4. The referenced spectra were processed in Topspin 3.2 (Bruker Biospin) and converted to ucsf format for analysis in CARA (Computer Aided Resonance Assignment) v1.9.1.7.[9]

Table 3.2: Experimental Parameters for NMR data collected for the Resonance assignment of TRBP2-dsRBD1.

Experiment (Pulse Sequence used)	Nucleus	TD^a	SW^b (ppm)	Offset (ppm)	NS^c	$d1^d$ (s)
^{1}H-^{15}N-HSQC (hsqcetf3gpsi)	^{1}H	2048	12	4.69	2	1.0
	^{15}N	256	28	117.00		
HNCA (hncagpwg3d)	^{1}H	2048	12	4.70	16	1.0
	^{15}N	40	28	117.00		
	^{13}C	128	32	54.00		
HN(CO)CA (hncocagpwg3d)	^{1}H	2048	12	4.70	16	1.0
	^{15}N	40	28	117.00		
	^{13}C	128	32	54.00		
CBCANH (cbcanhgpwg3d)	^{1}H	2048	12	4.69	16	1.5
	^{15}N	40	28	117.00		
	^{13}C	128	80	43.00		

Experiment (Pulse Sequence used)	Nucleus	TD[a]	SW[b] (ppm)	Offset (ppm)	NS[c]	d1[d] (s)
CBCA(CO)NH (cbcaconhgpwg3d)	^{1}H	2048	12	4.69	16	1.5
	^{15}N	40	28	117.00		
	^{13}C	128	80	43.00		
HNCO (hncogpwg3d)	^{1}H	2048	12	4.69	8	1.0
	^{15}N	40	28	117.00		
	^{13}C	128	22	176.00		
HN(CA)CO (hncacogpwg3d)	^{1}H	2048	12	4.69	32	1.0
	^{15}N	40	28	117.00		
	^{13}C	128	22	176.00		
^{1}H-^{15}N-TOCSY-HSQC (mlevhcqsetf3gpsi)	^{1}H	2048	12	4.69	16	1.0
	^{15}N	40	28	117.00		
	^{1}H	128	12	4.69		

[a]TD: Number of data points/size of fid, [b]SW: Spectral Width, [c]NS: Number of scans, [d]d1: relaxation delay

3.2.1.4. NMR data analysis in CARA

For the analysis of NMR data collected, a project was created in CARA and the amino acid sequence of the TRBP2-dsRBD1 was added in the sequence (.seq) format[9]. This was followed by importing all the NMR spectra formatted in ucsf file formats into the CARA project. The peaks picking for all the peaks in the HSQC spectrum, triple-resonance NMR experiments, and ^{1}H-^{15}N-TOCSY-HSQC were performed as per guidelines in CARA manual[9]. Then, using stripscope mode in CARA, the successor and the precursor for each of the amide resonance were identified and confirmed following the appearance of the resonances in the strips of multiple spectra. This was supported by the identification of the type of residue using ^{1}H-^{15}N-TOCSY-HSQC data and their alignment with the amino acid sequence of the protein.

3.2.1.5. Structure Calculation and Validation

The assigned backbone chemical shifts (H^N, N, C′, C$_\alpha$, and H$_\alpha$) were used to calculate the structure of the protein using CS-Rosetta program[3] (https://csrosetta.bmrb.wisc.edu/csrosetta/submit) available at BMRB. During structure calculations, three thousand structures were allowed to generate to get the best structure for the chemical shift data. The calculations were performed by disabling the option to remove the flexible tails. The structure, thus calculated, was further validated by using Ramachandran plots[10] for all best-fit models from CS-rosetta generated at MolProbity webserver[11,12] (http://molprobity.biochem.duke.edu/).

3.2.1.6. Calculation of Chemical Shift Perturbations

Given, the chemical shift change in ^{1}H and ^{15}N dimension respectively are $\Delta\delta_N$ and $\Delta\delta_H$ respectively, the overall chemical shift perturbations ($\Delta\delta$) were calculated using the following formula:

$$\Delta\delta = \sqrt{\frac{(\Delta\delta_N/5)^2 + \Delta\delta_H{}^2}{2}}$$

(3.1)

3.2.2. Resonance Assignment for dADAR-dsRBD1

3.2.2.1. Protein expression and Purification

Plasmid for dADAR-dsRBD1 was provided as a gift sample by Prof. Frederic H.T. Allain (ETH, Zurich, Switzerland). The overexpression and purification were performed as described by Barraud et al.[13]. Briefly, the plasmid-encoded in the pET28a(+) vector was transformed into *E. coli* BL21(DE3) cells. The cells were grown in 20 ml of LB broth overnight at 37°C in shaker-incubator rotating at 225 rpm. The overnight culture was then added to 1 liter of LB broth and allowed to grow till OD_{600} ~0.8 was observed. Protein over-expression was then carried out with IPTG as an inducer at 0.5 mM final concentration for 15 hours at 30°C. The cells were harvested as described for TRBP2-dsRBD1 in section 3.2.1.1. The cells were lysed as described for TRBP2-dsRBD1 by using lysis buffer (20 mM Tris-HCl, 1 M NaCl, 1 mM DTT) pH 8.0. The protein was then circulated through the Ni-affinity column (HisTrap column, 5 ml, GE healthcare) and the tagged protein was eluted using elution buffer (20 mM Tris-HCl, 1 M NaCl, 30 mM Imidazole, 1 mM DTT) pH 8.0. The eluted protein was then purified from the Gel filtration column (Sephacryl S100 HR, GE healthcare) using 20 mM Tris-HCl, 1 M NaCl, 1 mM DTT, pH 8.0 as elution buffer. The purified protein has amino acid sequence as:

```
                    50          60          70          80
    MGSSHHHHHHSSGLVPRGSHM SDP KKKMCKERIP QPKNTVAMLN ELRHGLIYKL

      90          100         110         120         130         140
    ESQTGPVHAP LFTISVEVDG QKYLGQGRSK KVARIEAAAT ALRSFIQFKD GAVLSPLKPA
```

where the residue MGSSHHHHHHSSGLVPRGSHM at the N-terminus (Underlined in the sequence above) of the protein are non-native residues that are expressed from the plasmid along with the protein of interest.

3.2.2.2. Preparation of isotopically labeled protein sample

^{15}N-ADAR-dsRBD1 sample was prepared by using ^{15}N-NH$_4$Cl (Sigma-Aldrich) as the sole source of nitrogen in minimal media (Table 3.1) used for cell growth.

3.2.2.3. Experimental data collection

For the resonance assignment of the ^{15}N-labeled dADAR-dsRBD1, a sample was prepared in NMR buffer (10 mM sodium phosphate, 100 mM NaCl, 1 mM EDTA and 1 mM DTT), pH 6.4 and the ^{1}H-^{15}N-HSQC spectrum was recorded. The spectrum was then processed in Topspin3.2 and converted to ucsf format. The assignment available in BMRB database[4] (BMRB accession number: 17936[13]) was then transferred by using the "*simulate and transfer assignment*" tool in the NMRFAM-Sparky[14].

3.3.   Results

3.3.1.   Resonance Assignment for TRBP2-dsRBD1

3.3.1.1. Protein expression and purification

The overexpression of the TRBP2-dsRBD1 protein was optimized by varying the time, temperature and concentration of IPTG used for induction. The expression of the protein was monitored at 16°C, 28°C, and 37°C by adding 0.1 mM, 0.5 mM, and 1.0 mM final IPTG concentration for 16 hours at an interval of 2 hours. An aliquot of 1 ml from the cell culture was collected every 2 hours; cells were pelleted; lysed; and loaded onto a 15 % SDS-PAGE gel to check the induction of the protein. The maximum expression of the protein was observed when cells were induced with 1.0 mM IPTG at 28°C for 8 hours. The gel image in Figure 3.1 shows the induction of TRBP2-dsRBD1 protein monitored at every 2 hours interval (for 16 hours) when cells were induced with 1.0 mM IPTG at 28°C.
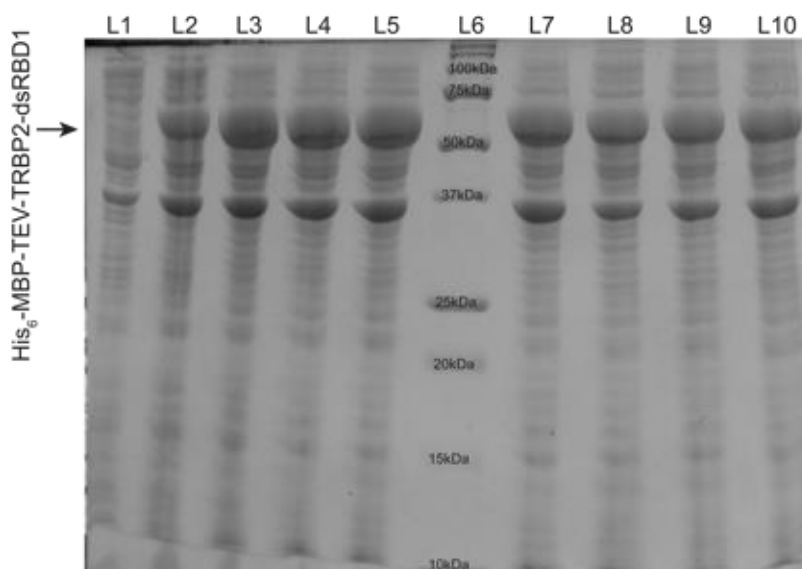
Figure 3.1: SDS-PAGE for Induction time optimization for over-expression of TRBP2-dsRBD1 when induced with 1 mM IPTG at 28°C. The lanes in the gel have been labeled for the time-point at which samples were collected - L1:0 hr, L2: 2 hr, L3: 4 hr, L4: 6 hr, L5: 8 hr, L7: 10 hr, L8: 12 hr, L9: 14 hr, L10: 16 hr. The lane L6 contains the protein ladder (Bio-rad Laboratories).

The over-expressed protein was then purified using the protocol as mentioned in the Methods section. However, this protocol yielded protein with some nucleic acid contamination as indicated by higher A260/280 ratios. Thus the protocol was further modified to remove the contaminating nucleic acids from the lysate by: (1) precipitation of nucleic acids using 5% polyethylene(imine) solution; (2) followed by precipitation of protein using saturated ammonium sulfate solution to 60% saturation; and (3) dialysis in lysis buffer to remove the ammonium sulfate in order to bind the protein in solution to Ni-affinity column. The cell lysate without any contaminating nucleic acids was further purified by Ni-affinity chromatography.
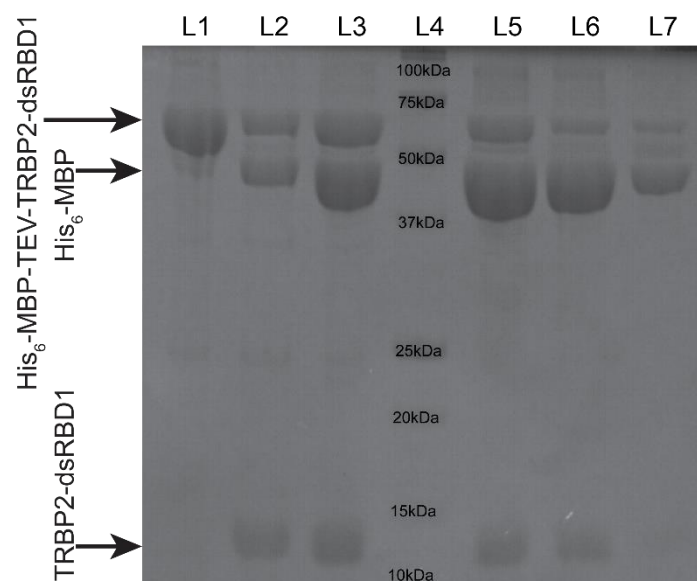
Figure 3.2: SDS-PAGE showing the optimization of cleavage conditions for cleavage of the tagged protein by TEV protease. The lanes are labeled with the ratio of the TEV protease to tagged protein as- L1: Uncleaved protein, L2: (1:1000), L3: (1:500), L4: Protein Ladder (Bio-rad Laboratories), L5: (1:200), L6: (1:100), L7: (1:30), respectively.

Expression	• Overexpress in *E.coli* BL21(DE3) using 1 mM IPTG at 28°C for 8 hr
Cell lysis	• Using Triton x-100 (detergent), Lysozyme • Sonication
Removal of Nucleic Acids	• Precipitation of RNA by Polyethylene(imine) • Precipitation of protein by Ammonium sulfate
Affinity purification 1	• Separation of His_6 tagged protein from TSP using Ni-Affinity chromatography
TEV cleavage	• Removal of Fusion tag using TEV protease at 1:100 protease to protein ratio for 16 hr at 4°C
Affinity purification 2	• Separation from His_6 tagged protein and the cleaved tag using Ni-Affinity chromatography
Gel Filtration purification	• Separation based on molecular weight

Figure 3.3: Overview of optimized protocol for purification of TRBP2-dsRBD1 protein

The TEV cleavage conditions were further optimized to obtain efficient cleavage of the tagged protein with a minimum amount of TEV protease by varying the protein to protease ratio. The efficiency of cleavage reaction at different relative concentrations of protease was assessed by the SDS-PAGE after 16 hours of cleavage at 4°C. Figure 3.2 shows that the optimum cleavage can be obtained at a ratio of 1:100 of TEV protease to the tagged protein. Post-cleavage, the tag and the cleaved protein were separated by another round of Ni-affinity purification and the cleaved protein without tag (TRBP2-dsRBD1) was collected in column washing. The purity of the protein was then assessed by running it

through the gel filtration column (Figure 3.4). This optimized protocol (as shown in Figure 3.3) was then used to overexpress and purify the protein with ^{15}N and/or ^{13}C NMR active nuclei using Minimal media. A gel showing protein at various stages of purification has been depicted in Figure 3.4. A detailed optimized protocol for overexpression and purification of TRBP2-dsRBD1 protein is available in Appendix 1.
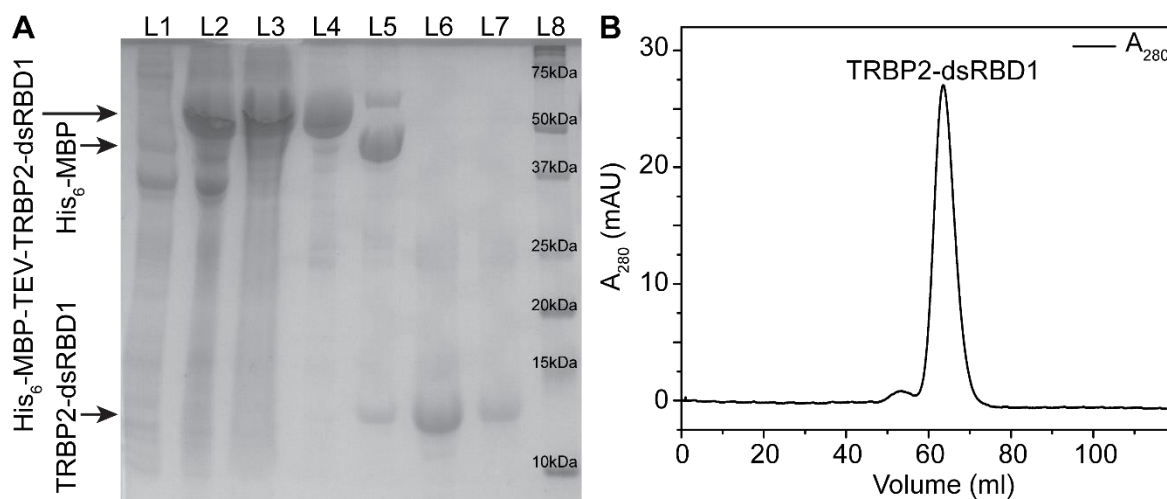
Figure 3.4: (**A**) SDS-PAGE showing TRBP2-dsRBD1 protein at various stages of purification: Lanes labeled as L1-L8 indicate- L1: Pre-induction, L2: Post-induction, L3: Total Soluble Protein, L4: Elution from Ni-affinity column, L5: Post-TEV cleavage, L6: Concentrated washing from Ni-affinity column after TEV cleavage, L7: Purified protein collected from after Gel filtration purification, L8: Protein ladder (Bio-rad Laboratories). (**B**) Gel filtration chromatogram showing the purity of the protein TRBP2-dsRBD1.

3.3.1.2. NMR data analysis

The backbone resonance assignment for the residue 19-228 of TRBP2 which includes dsRBD1 and dsRBD2 was available in literature[15]. The reports by Wilson *et al*. and Benoit *et al*. have shown that the presence of either dsRBD does not affect the chemical shifts of the other[16,17]. However, the overlay of the ^{1}H-^{15}N-HSQC spectrum recorded for TRBP2-dsRBD1 (1-105 aa) used in this study with ^{1}H-^{15}N-TROSY-HSQC (BMRB accession Number:18324) does not show a one-to-one correlation of HSQC peaks for the common residues (19-105 aa) as shown in Figure 3.5. This suggested that the presence of an additional 21 amino-acids at the N-terminal of the protein might have an impact on the structure of dsRBD1 of TRBP2. Therefore, it was essential to perform the detailed backbone assignment of TRBP2-dsRBD1.

A set of triple-resonance NMR experiments as listed in the method section and a ^{1}H-^{15}N-TOCSY-HSQC experiment for the TRBP2-dsRBD1 protein were recorded as described in the Methods section. The NMR data recorded were referenced directly in the ^{1}H dimension and indirectly in ^{15}N and ^{13}C dimension with respect to DSS[7,8]. The data recorded was then processed in Topspin 3.2 (Bruker Biospin) and converted to ucsf format. These files were then transferred to program CARA for the peak picking and further analysis. The type of amino acid corresponding to a peak in HSQC was identified using a pattern of TOCSY connections observed in the strips of the ^{1}H-^{15}N-TOCSY-HSQC spectrum.
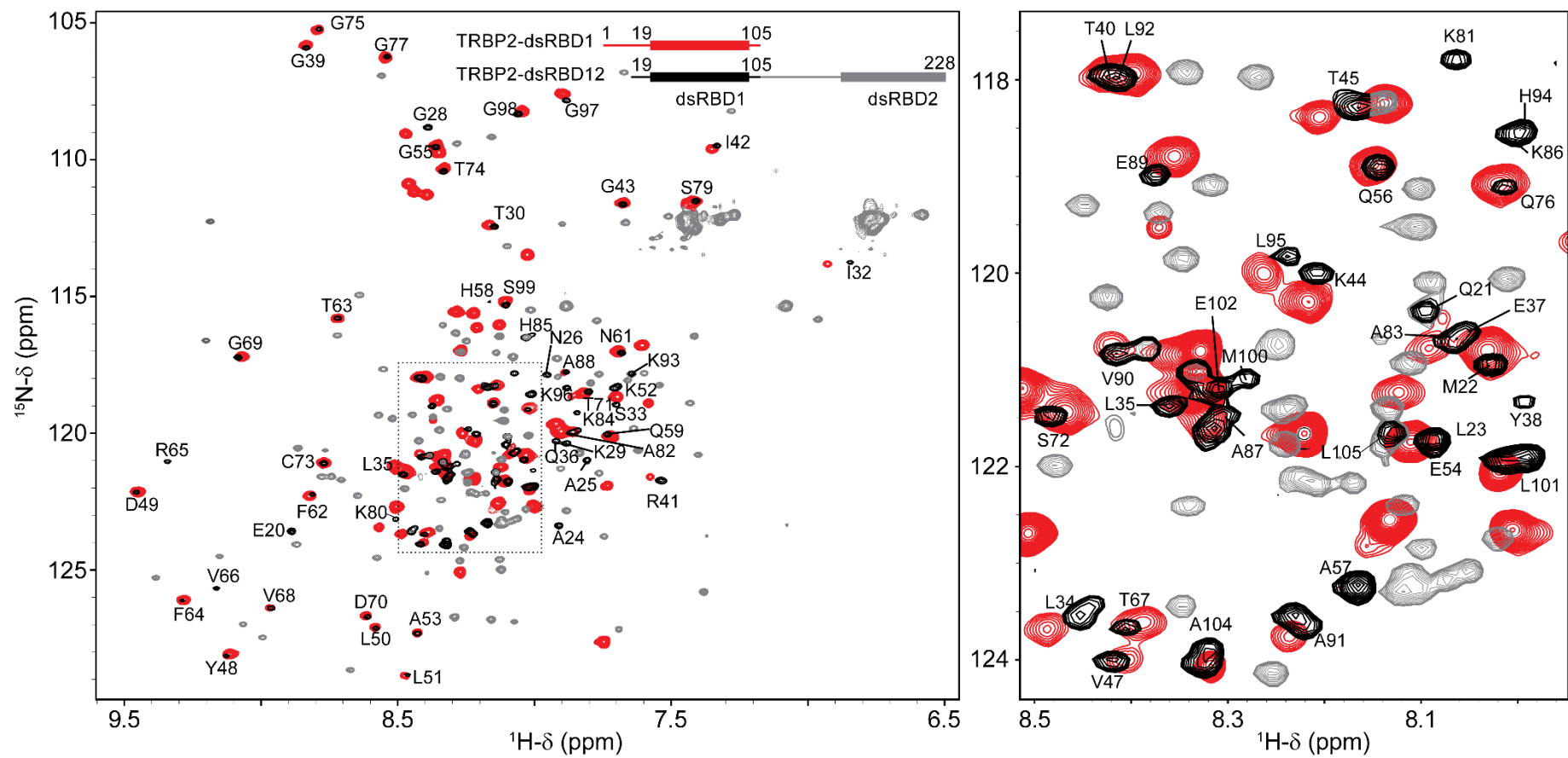
Figure 3.5: Overlay of the ^{1}H-^{15}N-TROSY-HSQC assignment of TRBP2-dsRBD12 (19-228 aa) on the ^{1}H-^{15}N-HSQC spectrum of TRBP2-dsRBD1 (1-105 aa). The color-coding of the two spectra is as shown in the inset in the left panel.

For example, for a peak in HSQC, Glycine shows only two peaks – one at ~3.9 ppm which originates from H_α protons and other from the backbone amide (H^N). The identification of the residue type was also assisted by the C_α and C_β chemical shifts observed in the strip of the CBCANH spectrum. For example, Alanine shows C_β chemical shift most up-field in 10-20 ppm range; Serine and Threonine show C_β peaks down-field than the corresponding C_α chemical shift. The sequential connections in the strips of the HNCA, CBCANH, and HN(CA)CO spectra along with the type of residue identified from the ^1H-^{15}N-TOCSY-HSQC spectrum guided through the protein sequence to get the protein backbone resonance assignment. An example of the sequential connections in the HNCA strips has been shown in Figure 3.6.
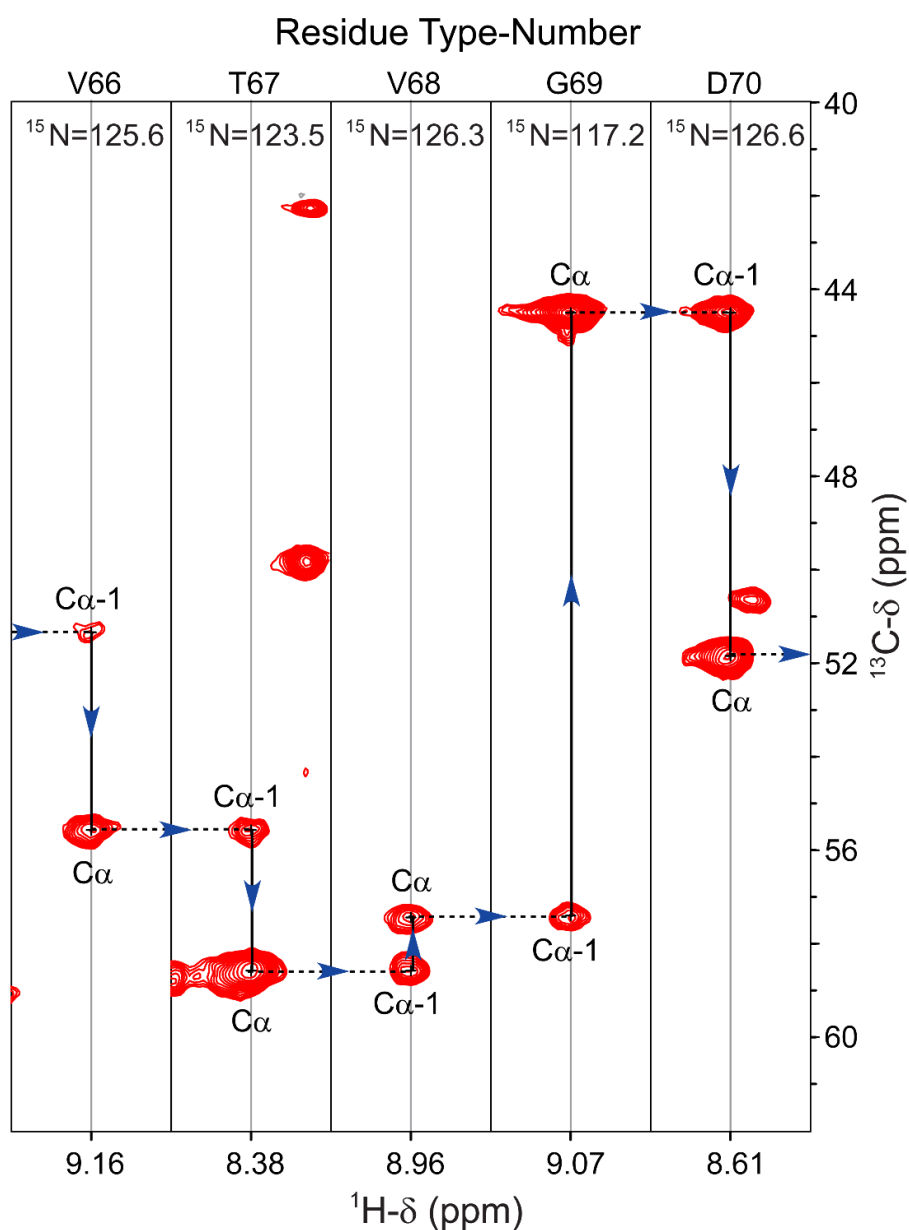
Figure 3.6: Sequential connectivities along the protein backbone using HNCA strips. The intra-residual and inter-residual connections are represented by solid and dashed lines respectively.

Using this approach, ~98% of the non-proline backbone amide groups were assigned (**Figure 3.7**). Along with this, assignment for 75% of C′, 94% of C_α and 67% of C_β carbons, and 93 % of H_α and 47% of H_β hydrogens were achieved. The list of assigned resonances, generated in NMR-STAR3.1 format from the program CARA, have been deposited to the Biological Magnetic Resonance Bank (BMRB) database. The chemical shift information is available at BMRB with accession number 27262[18]. The assigned peaks in the HSQC spectra have been labeled in Figure 3.7. There are five unassigned peaks that are found at low intensity that may represent peaks for unassigned residues (I19 and E20) and three non-native residues (GGA) left at the N-terminus of the protein after cleaving the fusion tag using TEV protease.
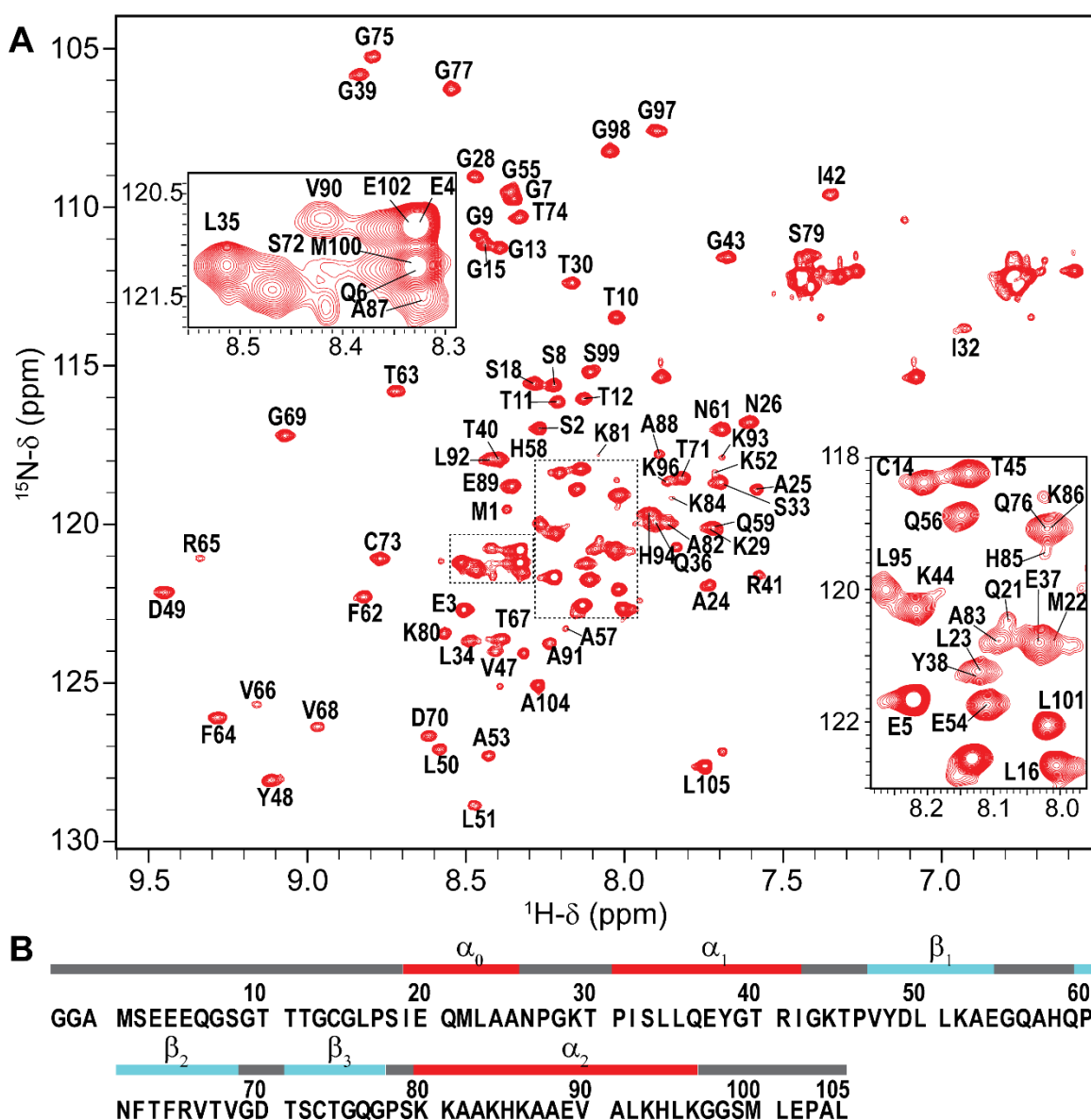
Figure 3.7: (**A**) Assignment of backbone resonance in the ^{1}H-^{15}N-HSQC spectrum for TRBP2-dsRBD1. (**B**) Primary sequence of the protein construct used in the study with the secondary structure of the protein marked on the sequence.

3.3.1.3. Structure Calculation

The backbone chemical shifts (H^N, N, C′, C_α, and H_α) were then used to calculate the structure of the protein at the CS-rosetta program (as described in the Methods section). The calculated structure contained ten best fit models defined by energy minimization. All of the ten best-fit models showed the presence of typical dsRBD fold α_1-β_1-β_2-β_3-α_2. In addition, models also showed the presence of an additional α helix, labeled hereafter as helix α_0, at the N-terminal of the dsRBD1 spanning 19-25 aa (Figure 3.8). The assessment of the quality of the structure was performed at the MolProbity web server (http://molprobity.biochem.duke.edu/) by using Ramachandran analysis for all the models in the ensemble generated by CS-rosetta. The results show that for all the residues, the torsion angles defined by all the models were present in the allowed regions of the Ramachandran plot, thus validating the structure geometrically[10,11]. The report of the Ramachandran analysis has been attached as Appendix 2.
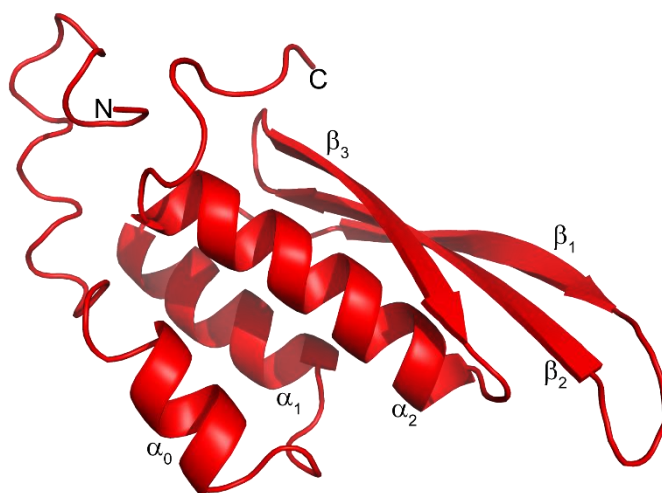
Figure 3.8: Structure of TRBP2-dsRBD1 calculated using the backbone chemical shifts from the CS-Rosetta program.

3.3.1.4. Calculation of Chemical Shift Perturbations

The chemical shifts of the TRBP2-dsRBD1 (1-105 aa) obtained from the resonance assignment (BMRB accession No.: 27262) were compared with the previously reported chemical shifts of TRBP2-dsRBD12 spanning length from 19-228 aa (BMRB accession No.:18324) by calculating Chemical Shift Perturbations (CSP) for the common residues (as described in the Methods section). The CSP values were plotted against the residue number (Figure 3.9). The plot shows a large deviation in chemical shift perturbation for the residue L23-N26, K29, H58, H85 and L105 from the average CSP observed for the common residues (19-105).
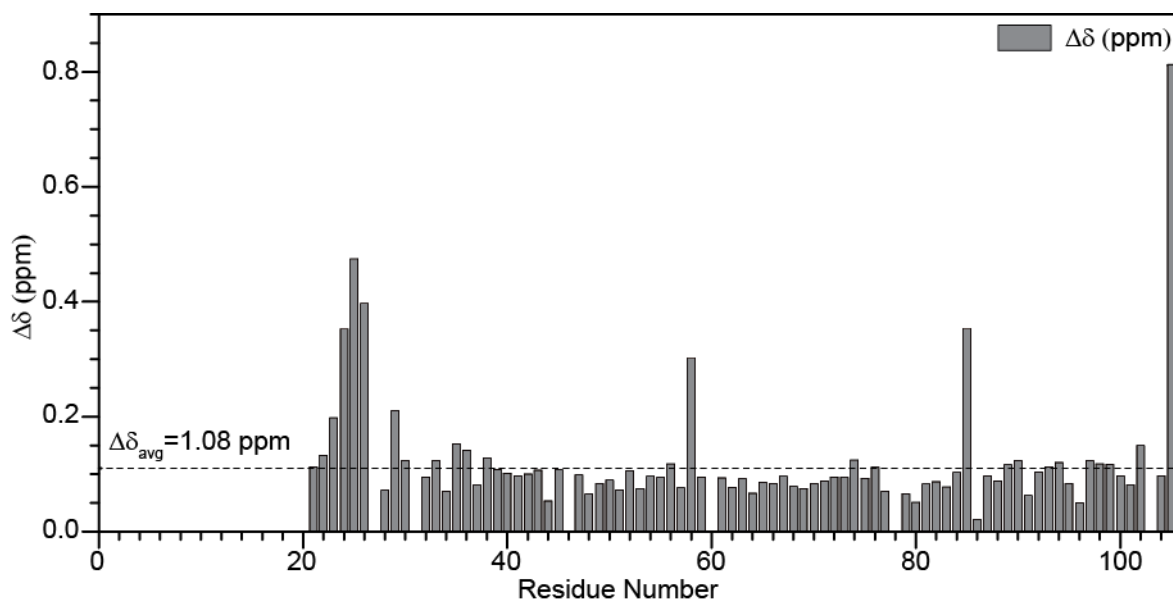
Figure 3.9: Chemical shift perturbations for residue 19-105 calculated from the new assignment of TRBP2-dsRBD1 (1-105 aa) and previously available assignment of TRBP2-dsRBD12 (19-228 aa).

3.3.2. Resonance Assignment for dADAR-dsRBD1

3.3.2.1. Protein expression and purification

Overexpression and the purification of the dADAR-dsRBD1 protein was performed as mentioned in the Methods section. As for TRBP2-dsRBD1, the presence of any nucleic acid contamination was avoided by the treatment of polyethylene(imine) to the TSP obtained from the cell lysate. This is followed by precipitation of protein using saturated ammonium sulfate solution to 60% saturation in the polyethylene(imine) treated TSP solution. The precipitated proteins were then re-suspended and dialyzed in lysis buffer pH 8.0. Further purification by Ni-affinity chromatography and gel filtration chromatography was performed as described in the method section. The optimized protocol used for labeled protein purification has been outlined in Figure 3.10. Figure 3.11 shows the SDS-PAGE for the dADAR-dsRBD1 protein at various stages of purification and the chromatogram from gel filtration purification of the dADAR-dsRBD1 protein ensuring the purity of the sample used for the NMR studies. A detailed optimized protocol for overexpression and purification of dADAR-dsRBD1 protein is available in Appendix 1.

Expression	• Overexpress in *E.coli* BL21(DE3) using 0.5 mM IPTG at 30°C for 15 hr
Cell lysis	• Using Triton x-100 (detergent), Lysozyme • Sonication
Removal of Nucleic Acids	• Precipitation of RNA by Polyethylene(imine) • Precipitation of protein by Ammonium sulfate
Affinity purification	• Separation of His6 tagged protein from TSP using Ni-Affinity chromatography
Gel Filtration purification	• Separation based on molecular weight

Figure 3.10: Overview of optimized protocol for purification of the dADAR-dsRBD1 protein construct.
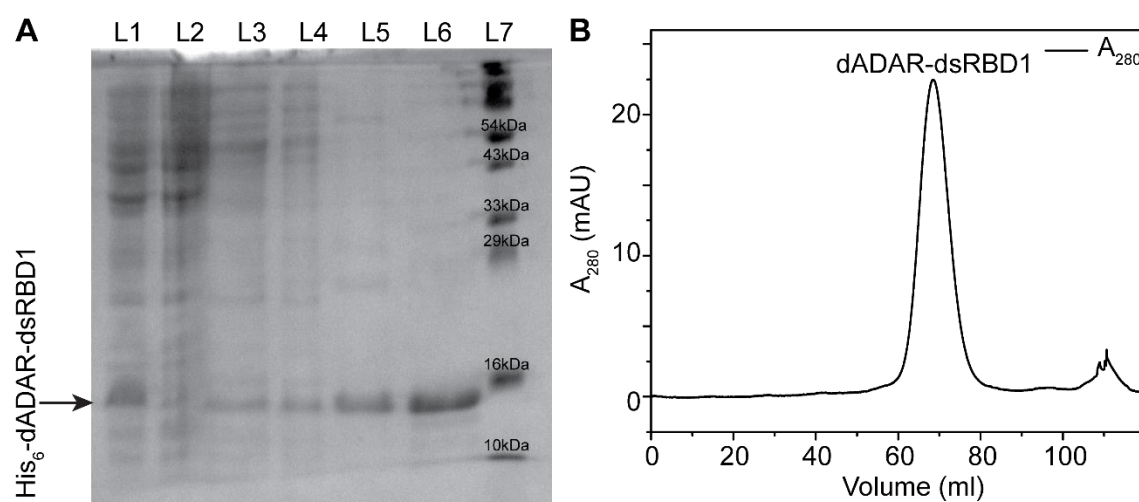
Figure 3.11: (**A**) SDS-PAGE showing dADAR-dsRBD1 protein at various stages of purification: Lanes are labeled as L1-L7 indicate- L1: Post-induction, L2: Pre-induction, L3: Cell lysate, L4: Total Soluble Protein, L5: Elution from Ni-affinity column, L6: Purified protein collected from after Gel filtration purification, L7: Protein ladder (Puregene). (**B**) Gel filtration chromatogram showing the purity of the protein dADAR-dsRBD1.

3.3.2.2. NMR data Analysis

The backbone resonance assignment for the dsRBD1 of dADAR was reported by Barraud *et al*. under BMRB accession number 17936 and the solution structure obtained from these assignments was deposited in Protein Data Bank (PDB ID:2LJH)[13]. The assignment was then transferred from the BMRB database to the HSQC recorded with the ^{15}N-labeled dADAR-dsRBD1 protein using the "simulate and transfer" tool of the NMRFAM-Sparky. Figure 3.12 shows the transferred assignment for 74 residues ^{1}H-^{15}N-HSQC spectrum for dADAR-dsRBD1 (48-140 aa) from the assignment for 75 residues available in BMRB.
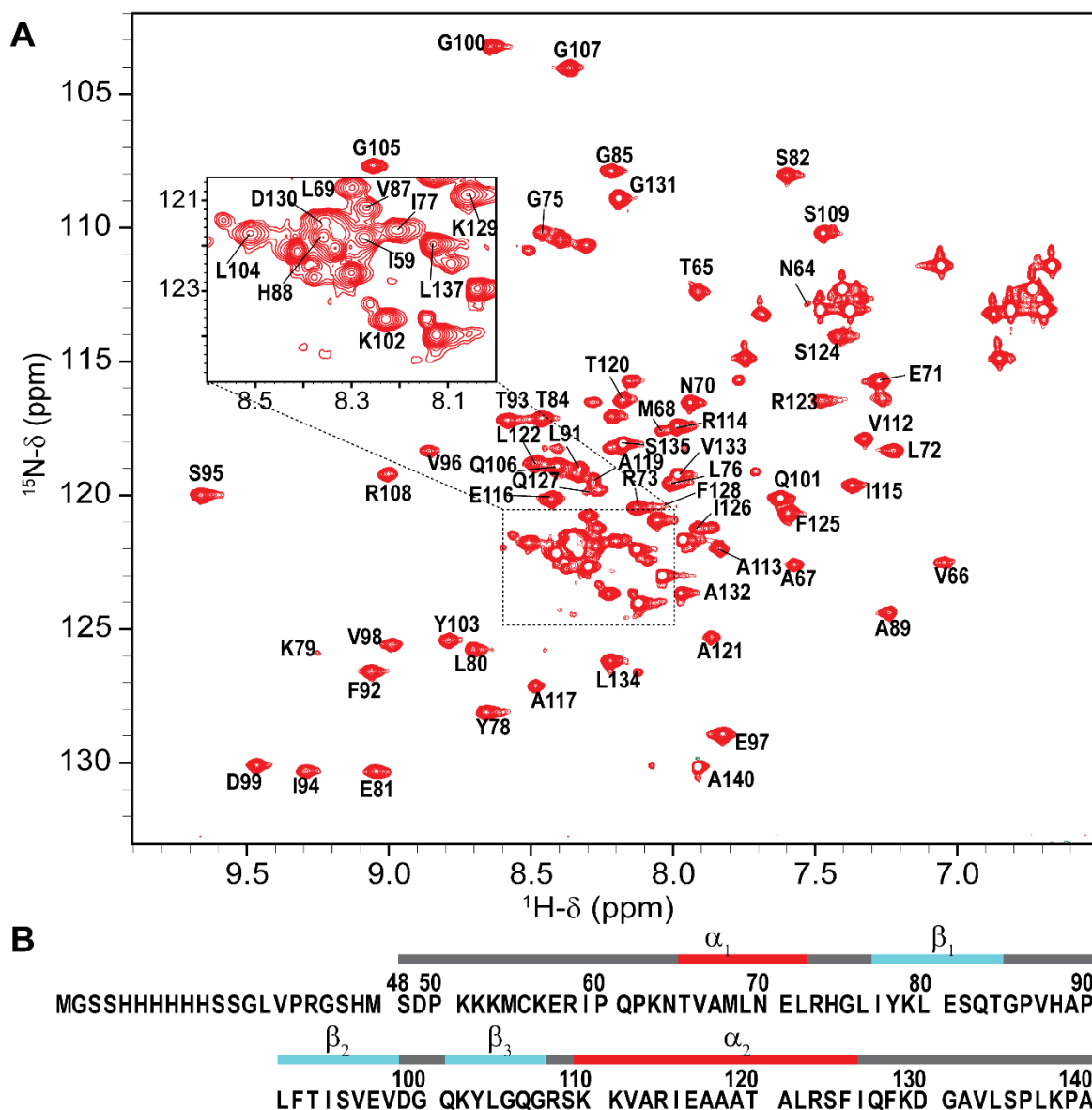
Figure 3.12: (**A**) Assignment of backbone resonance in the ^{1}H-^{15}N-HSQC spectrum for dADAR-dsRBD1. (**B**) Primary sequence of the protein construct used in the study with the secondary structure of the protein marked on the sequence.

3.4. Discussion

Though it was known that TRBP is expressed as two isoforms in humans that differ only in 21 amino acids at N-terminus, the structural or functional characterization of these residues was still not available. The structure calculated using resonance assignment for a protein construct containing these residues helped to identify that these additional residues form an additional helix α_0 which was not reported earlier. Masliah *et al.* simultaneously reported the presence of the additional helix α_0 in their independent work[19]. The comparison of the structure of the dsRBD1 of TRBP2 with the N-terminal residues – determined from CS-rosetta with the resonance assignment performed – and without the N-terminal residues – crystal structure[20] (PDB ID: 3LLH) – indicates that there is no significant change in the tertiary structure of the dsRBD core due to these residues. The RMSD between the calculated

structure and the crystal structure of the dsRBD1 of TRBP (28-96 aa) shows 1.14 Å, indicating a good match between the two structures (Figure 3.13). However, a small shift in the orientation of the helix α_1 was observed with respect to the helix α_2 in the calculated structure when compared with the crystal structure. Also, the β_1 strand in the solution structure shows more twisting at its C-terminus than observed in the Crystal structure. Further, the plot of CSP between previous assignment by Benoit and coworkers and the new assignment shows that more than average CSPs were observed in the residues helix α_0 (L23-N26) and in the residue K29 which are due to the formation of the of helix α_0 in polypeptide chain which may exist as flexible terminal in the protein construct without N-terminal residues (M1-Q21). However, the presence of additional residues has also resulted in a significant shift in the residues known to be involved in dsRNA-binding (residue H58 and H85). The residue H85 is present in the close spatial proximity to the newly identified α_0 helix, that might affect the local chemical environment of the residue observed as change in the chemical shift of H85. Further, since the hydrophobic region contributed by the A82, A83 residues of α_2 helix and F62, F64 at the termini of β_1-β_2 loop will might have affected the chemical environment of the H58 resulting in the CSP observed. Thus the presence of additional residues in the chain may have an impact on the dsRNA-binding, perturbing the interaction between the dsRNA and TRBP2-dsRBD1. The large CSP observed in the residue L105 is due to the flexibility at the terminal of the protein chain.
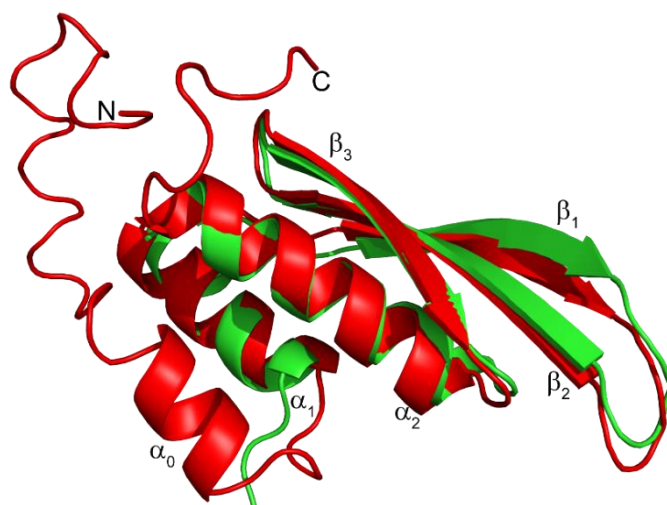
Figure 3.13: Comparison of common residues between the calculated solution NMR structure (Red) and the previously reported crystal structure (PDB ID: 3LLH - Green).

The structure of dsRBD1 of TRBP2[18] and dADAR[13] show the common structural feature particular of a dsRBD and contain α_1-β_1-β_2-β_3-α_2 fold. The comparison of the sequences of the two proteins shows that they possess a sequence identity of 23.6 % and a similarity of 33.3 %. Though they show limited similarity in the sequence, comparison of common structural dsRBD fold of the two dsRBDs (Figure 3.14) shows that they are structurally very close with RMSD between the two of 1.41 Å. This ensures that regardless of the difference in the primary sequences of the two proteins and being

from different species, the dsRBDs hold conserved structural characteristics that may support its non-sequence specific interactions with the dsRNAs.
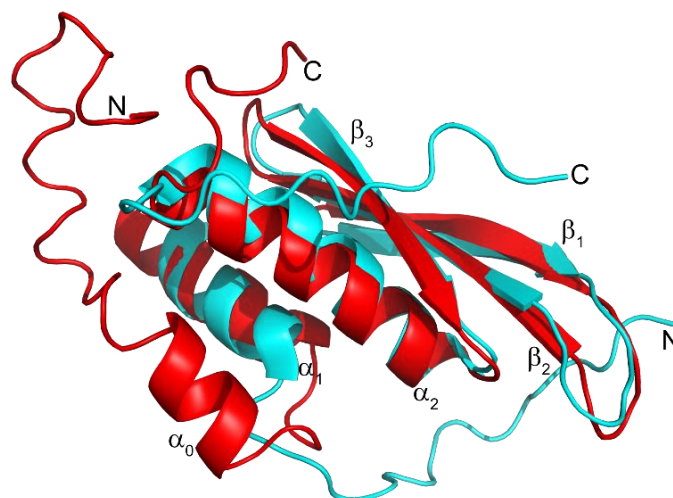
Figure 3.14: Comparison of the solution structure of TRBP2-dsRBD1 (Red) determined at CS-rosetta using assigned chemical shifts and dADAR-dsRBD1 (PDB ID: 2LJH - Cyan).

3.5. Summary

Here, we have successfully purified both the proteins (TRBP2-dsRBD1 and dADAR-dsRBD1) to >95% purity. The resonance assignment for the TRBP2-dsRBD1 protein was performed using a set of triple-resonance NMR experiments. The structure calculated using the assigned backbone chemical shifts was shown to match well with the crystal structure reported earlier with RMSD of 1.14 Å. The chemical shift perturbations between the assignment of dsRBD1 of TRBP2 with and without N-terminal residue (1-18 aa) indicate that these residues may affect the dsRNA recognition by dsRBD1 of TRBP2. The ^{1}H and ^{15}N assignments for backbone NH of dsRBD1 of dADAR are also successfully transferred. The comparison of the two dsRBDs from two different proteins belonging to two different species indicates that the dsRBD fold is independent of the sequence of the protein chain and contains features sufficient for RNA-binding.

3.6. References

1   G. S. Rule and T. K. Hitchens, *Fundamentals of Protein NMR Spectroscopy. Focus on Structural Biology*, Springer Netherlands, 2006, vol. 53.

2   J. Cavanagh, *Protein NMR spectroscopy : principles and practice*, Academic Press, Amsterdam ; Boston, 2nd edn., 2007.

3   Y. Shen, R. Vernon, D. Baker and A. Bax, De novo protein structure generation from incomplete chemical shift assignments, *J. Biomol. NMR*, 2009, **43**, 63–78.

4   E. L. Ulrich, H. Akutsu, J. F. Doreleijers, Y. Harano, Y. E. Ioannidis, J. Lin, M. Livny, S.

Mading, D. Maziuk, Z. Miller, E. Nakatani, C. F. Schulte, D. E. Tolmie, R. Kent Wenger, H. Yao and J. L. Markley, BioMagResBank, *Nucleic Acids Res.*, 2008, **36**, 402–408.

5   D. Esposito and D. K. Chatterjee, Enhancement of soluble protein expression through the use of fusion tags, *Curr. Opin. Biotechnol.*, 2006, **17**, 353–358.

6   P. Sun, J. E. Tropea and D. S. Waugh, in *Heterologous Gene Expression in E. coli, Methods in Molecular Biology*, eds. J. Evans Thomas C. and M.-Q. Xu, Humana Press, Totowa, NJ, 2011, pp. 259–274.

7   D. S. Wishart, C. G. Bigam, J. Yao, F. Abildgaard, H. J. Dyson, E. Oldfield, J. L. Markley and B. D. Sykes, 1H, 13C and 15N chemical shift referencing in biomolecular NMR, *J. Biomol. NMR*, 1995, **6**, 135–140.

8   D. S. Wishart and A. M. Nip, Protein chemical shift analysis: a practical guide, *Biochem Cell Biol*, 1998, **76**, 153–163.

9   R. Keller, *The computer aided resonance assignment tutorial*, 1st edn., 2004.

10   G. N. Ramachandran, C. Ramakrishnan and V. Sasisekharan, Stereochemistry of polypeptide chain configurations, *J Mol Biol*, 1963, **7**, 95–99.

11   I. W. Davis, A. Leaver-Fay, V. B. Chen, J. N. Block, G. J. Kapral, X. Wang, L. W. Murray, W. B. Arendall, J. Snoeyink, J. S. Richardson and D. C. Richardson, MolProbity: All-atom contacts and structure validation for proteins and nucleic acids, *Nucleic Acids Res.*, 2007, **35**, 375–383.

12   C. J. Williams, J. J. Headd, N. W. Moriarty, M. G. Prisant, L. L. Videau, L. N. Deis, V. Verma, D. A. Keedy, B. J. Hintze, V. B. Chen, S. Jain, S. M. Lewis, W. B. Arendall, J. Snoeyink, P. D. Adams, S. C. Lovell, J. S. Richardson and D. C. Richardson, MolProbity: More and better reference data for improved all-atom structure validation, *Protein Sci.*, 2018, **27**, 293–315.

13   P. Barraud, B. S. E. Heale, M. A. O'Connell and F. H. T. Allain, Solution structure of the N-terminal dsRBD of Drosophila ADAR and interaction studies with RNA, *Biochimie*, 2012, **94**, 1499–1509.

14   W. Lee, M. Tonelli and J. L. Markley, NMRFAM-SPARKY: Enhanced software for biomolecular NMR spectroscopy, *Bioinformatics*, 2015, **31**, 1325–1327.

15   M. P. M. H. Benoit and M. J. Plevin, Backbone resonance assignments of the micro-RNA precursor binding region of human TRBP, *Biomol. NMR Assign.*, 2013, **7**, 229–233.

16   R. C. Wilson, A. Tambe, M. A. Kidwell, C. L. Noland, C. P. Schneider and J. A. Doudna, Dicer-TRBP complex formation ensures accurate mammalian MicroRNA biogenesis, *Mol. Cell*, 2015, **57**, 397–408.

17   M. P. M. H. Benoit, L. Imbert, A. Palencia, J. Pérard, C. Ebel, J. Boisbouvier and M. J. Plevin, The RNA-binding region of human TRBP interacts with microRNA precursors through two independent domains, *Nucleic Acids Res.*, 2013, **41**, 4241–4252.

18   H. Paithankar, P. V. Jadhav, A. S. Naglekar, S. Sharma and J. Chugh, 1H, 13C and 15N resonance assignment of domain 1 of trans-activation response element (TAR) RNA binding protein isoform 1 (TRBP2) and its comparison with that of isoform 2 (TRBP1), *Biomol. NMR Assign.*, 2018, **12**, 189–194.

19   G. Masliah, C. Maris, S. L. König, M. Yulikov, F. Aeschimann, A. L. Malinowska, J. Mabille, J. Weiler, A. Holla, J. Hunziker, N. Meisner-Kober, B. Schuler, G. Jeschke and F. H. Allain, Structural basis of siRNA recognition by TRBP double-stranded RNA binding domains, *EMBO J.*, 2018, e97089.

20   S. Yamashita, T. Nagata, M. Kawazoe, C. Takemoto, T. Kigawa, P. Güntert, N. Kobayashi, T. Terada, M. Shirouzu, M. Wakiyama, Y. Muto and S. Yokoyama, Structures of the first and second double-stranded RNA-binding domains of human TAR RNA-binding protein, *Protein Sci.*, 2011, **20**, 118–130.

Chapter 4 Characterization of Intrinsic dynamics of dsRBDs

4.1.   Introduction

Though the structure of the protein indicates the lowest energy conformation that may represent the native fold, proteins may switch between one or more conformations leading to their functions[1]. NMR spectroscopy is commonly used to study the conformational dynamics in proteins at the atomic level as discussed in Chapter 2. The use of NMR spectroscopy is particularly advantageous because it can quantify the dynamics on a wide range of time scale at an atomic level.

In this chapter, we aimed to characterize the intrinsic dynamics in the two model dsRBDs by NMR spectroscopy to enhance the understanding of its role in the interaction of dsRBDs with dsRNAs. Since the pool of dsRNAs – which may contain helical imperfections like bulge and/or mismatch – present in the cellular matrix includes conformationally distinct substrates for dsRBDs, we hypothesized that the dsRBDs may span distinct conformations that could allow them to interact with these RNAs. In the following studies, the characterization of dsRBDs was accomplished by SEC-MALS, CD, and NMR-based studies. First, SEC-MALS analysis was used to determine the polydispersity of the dsRBDs in solution to be used for NMR analysis. Then, CD analysis was performed to explore the thermal stability of the protein at the NMR working conditions. This was followed by a detailed characterization of dynamics by NMR spectroscopy at different timescale by ^{15}N-relaxation experiments. The NMR experiments for ps-ns and μs-ms timescale dynamics in the dsRBDs were collected (as discussed in Chapter 2) and the data were analyzed to evaluate the functional significance of these motions.

4.2.   Materials and Methods

4.2.1.   Size-Exclusion Chromatography - Multi-Angle Light Scattering Analysis

Size Exclusion Chromatography - Multi-Angle Light Scattering (SEC-MALS) experiments were performed on the Agilent HPLC system equipped with a refractive index detector (Wyatt Optilab T-rEX) and 18-angle light scattering detector (Wyatt Dwan HELIOS II). The Superdex 75 10/300 GL column (GE Healthcare) was used for the size-based separation of sample components with an injection volume of 100 μl each. The system was calibrated with a known standard – Bovine Serum Albumin (BSA) solution (Thermo-Scientific) at 30 μM concentration. SEC-MALS data for protein samples were collected in duplicate at a concentration of 1.1 mM and 0.459 mM of TRBP2-dsRBD1 and dADAR-dsRBD1, respectively. Each protein sample was centrifuged at 21000 x g at 4°C for 15 minutes before injecting into the chromatography system. Molecular Weights at the peaks in the SEC-MALS data were determined using the Zimm model in ASTA software (Wyatt Technologies) version 6.1.7.17.

4.2.2. *Circular Dichroism Spectropolarimetry*

Circular Dichroism (CD) experiments were performed on a Jasco J-815 CD spectropolarimeter using 200 μl of protein samples – TRBP2-dsRBD1 and dADAR-dsRBD1 – in NMR buffer pH 6.4 at 20 μM protein concentration. The CD spectra were recorded using a rectangular quartz cuvette with a path length of 2 mm. The bandwidth was set at 1 nm and the data were acquired with a scanning speed of 200 nm/min with digital integration time (D.I.T.) of 1 sec. Data was collected as an average of 3 scans in the wavelength range of 200-250 nm in the far-UV region at a temperature ranging from 10°C to 80°C at an interval of 5°C. The sample was allowed to equilibrate at each temperature for 10 min before starting data collection.

All the CD spectra collected were baseline corrected by the buffer. The data was then smoothened using the five-point adjacent averaging method. The fraction of folded protein (α) at each temperature was calculated as (Equation 4.1)[2]:

$$\alpha = \frac{S_{obs} - S_U}{S_F - S_U} \tag{4.1}$$

where, S_{obs}, S_F and S_U are the CD signal at 222 nm at observed temperature, for completely folded protein and for completely unfolded protein respectively. The melting temperature of the protein was determined from the first derivative plot where the maxima of the plot indicate the melting temperature[2].

4.2.3. *NMR Spectroscopy*

Protein dynamics in the two dsRBDs at two different timescales – ps-ns and μs-ms – were probed by nuclear spin relaxation and relaxation dispersion methods. Proteins were overexpressed and purified as discussed in section 3.2.1.1 and 3.2.2.1. The protein samples at concentrations of 1.8 mM and 0.69 mM for TRBP2-dsRBD1 and dADAR-dsRBD1, respectively were prepared by exchanging protein in NMR buffer (10 mM Sodium phosphate, 100 mM NaCl, 1 mM EDTA, 1 mM DTT) pH 6.4 and adding 10% D_2O (for field locking) and each sample was loaded in 5 mm Shigemi tube. All the NMR relaxation experiments were recorded at 25°C on a Bruker 600MHz NMR spectrometer equipped with quad-channel (^{1}H/^{13}C/^{15}N/^{31}P) 5 mm cryogenic probe with X-, Y- and Z- gradients and dual receiver operating (in-house) or Bruker 750 MHz NMR spectrometer equipped with TXI probe with Z-gradient and deuterium decoupling (at IIT-Bombay). An inter-scan delay of 2.5 s and 3 s was used in all relaxation experiments for TRBP2-dsRBD1 and dADAR-dsRBD1, respectively. For all the relaxation data, the spectra collected were processed in NMRpipe/NMRDraw[3] and then converted to ucsf format for peak-picking in Sparky[4]. The intensity of each peak was then used for further data analysis as discussed below.

4.2.3.1. Nuclear Spin Relaxation Experiments

Nuclear spin relaxation experiments (R_1, R_2, and [^{1}H]-^{15}N-NOE) were recorded at two magnetic field strengths of 600 MHz and 750 MHz. ^{15}N-longitudinal relaxation rates (R_1) were measured using a set of inversion recovery delays of 10, 30, 50, 100, 200, 300, 450, 600, 750, and 900 ms and ^{15}N-transverse relaxation rates (R_2) was measured with CPMG delays of 17, 34, 51, 68, 85, 102, 136, and 170 ms for TRBP2-dsRBD1. For dADAR-dsRBD1, inversion recovery delays of 10, 30, 50, 100, 200, 350, 500, and 750 and CPMG delays (with a CPMG block length of 17 ms) of 17, 34, 68, 102, 136, 170, and 204 were used for measurement of R_1 and R_2 rates respectively. Data at relaxation delays underlined were recorded in duplicate for error estimation. Steady-state [^{1}H]-^{15}N-NOEs were measured with a ^{1}H saturation time of 3 s and a relaxation delay of 2 s for both the proteins. Relaxation delay of 5 s was used for experiments without ^{1}H saturation. The details of the experimental parameters used for the relaxation experiments for TRBP2-dsRBD1 have been listed in Table 4.1.

The Relaxation rates R_1 and R_2 for every residue were calculated by fitting the peak intensities – obtained from peak-picking in Sparky – against relaxation delay to a two-parameter exponential decay function (Equation 4.2) in Mathematica 5.2[5].

$$I(t) = I(0)e^{-R_{1,2}t} \tag{4.2}$$

Errors in relaxation rates were estimated from the points measured in duplicate and 500 Monte-Carlo simulations. Steady-state [^{1}H]-^{15}N-NOE values were calculated as a ratio of intensity from the spectrum with and without proton saturation (I_{sat}/I_{unsat}). Errors in NOE values σ_{NOE} were calculated as (Equation 4.3):

$$\sigma_{NOE} = NOE * \sqrt{\left(\frac{\sigma_{unsat}}{I_{unsat}}\right)^2 + \left(\frac{\sigma_{sat}}{I_{sat}}\right)^2} \tag{4.3}$$

where σ_{unsat} and σ_{sat} are the root mean square (RMS) value of noise for unsaturated and saturated spectrum, respectively.

The nuclear spin relaxation rates thus obtained at two magnetic field strengths were analyzed using an extended model-free approach using software Relax v4.0.3[6,7]. The global diffusion tensor parameters of the two protein molecules among different diffusion models – isotropic, axially symmetric or anisotropic – were optimized using *quadric_diffusion* program[8] with Chemical Shift Anisotropy (CSA) of -172 ppm and ^{1}H-^{15}N bond length of 1.02 Å as default values from Relax protocol. The solution structure of the two proteins – TRBP2-dsRBD1[9] and dADAR-dsRBD1 (PDB ID: 2LJH)[10] – were used as input for the *quadric_diffusion* program and further analysis. Then the diffusion tensor parameters obtained from the *quadric_diffusion* program were used as a starting point for the optimization of local model-free parameters in Relax.

The calculations in the Relax were initiated by optimizing the local τ_M model with no diffusion tensor parameter defined, using the Nuclear spin relaxation rates obtained at two magnetic fields. Then

by defining the global diffusion parameters – obtained from *quadric_diffusion* program – as starting values local model-free models were optimized based on the Akaike's Information Criterion. This is followed by further optimization of the global model with optimized local model-free models. This process was repeated until all the model-free parameters (both local and global) converged. The global diffusion model was then selected based on the chi-squared values obtained. After fixing the local and the global model, the errors were estimated using 500 Monte-Carlo simulations.

4.2.3.2. Relaxation Dispersion Experiments

CPMG relaxation dispersion experiments[11] with constant time CPMG block were recorded at two magnetic field strengths of 600 MHz and 750 MHz. The constant CPMG block length (T_{relax}) of 40 ms was used for TRBP2-dsRBD1, at different CPMG frequencies (v_{CPMG}) of 0, 25, 50, 100, 200, 350, 500, 650, 800, and 1000 Hz. For dADAR-dsRBD1, CPMG block length (T_{relax}) of 20 ms and CPMG frequencies (v_{CPMG}) of 0, 50, 100, 150, 200, 300, 450, 600, 800, and 1000 Hz were used. Data at CPMG frequencies underlined were recorded in duplicate for error estimation. The acquisition parameters for the CPMG-RD experiment have been listed in Table 4.1.

The effective transverse relaxation rates (R_{2eff}) at each CPMG frequency were calculated using the following Equation 4.4[1]:

$$R_{2eff} \ = \ -\frac{1}{T_{relax}}\ln(\frac{I_{v_{CPMG}}}{I_0}) \tag{4.4}$$

where I_0 is the peak intensity in the reference spectrum and $I_{v_{CPMG}}$ is the intensity with CPMG frequency of v_{CPMG} The effective relaxation rates (R_{2eff}) were then plotted against CPMG frequency v_{CPMG}.

Hetero-nuclear Adiabatic Relaxation Dispersion (HARD) experiments[12–14] were performed at a magnetic field strength of 600 MHz according to the geoHARD[14] method for both the protein samples. A composite pulse containing four hyperbolic secant family (HSn, where n= stretching factor) adiabatic pulses with different stretching factors (n = 1,2,4,6,8) were used to create relaxation dispersion in both $R_{1\rho}$ and $R_{2\rho}$ experiments. Relaxation rates ($R_{1\rho}$ and $R_{2\rho}$) with every pulse were measured by varying the relaxation delay by varying the number of pulses applied from 0, 1, 2, 3, and 4. This lead to the generation of relaxation delays corresponding to 0, 16, 32, 48, and 64 ms, respectively. R_1 experiments were recorded in the same way without using an adiabatic pulse during evolution. Relaxation delays as multiple loops of a fixed delay of 16 ms, which is a duration of application of adiabatic pulses in $R_{1\rho}$ and $R_{2\rho}$ experiments, used for R_1 experiments were 16, 48, 96, 192, 320, and 480 ms. The details of the acquisition parameters for the HARD experiment have been listed in Table 4.1.

For HARD data analysis, the relaxation rates (R_1, $R_{1\rho}$, and $R_{2\rho}$) were calculated by using the mono-exponential decay equation (Equation 4.2) in Mathematica5.2[5], as described for Nuclear spin relaxation rates. These relaxation rates in the rotating frame ($R_{1\rho}$ and $R_{2\rho}$) along with the global rotational

correlation time (τ_C) calculated from the model-free analysis and intrinsic R_1 rates were used to fit the time-dependent Bloch-McConnell equation assuming two-site exchange model. A grid search by Monte Carlo method from the solution surfaces of the data points generated from the Bloch-McConnell equation by geometric approximation method allowed to extract the chemical exchange parameters which included exchange rate between two states – state A and state B – (k_{ex}), chemical shift difference between the two states ($\Delta\omega$) and populations of the two states (p_A/p_B).

Table 4.1: Experimental parameters used for the relaxation data acquisition for TRBP2-dsRBD1 and dADAR-dsRBD1.

Experiment (Pulse Sequence used)	Nucleus	TD[a]	SW[b] (ppm)	Offset (ppm)	NS[c]	d1[d] (s)
^{15}N-R_1 (hsqct1etf3gpsi3d)	^{1}H ^{15}N Delay	2048 128 12	12 28	4.69 117.00	8	2.5
^{15}N-R_2 (hsqct2etf3gpsi3d)	^{1}H ^{15}N Delay	2048 128 10	12 28	4.70 117.00	8	2.5
[^{1}H]-^{15}N-NOE (hsqcnoef3gpsi)	^{1}H ^{15}N	2048 40	12 28	4.70 117.00	16	5.0
^{15}N-CPMG-RD (hsqcrexetf3gpsi3d)	^{1}H ^{15}N Delay	2048 256 12	12 28	4.71 117.00	16	2.5
^{15}N-R_1 - HARD (r1.fc)	^{1}H ^{15}N	2048 256	12 28	4.69 117.00	8	2.5
^{15}N-$R_{1\rho}$ - HARD (r1rho.fc)	^{1}H ^{15}N	2048 200	12 28	4.69 117.00	16	2.5
^{15}N-$R_{2\rho}$ - HARD (r2rho.fc)	^{1}H ^{15}N	2048 200	12 28	4.69 117.00	16	2.5
^{15}N-R_1 (hsqct1etf3gpsi3d)	^{1}H ^{15}N Delay	2048 256 10	12 31	4.69 117.00	24	3.0
^{15}N-R_2 (hsqct2etf3gpsi3d)	^{1}H ^{15}N Delay	2048 256 10	12 31	4.69 117.00	24	3.0
[^{1}H]-^{15}N-NOE (hsqcnoef3gpsi)	^{1}H ^{15}N	2048 256	12 31	4.69 117.00	48	5.0
^{15}N-CPMG-RD (hsqcrexetf3gpsi3d)	^{1}H ^{15}N Delay	2048 256 12	12 31	4.69 117.00	24	3.0
^{15}N-R_1 - HARD (r1.fc)	^{1}H ^{15}N	2048 256	12 31	4.71 117.00	16	3.0
^{15}N-$R_{1\rho}$ - HARD (r1rho.fc)	^{1}H ^{15}N	2048 200	12 31	4.71 117.00	24	3.0
^{15}N-$R_{2\rho}$ - HARD (r2rho.fc)	^{1}H ^{15}N	2048 200	12 31	4.70 117.00	24	3.0

[a]TD: Number of data points/size of fid, [b]SW: Spectral Width, [c]NS: Number of scans, [d]d1: relaxation delay

4.3.   *Results*

4.3.1.   *Size-Exclusion Chromatography - Multi-Angle Light Scattering Analysis*

Homogeneity of the protein samples used in this study to record the NMR experiments were analyzed using SEC-MALS analysis using unlabeled protein samples. The analysis of the BSA sample by SEC-MALS showed a distinct peak at a molecular weight of 62.12 kDa (±0.39%). This was used as a reference point to eliminate any errors in the SEC-MALS system. SEC-MALS data shows two peaks for TRBP2-dsRBD1 with molecular weights of 38.98 kDa (±0.95%) and 10.24 kDa (±1.16%), which correspond to a tetrameric and a monomeric form, respectively, of the protein (Figure 4.1). The quantification of peaks for TRBP2-dsRBD1 shows that the monomer to tetramer ratio was 4:1 at the experimental conditions. For dADAR-dsRBD1, a single peak corresponding to the molecular weight of 12.46 kDa (±1.49%) was observed, which corresponded to the molecular weight of the monomeric protein used in the study.
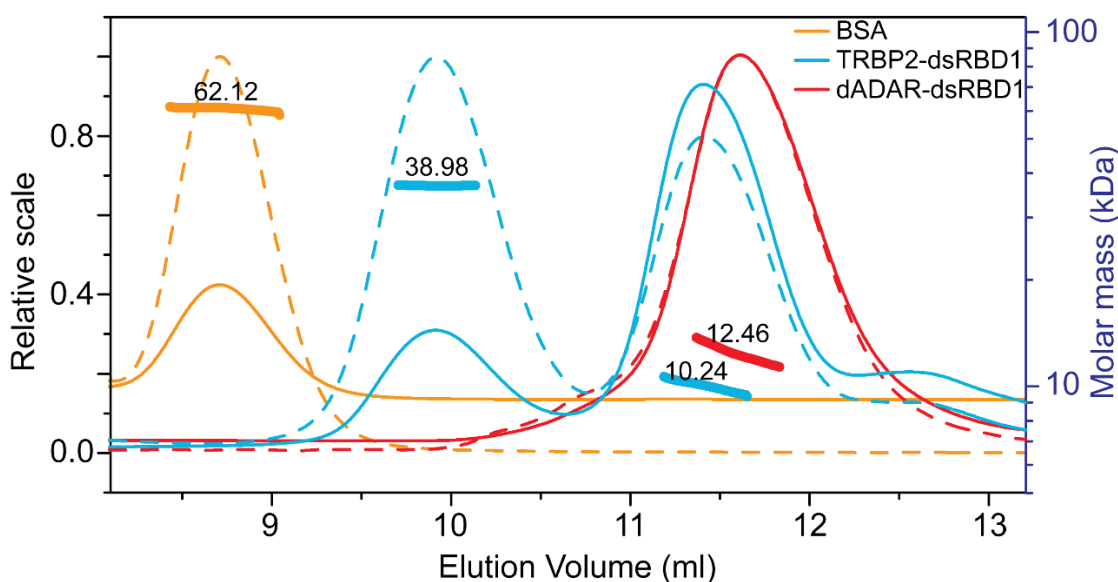
Figure 4.1: SEC-MALS analysis of Reference protein BSA (Orange), TRBP2-dsRBD1 (Cyan) and dADAR-dsRBD1 (Red). The plots show the signal from the MALS detector (Dashed line) and from the RI detector (Solid line) and the molecular mass calculated is marked as a bold bar for each peak and mentioned on the bar.

4.3.2.   *Circular Dichroism Spectropolarimetry*

To test the thermal stability of the protein at the NMR working conditions, CD-based melting studies were performed. An increase in the CD signal recorded in the far-UV region with increasing temperature suggested unfolding of the secondary structures in the protein as shown in Figure 4.2 A, B. The first order derivative plot of fraction folded at each temperature[2] helped to extract the melting temperature of unfolding event (Figure 4.2 C, D). Both the proteins showed a melting temperature of 45°C suggesting lower thermal stability present in two proteins.
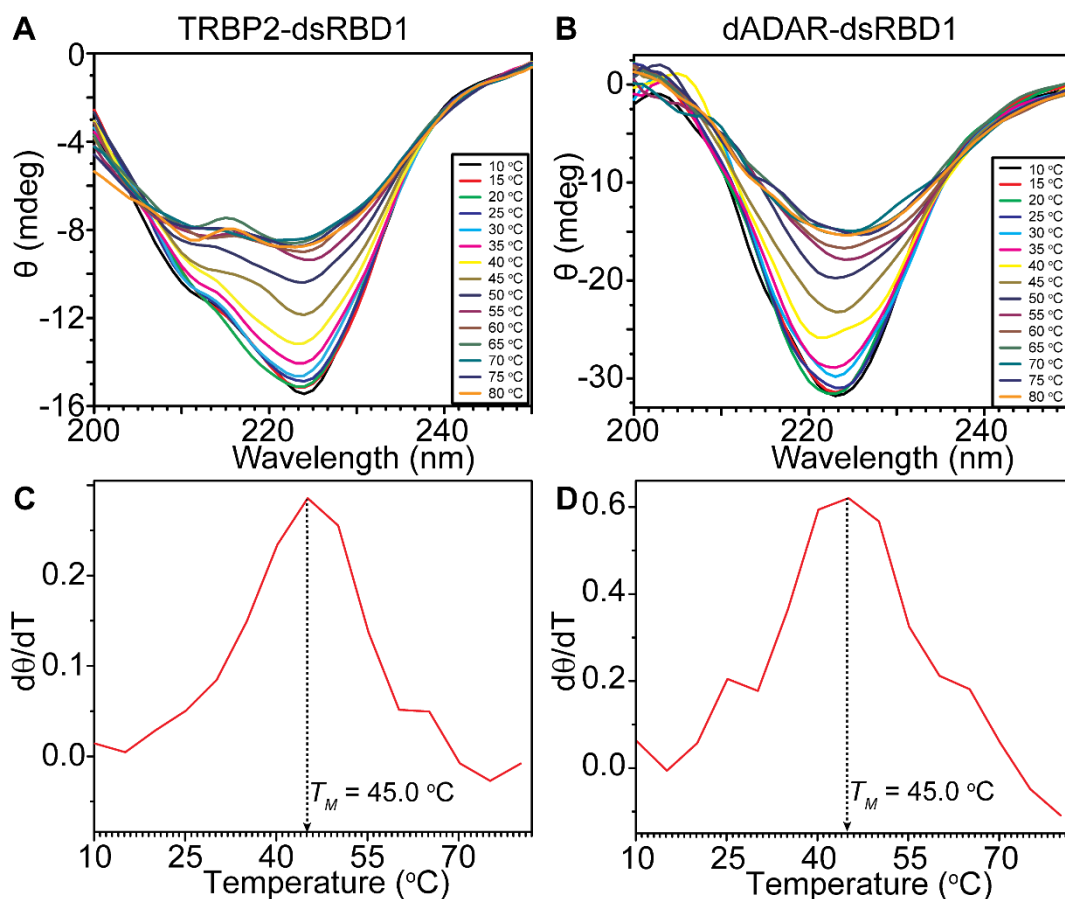
Figure 4.2: Thermal melting studies for TRBP2-dsRBD1 and dADAR-dsRBD1 by Circular Dichroism. Far-UV CD-spectra for (**A**) TRBP2-dsRBD1 and (**B**) dADAR-dsRBD1 recorded at a temperature ranging from 10°C to 80°C at an interval of 5°C. The first derivative plot of Fraction folded (calculated from Equation 1) against temperature to determine melting temperature of unfolding for (**C**) TRBP2-dsRBD1 and (**D**) dADAR-dsRBD1.

4.3.3. *NMR Spectroscopy: Nuclear Spin Relaxation*

To characterize the motions occurring at ps-ns timescale in both the proteins, 69 out of 96 and 58 out of 74 non-overlapping peaks in ^{1}H-^{15}N-HSQC spectra for TRBP2-dsRBD1 and dADAR-dsRBD1, respectively, were analyzed. The calculated nuclear spin relaxation rates (R_1, R_2 and [^{1}H]-^{15}N-NOE) have been plotted against the residue number in Figure 4.3 and have been listed in Appendix Table A.1 and Table A.2.

It was observed from the analysis of this primary data that the residues in the structured region show lower R_1 rates at 750 Hz than those at 600 Hz for both the proteins; while the N-terminal of TRBP2-dsRBD1 clearly show higher rates at 750 Hz. Thus, we hypothesized that residues in structured regions contribute to the global motions of the protein at ps-ns timescale. Dispersion in the R_2 rates in the residues along the protein chain and the higher R_2 rates at 750 MHz than at 600 MHz point toward the presence of slow timescale motions at µs-ms timescale in these residues in both the proteins. Specifically, residue L35, K44, T45, Q56, A57, A82, A88, E89 in TRBP2-dsRBD1 and G85, A89, K102, Y103, A119, A121 in dADAR-dsRBD1 which are present either in the RNA-Binding regions or

in their close proximity or present in the loop areas of the protein chain show significant deviation from the nearby residues. [^{1}H]-^{15}N-NOE values show a dip at the loop regions and the RNA-binding regions suggesting the presence of higher flexibility in these residues relative to the rest of the structured region of the protein. From this preliminary analysis, the data were further analyzed using an extended model-free approach[15–18] to extract the dynamics parameters. The plot of residue specific correlation time (represented as local τ_M) for both the proteins (Appendix Figure A.1) shows that the terminal regions and the loop areas of the protein have relatively fast motions at ps-ns timescale than the structured region of the protein. The field dependent variation in the Tm values further supports the presence of conformational exchange processes occurring on μs-ms timescale as proposed from the R_2 rates. The calculated model-free parameters have been listed in Table 4.2 and Table 4.3 for TRBP2-dsRBD1 and dADAR-dsRBD1, respectively.
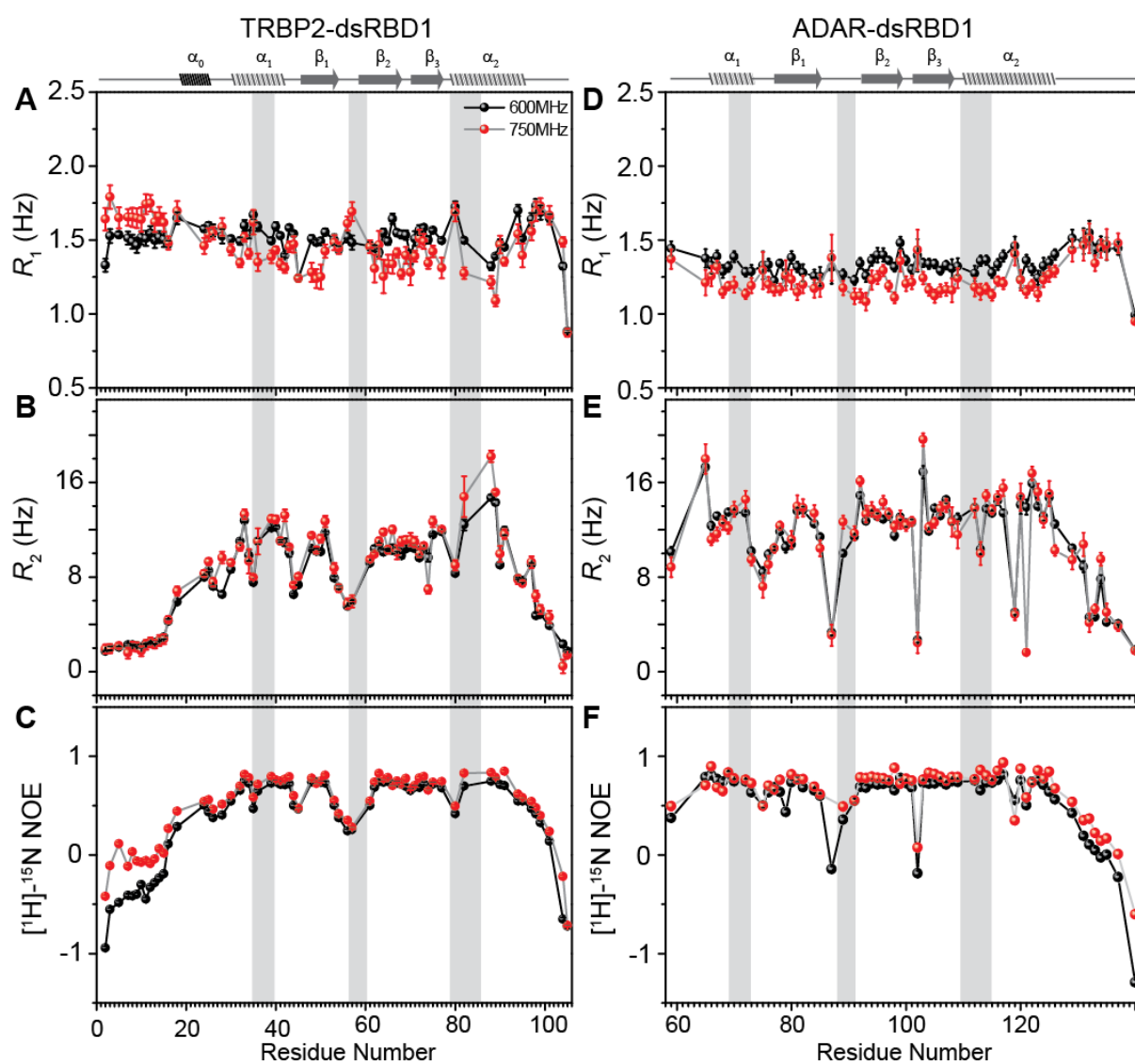
Figure 4.3: ^{15}N-Nuclear spin relaxation rates R_1 (**A** and **D**), R_2 (**B** and **E**) and [^{1}H]-^{15}N-NOE (**C** and **F**) for TRBP2-dsRBD1 and dADAR-dsRBD1. Data recorded at 600 MHz is represented in Black and data at 750 MHz is represented in Red. The secondary structure of the protein has been marked on top of each column and RNA-binding regions have been highlighted in grey.

The initial optimization of global diffusion tensor parameters for TRBP2-dsRBD1 by *quadric_diffusion*[8] protocol suggested that the anisotropic diffusion model could best explain the global motion of the protein. The global and local motions in the protein were then analyzed using the Relax[6,7] program, as discussed in the Methods section. The residue-specific order parameters (S^2) calculated for TRBP2-dsRBD1 were plotted against residue numbers and have been shown in Figure 4.4. As can be observed from Figure 4.4, large variations of S^2 values were observed in the structured regions of the protein. The N- and C-terminal showed values close to zero which were suggestive of high amplitude motions occurring in these terminal residues. The residues in the α_0 helix showed S^2 value higher than the terminal residues but lower than the dsRBD core suggesting higher flexibility in the residues than dsRBD core. The average S^2 value of the structured dsRBD core (31 - 95 aa) was 0.61, which suggested large flexibility in the dsRBD core. This was further supported by 78% of the residues analyzed that showed the best fit for the model-free models with two timescales. The faster motions at 40-150 ps reflected the random thermal motions that were mainly observed in the flexible termini and the loop regions of the protein, while motions at 1-4 ns timescale were also detected throughout the protein chain. Optimization of global diffusion tensor with the internal model-free models defined showed that anisotropic model can best define the diffusion tensor with a rotational correlation time of 7.64 ns. The anisotropic diffusion motion of the protein was also represented by the D_{xx} = 0.75e-7 rad/s, D_{yy} = 1.31e-7 rad/s and D_{zz} = 4.52e-7 rad/s and the Euler angles as α = 1.12 rad, β = 1.87 rad, and γ = 2.06 rad.

The global motions for dADAR-dsRBD1 were also predicted to be represented by the anisotropic model by the *quadric_diffusion*[8] program and further optimized by the Relax[6,7] program. The order parameters calculated for dADAR-dsRBD1 showed relatively rigid protein than TRBP-dsRBD1 with average order parameters of 0.80 in structured regions (65-125 aa) (Figure 4.4). The order parameters in the RNA-binding regions and the loop had lower S^2 value suggesting a higher amplitude of motions than the structured area in the protein at ps-ns time scale. 59% of the analyzed residues showed best fit to the model-free model with two timescales of faster 10-100 ps and slower ns motions at about 2 ns that were spread across the residues in the structured regions of the protein. The global rotational correlation time for dsRBD1 of dADAR was calculated to be 9.39 ns with anisotropic model defining the global motion of the protein. The diffusion tensor parameters for dADAR-dsRBD1 were obtained as D_{xx} = 1.25e-7 rad/s, D_{yy} = 1.75e-7 rad/s and D_{zz} = 2.33e-7 rad/s and the Euler angles as α = 1.13 rad, β = 2.05 rad, and γ = 1.44 rad.
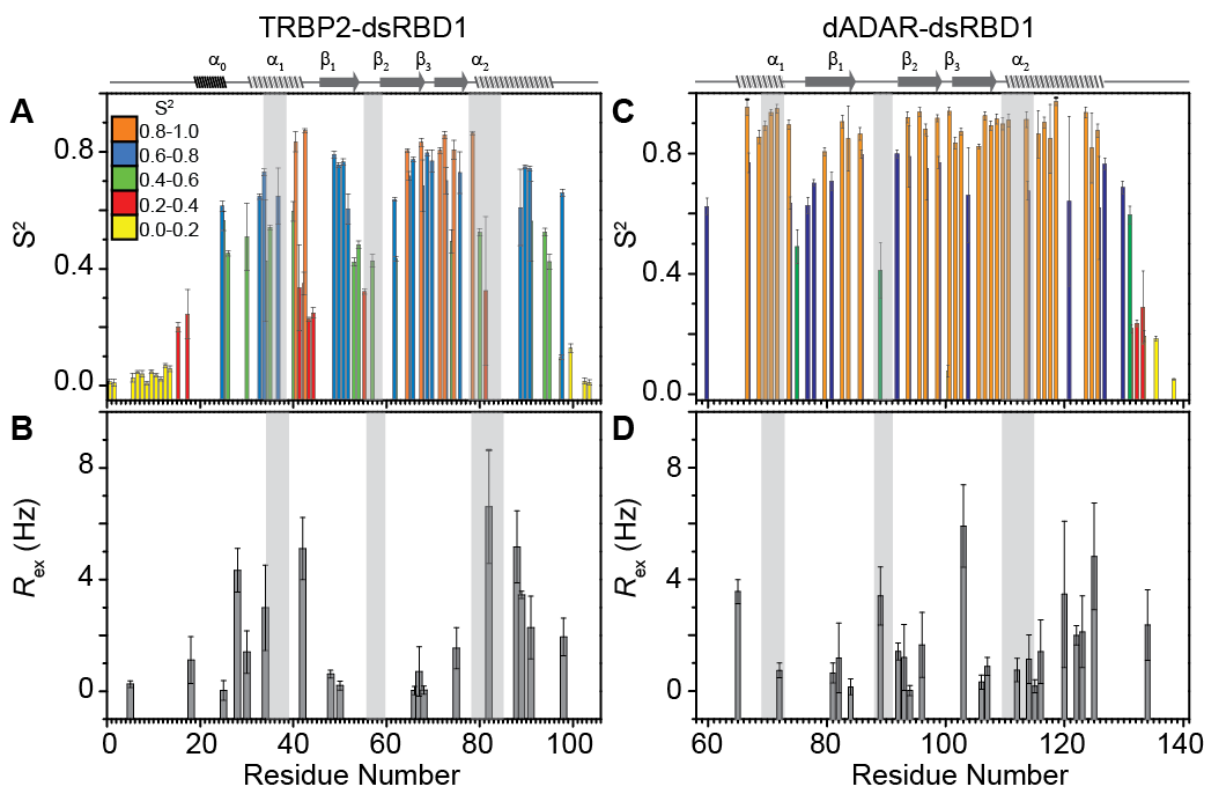
Figure 4.4: Model-free analysis of TRBP2-dsRBD1 and dADAR-dsRBD1. Plot of Order parameters (S^2) against residue number (**A**) for TRBP2-dsRBD1 and (**C**) for dADAR-dsRBD1. The colour codes used to represent the S^2 values have been mentioned as the inset in panel A. The plot of R_{ex} values indicating the presence of slow motions in (**B**) TRBP2-dsRBD1 and (**D**) dADAR-dsRBD1. The secondary structure of the protein has been marked on top of each column and RNA-binding regions have been highlighted in grey.

The model-free approach also showed residues having slower motions at µs-ms timescale as indicated by best fit to the model containing exchange R_{ex} term. Both dsRBD1 of TRBP2 and dADAR showed the presence of residues that have slow motions present spread in different residues along the protein backbone (Figure 4.4) and are not limited to the RNA-binding residues. TRBP2-dsRBD1 showed the presence of R_{ex} in residues close to RNA-binding regions (L34, G75, A82) and also in the residues (E5, S18, A25, G28, T30, I42, Y48, L50, V66, T67, V68, A88, E89, A91, and G98). Similarly, dADAR-dsRBD1 showed conformational exchange in residues in the vicinity of the RNA-binding residues (T65, L72, A89, F92, Q106, G107, V112, R114, I115, E116) and other residues (E81, S82, T84, T93, I94, V96, Y103, T120, L122, R123, F125, L134). Although some of the residues showed minimum R_{ex} values (< 2 Hz) in both the proteins, the presence of any slower motions need to be tested in more details by relaxation dispersion experiments.

Table 4.2: Model-free parameters for TRBP2-dsRBD1 extracted from the nuclear spin relaxation data recorded at 600 MHz and 750 MHz NMR spectrometer.

Residue Number	S^2		R_{ex} (Hz)		S^2_f		S^2_s		τ_e (ps)		τ_f (ps)		τ_s (ps)	
	value	error	value	error	value	error	value	error	value	error	value	error	value	error
S2	0.01	0.01			0.73	0.04	0.02	0.01			100	23	757	47
E3	0.01	0.01			0.77	0.04	0.01	0.02			96	23	921	53
E5	0.00	0.01	0.25	0.12	0.83	0.01							891	13

Residue Number	S^2		R_{ex} (Hz)		S^2_f		S^2_s		τ_e (ps)		τ_f (ps)		τ_s (ps)	
	value	error	value	error	value	error	value		value	error	value	error	value	error
G7	0.03	0.01			0.58	0.03	0.05	0.02			118	10	1348	119
S8	0.05	0.01			0.84	0.02	0.06	0.01					846	8
G9	0.04	0.01			0.65	0.03	0.06	0.02			92	12	1145	87
T10	0.01	0.01			0.51	0.02	0.03	0.01			105	7	1627	142
T11	0.05	0.01			0.74	0.04	0.07	0.01			95	18	990	63
T12	0.04	0.01			0.56	0.03	0.08	0.01			134	11	1533	141
G13	0.02	0.01			0.54	0.02	0.10	0.01			101	9	1407	105
C14	0.07	0.01			0.67	0.03	0.12	0.01			78	9	1200	83
G15	0.06	0.01			0.56	0.03	0.18	0.02			98	8	1553	140
L16	0.20	0.02			0.63	0.02	0.38	0.02			56	6	1529	153
S18	0.24	0.08	1.12	0.84	0.73	0.06	0.36	0.10			43	11	1586	269
A24	0.61	0.02			0.78	0.02	0.80	0.02			52	10	1506	770
A25	0.56	0.03	0.03	0.35	0.90	0.02	0.66	0.03					1084	55
N26	0.45	0.01			0.78	0.03	0.68	0.02			65	12	1623	279
G28	0.00	0.05	4.33	0.78	0.54	0.04					25	5	2287	247
T30	0.51	0.12	1.40	0.76	0.70	0.06	0.69	0.13			23	8	1685	1125
I32	0.65	0.01			0.88	0.01	0.92	0.01					1574	76
S33	0.73	0.01							2552	231				
L34	0.43	0.21	2.99	1.53	0.70	0.08	0.58	0.25					3121	1148
L35	0.54	0.01			0.87	0.01	0.60	0.01					1156	40
Q36	0.65	0.10			0.91	0.06	0.84	0.08					1679	210
G39	0.83	0.03			0.93	0.02	0.95	0.02					1457	265
T40	0.60	0.03			0.91	0.02	0.90	0.02					2613	214
R41	0.87	0.01							43	5				
I42	0.34	0.15	5.11	1.11	0.62	0.06	0.51	0.20					2933	743
G43	0.35	0.04			0.77	0.02	0.75	0.04					3037	234
K44	0.23	0.01			0.68	0.02	0.61	0.01			21	6	2179	268
T45	0.25	0.02			0.59	0.02	0.71	0.02			31	3	2434	299
Y48	0.79	0.01	0.61	0.14					16	3				
D49	0.76	0.01							20	3				
L50	0.77	0.01	0.21	0.16					19	3				
L51	0.61	0.05			0.88	0.03	0.87	0.04					2836	332
A53	0.42	0.01			0.74	0.02	0.73	0.02			42	7	2264	444
E54	0.48	0.01			0.69	0.02	0.68	0.02			54	7	1623	405
Q56	0.32	0.01			0.69	0.03	0.47	0.02			63	8	1630	247
A57	0.43	0.02			0.65	0.02	0.56	0.03			87	8	2077	812
N61	0.64	0.01			0.80	0.02	0.83	0.02			50	12	1369	454
F62	0.43	0.01			0.75	0.01	0.89	0.01					2367	138
T63	0.80	0.01							8	3				
F64	0.72	0.01			0.85	0.01	0.94	0.02					1825	220
R65	0.77	0.01							14	3				
V66	0.83	0.01	0.03	0.15					42	6				
T67	0.68	0.09	0.71	0.88	0.82	0.04	0.80	0.07					1719	501
V68	0.80	0.01	0.04	0.14					31	3				

Residue Number	S^2 value	error	R_{ex} (Hz) value	error	S^2_f value	error	S^2_s value	error	τ_e (ps) value	error	τ_f (ps) value	error	τ_s (ps) value	error
G69	0.77	0.04			0.85	0.02	0.92	0.03					1072	293
D70	0.81	0.01							45	4				
T71	0.86	0.01							56	7				
S72	0.70	0.04			0.84	0.02	0.88	0.04					1608	258
C73	0.81	0.03			0.86	0.02	0.96	0.03					993	367
T74	0.49	0.04			0.69	0.01	0.83	0.05			25	4	6605	2360
G75	0.73	0.07	1.54	0.74	0.84	0.03	0.84	0.05					1283	464
G77	0.86	0.01							46	5				
K80	0.52	0.01			0.84	0.03	0.71	0.02			98	18	1706	365
A82	0.32	0.25	6.61	2.03	0.63	0.09	0.45	0.33					3985	1712
A88	0.61	0.13	5.17	1.29	0.75	0.06	0.84	0.12					2925	1309
E89	0.75	0.01	3.45	0.13					10	2				
V90	0.74	0.01												
A91	0.56	0.14	2.28	1.12	0.74	0.06	0.69	0.14					2661	932
H94	0.53	0.01			0.79	0.02	0.67	0.02			36	12	1966	640
L95	0.42	0.02			0.70	0.02	0.74	0.03			36	5	2920	1135
G97	0.66	0.01			0.85	0.03	0.74	0.03			55	23	1049	375
G98	0.00	0.08	1.95	0.67	0.58	0.04					44	6	3521	594
S99	0.10	0.01			0.63	0.02	0.37	0.01			66	6	2383	274
L101	0.13	0.01			0.59	0.02	0.28	0.02			84	5	2246	282
A104	0.02	0.01			0.64	0.03	0.03	0.02			74	9	865	43
L105	0.01	0.01			0.21	0.00	0.07	0.04			70	1	3760	473

Table 4.3: Model-free parameters for dADAR-dsRBD1 calculated from the nuclear spin relaxation data recorded at 600 MHz and 750 MHz NMR spectrometer.

Residue Number	S^2 value	error	R_{ex} (Hz) value	error	S^2_f value	error	S^2_s value	error	τ_e (ps) value	error	τ_f (ps) value	error	τ_s (ps) value	error
I59	0.62	0.03			0.92	0.02	0.70	0.02					874	61
T65	0.95	0.03	3.56	0.43					91	326				
V66	0.77	0.03			0.86	0.02	0.93	0.04					4235	2292
A67	0.85	0.02			0.95	0.02	0.92	0.02					1398	357
M68	0.89	0.01							64	16				
L69	0.94	0.01												
N70	0.95	0.02							94	102				
L72	0.90	0.02	0.74	0.27					43	12				
R73	0.63	0.02			0.81	0.02	0.81	0.02					1354	138
G75	0.49	0.06			0.69	0.03	0.74	0.07			48	13	3040	2513
L76	0.63	0.03			0.81	0.02	0.80	0.02					1381	144
I77	0.70	0.01			0.82	0.01	0.88	0.01					1127	144
Y78	0.81	0.01			0.91	0.01	0.92	0.01					841	118
L80	0.71	0.03			0.84	0.02	0.87	0.02					2022	589
E81	0.91	0.02	0.65	0.35					39	18				
S82	0.85	0.11	1.19	1.25	0.92	0.07	0.92	0.06					799	584
T84	0.86	0.02	0.15	0.29					66	15				

Residue Number	S^2		R_{ex} (Hz)		S^2_f		S^2_s		τ_e (ps)		τ_f (ps)		τ_s (ps)	
	value	error	value	error	value	error	value		value	error	value	error	value	error
G85	0.80	0.01							56	8				
A89	0.41	0.09	3.41	1.03	0.73	0.05	0.57	0.09					1063	145
L91	0.80	0.01							72	8				
F92	0.92	0.02	1.42	0.31					80	57				
T93	0.79	0.10	1.20	1.18	0.86	0.07	0.92	0.06					803	624
I94	0.94	0.01	0.02	0.19					80	43				
S95	0.88	0.02			0.97	0.01	0.93	0.01					1089	225
V96	0.75	0.11	1.65	1.16	0.90	0.06	0.84	0.06					1709	504
E97	0.92	0.01							67	16				
V98	0.77	0.02			0.87	0.01	0.91	0.01					1126	197
D99	0.94	0.01							84	98				
G100	0.83	0.02			0.91	0.01	0.94	0.01					1107	241
Q101	0.87	0.01							55	10				
K102	0.08	0.02			0.59	0.06	0.13	0.03			62	16	1247	196
Y103	0.66	0.16	5.91	1.47	0.81	0.09	0.81	0.13					1917	825
L104	0.82	0.01			0.90	0.01	0.94	0.01					1231	275
G105	0.92	0.01							56	17				
Q106	0.89	0.01	0.32	0.25					35	11				
G107	0.91	0.02	0.88	0.32					70	31				
R108	0.90	0.02							38	34				
S109	0.91	0.02							49	77				
V112	0.91	0.03	0.75	0.42					46	68				
A113	0.68	0.03			0.83	0.02	0.84	0.02					1546	229
R114	0.86	0.08	1.14	0.87	0.93	0.05	0.94	0.04					1075	665
I115	0.90	0.02	0.17	0.23					51	14				
E116	0.85	0.11	1.41	1.14	0.92	0.06	0.92	0.07					1641	1408
A117	0.97	0.01												
T120	0.64	0.28	3.46	2.62	0.77	0.15	0.83	0.29					2614	2205
L122	0.94	0.02	1.99	0.35					87	85				
R123	0.82	0.12	2.12	1.28	0.87	0.08	0.94	0.07					1459	1547
S124	0.88	0.02			0.95	0.02	0.94	0.02					957	266
F125	0.62	0.17	4.82	1.91	0.81	0.10	0.76	0.15					1648	577
I126	0.76	0.02			0.94	0.01	0.84	0.02					926	88
K129	0.69	0.02							922	59				
G131	0.60	0.03							763	53				
A132	0.22	0.01			0.81	0.03	0.28	0.02					1059	27
V133	0.24	0.01			0.65	0.05	0.38	0.02			60	16	1354	275
L134	0.29	0.12	2.37	1.26	0.69	0.10	0.42	0.14			91	40	1257	468
S135	0.19	0.02			0.62	0.05	0.32	0.03			72	15	1475	333
L137	0.18	0.01			0.66	0.06	0.29	0.03			93	19	1153	213
A140	0.05	0.00			0.68	0.00	0.08	0.00					505	6

4.3.4. NMR Spectroscopy: Relaxation Dispersion

4.3.4.1. CPMG Relaxation Dispersion

Having identified the presence of slow μs-ms motions in different residues distributed along the protein chain was a driving factor to characterize these motions by relaxation dispersion method. The CPMG relaxation dispersion[1,11] method was applied to extract the dynamics parameters. CPMG relaxation dispersion method is suitable to characterize exchange events occurring at 0.3-10 ms timescale ($k_{ex} \approx$ 10-3000 s^{-1})[1]. The effective relaxation rates (R_{2eff}) at a range of applied CPMG frequencies were calculated by Equation 4.7. These rates measured at different CPMG frequencies have been listed in Appendix Table A.3 - Table A.6 and plotted against the CPMG frequencies (ν_{CPMG}). The plots showed no dispersion in the relaxation rates in all the residues for TRBP2-dsRBD1 (Figure 4.5) and for dADAR-dsRBD1 (Figure 4.6). This could occur if there are no motions occurring at μs-ms timescale or the motions are outside the detection limit of the CPMG relaxation dispersion method. Since the presence of slow-motions in the protein is indicated by R_{ex} values detected from the model-free analysis and no dispersion is observed in the R_{2eff} values, it can be concluded that the dynamics in dsRBDs studied are outside this exchange regime and may involve motions at μs timescale.
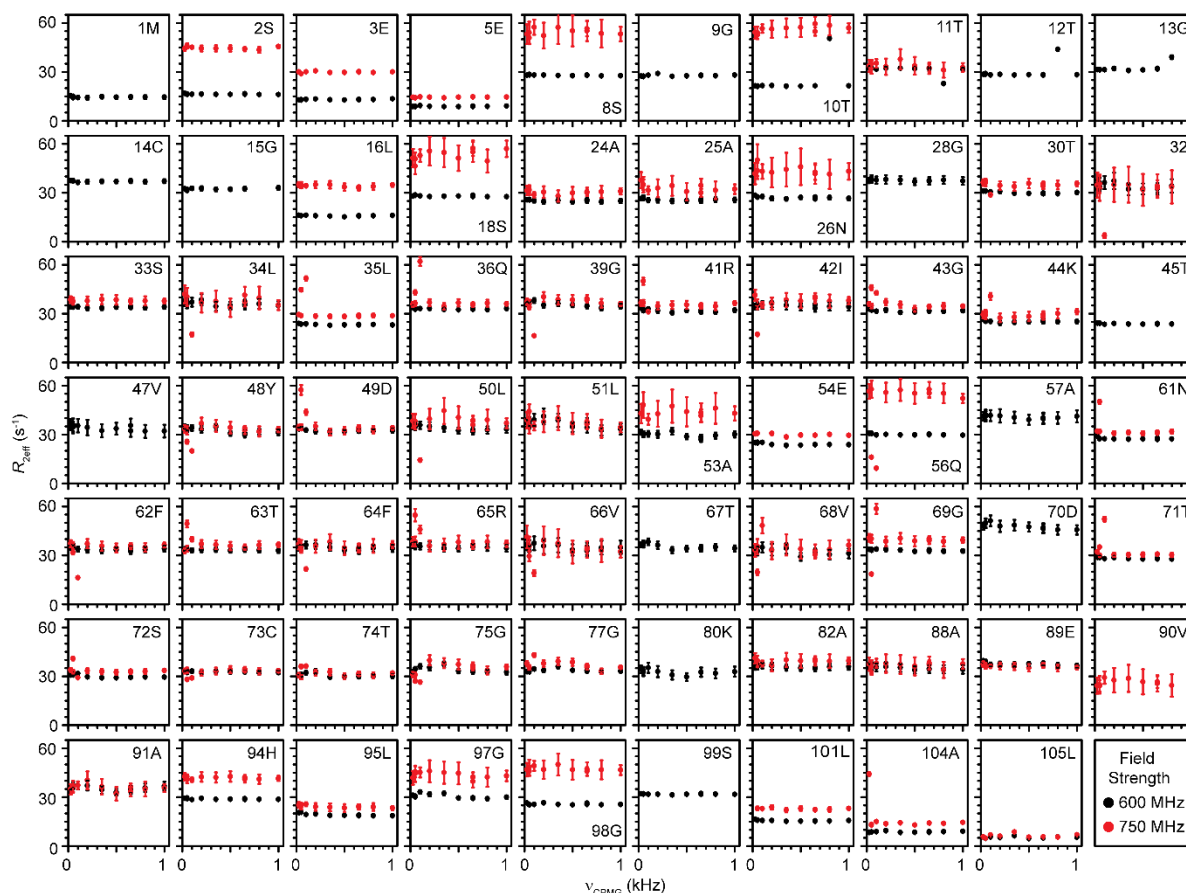
Figure 4.5: Effective relaxation rates (R_{2eff}) plotted against for CPMG frequencies for TRBP2-dsRBD1 (Residue name and number are indicated in each plot).
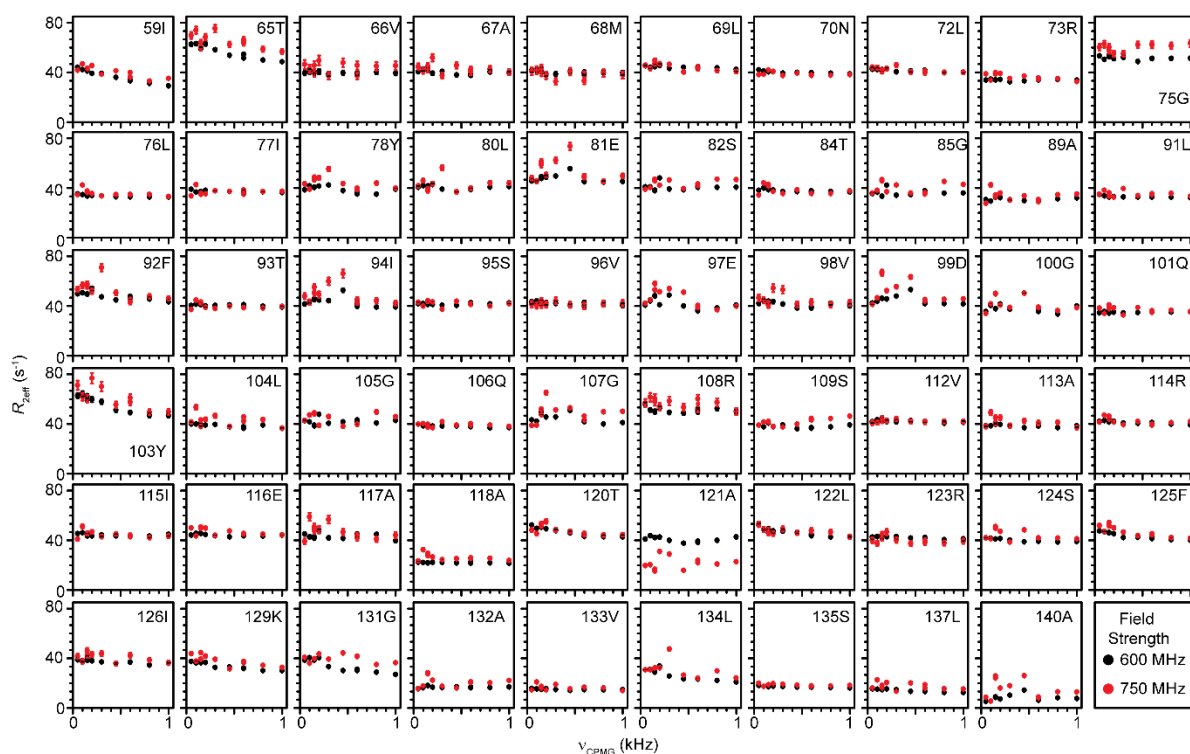
Figure 4.6: Effective relaxation rates ($R_{2\text{eff}}$) plotted against for CPMG frequencies for dADAR-dsRBD1 (Residue name and number are indicated in each plot).

4.3.4.2. Hetero-nuclear Adiabatic Relaxation Dispersion

Since the CPMG relaxation dispersion method was not able to detect the exchange event in the dsRBDs, we moved to an advanced $R_{1\rho}$ type of relaxation dispersion method – Heteronuclear Adiabatic Relaxation Dispersion method. The adiabatic relaxation rates (longitudinal $R_{1\rho}$ and transverse $R_{2\rho}$) were determined for 69 and 59 non-overlapping peaks for TRBP2-dsRBD1 and dADAR-dsRBD1, respectively. As described in section 2.5.2.2, the HARD NMR experiments use hyperbolic secant family (HSn, where n = stretching factor) adiabatic pulses of different shapes (created by different stretching factors n = 1,2,4,6,8) that lead to the application of different spin-lock field strengths. These different spin-lock allows to create dispersion in the detected adiabatic relaxation rates. The $R_{1\rho}$ and $R_{2\rho}$ relaxation rates thus obtained have been listed in Appendix Table A.7 - Table A.10. The plot of the longitudinal ($R_{1\rho}$) and transverse ($R_{2\rho}$) relaxation rates in the rotating frame as a function of the stretching factor have been shown in Figure 4.7 for a few residues in the two proteins. The observed dispersion in the relaxation rates ($R_{1\rho}$ and $R_{2\rho}$) indicate that the method was able to detect the chemical exchange phenomenon in these residues in the proteins. Such dispersion in the $R_{1\rho}$ and $R_{2\rho}$ relaxation rates was observed in the several residues present along the protein chain as the shape of the applied adiabatic pulse was changed (Figure 4.8). As observed in the case of the R_{ex} values determined from the model-free analysis, the dispersion in adiabatic relaxation rates was found to be present in many residues in the protein and was not limited only to the RNA-binding regions.
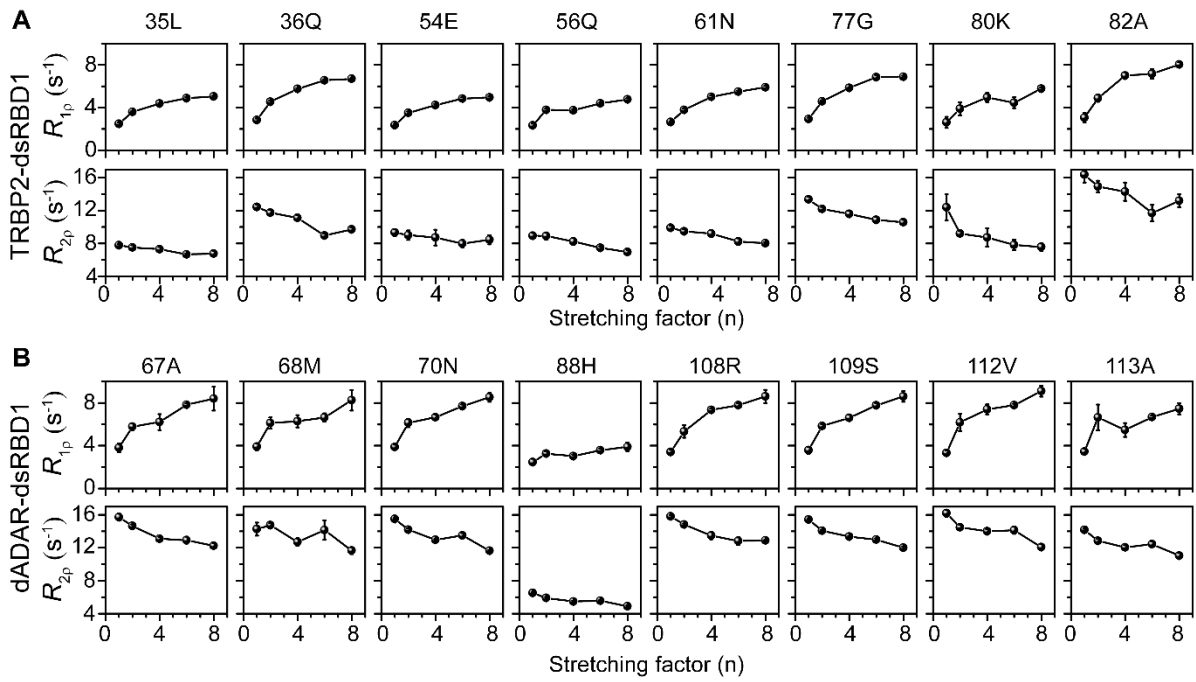
Figure 4.7: Representative plot of $R_{1\rho}$ and $R_{2\rho}$ rates against stretching factor (n) of Hyperbolic Secant pulses for a few residues in the (**A**) TRBP2-dsRB1 and (**B**) dADAR-dsRBD1. The protein name is indicated at the left side of the plots and the residue number is indicated on top of each set plot ($R_{1\rho}$ and $R_{2\rho}$).
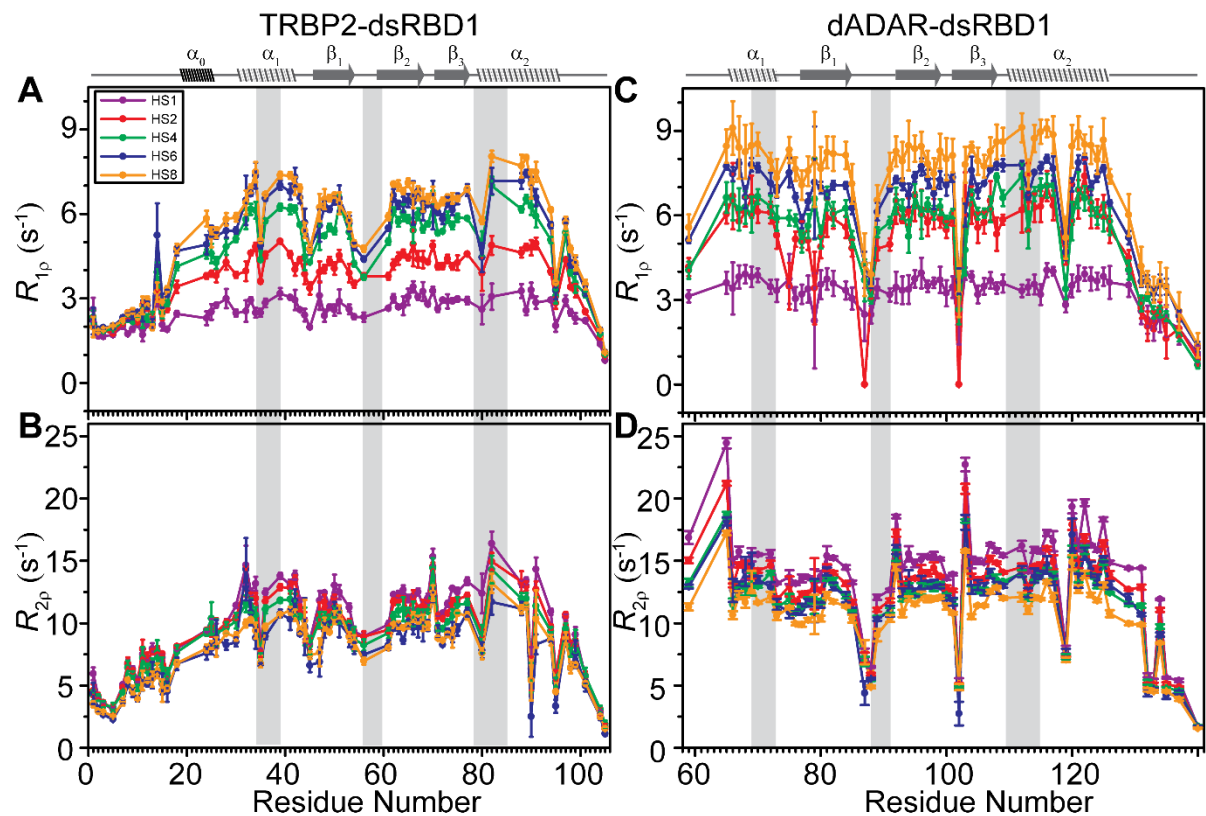
Figure 4.8: Dispersion in the adiabatic relaxation rates in dsRBDs. The plot of $R_{1\rho}$ (**A**) and $R_{2\rho}$ (**B**) rates against residue number for TRBP2-dsRBD1 and $R_{1\rho}$ (**C**) and $R_{2\rho}$ (**D**) rates against residue number for dADAR-dsRBD1. The colours indicate the Hyperbolic Secant (HSn, where n=1,2,4,6,8) adiabatic pulse used for spin-locking and have been mentioned in the inset. The secondary structure of the protein has been marked on top of each column and RNA-binding regions have been highlighted in grey.

These adiabatic relaxation rates were fit to the Bloch-McConnell equation assuming a two-site exchange model to calculate the dynamics parameters describing the chemical exchange event i.e. k_{ex} (kinetic), $\Delta\omega$ (structural), and p_B (thermodynamics) by geometric approximation method. The calculated parameters were mapped on to the structures as shown in Figure 4.9 and listed in Appendix Table A.11 and Table A.12.
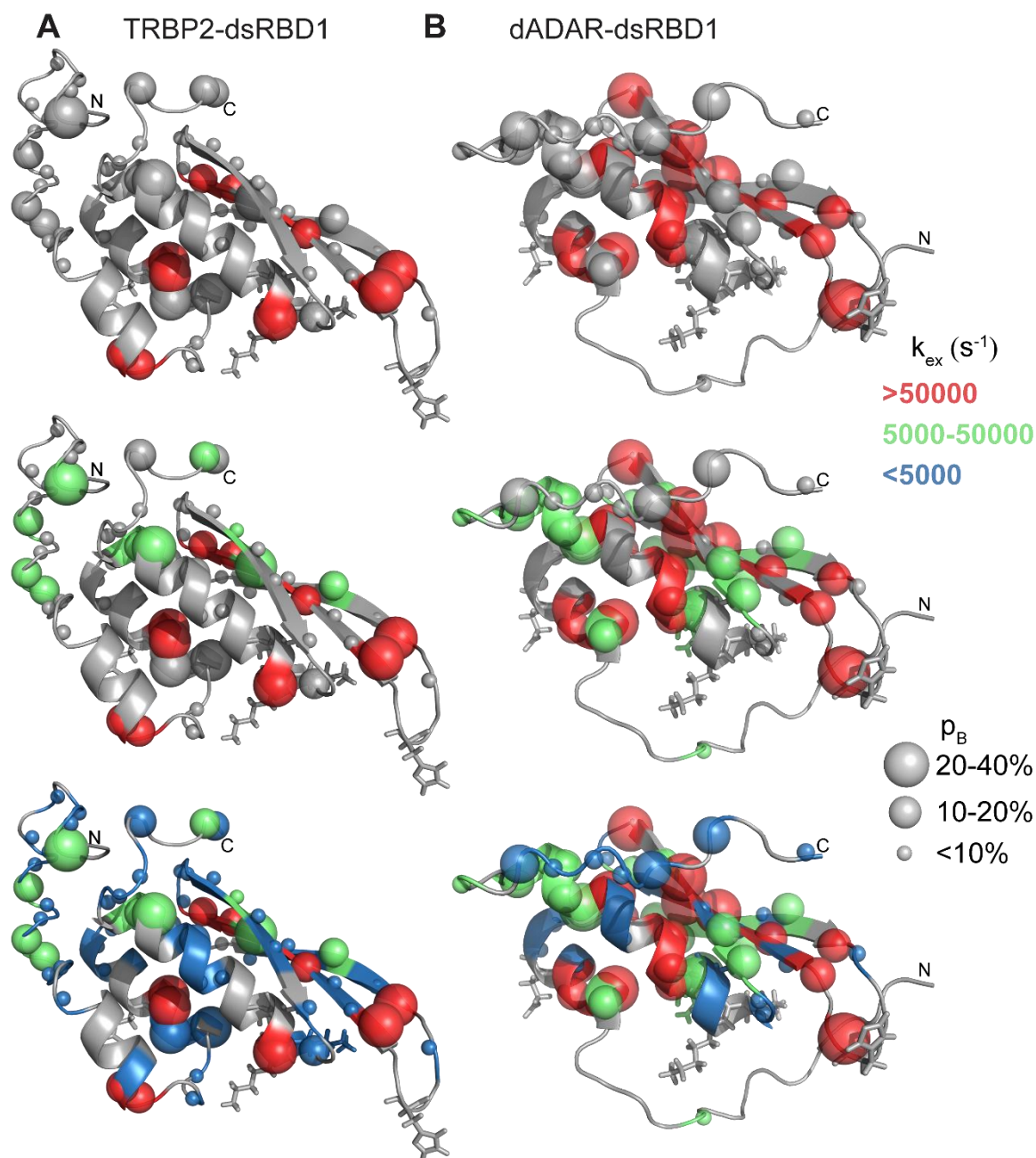
Figure 4.9: Mapping of Dynamics parameters extracted from the HARD NMR data using the geometric approximation method for TRBP2-dsRBD1 and dADAR-dsRBD1. The k_{ex} values are marked in color and the sphere size indicates the population of the excited state (p_B) as shown on the right of the figure. The RNA-binding residues are shown in stick representation.

Attentive analysis of the exchange rates (k_{ex}) for TRBP2-dsRBD1 indicated that the residues in the RNA-binding region or in the close vicinity show a rapid exchange between the two states – a ground state or state A and an excited state or state B – with exchange rates (k_{ex}) of 50000 s^{-1} or more (Figure 4.9). These residues include: (1) L35 and Q36 from α_1-helix, (2) E54 and N61 which are at the termini of β_1-β_2 loop, and (3) A82 in KKxAK motif at N-terminus of α_2-helix and have about 25% population (p_B) in the state B. Few other residues (M1, T10, G13, C14, L51, V66, C73, H94, L95, A104) showed chemical exchange rates between 50000 s^{-1} and 5000 s^{-1} with excited state population of 10-40%. Interestingly, some of the non-RNA-binding residues A25, N26, F64, T67, and V68 also showed exchange rates of more than 50000 s^{-1} with a 10-20% population of excited-state. The exchange observed in these residues might have resulted from a network of interactions responsible for maintaining the tertiary structure of the protein. These interactions include hydrophobic interactions, H-bonding interactions or dipole-dipole interactions between different residues in the protein chain. The rest of the residues exhibited exchange rates of less than 5000 s^{-1} with an excited-state population of less than 10%. The exchange observed in the protein is further supported by the large chemical shift difference between the two states of 5 Hz to 1100 Hz (Appendix Table A.11). This indicated the availability of large conformational space that the residues can sample to interact efficiently with substrate dsRNAs of diverse topologies.

Even though the two proteins have limited sequence similarity and differential ps-ns timescale dynamics, the analysis of k_{ex} and p_B for dADAR-dsRBD1 also showed an analogous distribution of the exchange parameters (Figure 4.9). The residues involved in RNA-binding or in their close vicinity showed an exchange rate of 50000 s^{-1} or more. For example, RNA-binding residues V66, A67, M68, N70 in α_1-helix; A 89 in the loop connecting β_1-β_2 strands, and R114, I115 in α_2-helix showed exchange rate of > 50000 s^{-1}. A few other non-RNA-binding residues that are in close proximity like T84 and L91 that are at the C- and N- terminus of β_1 and β_2 strand, respectively; and residue E116 and A117 in α_2-helix showed k_{ex} more than 50000 s^{-1}. All these residues showed more than 15% of the population in the excited state. Similar to the TRBP2-dsRBD1, a few of the allosteric residues like L76 of β_1-strand, T93, I94, S95 and V96 of β_2-strand, and Q101 and L104 of β_3-strand that are at the rare face from the RNA-binding region in dADAR-dsRBD1 also to have chemical exchange rate of about 50000 s^{-1} with 15% or more population in excited state (except for I94) as observed for TRBP2-dsRBD1. Some of the residues in non-RNA-binding regions of loops or β-strands or in α_2-helix showed 10% or more population in the excited state having k_{ex} between 5000 to 50000 s^{-1}. The rest of the residues showed an exchange event occurring at <5000 s^{-1} with a <10 % population in an excited state. This similar profile of exchange rates and the populations for dADAR-dsRBD1 also resulted in a similar dispersion of chemical shift difference between (48 Hz - 1050 Hz) the two states as for dADAR-dsRBD1 (Appendix Table A.12).

4.4.   *Discussion*

Though the dsRBD1 of the two proteins – TRBP2 and dADAR – has a limited sequence identity of 23.6 % and similarity of 33.3 %, they exhibit similar structural fold common to all dsRBDs. The solution state homogeneity of the TRBP2-dsRBD1 was determined by SEC-MALS showed that one-fifth fraction of the protein coexists as a tetramer with the monomeric protein. A similar study for dADAR-dsRBD1 showed only monomeric protein present in the solution. Regardless of the differences in the primary sequence and the oligomeric state, both the dsRBDs possess similar thermal stability with a melting temperature of 45°C. Also, both the proteins showed ~95 % of the population that exists in folded state at NMR working temperature of 25°C. The analysis of the thermal unfolding profile of the two proteins further shows that TRBP2-dsRBD1 requires additional heat change for the unfolding as indicated by higher enthalpic contribution. This additional enthalpic contribution required in the case of TRBP2-dsRBD1 over dADAR-dsRBD1 might arise due to the coexisting tetramer population (about 20 %) for TRBP2-dsRBD1 in solution as observed from SEC-MALS study. Though we observed the presence of 20 % of the tetramer for TRBP2-dsRBD1, the ^{1}H-^{15}N-HSQC spectra do not show any additional peaks that may correspond to an additional species in solution. This suggests that either (1) the peaks for tetramer show significant line broadening such that they could not be detected; or (2) TRBP2-dsRBD1 forms a symmetric tetramer and thus the resultant peaks overlap as they will have similar chemical environment. To test this probability, the global diffusion parameters were calculated by *quadric_diffusion* program by excluding the terminal flexible residues which will be affected if these peaks correspond to overlapped peaks of monomer and tetramer. However, no such change in diffusion tensor parameters was observed suggesting that the peaks belong to a single entity in the solution which can be the monomeric form of the protein. Though TRBP2-dsRBD1 exists in tetrameric state, it is reported that the RNA-binding shifts the monomer-oligomer equilibrium for TRBP-dsRBD12 towards monomer and the protein interacts with the RNA in its monomeric form[19].

From the empirical correlation of the global tumbling time with the molecular size, the global tumbling time for the proteins of about 10 kDa was expected to be ~5 ns provided the protein exists as a compact globular molecule. However, analysis of the secondary structure composition of the two proteins shows that 45 % and 59 % of the residues of TRBP2-dsRBD1 and dADAR-dsRBD1, respectively are in the unstructured region of the protein. This leads to the anisotropic nature of the diffusion tensor of the two proteins and thus to the higher global rotational correlation time calculated from model-free analysis than the globular protein of this size. Similar higher rotational correlation times of 7.2 ns, 6.29 ns, and 6.35 ns have been reported previously for DGCR8-dsRBD1, Drosha-dsRBD, and Dicer-dsRBD[20,21], respectively. The difference in the rotational correlation time of TRBP2-dsRBD1 and dADAR-dsRBD1 can be assigned to the difference in the theoretical molecular mass of the two protein constructs, 11.2 kDa being for TRBP2-dsRBD1 and 12.5 kDa for dADAR-dsRBD1, respectively. The higher rotational correlation time obtained for dADAR-dsRBD1 is could also have

contribution from the non-native tail of ~20 residues at the N-terminus of the construct that add to the anisotropy of the molecule in addition to the inherent anisotropic shape of the dsRBDs – as represented by higher rotational correlation times of ~ 7 ns for other dsRBDs. Further, the global tumbling time for TRBP2-dsRBD1, calculated from the model-free analysis is 7.64 ns which can only be assigned to monomeric species with a molecular mass of about 11 kDa (for TRBP2-dsRBD1) as the tetramer will result in molecular mass of about 45 kDa and thus require a much longer time for tumbling in solution. This also assures that the peaks in the ^{1}H-^{15}N-HSQC spectrum and in the analyzed ^{15}N-spin relaxation data for TRBP2-dsRBD1 characterize the dynamics of the monomeric form of the protein.

Analysis of the ps-ns timescale dynamics by nuclear spin relaxation data using extended model-free approach resulted in a range of order parameter values in the structured region of the TRBP2-dsRBD1 protein. For a structured region of a globular protein, generally, the order parameters have a value of more than 0.8 suggesting the limited flexibility. However, in the case of TRBP2-dsRBD1, the residues in the dsRBD core showed S^2 values ranging from 0.23 to 0.87 with average S^2 being 0.61 for dsRBD core with lower S^2 values for residues not only in the loop regions but also in the structured regions of the protein. This supports the higher flexibility at ps-ns timescale present in the protein. The profile of S^2 for dADAR-dsRBD1, however, follows the routine pattern, where the structured regions show order parameters of about 0.8 or more and the loop regions have lower values. The average S^2 value for the dADAR-dsRBD1 core was found to be 0.80 suggesting restricted motions in residues at ps-ns timescale. Thus, the two proteins showed different profiles of dynamics present at ps-ns timescale. Interestingly, the presence of slow motions was detected by model-free analysis and HARD NMR experiments in both the proteins.

Analysis of HARD NMR data allowed to further characterize these motions and suggested similar distribution of chemical exchange events occurring in the protein. The extracted exchange parameters show that RNA-binding residues (e.g. in middle of α_1-helix) or those in the vicinity of RNA-binding region (eg. at the N-terminus and C-terminus of β_1-β_2 loop) and few other allosteric residues (distributed in three antiparallel β-strands) have a chemical exchange rate of 50000 s^{-1} or more with a significant population (more than 15%) in the excited state(s) in both the dsRBDs. Though the results of HARD NMR data, showed >15% population of these residues in excited state(s), these residues show intermediate timescale exchange with the ground state resulting in significant line-broadening of the peaks. Also, though the data is fit using a two-state exchange model, which is highly simplistic model, the actual number of alternative conformational states could be higher. Thus the peaks for the excited states could not be observed in the ^{1}H-^{15}N-HSQC spectra of the two proteins. Some residues in close proximity to the RNA-binding residues (at C-terminal of α_2 helix) showed a k_{ex} value of 5000-50000 s^{-1} with at least a 10 % population in the excited state(s). Along with these fast µs motions, 49 out of 69 analyzed residues in TRBP2-dsRBD1 and 25 out of 59 analyzed residues in dADAR-dsRBD1, distributed along the protein chain, showed conformational exchange with $k_{ex} < 5000$ s^{-1}. The

conformational dynamics present in multiple residues along the protein chain leads to the availability of the large conformational space for the two dsRBDs. This was reinforced by the large chemical shift difference ($\Delta\omega$) observed between the ground and the excited state of the two dsRBDs. Since the sign of ($\Delta\omega$) cannot be obtained from the HARD experiment the structure of the excited state conformation of the protein cannot be determined. Interestingly, though the two dsRBDs studied here belong to two different species and have differences in their primary sequence, showed different dynamics profile at ps-ns timescale with different oligomerization patterns, they show similar profiles of motions at μs-ms timescale. In addition, the similarity in the dynamics is not only limited to the RNA-binding region but also observed in allosteric regions. This implies that these motions are intrinsic to the dsRBD structural fold and do not reflect the aggregation behavior observed in the case TRBP2-dsRBD1. These concerted motions in multiple sites in dsRBDs can allow adaption to multiple conformations by undergoing conformational rearrangement. In addition, from the CD melting profile, both the proteins show about a 5 % unfolded population at 25°C – where all the NMR experiments were recorded. This also suggests the lower energy barrier for the two dsRBDs to access the non-native conformation(s) (which can be an unfolded state). This is reflected in the presence of conformational dynamics present all along the protein chain in both the dsRBDs. Being present all along the protein chain, this dynamic behavior in dsRBDs allows them to exists as an ensemble of conformations ensemble that may have a functional role. These conformations might allow dsRBDs to interact with a topologically diverse set of dsRNAs in the cellular pool and ensure accurate processing of the substrate by their protein partners like Dicer and Ago.

4.5.   *Summary*

The characterization of the dynamics of two dsRBDs from two different proteins from two different species showed that they show similar thermal stability as indicated by similar CD melting behavior. However, the SEC-MALS study showed that they have different aggregation patterns. The ps-ns timescale dynamics studied by NMR showed that they possess a differential dynamic profile at this timescale, however, the model-free analysis suggested the presence of slow motions at μs-ms timescale distributed along the protein chain. Further, relaxation dispersion studies have helped to confirm and characterize these motions and indicated that these motions occur at μs timescale and present in most of the residues along the length of the protein and not restricted to RNA-binding sites in both the dsRBDs. The presence of these motions at multiple sites suggests possible conformational rearrangements in the protein chain. This corroborates the conformational adaptability in dsRBDs originating from the intrinsic dynamics which might support their interaction with topologically different dsRNAs present in the cellular environment.

4.6. References

1   I. R. Kleckner and M. P. Foster, An introduction to NMR-based approaches for measuring protein dynamics, *Biochim. Biophys. Acta - Proteins Proteomics*, 2011, **1814**, 942–968.

2   N. J. Greenfield, Using circular dichroism collected as a function of temperature to determine the thermodynamics of protein unfolding and binding interactions, *Nat. Protoc.*, 2006, **1**, 2527–2535.

3   F. Delaglio, S. Grzesiek, G. W. Vuister, G. Zhu, J. Pfeifer and A. Bax, NMRPipe: a multidimensional spectral processing system based on UNIX pipes, *J Biomol NMR*, 1995, **6**, 277–293.

4   W. Lee, M. Tonelli and J. L. Markley, NMRFAM-SPARKY: Enhanced software for biomolecular NMR spectroscopy, *Bioinformatics*, 2015, **31**, 1325–1327.

5   L. Spyracopoulos, A suite of Mathematica notebooks for the analysis of protein main chain 15N NMR relaxation data, *J. Biomol. NMR*, 2006, **36**, 215–224.

6   E. J. d'Auvergne, University of Melbourne, 2006.

7   M. Bieri, E. J. d'Auvergne and P. R. Gooley, relaxGUI: a new software for fast and simple NMR relaxation data analysis and calculation of ps-ns and mus motion of proteins, *J Biomol NMR*, 2011, **50**, 147–155.

8   L. K. Lee, M. Rance, W. J. Chazin and A. G. Palmer 3rd, Rotational diffusion anisotropy of proteins from simultaneous analysis of 15N and 13C alpha nuclear spin relaxation, *J Biomol NMR*, 1997, **9**, 287–298.

9   H. Paithankar, P. V. Jadhav, A. S. Naglekar, S. Sharma and J. Chugh, 1H, 13C and 15N resonance assignment of domain 1 of trans-activation response element (TAR) RNA binding protein isoform 1 (TRBP2) and its comparison with that of isoform 2 (TRBP1), *Biomol. NMR Assign.*, 2018, **12**, 189–194.

10 P. Barraud, B. S. E. Heale, M. A. O'Connell and F. H. T. Allain, Solution structure of the N-terminal dsRBD of Drosophila ADAR and interaction studies with RNA, *Biochimie*, 2012, **94**, 1499–1509.

11 M. Tollinger, N. R. Skrynnikov, F. A. Mulder, J. D. Forman-Kay and L. E. Kay, Slow dynamics in folded and unfolded states of an SH3 domain, *J Am Chem Soc*, 2001, **123**, 11341–11352.

12 S. Mangia, N. J. Traaseth, G. Veglia, M. Garwood and S. Michaeli, Probing slow protein dynamics by adiabatic R(1rho) and R(2rho) NMR experiments, *J Am Chem Soc*, 2010, **132**, 9979–9981.

13   N. J. Traaseth, F. A. Chao, L. R. Masterson, S. Mangia, M. Garwood, S. Michaeli, B. Seelig and G. Veglia, Heteronuclear Adiabatic Relaxation Dispersion (HARD) for quantitative analysis of conformational dynamics in proteins, *J Magn Reson*, 2012, **219**, 75–82.

14   F. A. Chao and R. A. Byrd, Geometric Approximation: A New Computational Approach To Characterize Protein Dynamics from NMR Adiabatic Relaxation Dispersion Experiments, *J Am Chem Soc*, 2016, **138**, 7337–7345.

15   G. Lipari and A. Szabo, Model-Free Approach to the Interpretation of Nuclear Magnetic-Resonance Relaxation in Macromolecules .1. Theory and Range of Validity, *J. Am. Chem. Soc.*, 1982, **104**, 4546–4559.

16   G. Lipari and A. Szabo, Model-Free Approach to the Interpretation of Nuclear Magnetic-Resonance Relaxation in Macromolecules .2. Analysis of Experimental Results, *J. Am. Chem. Soc.*, 1982, **104**, 4559–4570.

17   G. Lipari and A. Szabo, Analysis of Nmr Relaxation Data on Macromolecules Using the Model-Free Approach, *Biophys. J.*, 1982, **37**, A380–A380.

18   G. M. Clore, A. Szabo, A. Bax, L. E. Kay, P. C. Driscoll and A. M. Gronenborn, Deviations from the simple two-parameter model-free approach to the interpretation of nitrogen-15 nuclear magnetic relaxation of proteins, *J. Am. Chem. Soc.*, 1990, **112**, 4989–4991.

19   T. Takahashi, T. Miyakawa, S. Zenno, K. Nishi, M. Tanokura and K. Ui-Tei, Distinguishable In Vitro Binding Mode of Monomeric TRBP and Dimeric PACT with siRNA, *PLoS One*, , DOI:10.1371/journal.pone.0063434.

20   C. Wostenberg, K. A. Quarles and S. A. Showalter, Dynamic origins of differential RNA binding function in two dsRBDs from the miRNA 'Microprocessor' complex, *Biochemistry*, 2010, **49**, 10728–10736.

21   C. Wostenberg, J. W. Lary, D. Sahu, R. Acevedo, K. A. Quarles, J. L. Cole and S. A. Showalter, The role of human Dicer-dsRBD in processing small regulatory RNAs, *PLoS One*, 2012, **7**, e51829.

Chapter 5 Effect of dsRNA substrates on dsRBD dynamics

5.1. Introduction

The interaction between any two molecules is associated with a change in the internal energy of the system either in the form of gain from or loss to the surrounding. With respect to RNA-protein interactions, these changes involve direct or solvent-mediated interactions like hydrogen bonding, or electrostatic, or dipole-dipole interaction, etc[1–3]. The mechanistic insights into the interaction between an RNA-protein pair can be understood by performing a detailed characterization of the changes that affect proteins and/or RNA at the thermodynamic, kinetic, and structural levels.

In order to explore the mechanism of recognition of dsRNA – with or without any imperfection in the A-form helix of the dsRNA – by dsRBDs, we aimed to characterize the effect of different dsRNA topologies (that is perturbed based on the secondary structural changes in the RNA[4]) on the dsRBD-dsRNA interaction. In Chapter 4, we have identified that the dsRBDs exists as an ensemble of conformations due to the presence of inherent microsecond timescale dynamics[5]. In this Chapter, we tested the binding modes of topologically different dsRNAs by isothermal titration calorimetry (ITC) and NMR-based studies. RNA duplexes of varying shapes were designed from a known binder – miR-16-1 RNA duplex[6], of TRBP2-dsRBD1 by creating mutations in the native sequence. Determination of the thermodynamic parameters from ITC studies offered to explore similarities and the differences between interactions of dsRBDs with dsRNAs. Since the dsRBDs exist as an ensemble of conformations due to the intrinsic dynamics, the effect of dsRNAs with different shapes on the structure and dynamics of dsRBDs were probed by using NMR-based titration and NMR-based relaxation experiments that allowed us to probe the effect of dsRNA topologies on the dsRBD at the atomic level. Detailed characterization of the dsRBD dynamics with a small dsRNA construct suggested the role of intrinsic dsRBD dynamics in the recognition process, reinforcing the proposed conformational rearrangement as the mechanism of interaction of dsRBD with dsRNAs.

5.2. Materials and Methods

5.2.1. Protein overexpression and purification

TRBP2-dsRBD1 and dADAR-dsRBD1 proteins (unlabeled and ^{15}N labeled) were overexpressed and purified as described in Chapter 3.

5.2.2. Selection and design of RNA substrate

The selection of the substrate RNA was based on the fact that precursors of miRNA-16-1 were used to study their interactions with many dsRBDs (Drosha, Dicer, DGCR8, and TRBP)[6–8]. The duplex of the miR-16-1 contains a mismatch (A•A) and a bulge (from unpaired U) in the potential TRBP binding region[9], as shown in Figure 1.7. Thus, to study the effect of perturbations in the A-form helical

structure of RNA duplex, the nucleobases in the passenger strand of the RNA were altered to create different topologies. The modifications were made to generate following mutant RNAs: (1) miR-16-1-M: RNA with only mismatch by removing the unpaired U from the passenger strand; (2) miR-16-1-B: RNA with only bulge by replacing A by U in the A•A mismatch position in the passenger strand; and (3) miR-16-1-D: RNA with all base-pairs, by removing U bulge and replacing A by U in passenger strand at A•A mismatch. A short RNA having a length of 10 bp – hereafter referred to as D10-RNA – sufficient to bind to dsRBD was also designed from perfectly duplex RNA (miR-16-1-D).

All the RNA oligonucleotides were purchased from Integrated DNA technology or Sigma Aldrich and have been listed in Table 5.1. RNA annealing was done by mixing the guide and the passenger strand for each RNA duplex in a 1:1 molar ratio, followed by heating at 95°C for 5 min for denaturation, and finally renaturing at 4°C for 10 min. The annealing of the two strands for each RNA duplex was confirmed by the presence of imino protons (Appendix Figure A.2) in the ^{1}H NMR spectrum with each sample in NMR buffer.

Table 5.1: RNA sequences used to study interaction with dsRBDs.

Name	Strand	Sequence (5′ → 3′)
miR-16-1	Guide	5′- UAGCAGCACGUAAAUAUUGGCG -3′
	Passenger	5′- CCAGUAUUAACUGUGCUGCUGAA -3′
miR-16-1-D	Guide	5′- UAGCAGCACGUAAAUAUUGGCG -3′
	Passenger	5′- CCAGUAUUUACGUGCUGCUGAA -3′
miR-16-1-M	Guide	5′- UAGCAGCACGUAAAUAUUGGCG -3′
	Passenger	5′- CCAGUAUUAACGUGCUGCUGAA -3′
miR-16-1-B	Guide	5′- UAGCAGCACGUAAAUAUUGGCG -3′
	Passenger	5′- CCAGUAUUAACGUGCUGCUGAA -3′
D10 RNA	Guide	5′- UUAUAAAUGC -3′
	Passenger	5′- GCAUUUAUGA -3′

5.2.3. RNA structure modeling

The secondary structure of each RNA duplex was determined by prediction from the DINAmelt program[10,11] (http://unafold.rna.albany.edu/?q=DINAMelt/Hybrid2). The tertiary structure of each RNA duplex was modeled using SimRNA webserver[12,13] (https://genesilico.pl/SimRNAweb/). The program works on the algorithm based on the coarse-grained representation of the RNA molecule with the help of the Monte-Carlo method for conformational sampling. The simulations were carried out with the secondary structures of each duplex obtained from DINAmelt[10] as input to the program.

5.2.4. Isothermal titration calorimetry

All the ITC experiments were performed at 25°C on the MicroCal VP –iTC200 instrument (at UM-DAE, CEBS, Mumbai). For all the titrations, both protein and RNA samples were exchanged into NMR buffer (10 mM Sodium Phosphate, 100 mM NaCl, 1 mM EDTA, 1 mM DTT), pH 6.4. Diluted protein samples (TRBP2-dsRBD1 or dADAR-dsRBD1) at 30 µM concentration were used in the sample cell for all experiments. The molar ratio of the protein to RNA duplex (prepared by annealing two strands as mentioned in Table 5.1) was optimized for all RNAs to get the saturated calorimetric signal at the end of the titration. The optimized concentrations for various RNAs were miR-16-1 = 90 µM, miR-16-1-D = 120 µM, miR-16-1-M = 300 µM, miR-16-1-B = 150 µM, and D10-RNA = 240 µM. Blank titration was carried out by measuring the heat of dilution of RNA into NMR buffer, by using the buffer in the sample cell instead of protein. For every injection, 2 µl of the RNA was injected into the sample cell over 4 seconds with an equilibration time of 120 seconds. The heat change during the titration was measured and recorded as a calorimetric signal for every injection. The heat change was converted to the corresponding enthalpy change and the data were baseline corrected by subtracting the heat of dilution of the RNA into the buffer. The data, thus obtained, was fitted to the one set of sites model (assuming no dependence in the multiple binding events) to calculate thermodynamic parameters (N, K_a, ΔH, ΔS) of the binding event in Origin 7.0 provided with the instrument.

5.2.5. NMR Spectroscopy

5.2.5.1. NMR based titration with RNA duplexes with different topologies

All the titration experiments were recorded on an in-house Bruker 600 MHz NMR spectrometer equipped with Quad-Channel (^{1}H, ^{13}C, ^{15}N, ^{31}P) Cryoprobe or on Bruker 600 MHz NMR spectrometer equipped with ^{13}C-enhanced TCI cryoprobe (located at NCBS, Bangalore). Each of the duplex RNA was titrated against the fixed protein concentration of 80 µM of ^{15}N-TRBP2-dsRBD1 in NMR buffer pH 6.4 in the concentration range of 0.0 to 0.25 equivalents of the RNA duplex (0.0 to 2.5 equivalents in case of D10-RNA). At every step, the protein was allowed to equilibrate for ~30 min before recording the ^{1}H-^{15}N HSQC spectrum. All the spectra were recorded with 2048 and 128 points with a spectral width of 12 and 28 ppm in ^{1}H and ^{15}N dimension, respectively. The offsets were set at water resonance (~4.70 ppm) in ^{1}H dimension and 117.00 ppm in ^{15}N dimension and data was collected with 96 scans. All the spectra were processed in NMRpipe/NMRDraw[14] and analyzed in Sparky[15] to monitor changes in the intensities and the chemical shift of the individual peak in the HSQC. Changes in the intensity of the peaks were plotted by normalizing with respect to peak intensity in the apo-state of the protein against increasing RNA concentration for every peak in HSQC spectra. The change in a chemical shift as chemical shift perturbations ($\Delta\delta$) was calculated by using Equation 5.1[16]:

$$\Delta\boldsymbol{\delta} = \sqrt{(\Delta\boldsymbol{\delta_N}/6.5)^2 + \Delta\boldsymbol{\delta_H}^2} \qquad\qquad (5.1)$$

where $\Delta\delta_N$ and $\Delta\delta_H$ represent the change in the chemical shift in the ^{15}N and ^{1}H dimension, respectively, after the addition of a known equivalent of RNA.

5.2.5.2. NMR-based relaxation experiments without and with RNA duplex

All NMR-based relaxation experiments were recorded on Bruker 950 MHz NMR spectrometer equipped with a TCI cryoprobe (at Institute for Protein Research, Osaka University, Japan). The nuclear spin relaxation experiments (R_1, R_2, and [^{1}H]-^{15}N-NOE) were recorded with a protein concentration of 200 μM in the absence of any RNA added. The inversion recovery delays used for R_1 experiments were 10, 50, 100, 150, 400, 650, 900 ms and CPMG delays used for R_2 experiments were 15.84, 31.68, 47.52, 63.36, 95.04, 142.56, 158.40 ms. [^{1}H]-^{15}N-NOE experiments were recorded as two HSQCs, one with ^{1}H saturation where a ^{1}H saturation delay of 3.0 s and a relaxation delay of 2.0 s was used, and another without ^{1}H saturation where a relaxation delay of 5.0 s was used. All these experiments were recorded in an interleaved fashion to average out any temperature fluctuation during relaxation data measurement. Further, the same set of experiments was recorded in the presence of four topologically different RNA duplexes at 0.05 equivalent of RNA added to the protein individually. For R_1 experiments, inversion recovery delays of 10, 30, 70, 150, 300, 600, and 750 ms were used protein in presence of miR-16-1 RNA and that of 10, 30, 70, 150, 300, 400, 500 ms were used in case of all other three RNAs. The CPMG relaxation delays of 10, 30, 50, 90, 130, 170, 220 ms were used for R_2 experiments for protein complexed with all four RNAs. These experiments were recorded as separate HSQCs with a randomized order of delays. The delays underlined were measured in duplicate for error estimation. [^{1}H]-^{15}N-NOE experiment was recorded with a ^{1}H saturation delay of 0.9 s and a relaxation delay of 1.5 s was used for the experiment without ^{1}H saturation in an interleaved manner. The longitudinal (R_1) and transverse (R_2) relaxation rates and the NOE ratios were calculated, as described in section 4.2.3.1, for the observed non-overlapping peaks with measurable intensities in absence of RNA or presence of each of the four RNAs and plotted against residue number. The details of the experimental parameters used for recording relaxation experiments have been listed in Table 5.2.

Table 5.2: Experimental parameters for relaxation data acquisition for TRBP2-dsRBD1 in the absence of RNA and in presence of miR-16-1 and its mutants (RNAs with different topologies)

Experiment (Pulse Sequence used)	Nucleus	TD[a]	SW[b] (ppm)	Offset (ppm)	NS[c]	d1[d] (s)
TRBP2-dsRBD1 in absence of RNA						
^{15}N-R_1 (hsqct1etf3gpsi3d)	^{1}H ^{15}N Delay	2048 256 9	12 28	4.70 117.00	16	2.5

Experiment (Pulse Sequence used)	Nucleus	TD[a]	SW[b] (ppm)	Offset (ppm)	NS[c]	d1[d] (s)
TRBP2-dsRBD1 in absence of RNA						
[15]N-R_2 (hsqct2etf3gpsi3d)	[1]H	2048	12	4.70	16	2.5
	[15]N	256	28	117.00		
	Delay	9				
[^{1}H]-^{15}N-NOE (hsqcnoef3gpsi)	[1]H	2048	12	4.70	16	5.0
	[15]N	512	28	117.00		
TRBP2-dsRBD1 in the presence of RNA						
[15]N-R_1 (hsqct1etf3gpsi)	[1]H	2048	10	4.70	16	1.5
	[15]N	256	26	117.00		
[15]N-R_2 (hsqct2etf3gpsi)	[1]H	2048	10	4.70	16	1.5
	[15]N	256	26	117.00		
[^{1}H]-^{15}N-NOE (hsqcnoef3gpsi)	[1]H	2048	10	4.70	32	1.5
	[15]N	512	26	117.00		

[a]TD: Number of data points/size of fid, [b]SW: Spectral Width, [c]NS: Number of scans, [d]d1: relaxation delay

All the NMR-based relaxation experiments for TRBP2-dsRBD1 in presence of D10-RNA were recorded on an in-house Bruker 600 MHz NMR spectrometer. For all the experiments, the protein sample at a concentration of 200 μM complexed with 0.5 equivalent of D10-RNA was used. For R_1 experiments, the 8 inversion recovery delays of 10, 30, 50, 100, 200, 350, 500, 700 ms were used and for R_2 experiments, 8 CPMG delays of 17, 34, 51, 68, 85, 102, 136, 170 ms were used. The delays underlined were measured in duplicate for error estimation. [^{1}H]-^{15}N-NOE experiment was recorded with a ^{1}H saturation delay of 3.0 s and the experiment without ^{1}H saturation was recorded with a recovery delay of 5.0 s. All these experiments were collected in an interleaved fashion. ^{15}N-CPMG relaxation dispersion experiment[17] was recorded with constant relaxation time, T_{relax}, of 40 ms during which CPMG blocks are applied. A series of HSQCs with CPMG frequencies of 0, 25, 50, 100, 200, 350, 500, 650, 800, 1000 Hz were recorded in an interleaved manner. The rates at underlined CPMG frequencies were collected in duplicate for error estimation. The effective relaxation rates were determined as described in section 4.2.3.2.

Heteronuclear adiabatic relaxation dispersion (HARD)[18,19] experiments were recorded for the protein in D10-RNA bound state. A set of four hyperbolic secant family pulses of 4 ms each was used for spin-locking the magnetization in the rotating frame. For $R_{1\rho}$ and $R_{2\rho}$ experiments, relaxation rates in the rotating frame were measured by using relaxation delays of 0, 16, 32 and 64 ms (corresponding to L4 = 0, 1, 2, 4). The dispersion in relaxation rates was created by varying the stretching factor (n) of the hyperbolic secant (HSn) family adiabatic pulses from 1 to 8 (n=1,2,4,6,8). For the R_1 experiment as a part of HARD experiments, relaxation delays of 16, 48, 96, 192, 320, 480 and 640 ms were used. Relaxation rates ($R_{1\rho}$, $R_{2\rho}$, and R_1), thus obtained, were fitted to the time-dependent Bloch-McConnell equation by geometric approximation method to extract the dynamic parameters assuming the two-state

model. The details of the experimental parameters used for NMR data collection have been listed in Table 5.3.

Table 5.3: Experimental parameters for relaxation data acquisition for TRBP2-dsRBD1 in presence of 0.5 equivalents of D10-RNA.

Experiment (Pulse Sequence used)	Nucleus	TD[a]	SW[b] (ppm)	Offset (ppm)	NS[c]	d1[d] (s)
^{15}N-R_1 (hsqct1etf3gpsi3d)	^{1}H ^{15}N Delay	2048 128 10	12 28	4.69 117.00	24	2.5
^{15}N-R_2 (hsqct2etf3gpsi3d)	^{1}H ^{15}N Delay	2048 128 10	12 28	4.69 117.00	24	2.5
[^{1}H]-^{15}N-NOE (hsqcnoef3gpsi)	^{1}H ^{15}N	2048 256	12 28	4.69 117.00	64	5.0
^{15}N-CPMG-RD (hsqcrexetf3gpsi3d)	^{1}H ^{15}N Delay	2048 128 12	12 28	4.69 117.00	24	2.5
^{15}N-R_1 - HARD (r1.fc)	^{1}H ^{15}N	2048 128	12 28	4.69 117.00	24	2.5
^{15}N-$R_{1\rho}$ - HARD (r1rho.fc)	^{1}H ^{15}N	2048 128	12 28	4.69 117.00	24	2.5
^{15}N-$R_{2\rho}$ - HARD (r2rho.fc)	^{1}H ^{15}N	2048 128	12 28	4.69 117.00	24	2.5

[a]TD: Number of data points/size of fid, [b]SW: Spectral Width, [c]NS: Number of scans, [d]d1: relaxation delay

5.3.   Results

5.3.1.   RNA design and 3D structure modeling

The secondary structure analysis of precursor of miR-16-1 shows that it contains a mismatch and a single nucleotide bulge, thus showing the imperfections in the duplex structure. The RNA duplex with imperfections was altered to create three mutants, one without any imperfection in the duplex – miR-16-1-D; and two with a single imperfection – miR-16-1-M and miR-16-1-B. The structures of all four RNAs were modeled using the SimRNA webserver,[12,13] with the secondary structure predicted from DINAmelt[10]. The models generated from the SimRNA have been shown in Figure 5.1 with the TRBP binding residues highlighted in orange. These structures clearly show that the imperfections in the RNA duplex observed in the secondary structure result in the corresponding change in the tertiary structure of the molecule[4]. Furthermore, the measurement of length of the RNA determined between 5′-phosphate of UMP in the guide strand and 5′-phosphate of CMP in the passenger strand forming the RNA duplex shows that the four RNA have different length of 59.3 Å (miR-16-1), 43.8 Å (miR-16-1-D), 34.2 Å (miR-16-1-M) and 52.7 Å (miR-16-1-B), respectively. This confirms that the topological differences get induced due to the helical imperfections in the RNA duplex.

miR-16-1
```
U A G C A G C A C - G U A A A U A U U G G C G
| | | | | | | | |   | |   | | | | | | | | | |
A A G U C G U C G U G U C A A U U A U G A C C
```

miR-16-1-D
```
U A G C A G C A C G U A A A U A U U G G C G
| | | | | | | | | | | | | | | | | | | | | |
A A G U C G U C G U G C A U U U A U G A C C
```

miR-16-1-M
```
U A G C A G C A C G U A A A U A U U G G C G
| | | | | | | | | | | | | | | | | | | |
A A G U C G U C G U G C A A U U A U G A C C
```

miR-16-1-B
```
U A G C A G C A C - G U A A A U A U U G G C G
| | | | | | | | |   | |   | | | | | | | | | |
A A G U C G U C G U G U C A U U U A U G A C C
```

Figure 5.1: Secondary and tertiary structure of RNA (miR-16-1) and its mutants used in the study. The structures (as obtained from DINAmelt and SimRNA programs) of duplexes of miR-16-1 (native form), miR-16-1-D (without any imperfections in a duplex), miR-16-1-M (with mismatch only), and miR-16-1-B (with bulge only) are shown. The imperfections in the RNA duplex and the corresponding mutations are marked in Blue-box.

5.3.2. *dsRBD-dsRNA binding studies by isothermal titration calorimetry*

The isothermal titrations of each of the four RNAs into each of the protein – TRBP2-dsRBD1 and dADAR-dsRBD1 – showed that irrespective of the structure of the RNA and the origin of the dsRBD, they can interact with each other (Figure 5.2). Though the heat change observed during the interaction is positive or negative in some cases, the net change in enthalpy is always negative. The different heat change observed is due to different heat of dilution of each of the RNA. The thermodynamic parameters obtained from fitting of the ITC data to the one set of sites model describing the interaction between a dsRBD and a dsRNA have been shown in Figure 5.3 and listed in Appendix Table A.13. The binding constants, K_d, calculated for TRBP2-dsRBD1 ranged from 0.50 ± 0.04 μM to 2.12 ± 0.22 μM and that for dADAR-dsRBD1 ranged from 0.27 ± 0.05 μM to 0.78 ± 0.24 μM. This suggests that both dsRBDs can bind to either of the four dsRNAs with similar affinities. The interactions with TRBP2-dsRBD1 have shown that enthalpic (ΔH) and entropic ($T\Delta S$) contribution to free energy change ranges from -9.4 ± 0.2 kcal.mol^{-1} to -34.8 ± 0.6 kcal.mol^{-1} and -1.6 ± 0.2 to -26.2 ± 0.6 kcal.mol^{-1}, respectively. The corresponding changes in ΔH and $T\Delta S$ for dADAR-dsRBD1 were -24.6 ± 1.1 kcal.mol^{-1} to -80.9 ± 3.2 kcal.mol^{-1} and -16.3 ± 0.9 to -72.1 ± 3.1 kcal.mol^{-1}, respectively. It was interesting to note that though the binding affinities were similar, the number of binding sites differed

Figure 5.2: Isothermal Titration Calorimetric data showing interactions of all four RNAs with (**A**) TRBP2-dsRBD1 and (**B**) dADAR-dsRBD1. The K_d values calculated from data fitting to one set of sites model shows that the binding affinities of both the dsRBDs for all four RNAs are similar.

for all four RNAs with a different combination of enthalpic and entropic contribution to the free energy of binding. miR-16-1-M was found to have a minimum number of binding sites for TRBP2-dsRBD1 and dADAR-dsRBD1 as 1.5 and 1.6, respectively and thus showed restricted binding among four RNAs.
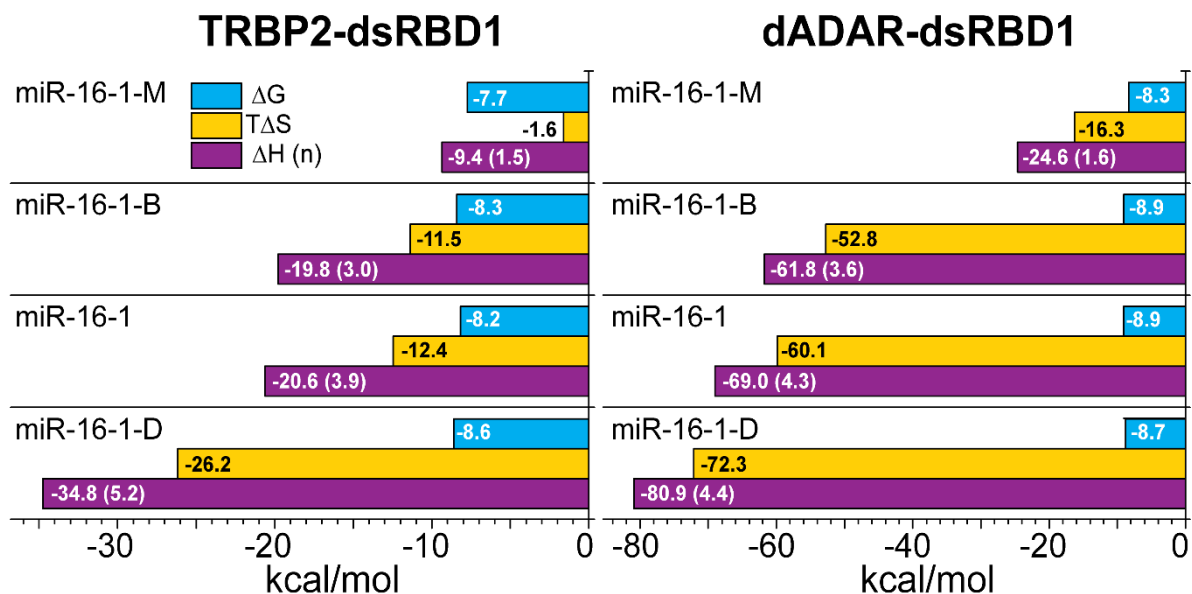
Figure 5.3: Thermodynamic parameters (ΔG, TΔS, ΔH and n) obtained from binding studies of TRBP2-dsRBD1 and dADAR-dsRBD1 with four topologically different RNAs using isothermal titration calorimetry. The values in the brackets indicate the stoichiometry (n) of the interaction.

5.3.3. *Interaction of dsRBD with RNA duplex and its mutant*

To gain atomic-level information of the interactions of dsRBD with dsRNA, all four RNAs were titrated against TRBP2-dsRBD1 individually and the ^{1}H-^{15}N HSQC spectra at increasing RNA concentrations were recorded. In such experiments, any change in the NMR observables (chemical shift or intensity) would indicate the interactions between the two biomolecules. The intensity and the chemical shifts of the HSQC peaks were monitored to envisage the timescale of motions leading to interactions (Figure 5.4). As higher concentrations up to 0.25 equivalents of the RNA were added to the protein, there was a significant decrease in the number of peaks due to a gradual increase in line-broadening. The resultant decays in peak intensities were plotted as a function of increasing RNA concentration for each of the detected residues by normalizing with peak intensity in the apo-state of the protein (Figure 5.5). The plots show that most of the residues in the structured region of the protein (18-95 aa) are affected due to the binding event, while the intensities of the terminal residues do not change suggesting that they do not participate in the binding event. Such line-broadening can be explained by either an increase in intrinsic transverse relaxation time (T_2) due to the complex formation or by intermediate timescale exchange (at NMR timescale) between apo- and RNA-bound state of the protein. The line-broadening profile was mapped on the protein chain as shown in Figure 5.6. A comparison of the line-broadening pattern suggested it is unique for each of the four RNAs at a given

RNA concentration suggesting that the residues affected due to the dsRBD-dsRNA interaction vary in dsRNA shape-dependent fashion. To test the structural change in the protein, the chemical shift perturbations at a concentration of 0.1 equivalents of protein were calculated and have been plotted against residue number with corresponding intensity change (Figure 5.7). Minimal change in the chemical shift of the order of 0.01 ppm suggests no structural change in the protein when either of the four RNAs is added to the protein.
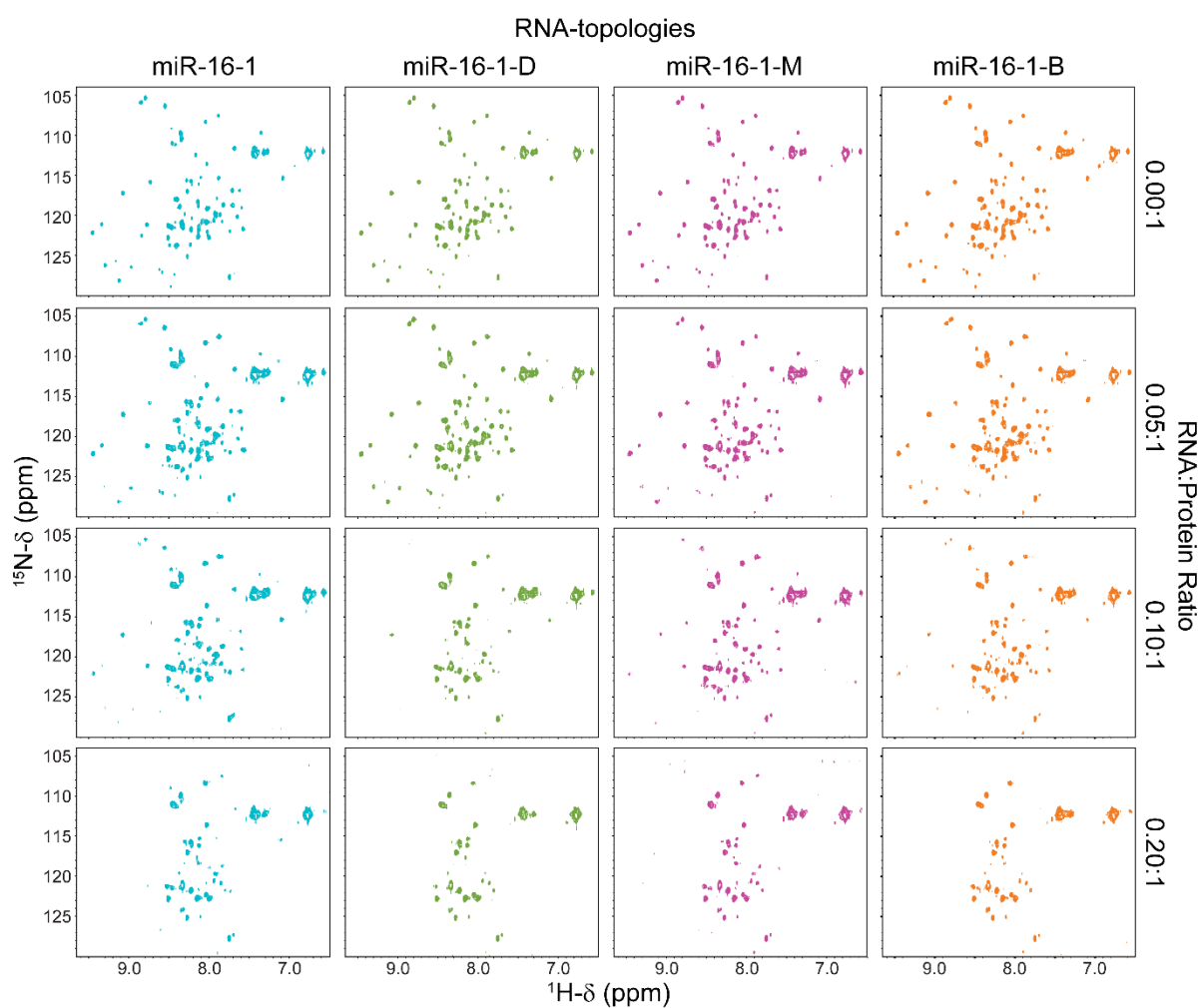
Figure 5.4: Comparison of ^{1}H-^{15}N-HSQC spectra of TRBP2-dsRBD1 titrated with for four topologically different RNAs monitored with increasing concentration. The different RNA:Protein ratios have been mentioned on the right panel.
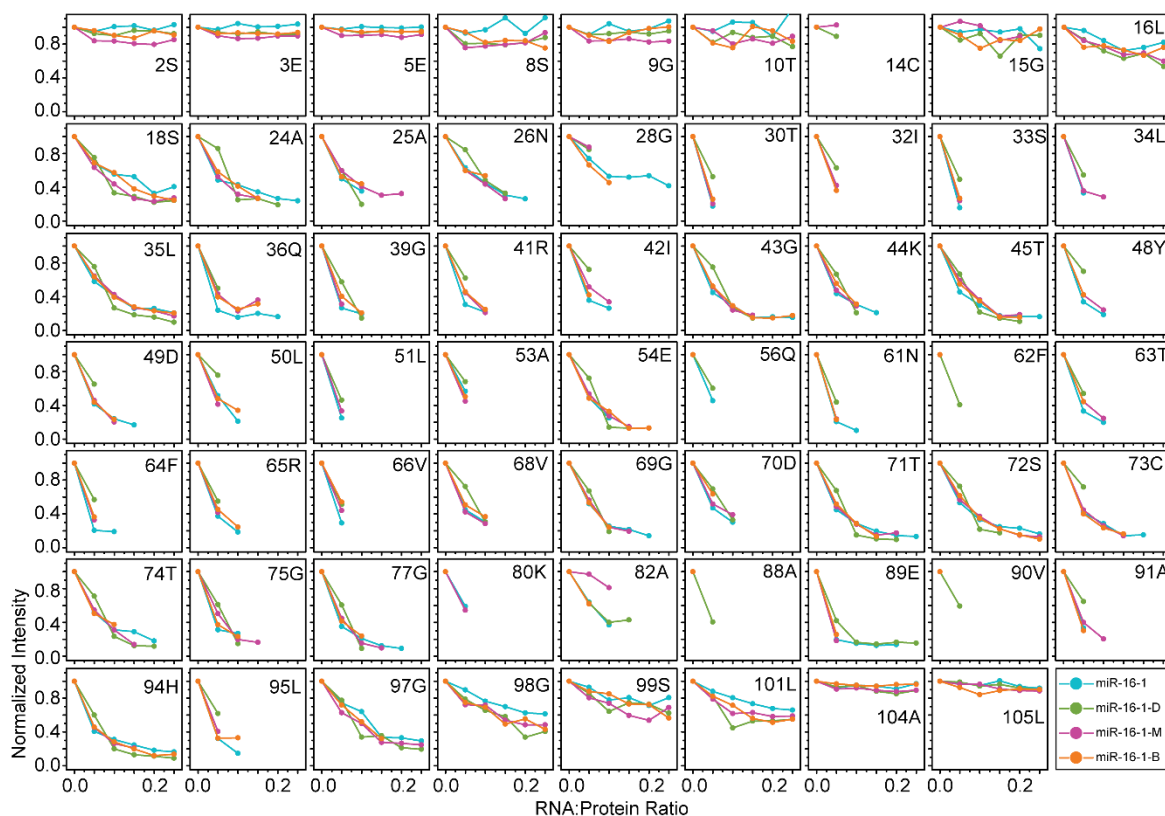
Figure 5.5: Intensity decay profile from titration of TRBP2-dsRBD1 with four RNA duplexes with different topologies plotted against increasing RNA:Protein ratio. The color codes used to indicate different RNAs have been listed in the bottom-right panel.
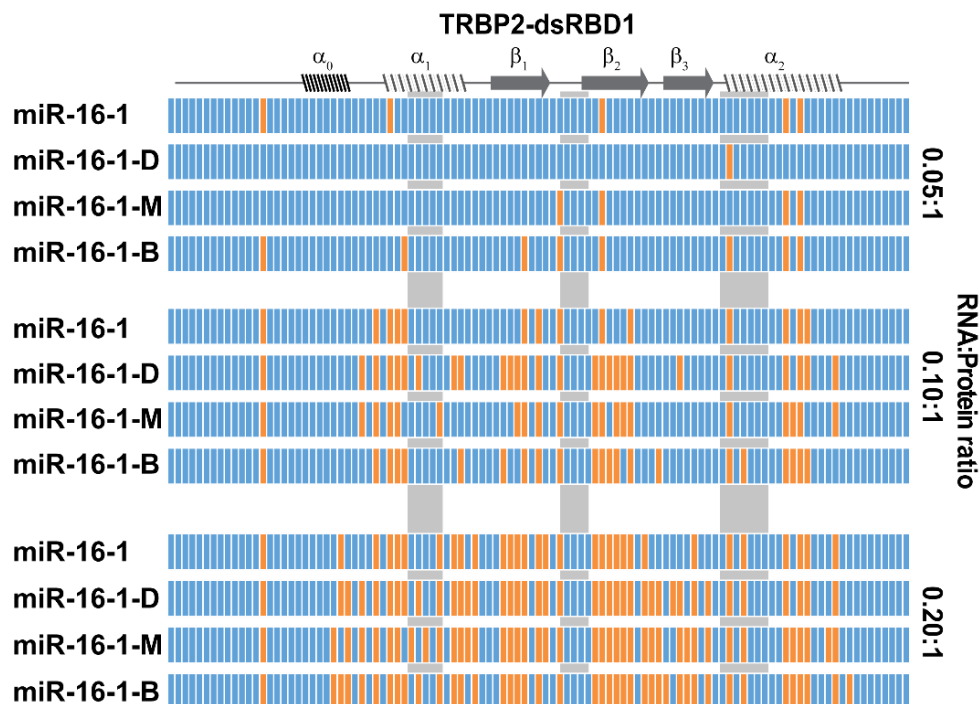
Figure 5.6: Mapping of the line-broadening profile of HSQC peaks of TRBP2-dsRBD1 on the addition of increasing concentration of RNA. Every cyan bar in the figure indicates an amino acid in the TRBP2-dsRBD1 and the orange bar indicates a disappeared peak due to the addition of topologically different dsRNAs (the name of each dsRNA has been mentioned on left of the bar). The RNA to protein ratio has been mentioned on the right of the figure. The secondary structure of the protein has been marked on the top and the RNA-binding regions have been highlighted in grey.
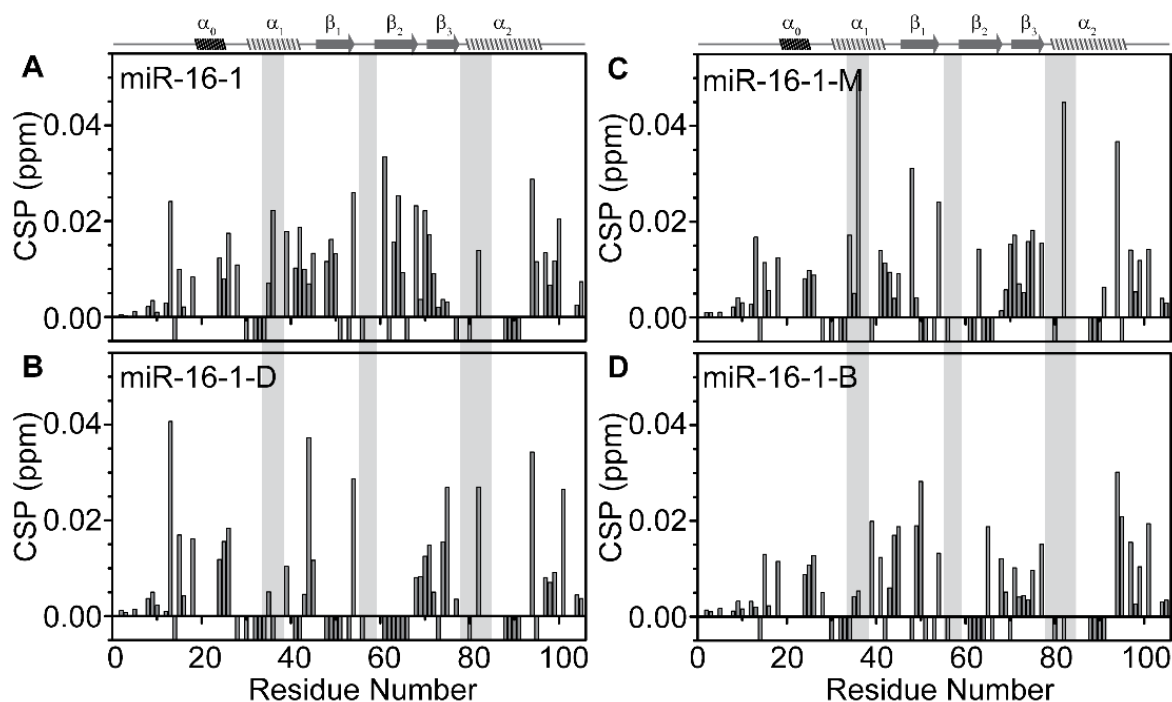
Figure 5.7: Chemical shift perturbations (CSP) calculated for TRBP2-dsRBD1 upon the addition of 0.1 equivalent of RNA. Four panels represent plots for (**A**) miR-16-1, (**B**) miR-16-1-D, (**C**) miR-16-1-M and (**D**) miR-16-1-B. The secondary structure of the protein has been marked on the top of each column and the RNA binding regions have been highlighted in grey in each plot. The negative bars for the CSPs are shown for the residues that broadened beyond detection at 0.1 equivalent of RNA concentration is added to the TRBP2-dsRBD1 protein sample.

To study the effect of dsRNA shape on the dynamics of the protein, nuclear spin relaxation experiments (R_1, R_2, and [^{1}H]-^{15}N-NOE) were performed by adding 0.05 equivalent of RNA to the TRBP2-dsRBD1. As the titration studies have shown a significant line-broadening, the relaxation rates (R_1 and R_2) and the [^{1}H]-^{15}N-NOE values for these peaks could not be determined at higher protein to RNA ratio. The nuclear spin relaxation parameters for the detectable peaks were calculated (as described in the Methods section) and have been plotted against residue numbers along with the rates for apo-protein (Figure 5.8). Figure 5.8 shows an increase in the R_1 rates for all the detected residues and for all shapes of the RNA, however, the increase in the R_1 rates varies for the topologically different RNAs. Similarly, R_2 rates also showed an increase to a different extent (observed mainly in the terminal regions of the protein) in the dsRNA shape-dependent manner. These changes supported the formation of dsRBD:dsRNA complex, which results in an increased rotational correlation time of the protein and thus increased R_1 rates. In addition, the significant line broadening with a corresponding increase in the R_2 rates might have originated from the increase in the conformational exchange between the apo- and RNA-bound state of the protein and/or due to complex formation. On the other hand, only minor changes were observed in the case of [^{1}H]-^{15}N-NOE values that are highly sensitive to the local motions at ps-ns timescale in the protein. Overall, these results suggest that along with the local motions in the protein at ps-ns timescale, motions at μs-ms timescale possibly get perturbed due to the RNA-binding interactions of dsRBDs.
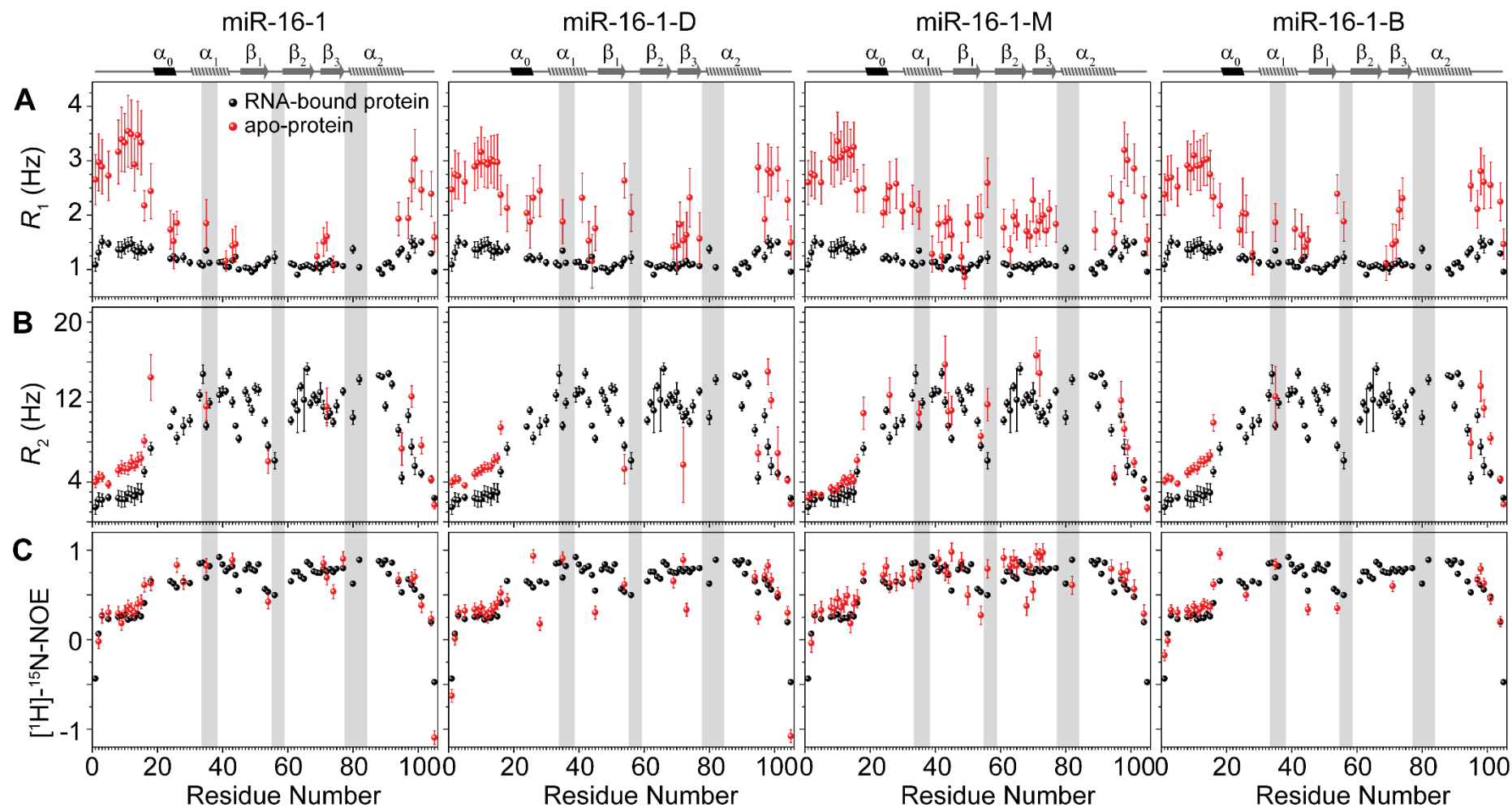
Figure 5.8: (**A**) ^{15}N-R_1, (**B**) ^{15}N-R_2 and (**C**) [^1H]-^{15}N-NOE for TRBP2-dsRBD1 protein in the absence (black) and in the presence (red) of RNA with different topologies as marked on the top of each column. The secondary structure of the protein has been marked on the top of each column and the RNA-binding regions have been highlighted in grey in each plot.

5.3.4. *Interaction of dsRBD with short RNA duplex*

The interaction between dsRBD and dsRNAs with distinct shapes have shown that they involve intermediate timescale exchange, it can be ascribed to the exchange between apo- and RNA-bound state of the protein or to the dsRBD diffusing along the length of the dsRNA (as has been reported by Sua Myong and coworkers[20]). This diffusion process is restricted by the length and any imperfections in the dsRNA[20,21]. Thus, to get more insights into the dynamics at dsRNA:dsRBD interface, a segment of miR-16-1-D – RNA without any helical imperfections – was used. The RNA segment (D10-RNA) selected included the known RNA-binding residues[9] with the shortest length of 10 base-pair used for interaction with TRBP in previously reported studies[22] (Figure 5.9). The interactions of the D10-RNA with TRBP2-dsRBD1 and dADAR-dsRBD1 were tested by isothermal titration calorimetry.
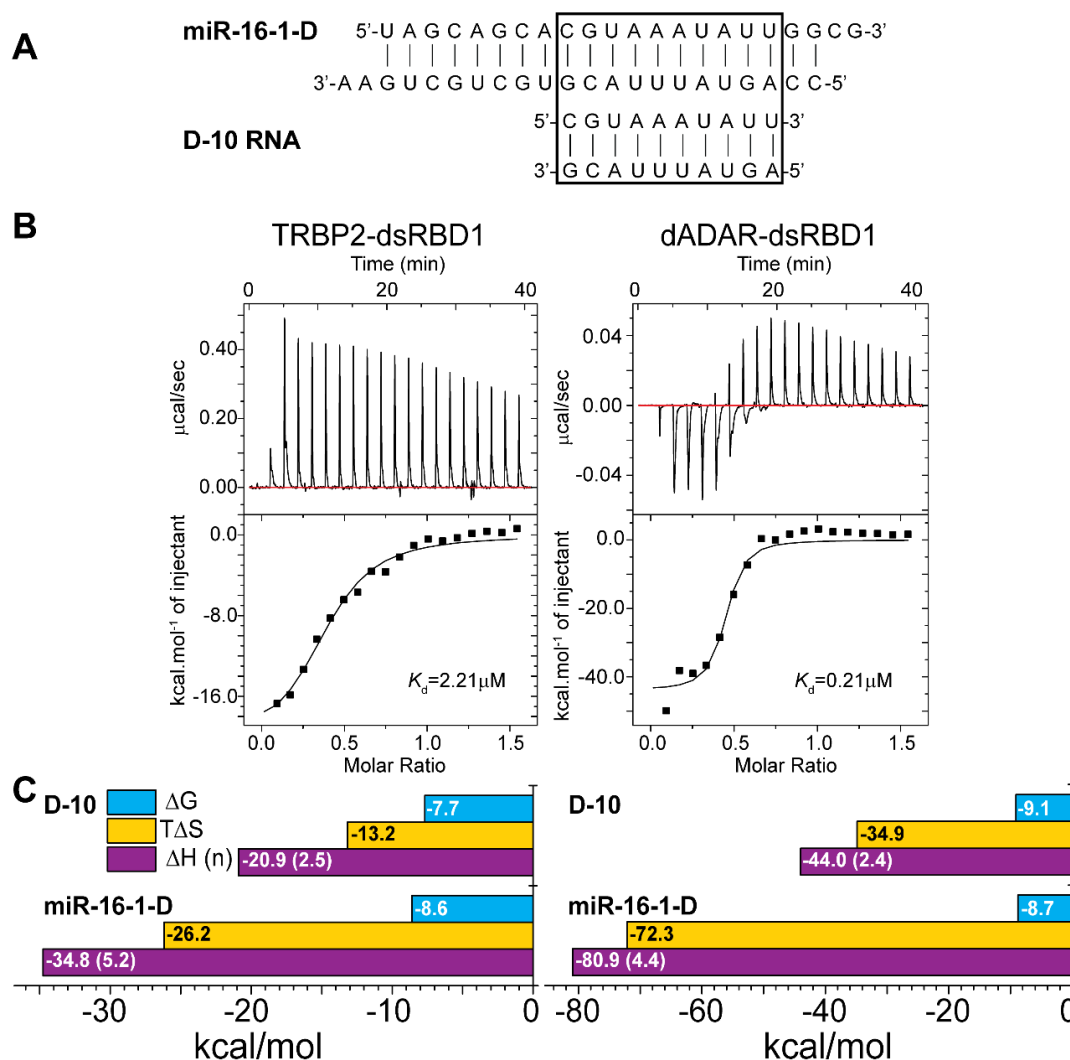
Figure 5.9: Interaction of D10-RNA with dsRBDs studied by ITC. (**A**) A sequence of D10-RNA has been derived from miR-16-1-D with minimum length required for binding to dsRBD as marked with a box. (**B**) Isothermal Titration Calorimetry data showing the interaction of D10-RNA with TRBP2-dsRBD1 and dADAR-dsRBD1. The K_d values have been calculated from the fitting of the data to one set of site binding model and have been indicated in the plot. (**C**) The comparison of thermodynamic parameters calculated from ITC data fitting for the interaction of dsRBDs and D10-RNA with that of dsRBDs and miR-16-1-D.

The titration shows that both the proteins were able to bind to the D10-RNA with similar binding affinity as that of longer RNA sequences with ΔG of -7.7 ± 0.1 kcal.mol^{-1} and -9.1 ± 0.3 kcal.mol^{-1} for TRBP2-dsRBD1 and dADAR-dsRBD1, respectively. The corresponding changes in *ΔH* and *TΔS* were found to be -20.9 ± 1.6 kcal.mol^{-1} and -13.2 ± 1.4 kcal.mol^{-1} for TRBP2-dsRBD1; and -44.0 ± 2.2 kcal.mol^{-1}, and -34.9 ± 2.0 kcal.mol^{-1} for dADAR-dsRBD1, respectively.
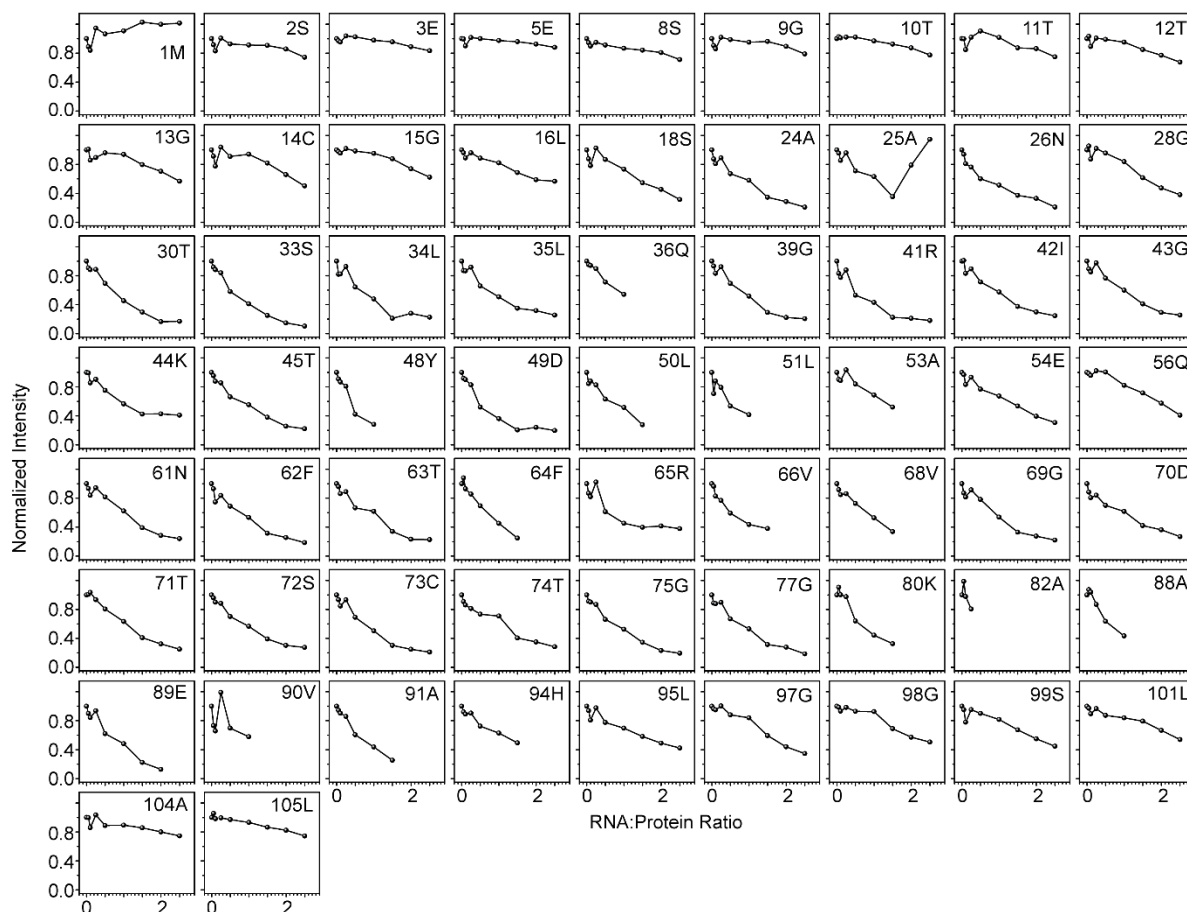
Figure 5.10: Intensity decay profile for TRBP2-dsRBD1 on interaction with D-10 RNA.
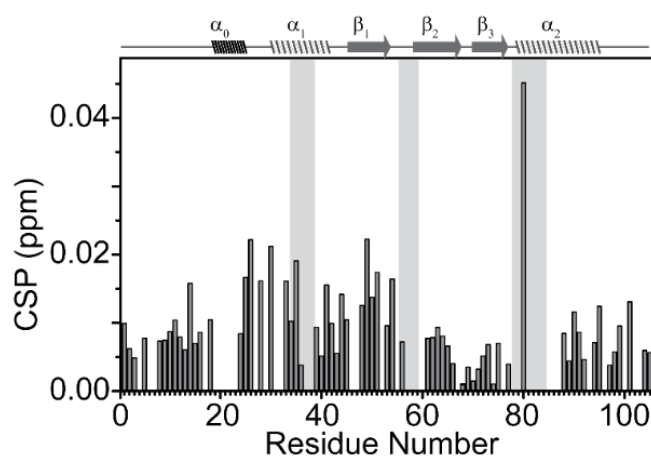
Figure 5.11: Chemical shift perturbations (CSP) calculated for TRBP2-dsRBD1 in presence of 0.5 equivalents of D10-RNA. The secondary structure of the protein has been marked on the top of the column and the RNA-binding regions have been highlighted in grey.

Further titrations of TRBP2-dsRBD1 with D10-RNA showed that it is able to bind to RNA, however, the peak broadening gets delayed and was observed only after protein-to-RNA ratio was increased further to 1:1. The decay in the peaks in the HSQC spectra was monitored up to 2.5 equivalents of RNA added to the protein and have been plotted for all four RNA (Figure 5.10). The plots show a gradual decrease in the peak intensity spread along the structured region of the protein as observed for longer RNA (Figure 5.10). This may represent the static binding[20,21] and the delay in the line-broadening could be due to the loss of the diffusive motions. The chemical shift perturbations determined at 1:0.5 Protein-to-RNA ratio (Figure 5.11) show no significant change in the structure of the protein as observed for other RNA duplexes. Since after adding 1.0 equivalents of RNA, HSQC peaks started to broaden, the studies of the dynamics in the bound-state of the protein were performed at 0.5 equivalents of D10-RNA. An HSQC spectrum with the resonance assignments in presence of 0.5 equivalents of D10-RNA is shown in Appendix Figure A.3.
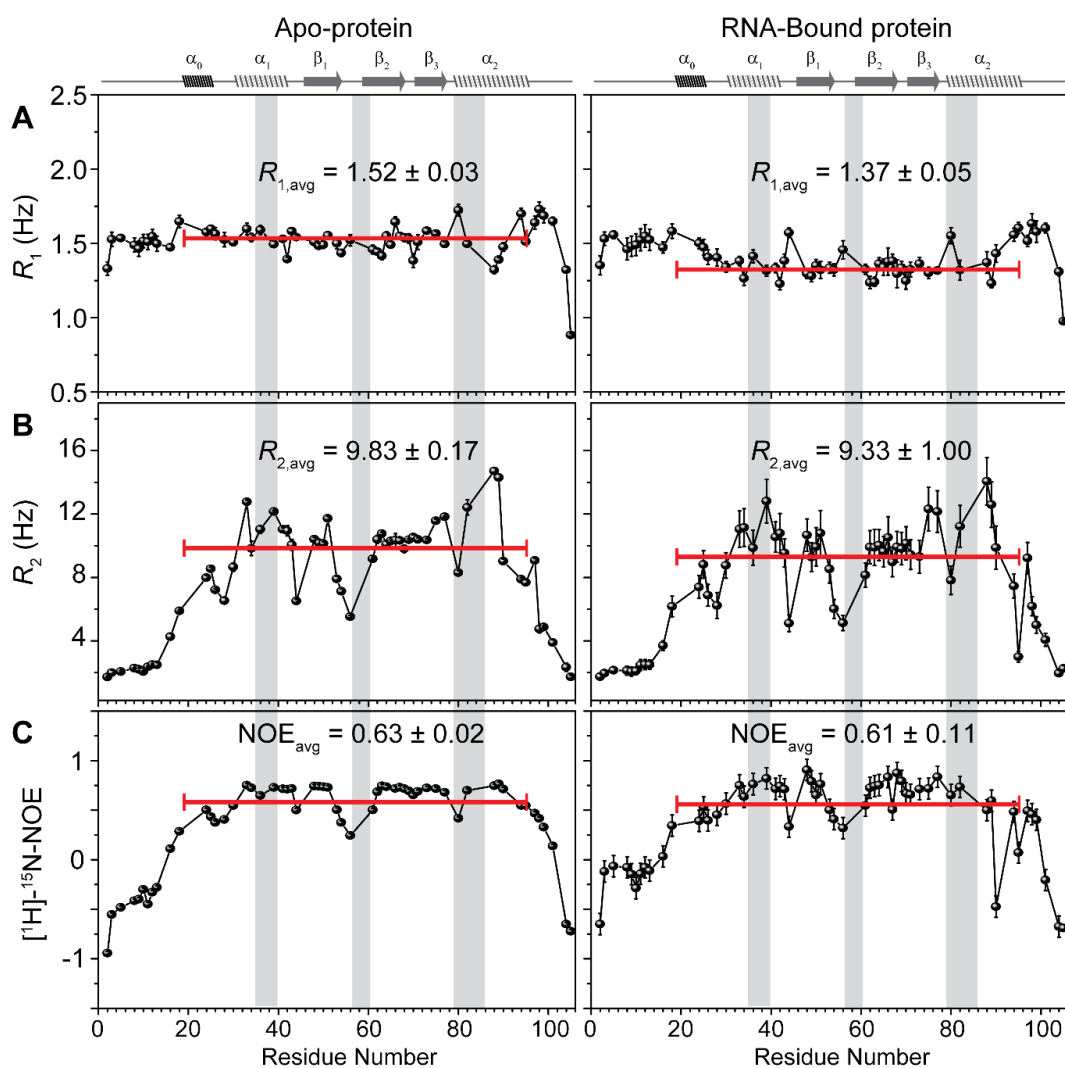
Figure 5.12: Comparison of ^{15}N-Relaxation parameters (**A**) ^{15}N-R_1, (**B**) ^{15}N-R_2 and (**C**) [^{1}H]-^{15}N-NOE values for TRBP2-dsRBD1 plotted against residue number for apo-protein and in presence of 0.5 equivalents of D10-RNA. The average values for the relaxation parameters for the residues in the structured region (18-95 aa) are mentioned in the figure. The secondary structure of the protein is marked on the top of each column and the RNA-binding regions are highlighted in grey in each plot.

Nuclear spin relaxation rates (R_1, R_2, and [^{1}H]-^{15}N-NOE) were calculated using 58 residues in presence of 0.5 equivalents of D-10 RNA (as described in the method section) and have been plotted against residue number (Figure 5.12) with the values for apo-protein and listed in Appendix Table A.14 - Table A.18. The average R_1, R_2 rates were 1.37 ± 0.05 and 9.33 ± 1.00 in RNA-bound protein, that were similar to the apo-state of the protein with average R_1 of 1.52 ± 0.03 and average R_2 of 9.83 ± 0.17. The NOE ratio also showed a similar pattern with an average [^{1}H]-^{15}N-NOE value of 0.41 ± 0.11 and 0.38 ± 0.02 for RNA-bound and apo-state of the protein, respectively. A comparison of these rates showed only minimal changes, which could be attributed to complex formation. Thus, the overall ps-ns dynamics in TRBP2-dsRBD1 were not affected due to the presence of the D10-RNA.

The slow dynamics at slower ms timescale in the protein were tested with the CPMG relaxation dispersion experiment. The $R_{2\text{eff}}$ calculated at different CPMG frequencies (ν_{CPMG}) for 55 residues with detectable peaks have been plotted against CPMG frequencies (Figure 5.13) and listed in Appendix Table A.20. Most of the residues do not show any dispersion in relaxation rates as observed for apo-protein except for a few residues in the β_1-strand (Y48, L50, L51, A53) and in the α_2-helix (A82, A88, and E89). The fitting of these relaxation rates to the Carver-Richards equation (in the fast exchange limit)[23,24] (Equation 5.2) could not yield a good fit due to large errors in the $R_{2\text{eff}}$ values.
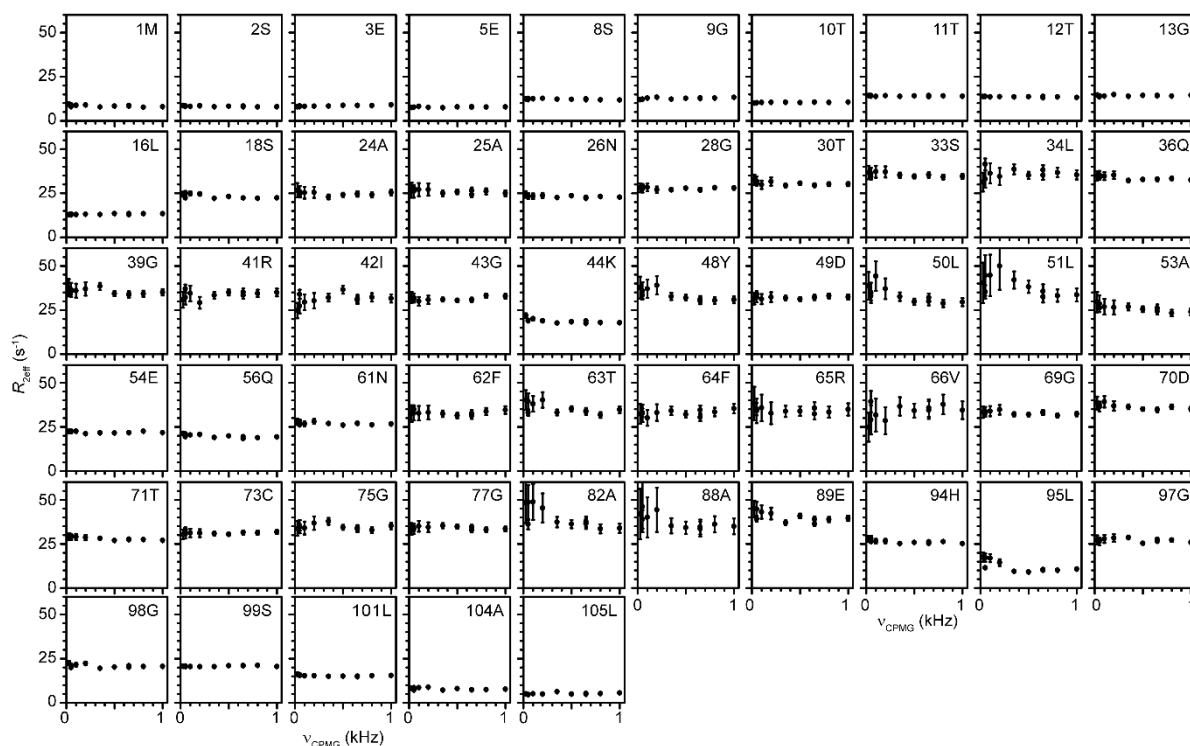
Figure 5.13: Plot of $R_{2\text{eff}}$ against CPMG frequency, ν_{CPMG}, for residues in TRBP2-dsRBD1 in presence of 0.5 equivalents of D10-RNA.

$$R_{2eff} = R_2 + \left(\frac{\varphi_{ex}}{k_{ex}}\right)\left(1 - \frac{2\,tanh(k_{ex}\tau)}{2k_{ex}\tau}\right) \tag{5.2}$$

where, R_2 is the intrinsic relaxation rate of each proton, $\varphi_{ex} = p_A p_B \Delta\omega^2$ is the exchange contribution to the effective relaxation rate and k_{ex} is the timescale of the exchange event.

Though the CPMG relaxation dispersion method was not able to detect the μs-ms timescale dynamics in the apo-state of the dsRBDs, it was detected by HARD NMR experiments. Therefore, to test the μs-ms dynamics in the RNA-bound state of the dsRBD (that are outside the CPMG-RD detection limit[24]), HARD NMR experiments[18,19,25] were performed and analyzed for the 60 peaks. The $R_{1\rho}$ and $R_{2\rho}$ rates were obtained by an exponential fit to the intensity data recorded with an increasing number of pulses applied during evolution thus increasing relaxation delay. The relaxation rates ($R_{1\rho}$ and $R_{2\rho}$), obtained by application of different adiabatic pulses of hyperbolic secant family (HSn), were plotted against residue number (listed in Appendix Table A.21 and Table A.22) and compared with the rates obtained for TRBP2-dsRBD1 protein in the absence of any RNA (Figure 5.14). The figure clearly shows dispersion in $R_{1\rho}$ and $R_{2\rho}$ rates suggesting the presence of motions at μs-ms timescale in the bound state of the protein. Further, the rates in the presence of RNA show more dispersion at certain sites than others and thus it is interesting to observe the dynamics present in the protein in the presence of RNA. The dynamics parameters (k_{ex}, p_B, and $\Delta\omega$) in the presence of D10-RNA were then calculated using a geometric approximation method[19] and have been listed in Appendix Table A.23 and mapped on the structure of the protein in Figure 5.15.
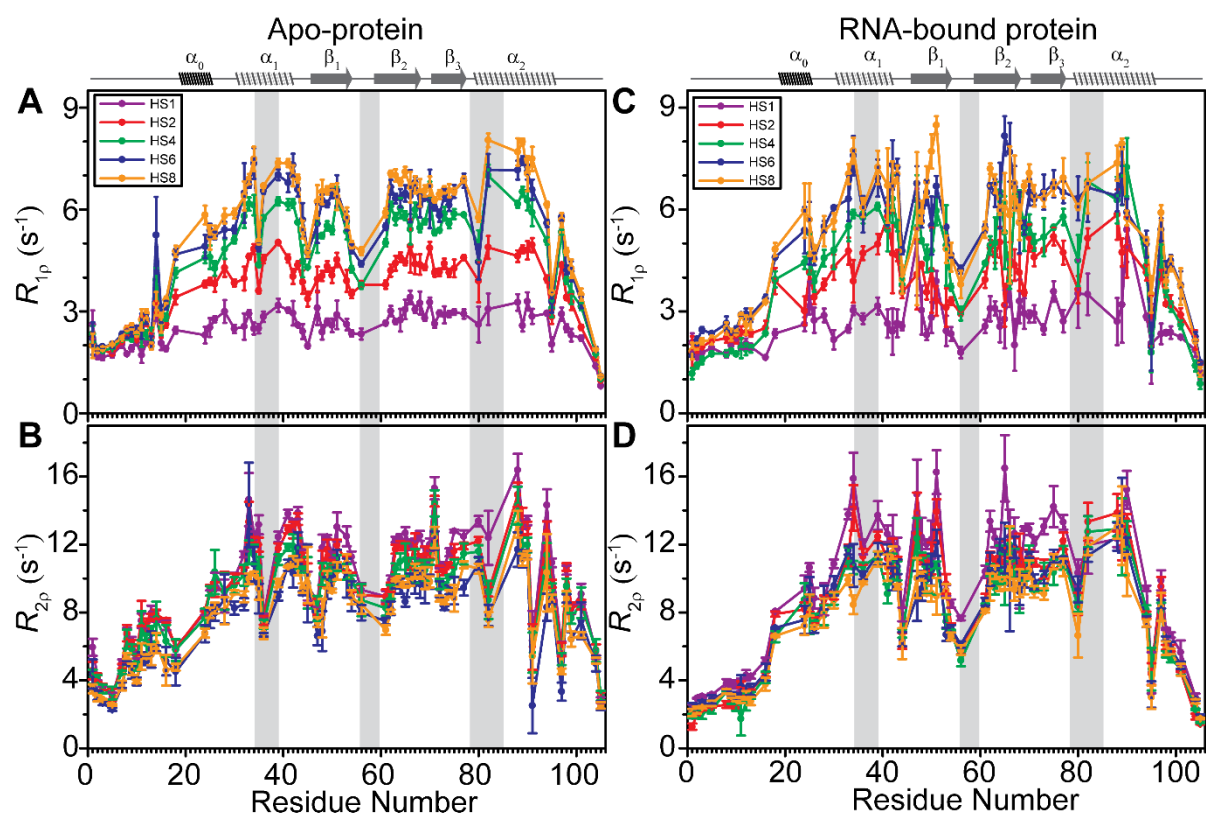
Figure 5.14: Comparison of Adiabatic $R_{1\rho}$ and $R_{2\rho}$ relaxation rates for TRBP2-dsRBD1 obtained in (**A** and **B**) apo-protein and in (**C** and **D**) RNA-bound protein with D10-RNA. The colors indicate the HSn pulse used for spin-locking during evolution. The secondary structure of the protein has been marked on the top of each column and the RNA-binding regions have been highlighted in grey in each plot.
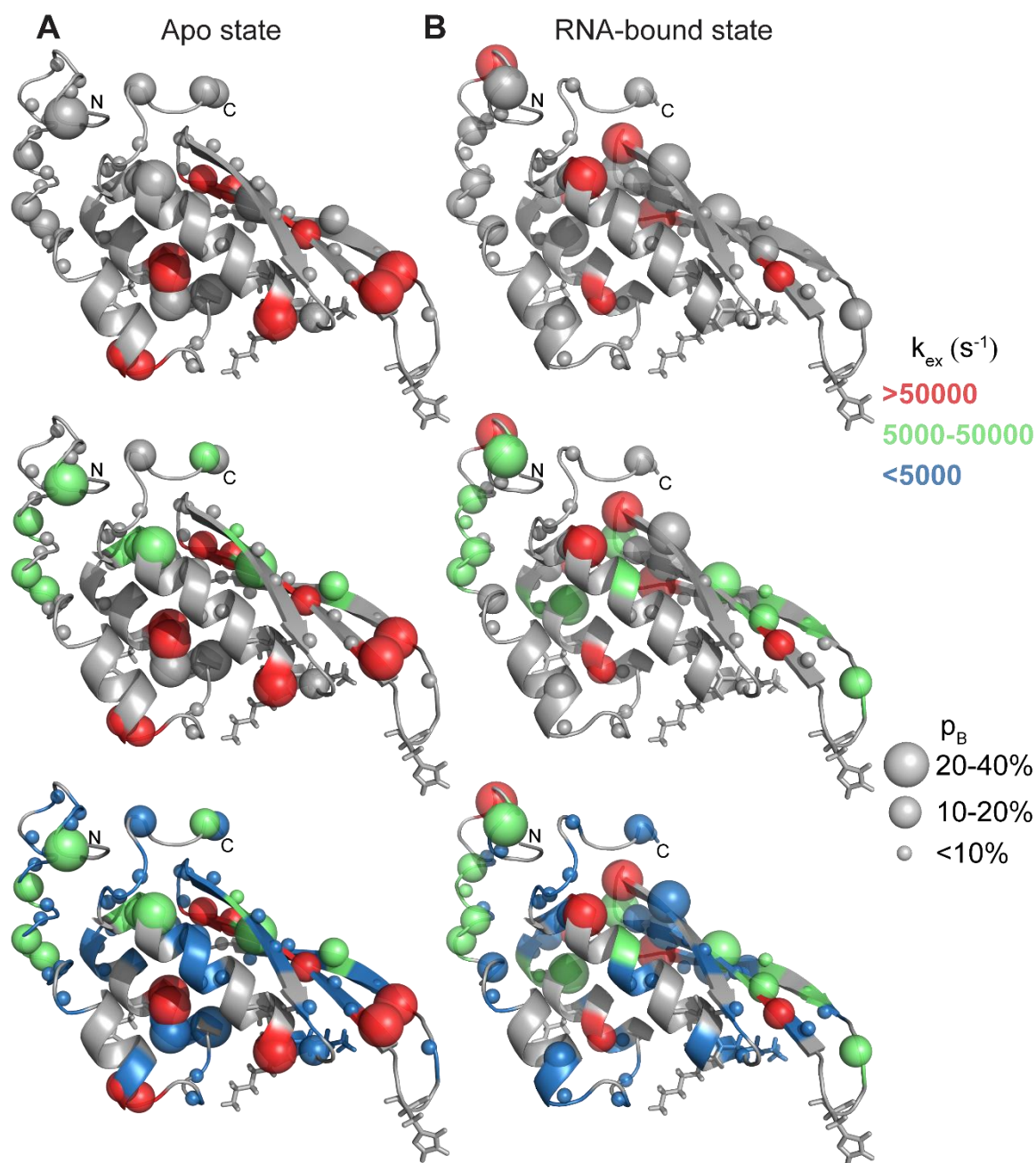
Figure 5.15: Mapping of dynamics parameters extracted from the HARD NMR data using the geometric approximation method for TRBP2-dsRBD1 in (**A**) apo- and (**B**) RNA-bound states. The k_{ex} values have been marked in color and the sphere size indicates the population of the excited state (p_B) (as shown on the right side of the figure). The RNA-binding residues have been shown in stick representation.

A careful analysis of k_{ex} and p_B values obtained in absence and presence of substrate RNA shows that the high-frequency motions (k_{ex} >50000 s^{-1}) present in and near RNA-binding residues (L35, Q36, E54, N61, and A82) are quenched in RNA-bound state and show most of the population in the RNA-bound state (p_B <5 %). The non-RNA-binding residue having exchange rate more than 50000 s^{-1} (A25, N26, F64, T67, V68) in apo-protein showed suppressed exchange – disappearance of red balls in Figure 5.15 – with exchange rates less than 5000 s^{-1} with higher population (>95 %) in the RNA-bound state (except for the residues T67 and V68 have excited state population of 21 and 16 % respectively). Surprisingly, few other residues L34, K44, V47, F62, T71, and H94 showed a higher exchange rate (k_{ex}

>50000 s^{-1}) in RNA-bound state with more than 15 % population in the excited state. In the RNA-bound state, residue S2, E3, G9, T10, G39, R41, L51, A53, Q56, R65, G69, T63, V90 showed exchange rates between 5000-50000 s^{-1} with about 10 % population in the excited state. The rest of the analyzed residues showed exchange rates of less than 5000 s^{-1}. Though the residues undergoing conformational exchange are changed from the apo-state to the RNA-Bound state of the protein, the spread of the conformational space available is similar as shown by a similar difference in the chemical shift ($\Delta\omega$) of the two states (a ground state in exchange with an excited state) up to ~1100 Hz.
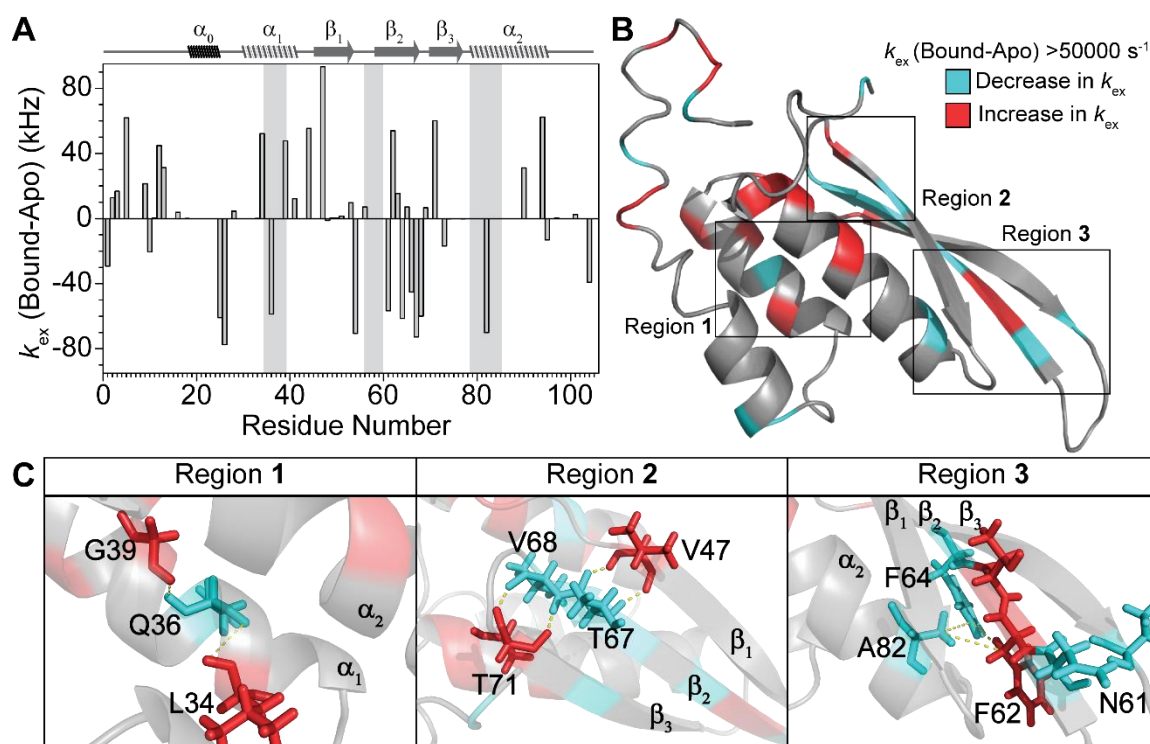
Figure 5.16: Effect of D10-RNA on conformational exchange in TRBP2-dsRBD1. (**A**) Plot of change in the conformational exchange rate (k_{ex}) for TRBP2-dsRBD1 from apo-state to RNA-bound state against residue number. The secondary structure of the protein is marked on the top of each column and the RNA-binding regions are highlighted in grey in each plot. (**B**) Mapping of residues on protein structure showing the change in k_{ex} greater than 50000 s^{-1} on RNA binding. (**C**) The regions marked in (**B**) showing transfer of conformational flexibility to nearby residues are enlarged and the connections between the residues are marked with dashed lines.

To compare the change in the conformational dynamics due to the presence of dsRNA, the difference of k_{ex} between the apo and bound state was calculated and has been plotted against residue number (Figure 5.16(A)). The plot suggests that the residue E5, L34, G39, K44, V47, F62, T71, and H94 show a large increase in the k_{ex} of about 50000 s^{-1} while residue A25, N26, Q36, E54, N61, F64, T67, V68, and A82 show a decrease in k_{ex} of about 50000 s^{-1}. The mapping of change in the k_{ex} on the protein structures showed that the residues with a suppressed and induced exchange in presence of RNA are present in the close vicinity to each other (Figure 5.16(B)). A closer look between the spatial separation of these residues shows that they are in close contact via either electrostatic or hydrogen bonding or hydrophobic interactions. For example, the residues involved in RNA binding in the α$_1$-helix Q36 show suppressed conformational exchange while the residues hydrogen bonded to it – due to

the connections stabilizing the helical structure – L34 and G39 show corresponding increase in the conformational exchange rates (Figure 5.16(C)). Similarly, residue T67 and V68 in β_2-strand showing suppressed exchange are connected to V47 in β_1-strand and T71 in β_3-strand respectively, with induced conformational exchange via dipolar interactions between the carbonyl oxygen and amide proton in the peptide backbone of these residues (Figure 5.16(C)). The methylene group of F62 with increased k_{ex} is in close vicinity to the phenyl ring of F64 and methyl group of A82 and may have hydrophobic interactions among them (Figure 5.16(C)).

5.4. *Discussion*

In order to explore the role of intrinsic dynamics in dsRBDs to interact dsRNAs in the cellular matrix, two dsRBDs – TRBP2-dsRBD1 and dADAR-dsRBD1 – were used along with four topologically different dsRNAs. As observed in Chapter 4, these dsRBDs exists as an ensemble of conformations, which are hypothesized to allow them to interact with multiple dsRNAs. From ITC based binding studies, it was observed that both dsRBDs show similar affinities to bind to the dsRNAs irrespective of imperfections in the structure. While this supports the TRBP2-dsRBD1 as a non-specific binder[6,16] for dsRNAs, it also sheds light on non-specificity of the dsRBD1 of dADAR. A careful analysis of the ΔH and $T\Delta S$ values obtained from the ITC data showed that it represents a case of a well-known concept of enthalpy-entropy compensation[26–29]. Furthermore, these results showed that enthalpic change during the dsRNA binding to dsRBD is compensated by the loss of entropy of the system with the net change in free energy of the system of ~8 kcal/mol. Another interesting thing to note is that the trend of the contribution of enthalpy and entropy varies with the dsRNA topologies and it follows a similar trend for the two dsRBDs. For example, the highest favorable enthalpy change is observed for miR-16-1-D during its interaction with either of the dsRBDs. Since interaction between dsRBD and dsRNA occurs via well-known contacts, the change in the enthalpic contribution can originate from the number of contacts (which includes hydrogen bonding or electrostatic or van der Walls interactions) that each dsRBD-dsRNA interface has. This is further supported by the number of binding sites that vary linearly with the enthalpy change for each of the dsRBD. Thus the interaction seems to be enthalpically driven process. In order to form these stable interactions with the dsRNA of varying shapes, it is necessary that the dsRBDs should have conformational adaptability to interact with their targets – which is our primary hypothesis. The formation of these interactions would alter the free energy barriers among conformational states and lead to redistribution of the conformational states favoring the formation of the bound state[26]. Yamashita *et al.* and Acevedo *et al.* have independently reported that the structure of either of the interacting partners – dsRBD or dsRNA – remains unaltered in the complexed state. Considering this fact, the shape of the RNA is the only variable among different pairs studied here[22,30]. As the shape of dsRNA varies with the imperfections in the secondary structure of the RNA, it will also change the spread of minor-major-minor grove responsible for interaction with dsRBDs. Since the number of interacting molecules (stoichiometry) and thus the enthalpy of interaction

varies with the shape of the RNA, suggests that the conformational redistribution should primarily be dsRNA-shape dependent This directs to the probable shape dependent conformational selection mechanism of the dsRBD-dsRNA interaction. Also, as the shape of the RNA varies, the enthalpic change is compensated by the corresponding entropic cost, in order to maintain the net change in free energy constant, that is a net result of solvent reorganization or the change in the overall flexibility of the protein and/or RNA molecule. As the similarity in the pattern of enthalpy-entropy compensation – varying with dsRNA-shape – was observed for both dsRBDs, the contribution for the recognition of dsRNA may be largely dependent on the dsRBD involved in the binding event. This suggests that the binding modes of dsRBDs with dsRNA are dsRNA shape-dependent. As the binding occurs in micro-molar concentration range suggesting possible involvement of dynamics in µs to ms timescale at protein-RNA interface.

NMR based titration experiments – monitored by ^{1}H-^{15}N HSQC spectra – have shown that most of the residues in the structured region of the protein are involved in the interaction with any of the dsRNA, however, the pattern of interactions is distinct for each of the dsRNA with a distinct topology Figure 5.6. This agrees with the conclusions from ITC-based titration experiments about the dsRNA shape-dependence of the interactions. Since minimal chemical shift perturbations were observed in presence of dsRNAs with substantial line-broadening observed in presence of 0.05 equivalents of RNA, structural changes if any in dsRBDs could not be determined. Further, the line-broadening in NMR signals observed in titration experiments Figure 5.6 and NMR-based relaxation experiments Figure 5.8 directed to the intermediate timescale exchange[24,31–34] between the apo- and RNA-bound states of the protein. The exchange might involve the diffusion of the dsRBDs along the length of the dsRNA as shown previously by Sua Myong and coworkers[20,21]. Since the diffusion process was reported to be length-dependent, a smaller RNA construct – 10 bp in length (D10-RNA) – was employed to study in detail the dynamics involved at the dsRBD-dsRNA interface. The thermodynamic parameters obtained from the ITC based binding studies with D10-RNA suggest that it binds with similar affinity as longer RNA constructs. The ΔH and $T\Delta S$ values support the enthalpy-entropy compensation with half the binding sites as that miR-16-1-D – from which the D10-RNA was derived – due to reduced RNA length. The titration monitored by HSQC spectra suggested that the interaction follows similar intermediate timescale exchange events as observed for longer RNA, however, the line-broadening is delayed and was observed after protein-to-RNA of 1:1. The chemical shift perturbations at 1:0.5 protein-to-RNA ratio shows a similar extent of perturbations as that of longer RNA. This is in line with the observation of Yamashita *et al*. showing no significant change in the apo- and RNA-bound structure of the dsRBD1 core (28-95 aa) of TRBP[22].

Comparison of nuclear spin relaxation parameters (R_1, R_2, and [^{1}H]-^{15}N-NOE) for D10RNA-bound TRBP2-dsRBD1 with those of apo-protein ensured that the ps-ns timescale dynamics of dsRBD are not affected due to the RNA binding. However, they also support a marginal reduction in R_1 rates

and an increase in R_2 rates that support the complex formation and may have a component due to intermediate exchange between apo and RNA-bound state of the protein. Though the RNA-binding was expected to suppress the exchange in the residues of the protein, however, it was fascinating to observe that in the bound state as well the protein had significant variations in R_2 (Figure 5.12) directing towards the possibility of the exchange in this state. The $R_{1\rho}$ and $R_{2\rho}$ plots of the HARD data showed that the variance in the R_2 observed in the RNA-bound state might originate from the µs-ms timescale exchange in the bound state of the protein. Further results from the analysis of HARD NMR data supported that binding has a significant effect on dynamics at µs-ms timescale. These results were quite exciting as a closer look at the clustering of residues undergoing significant change in the exchange ($k_{ex} > 50000$ s^{-1}) showed that the residues showing quenched exchange are in close spatial proximity to the residues with induced dynamics. The suppression in the exchange was not only restricted to the RNA-binding residues but also observed in the allosteric regions with higher k_{ex} in apo-protein. Such switching on and off of dynamics in residues in dsRBDs indicates a transfer of dynamics from a residue or a group of residues to neighboring ones via the tertiary structural contacts (Figure 5.16(B)). As suggested by Yamashita *et al.* and Acevedo *et al.* in their independent studies, neither dsRBD[22] nor dsRNA[30] change their shape upon the interaction between a dsRNA and a dsRBD. Thus, the switching of dynamics should lead to conformational transitions (occurring via hydrogen bonding or hydrophobic interactions, etc. (Figure 5.16(C))) necessary to maintain the overall tertiary fold of the dsRBD. This reinforces the adaptable nature of the dsRBDs in order to bind to dsRNAs. Though bound to dsRNA, the conformational space that can be sampled by the dsRBD was maintained as indicated by a similar spread of $\Delta\omega$ values. Since the dsRNA shape determines the dsRBD binding surface and is complemented by the adaptable nature of the dsRBDs, the intrinsic dynamics are important for the accurate targeting of the RNAs in the cellular environment.

5.5.   *Summary*

The examination of interactions among dsRBDs and dsRNAs by ITC titrations and NMR-based studies show that the interactions between the two binding partners are dsRNA shape-dependent. ITC titrations also suggested that these interactions are enthalpy driven and a typical case of enthalpy-entropy compensation. Further, the line-broadening profiles and relaxation studies in the presence of RNAs of different shapes and length indicate that the interactions involve intermediate timescale exchange. Probing of conformational exchange at µs timescale in RNA-bound state and its comparison to the similar timescale exchange in the absence of dsRNA showed that the transitions are switched between residues spatially close in the protein structure. This transfer of dynamics from RNA-binding and allosteric residues in the dsRBDs to the nearby residues focuses on the importance of the intrinsic dynamics in dsRBDs for the dsRBD-dsRNA interaction.

5.6. References

1   A. L. Feig, Applications of Isothermal Titration Calorimetry in RNA Biochemistry and Biophysics, *Biopolymers*, 2007, **87**, 293–301.

2   Kathleen B Hall, RNA–protein interactions, *Curr. Opin. Struct. Biol.*, 2002, **12**, 283–288.

3   Chirlmin Joo and D. Rueda, Eds., *Biophysics of RNA-Protein Interactions: A Mechanistic View*, Springer, 2019.

4   M. H. Bailor, X. Sun and H. M. Al-Hashimi, Topology links RNA secondary structure with global conformation, dynamics, and adaptation, *Science (80-.).*, 2010, **327**, 202–206.

5   H. Paithankar and J. Chugh, Characterization of conformational dynamics at microsecond timescale in the RNA-binding regions of dsRNA-binding domains, *bioRxiv*, 2019, 797449.

6   R. Acevedo, N. Orench-Rivera, K. A. Quarles and S. A. Showalter, Helical defects in MicroRNA influence protein binding by TAR RNA binding protein, *PLoS One*, 2015, **10**, e0116749.

7   C. Wostenberg, K. A. Quarles and S. A. Showalter, Dynamic origins of differential RNA binding function in two dsRBDs from the miRNA 'Microprocessor' complex, *Biochemistry*, 2010, **49**, 10728–10736.

8   C. Wostenberg, J. W. Lary, D. Sahu, R. Acevedo, K. A. Quarles, J. L. Cole and S. A. Showalter, The role of human Dicer-dsRBD in processing small regulatory RNAs, *PLoS One*, 2012, **7**, e51829.

9   T. Takahashi, S. Zenno, O. Ishibashi, T. Takizawa, K. Saigo and K. Ui-Tei, Interactions between the non-seed region of siRNA and RNA-binding RLC/RISC proteins, Ago and TRBP, in mammalian cells, *Nucleic Acids Res.*, 2014, **42**, 5256–5269.

10 N. R. Markham and M. Zuker, DINAMelt web server for nucleic acid melting prediction, *Nucleic Acids Res*, 2005, **33**, W577-81.

11 N. R. Markham and M. Zuker, UNAFold: software for nucleic acid folding and hybridization, *Methods Mol. Biol.*, 2008, **453**, 3–31.

12 M. J. Boniecki, G. Lach, W. K. Dawson, K. Tomala, P. Lukasz, T. Soltysinski, K. M. Rother and J. M. Bujnicki, SimRNA: a coarse-grained method for RNA folding simulations and 3D structure prediction, *Nucleic Acids Res.*, 2016, **44**, e63.

13 M. Magnus, M. J. Boniecki, W. Dawson and J. M. Bujnicki, SimRNAweb: a web server for RNA 3D structure modeling with optional restraints, *Nucleic Acids Res.*, 2016, **44**, W315-9.

14   F. Delaglio, S. Grzesiek, G. W. Vuister, G. Zhu, J. Pfeifer and A. Bax, NMRPipe: a multidimensional spectral processing system based on UNIX pipes, *J Biomol NMR*, 1995, **6**, 277–293.

15   W. Lee, M. Tonelli and J. L. Markley, NMRFAM-SPARKY: Enhanced software for biomolecular NMR spectroscopy, *Bioinformatics*, 2015, **31**, 1325–1327.

16   M. P. M. H. Benoit, L. Imbert, A. Palencia, J. Pérard, C. Ebel, J. Boisbouvier and M. J. Plevin, The RNA-binding region of human TRBP interacts with microRNA precursors through two independent domains, *Nucleic Acids Res.*, 2013, **41**, 4241–4252.

17   M. Tollinger, N. R. Skrynnikov, F. A. Mulder, J. D. Forman-Kay and L. E. Kay, Slow dynamics in folded and unfolded states of an SH3 domain, *J Am Chem Soc*, 2001, **123**, 11341–11352.

18   S. Mangia, N. J. Traaseth, G. Veglia, M. Garwood and S. Michaeli, Probing slow protein dynamics by adiabatic R(1rho) and R(2rho) NMR experiments, *J Am Chem Soc*, 2010, **132**, 9979–9981.

19   F. A. Chao and R. A. Byrd, Geometric Approximation: A New Computational Approach To Characterize Protein Dynamics from NMR Adiabatic Relaxation Dispersion Experiments, *J Am Chem Soc*, 2016, **138**, 7337–7345.

20   X. Wang, L. Vukovic, H. R. Koh, K. Schulten and S. Myong, Dynamic profiling of double-stranded RNA binding proteins, *Nucleic Acids Res.*, 2015, **43**, 7566–7576.

21   H. R. Koh, M. A. Kidwell, K. Ragunathan, J. A. Doudna and S. Myong, ATP-independent diffusion of double-stranded RNA binding proteins, *Proc. Natl. Acad. Sci. U. S. A.*, 2013, **110**, 151–156.

22   S. Yamashita, T. Nagata, M. Kawazoe, C. Takemoto, T. Kigawa, P. Güntert, N. Kobayashi, T. Terada, M. Shirouzu, M. Wakiyama, Y. Muto and S. Yokoyama, Structures of the first and second double-stranded RNA-binding domains of human TAR RNA-binding protein, *Protein Sci.*, 2011, **20**, 118–130.

23   O. Millet, J. P. Loria, C. D. Kroenke, M. Pons and A. G. Palmer, The static magnetic field dependence of chemical exchange linebroadening defines the NMR chemical shift time scale, *J. Am. Chem. Soc.*, 2000, **122**, 2867–2877.

24   I. R. Kleckner and M. P. Foster, An introduction to NMR-based approaches for measuring protein dynamics, *Biochim. Biophys. Acta - Proteins Proteomics*, 2011, **1814**, 942–968.

25   N. J. Traaseth, F. A. Chao, L. R. Masterson, S. Mangia, M. Garwood, S. Michaeli, B. Seelig and G. Veglia, Heteronuclear Adiabatic Relaxation Dispersion (HARD) for quantitative analysis of

conformational dynamics in proteins, *J Magn Reson*, 2012, **219**, 75–82.

26   J. M. Fox, M. Zhao, M. J. Fink, K. Kang and G. M. Whitesides, The Molecular Origin of Enthalpy/Entropy Compensation in Biomolecular Recognition, *Annu. Rev. Biophys.*, 2018, **47**, 223–250.

27   J. D. Dunitz, Win some, lose some: enthalpy-entropy compensation in weak intermolecular interactions, *Chem. Biol.*, 1995, **2**, 709–712.

28   L. Movileanu and E. A. Schiff, Entropy-enthalpy compensation of biomolecular systems in aqueous phase: A dry perspective, *Monatshefte fur Chemie*, 2013, **144**, 59–65.

29   A. T. Fenley, H. S. Muddana and M. K. Gilson, Entropy-enthalpy transduction caused by conformational shifts can obscure the forces driving protein-ligand binding, *Proc. Natl. Acad. Sci. U. S. A.*, 2012, **109**, 20006–20011.

30   R. Acevedo, D. Evans, K. A. Penrod and S. A. Showalter, Binding by TRBP-dsRBD2 Does Not Induce Bending of Double-Stranded RNA, *Biophysj*, 2016, **110**, 2610–2617.

31   C. Göbl and N. Tjandra, Application of solution NMR spectroscopy to study protein dynamics, *Entropy*, 2012, **14**, 581–598.

32   J. G. Kempf and J. P. Loria, Protein dynamics from solution NMR, *Cell Biochem. Biophys.*, 2002, **37**, 187–211.

33   A. G. Palmer, Chemical exchange in biomacromolecules: Past, present, and future, *J. Magn. Reson.*, 2014, **241**, 3–17.

34   A. G. Palmer, NMR characterization of the dynamics of biomacromolecules, *Chem. Rev.*, 2004, **104**, 3623–3640.

Chapter 6 Conclusion

The broad range of cellular activities – ranging from cell-growth, development, to death – involve interactions between double-stranded RNAs (dsRNAs) and dsRNA-binding domains (dsRBDs)[1,2]. The dsRBDs have a well-defined α-β-β-β-α structural fold[1,2] and interact with dsRNAs via minor-major-minor grooves in the A-form helical structure[3]. A handful of dsRBDs in the cellular matrix are exposed to topologically diverse dsRNAs. The difference in the topology[4] of the dsRNA originates from the imperfection in the duplex like an internal loop or a bulge, etc. In order to understand how dsRBDs recognize dsRNAs of diverse topologies, we employed two of these dsRBDs from two different species – TRBP2-dsRBD1 from *Homo sapiens* and dADAR-dsRBD1 from *Drosophila melanogaster* – and studied their interaction with the substrate using various biophysical techniques, with NMR spectroscopy as a primary technique.

As a first step, the two proteins were over-expressed in the bacterial expression system and purified to more than 95% purity. The backbone resonance assignment (with few sidechain resonances) for TRBP2-dsRBD1 was accomplished by using triple-resonance experiments and ^{15}N-edited-TOCSY-HSQC experiment. These resonances were used to calculate the structure of the protein using CS-rosetta program[5]. The structure showed the presence of an additional helix α_0 present at the N-terminus of the dsRBD structural fold[6,7]. A comparison of the dsRBD core with the previously reported crystal structure[8] showed a good match between the two structures. The resonance assignments in the HSQC spectrum of dADAR-dsRBD1 were transferred from the assignments reported in literature[9].

To gain some insights into the thermal stabilities of the two dsRBDs, CD-based melting studies were performed which showed a similar thermal melting profile of the two proteins with a melting temperature of 45°C. This suggested that the two proteins have low thermal stabilities. The analysis of nuclear spin relaxation parameters (R_1, R_2, and [^{1}H]-^{15}N-NOE) showed that the two dsRBDs exhibit differential dynamics profile at ps-ns timescale. The residues in dADAR-dsRBD1 were found to be more rigid than those in TRBP2-dsRBD1. However, both the proteins exhibited slower μs-ms timescale motions in the residues which were not restricted to the RNA-binding region but were rather spread across the backbone. Further characterization of these motions by relaxation dispersion methods showed that they exhibit a parallel dynamics profile in two dsRBDs studied. In both the proteins, the RNA-binding residues, and a few allosteric residues exhibited motions at faster μs timescale with $k_{ex} >$ 50000 s^{-1}. Many of the residues in both the proteins also showed presence of motions with 50000 s$^{-1} >$ $k_{ex} >$ 5000 s^{-1} or $k_{ex} <$ 5000 s^{-1}. The presence of dynamics at multiple sites suggested that the dsRBDs exist as a conformational ensemble which might support their interaction with dsRNAs.

To study the effect of different dsRNA topologies on dsRBD-dsRNA interaction, three mutant RNAs were designed from the miR-16-1 RNA duplex (a known binder) to create an assortment of topologies. The binding studies of four RNAs with each of the dsRBD by ITC showed that the dsRBDs bind to all four RNAs with similar affinities. However, the binding modes of dsRBDs varied with

variation in dsRNA topology. The interactions were driven by the enthalpic terms and were found to follow a well-studied case of enthalpy-entropy compensation. The shape-dependent effect on dsRBD-dsRNA interactions were upheld by the differential line-broadening pattern observed for TRBP2-dsRBD1 when titrated with four dsRNAs of different topologies. The line-broadening might have originated from intermediate timescale exchange between free and RNA-bound state of the protein and/or diffusion of dsRBD along dsRNA (as reported by Wang *et al*[10]). Similar conclusions can be drawn from the limited number of site-specific nuclear spin relaxation parameters (R_1, R_2, and [^{1}H]-^{15}N-NOE) obtained for TRBP2-dsRBD1 in presence of dsRNAs. Further characterization of µs-ms timescale motions in the dsRNA-bound state using a short RNA duplex revealed that high-frequency motions (at µs timescale) present in free dsRBDs are transferred to the neighboring residues during dsRBD-dsRNA interaction. These results support the conformational adaptability of the dsRBDs to interact with dsRNAs of diverse topologies originates from their inherent conformational dynamics.

In conclusion, our studies reported a detailed characterization of the intrinsic dynamics of dsRBDs at multiple timescales suggesting it as an inherent property of the structural fold of dsRBD. The binding studies further implied that these conformational dynamics play an important role in the interaction with dsRNA and allow dsRBDs to recognize with dsRNA irrespective of the structural variations.

References

1   G. Masliah, P. Barraud and F. H.-T. Allain, RNA recognition by double-stranded RNA binding domains: a matter of shape and sequence, *Cell. Mol. Life Sci.*, 2013, **70**, 1875–1895.

2   B. Tian, P. C. Bevilacqua, A. Diegelman-Parente and M. B. Mathews, The double-stranded-RNA-binding motif: Interference and much more, *Nat. Rev. Mol. Cell Biol.*, 2004, **5**, 1013–1023.

3   I. Fierro-Monti and M. B. Mathews, Proteins binding to duplexed RNA: one motif, multiple functions, *Trends Biochem. Sci.*, 2000, **25**, 241–246.

4   M. H. Bailor, X. Sun and H. M. Al-Hashimi, Topology links RNA secondary structure with global conformation, dynamics, and adaptation, *Science (80-.).*, 2010, **327**, 202–206.

5   Y. Shen, R. Vernon, D. Baker and A. Bax, De novo protein structure generation from incomplete chemical shift assignments, *J. Biomol. NMR*, 2009, **43**, 63–78.

6   H. Paithankar, P. V. Jadhav, A. S. Naglekar, S. Sharma and J. Chugh, 1H, 13C and 15N resonance assignment of domain 1 of trans-activation response element (TAR) RNA binding protein isoform 1 (TRBP2) and its comparison with that of isoform 2 (TRBP1), *Biomol. NMR Assign.*, 2018, **12**, 189–194.

7   G. Masliah, C. Maris, S. L. König, M. Yulikov, F. Aeschimann, A. L. Malinowska, J. Mabille, J. Weiler, A. Holla, J. Hunziker, N. Meisner-Kober, B. Schuler, G. Jeschke and F. H. Allain, Structural basis of siRNA recognition by TRBP double-stranded RNA binding domains, *EMBO J.*, 2018, e97089.

8   S. Yamashita, T. Nagata, M. Kawazoe, C. Takemoto, T. Kigawa, P. Güntert, N. Kobayashi, T. Terada, M. Shirouzu, M. Wakiyama, Y. Muto and S. Yokoyama, Structures of the first and second double-stranded RNA-binding domains of human TAR RNA-binding protein, *Protein Sci.*, 2011, **20**, 118–130.

9   P. Barraud, B. S. E. Heale, M. A. O'Connell and F. H. T. Allain, Solution structure of the N-terminal dsRBD of Drosophila ADAR and interaction studies with RNA, *Biochimie*, 2012, **94**, 1499–1509.

10   X. Wang, L. Vukovic, H. R. Koh, K. Schulten and S. Myong, Dynamic profiling of double-stranded RNA binding proteins, *Nucleic Acids Res.*, 2015, **43**, 7566–7576.

Appendix 1 Protein Over-expression and Purification Protocol

Preparation of Stock Solutions

LB media

- Make 1 x 1liter ml solutions (Dissolve 20 g in 1000 ml of distilled water in a conical flask covered with a non-absorbent cotton plug). Autoclave media and let it cool.
- Make 1 x 10 ml solutions (Dissolve 0.2 g in 10 ml of distilled water in a glass tube covered with a non-absorbent cotton plug). Autoclave media and let it cool.

Preparation stock solutions for buffers for protein purification

- 1 M Tris-HCl:

Dissolve 15.76 g of Tris-HCl in 900 ml autoclaved water. Keep overnight to stabilize. Adjust pH to 7.5 using HCl and make up the volume to 1 liter with autoclaved water. Autoclave and store at room temperature.

- 3 M Imidazole:

Dissolve 20.424 g of imidazole in 90 ml autoclaved water and make up the volume to 100 ml with autoclaved water. Autoclave and store at room temperature.

- 5 M NaCl:

Dissolve 292.2 g of NaCl in 900 ml of autoclaved water and make up the volume to 1 liter with autoclaved water. Autoclave and store at room temperature.

- 1 M DTT:

Dissolve 15.425 g of DTT in 100 ml Autoclaved water. Filter sterilize in sterile container and store at -20°C until use.

- 5% Polyethylene(imine):

Mix 100 µl of 50% polyethylene(imine) in 1 ml of autoclaved water.

- Saturated Ammonium sulfate solutions

Add 76.6 g of Ammonium sulfate to 100 ml autoclaved water. Allow to dissolve. Filter sterilize. (**Note:** Not all ammonium sulfate will dissolve in water some salt remains as such as the solution becomes saturated.)

- Kanamycin Stock solution (50 mg/ml)

Weigh 500 mg of Kanamycin di-sulfate. Dissolve in 10 ml autoclaved water. Filter sterilize in the hood. Make aliquots of 1 ml each and store at -20°C.

- 20 mg/ml Lysozyme:

Dissolve 100 mg of lysozyme in 5 ml of distilled water. Make aliquots of 1 ml in micro-centrifuge tubes. Store at -20°C until use.

- 1 M IPTG

Dissolve 2.383 g of IPTG in 10 ml of distilled water. Filter sterilize through a syringe-filter. Make aliquots of 1 ml each in micro-centrifuge tubes. Store at -20°C until use.

- Protease Inhibitor Cocktail (10X) solution

Dissolve 1 tablet of SigmaFast protease inhibitor cocktail in 10 ml of distilled water. Filter sterilize through a syringe-filter. Make aliquots of 1 ml each in micro-centrifuge tubes. Store at -20°C until use.

- 100 mM PMSF

Dissolve 0.174 g of PMSF in 10 ml of 2-propanol, anhydrous. Keep on rotospin to dissolve for about 15-30 min. Store at -20°C until use.

- 1 M Sodium Phosphate dibasic (Na_2HPO_4)

Dissolve 7.09 g of Sodium phosphate dibasic in about 40 ml of water and make up the volume to 50 ml with water. Filter and autoclave. Store at room temperature until use.

- 1 M Sodium Phosphate monobasic (NaH_2PO_4)

Dissolve 93.05 g of EDTA-disodium salt dihydrate in about 450 ml of water. Adjust pH to 8 to dissolve EDTA completely. Make up the volume to 500 ml. Filter and autoclave. Store at room temperature until use.

- 0.5 M EDTA

Dissolve 5.99 g of Sodium phosphate monobasic in about 40 ml of water and make up the volume to 50 ml with water. Filter and autoclave. Store at room temperature until use

Protocol for Over-expression and Purification of TRBP2-dsRBD1

Preparation of buffers for protein purification

(All volumes for buffer preparations to be taken from the stock solutions)

Equilibration Buffer	2000 ml
20 mM Tris HCl, pH 7.5	40 ml
500 mM NaCl	200 ml
10% Glycerol	200 ml
10 mM Imidazole	6.68 ml
1 mM DTT	2 ml

Wash Buffer	500 ml
20 mM Tris HCl, pH 7.5	10 ml
500 mM NaCl	50 ml
10% Glycerol	50 ml
30 mM Imidazole	5 ml
1 mM DTT	0.5 ml

Elution Buffer	100 ml
20 mM Tris HCl, pH 7.5	2 ml
500 mM NaCl	10 ml
10% Glycerol	10 ml
300 mM Imidazole	10 ml
1 mM DTT	0.1 ml

TEV Cleavage Buffer	250 ml
20 mM Tris HCl, pH 7.5	5 ml
25 mM NaCl	1.25 ml
10% Glycerol	25 ml
1 mM DTT	0.25 ml

Gel Filtration Buffer	1 L
20 mM Tris HCl, pH 7.5	20 ml
500 mM NaCl	100 ml
10% Glycerol	100 ml
1 mM DTT	1 ml

1. Add stock liquids (Tris HCl, imidazole, NaCl, Glycerol)
2. Add autoclaved water to 90% of the final volume.
3. Titrate pH to 7.5.
4. Makeup the volume with autoclaved water.
5. Filter sterilize into a sterile bottle.
6. Store all at 4°C.

Note: Add DTT just before use

NMR Buffer	100 ml
10 mM Sodium Phosphate	(367.5 µl of 1M NaH_2PO_4 + 132.5 µl of 1M Na_2HPO_4)
100 mM NaCl	2 ml
1mM EDTA	0.2 ml
1mM DTT	0.1 ml

Overexpression of TRBP2-dsRBD1 protein in a bacterial expression system

1. Prepare LB media
2. Add Kanamycin to the sterile LB media (10 ml) to a final concentration of 50 µg/ml.

3. Use a pipette-tip to scrap BL21(DE3) cells containing appropriate plasmid from Glycerol stock and transfer it to 10 ml LB medium containing antibiotic.

4. Allow cells to grow overnight at 37°C in incubator shaker with shaker speed set to 225 rpm.

5. Add 10 ml overnight culture to 1 liter of LB media containing Kanamycin (final conc. 50 μg/ml) and continue incubation with shaking.

6. Monitor the OD600 at every ½ hr till it reaches ~0.8-1.0. (Note: It takes not more than 3 hr to reach OD600 to ~0.8).

7. Add IPTG (1 M stock) to a final concentration of 1 mM and continue induction for 8 hr at 28°C with shaking.

8. Centrifuge solution for 20 min at 8000xg, 4°C in a high-speed centrifuge. Decant the supernatant.

Transfer the pellet to a 50 ml centrifuge tube by re-suspending it in the same LB media. Centrifuge at 4000 rpm for 20 min and Store the pellet at -20 °C until use. [Usually 1 liter culture→ 4-6 g (pellet weight)].

Cell Lysis and Purification of TRBP2-dsRBD1 protein

Important note: PMSF acts as a serine protease suicide inhibitor whose half-life is drastically shortened by the presence of water. It should, therefore, be prepared in 2-Propanol (not ethanol, as this is rarely 100% pure) immediately prior to use. There is some evidence that it can be stable when stored at -20°C. It is also extremely toxic!!!

1. Resuspend the cell pellet in 10-15 ml of Lysis buffer pH 7.5. Keep the cell pellet on the ice during lysis.

2. Add 1% volume of Triton-X 100 i.e. 500 μl of Triton-X 100 for 50 ml of the final volume.

Note: Add 500 μl of Triton-X 100 in ~10 ml of lysis buffer. Warm to dissolve and cool on ice and then use.

3. Add 62.5 μl of Lysozyme solution (20 mg/ml stock) to the above solution.

4. Incubate for 10 min on ice. (till you get viscous solution i.e. DNA is released in the solution).

5. Add 100 μl of PMSF and sonicate using probe sonicator.

(Sonication cycle: 10 s pulse-10 s gap-10 s pulse-10 s gap-10 s pulse, amplitude 70%)

6. Add 100 μl of PMSF again and repeat the sonication cycle. (Repeat till solution viscosity is reduced).

7. Add protease inhibitor. (2 ml of SigmaFAST protease inhibitor cocktail solution (10X) is required for 4 g of cell pellet)

8. Add cell lysate to 50 ml oak ridge tubes and centrifuge at 32000xg for 30 min at 4°C in the high-speed centrifuge.

9. Transfer the supernatant to a fresh 50 ml corning tube. (Total soluble protein TSP-I).

10. Add 250 μl of Polyethylene(imine) solution and allow it to incubate for 30 min on ice. Then centrifuge at 10000xg for 30 min at 4°C. Collect supernatant in a fresh tube.

11. Repeat step 10 till no precipitate is observed after centrifugation.

12. Then add saturated ammonium sulfate solution to 60% saturation. (Add 150 ml of saturated ammonium sulfate solution to 100 ml of the TSP.) Allow to incubate on ice overnight with mixing.

13. Centrifuge at 10000xg for 30 min and collect the precipitate. (Note: This precipitate floats over the solution and does not settle down. Take necessary precautions to avoid loss of precipitate).

14. Re-suspend the precipitate in ~30-40 ml of Lysis buffer and dialyze against lysis buffer to remove ammonium sulfate. (Repeat the dialysis step with at least 3 rounds of fresh lysis buffer).

15. Transfer the dialyzed protein solution to a fresh 50 ml centrifuge tube.

Purification of tagged protein by Ni-NTA Affinity Chromatography

1. Prepare HisTrap column for protein binding.
   a. Pass 5-6 Column Volume (CV) of autoclaved water through the Ni-NTA column (HisTrap 5 ml column, GE Healthcare).
   b. Equilibrate the column using 5-10 CV of Lysis buffer.

2. Circulate TSP-I through the Ni-NTA column for about 3 hr at 4°C to allow binding of the protein to the column.

3. Pass 40-50 CV of wash buffer (pH = 7.5) through the column to remove any non-specific protein binding.

4. Elute the bound protein by passing the elution buffer (pH = 7.5).
   a. Fill the column with elution buffer. Allow to equilibrate for 30 min.
   b. Elute by passing fresh 1 CV elution buffer. Collect the eluted fraction.
   c. Repeat till no protein is observed in the Bradford test or till stable A_{280} reading is observed.

5. Pool all the eluted fractions containing protein and concentrate to ~ 1 ml. Take a sample of concentrated protein.

TEV cleavage of the tagged protein

1. Calculate the total amount of protein using the formula:

$$Amount\ of\ protein\ (mg) = \frac{A_{280}}{70945} \times 56070.9 \times (Volume\ of\ elution)$$

2. Buffer exchange the protein to TEV cleavage buffer using Amicon concentrators (Membrane pore size 3 kDa).

3. Add TEV protease to TEV:protein ratio of 1:100. Allow cleavage of the protein for 16 hr at 4°C with end-to-end rotation.

Purification of TRBP2-dsRBD1 from the cleaved tag and un-cleaved protein

1. Prepare HisTrap column for protein binding.

    a. Pass 5-6 CV of autoclaved water through the Ni-NTA column (HisTrap 5 ml column, GE Healthcare).

    b. Equilibrate the column using 5-10 CV of Lysis buffer.

2. Circulate Post cleavage reaction mix through the HisTrap column for about 3 hr at 4°C to allow binding of His tagged protein to the column.

3. Wash column with ~50 ml of Gel filtration buffer. Concentrate the washings to ~550 µl. (This should contain the protein of interest – TRBP2-dsRBD1 – free from tag).

Gel Filtration Purification of the Protein

Chromatographic conditions

    a. Column: Sephacryl 16/60 100 HR (120ml, GE healthcare)

    b. Flow rate: 0.5 ml/min

    c. Delta column pressure limit: less than 0.15 Mbar

    d. Pre-column pressure limit: less than 0.5 Mbar

1. Pass 1-2 CV of autoclaved water through the Gel filtration column.

2. Equilibrate the column with 2 CV of Gel filtration buffer pH = 7.5.

3. Inject 500 µl of concentrated protein on to the gel filtration column

4. Elute the protein through a gel filtration column by passing 1.5 CV of gel filtration buffer.

5. Collect eluted protein, concentrate to final concentration of ~1 mM (Extinction coefficient = 2980 $M^{-1}.cm^{-1}$).

NMR sample preparation

1. Buffer exchange the concentrated protein to NMR buffer pH 6.4. Store at 4°C until further use.

2. Transfer the concentrated protein in NMR buffer to the washed Shigemi tube (NMR tube). Label the tube and close it using parafilm.

Protocol for Overexpression and Purification of dADAR-dsRBD1

Preparation of buffers for protein purification

(All volumes for buffer preparations to be taken from the stock solutions)

Equilibration Buffer	4000 ml
20 mM Tris HCl, pH 8.0	40 ml
1 M NaCl	200 ml
1 mM DTT	2 ml

Elution Buffer	500 ml
20 mM Tris HCl, pH 8.0	10 ml
1 M NaCl	50 ml
10 mM Imidazole	5 ml
1 mM DTT	0.5 ml

1. Add stock liquids (Tris HCl, imidazole, NaCl, Glycerol)

2. Add autoclaved water to 90% of the final volume.

3. Titrate pH to 7.5.

4. Makeup the volume with autoclaved water.

5. Filter sterilize into a sterile bottle.

6. Store all at 4°C.

Note: Add DTT just before use

NMR Buffer	**100 ml**
10 mM Sodium Phosphate (367.5 µl of 1M NaH_2PO_4 + 132.5 µl of 1M Na_2HPO_4)	
100 mM NaCl	2 ml
1 mM EDTA	0.2 ml
1mM DTT	0.1 ml

Overexpression of dADAR-dsRBD1 in a bacterial expression system

1. Prepare LB media

2. Add Kanamycin to the sterile LB media to a final concentration of 50 µg/ml.

3. Use a pipette tip to scrap BL21(DE3) cells containing appropriate plasmid from Glycerol stock and transfer it to 10 ml LB medium containing antibiotic.

4. Allow cells to grow overnight at 37°C in incubator shaker with shaker speed set to 225 rpm.

5. Add 10 ml overnight culture to 1 liter of LB media containing Kanamycin (final conc. 50 µg/ml) and continue incubation with shaking.

6. Monitor the OD600 at every ½ hr till it reaches ~0.8-1.0. (Note: It takes not more than 3 hrs to reach OD600 to ~0.8).

7. Add IPTG (1 M stock) to a final concentration of 0.5 mM and continue induction for 15 hr at 30°C with shaking.

8. Centrifuge solution for 20 min at 8000xg, 4°C in a high-speed centrifuge. Decant the supernatant.

9. Transfer the pellet to a 50 ml centrifuge tube by re-suspending it in the same LB media. Centrifuge at 4000 rpm for 20 min and Store the pellet at -20°C until use. [Usually 1 liter culture→ 4-6 g (pellet weight)].

Cell Lysis and Purification of TRBP2-dsRBD1 protein

Important note: PMSF acts as a serine protease suicide inhibitor whose half-life is drastically shortened by the presence of water. It should, therefore, be prepared in 2-Propanol (not ethanol, as this is rarely 100% pure) immediately prior to use. There is some evidence that it can be stable stored at -20°C. It is also extremely toxic!!!

1. Resuspend the cell pellet in the 10-15 ml of Equilibration buffer pH = 8.0. Keep the cell pellet on the ice during lysis.

2. Add 1% volume of Triton-X 100 i.e. 500 µl of Triton-X 100 for 50 ml of the final volume.

Note: Add 500 µl of Triton-X 100 in ~10 ml of equilibration buffer. Warm to dissolve and cool on ice and then use.

3. Add 62.5 µl of Lysozyme solution (20 mg/ml stock) to the above solution.

4. Incubate for 10 min on ice. (till you get viscous solution i.e. DNA is released in the solution).

5. Add 100 µl of PMSF and sonicate using probe sonicator.

(Sonication cycle: 10 s pulse-10 s gap-10 s pulse-10 s gap-10 s pulse, amplitude 70%)

6. Add 100 µl of PMSF again and repeat the sonication cycle. (Repeat till solution viscosity is reduced).

7. Add protease inhibitor. (2 ml of SigmaFAST protease inhibitor cocktail solution (10X) is required for 4 g of cell pellet)

8. Add cell lysate to 50 ml oak ridge tubes and centrifuge at 32000xg for 30 min at 4°C in a high-speed centrifuge.

9. Transfer the supernatant to a fresh 50 ml corning tube. (Total soluble protein TSP-I).

10. Add 250 µl of Polyethylene(imine) solution and allow it to incubate for 30 min on ice. Then centrifuge at 10000xg for 30 min at 4°C. Collect supernatant in a fresh tube.

11. Repeat step 10 till no precipitate is observed after centrifugation.

12. Then add saturated ammonium sulfate solution to 60% saturation. (Add 150 ml of saturated ammonium sulfate solution to 100 ml of the TSP.) Allow to incubate on ice overnight with mixing.

13. Centrifuge at 10000xg for 30 min and collect the precipitate. (Note: This precipitate floats over the solution and does not settle down. Take necessary precautions to avoid loss of precipitate).

14. Re-suspend the precipitate in ~30-40 ml of Lysis buffer and dialyze against equilibration buffer to remove ammonium sulfate. (Repeat the dialysis step with at least 3 rounds of fresh lysis buffer).

15. Transfer the dialyzed protein solution to a fresh 50 ml centrifuge tube.

Purification of tagged protein by Ni-NTA Affinity Chromatography

1. Prepare HisTrap column for protein binding.

   a. Pass 5-6 Column Volume (CV) of autoclaved water through the Ni-NTA column (HisTrap 5 ml column, GE Healthcare).

   b. Equilibrate the column using 5-10 CV of equilibration buffer.

2. Circulate TSP-I through the Ni-NTA column for about 3 hr at 4°C to allow binding of the protein to the column. Pass 40-50 CV of equilibration buffer (pH = 8.0) through the column to remove any non-specific protein binding.

3. Elute the bound protein by passing the elution buffer (pH = 8.0).

   a. Fill the column with elution buffer. Allow to equilibrate for 30 min.

   b. Elute by passing fresh 1 CV elution buffer. Collect the eluted fraction.

   c. Repeat till no protein is observed in the Bradford test or till stable A_{280} reading is observed.

4. Pool all the eluted fractions containing protein and concentrate to ~ 1 ml. Take a sample of concentrated protein.

Gel Filtration Purification of the Protein

Chromatographic conditions

   a. Column: Sephacryl 16/60 100 HR (120ml, GE healthcare)

   b. Flow rate: 0.5 ml/min

   c. Delta column pressure limit: less than 0.15 Mbar

   d. Pre-column pressure limit: less than 0.5 Mbar

1. Pass 1-2 CV of autoclaved water through the Gel filtration column.

2. Equilibrate the column with 2 CV of equilibration buffer pH = 8.0.

3. Inject 500 µl of concentrated protein on to the gel filtration column

4. Elute the protein through a gel filtration column by passing 1.5 CV of gel filtration buffer.

5. Collect eluted protein, concentrate to final concentration of ~1 mM (Extinction coefficient = 2980 $M^{-1}.cm^{-1}$).

NMR sample preparation

1. Buffer exchange the concentrated protein to NMR buffer pH 6.4. Store at 4°C until further use.

2. Transfer the concentrated protein in NMR buffer to the washed Shigemi tube (NMR tube). Label the tube and close it using parafilm.

Appendix 2 *Report of Ramachandran analysis for solution structures of TRBP2-dsRBD1*

MolProbity Ramachandran analysis

2rbdH.pdb, all models
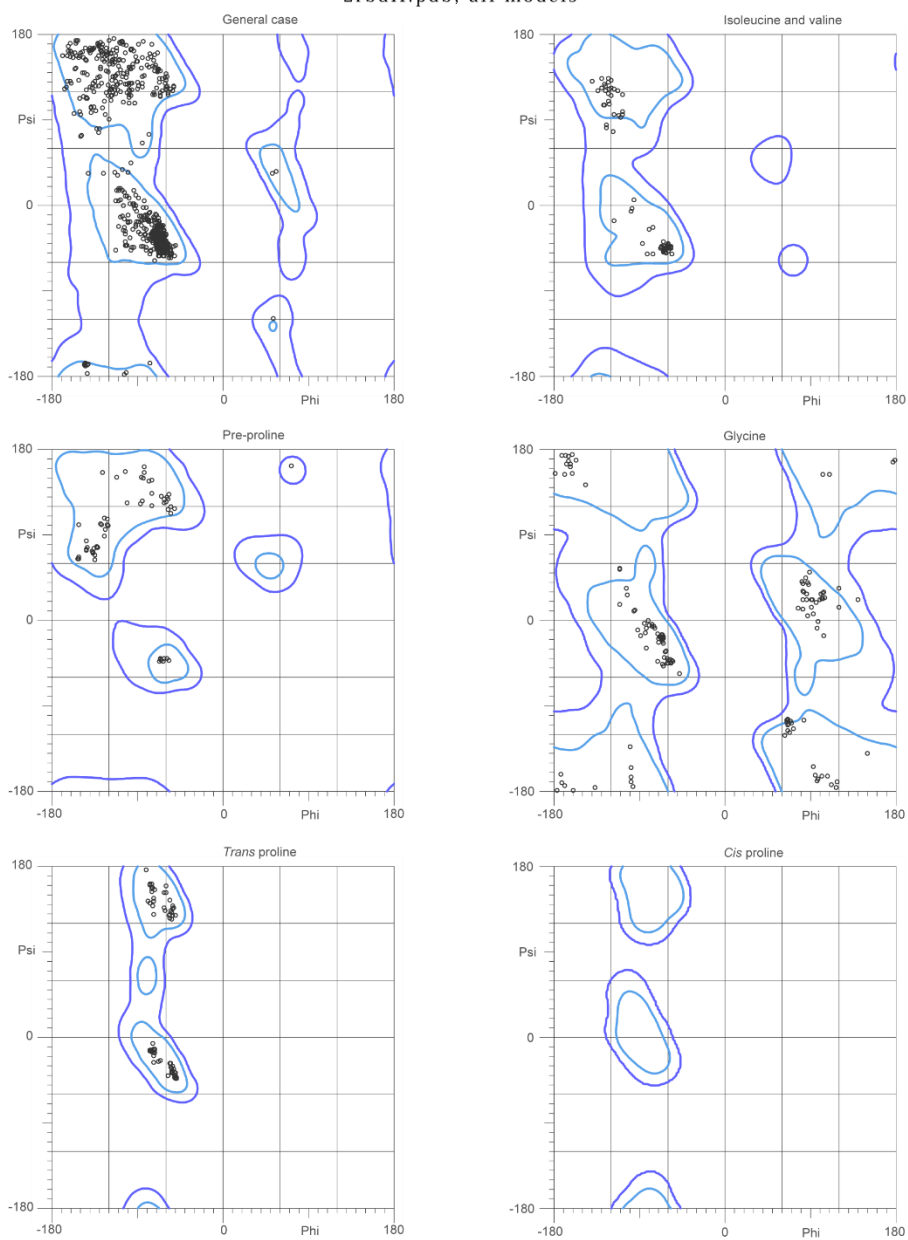
97.6% (1035/1060) of all residues were in favored (98%) regions.
100.0% (1060/1060) of all residues were in allowed (>99.8%) regions.

There were no outliers.

http://kinemage.biochem.duke.edu   Lovell, Davis, et al. Proteins 50:437 (2003)

MolProbity Ramachandran analysis

2rbdH.pdb, model 1

96.2% (102/106) of all residues were in favored (98%) regions.
100.0% (106/106) of all residues were in allowed (>99.8%) regions.

There were no outliers.

http://kinemage.biochem.duke.edu   Lovell, Davis, et al. Proteins 50:437 (2003)
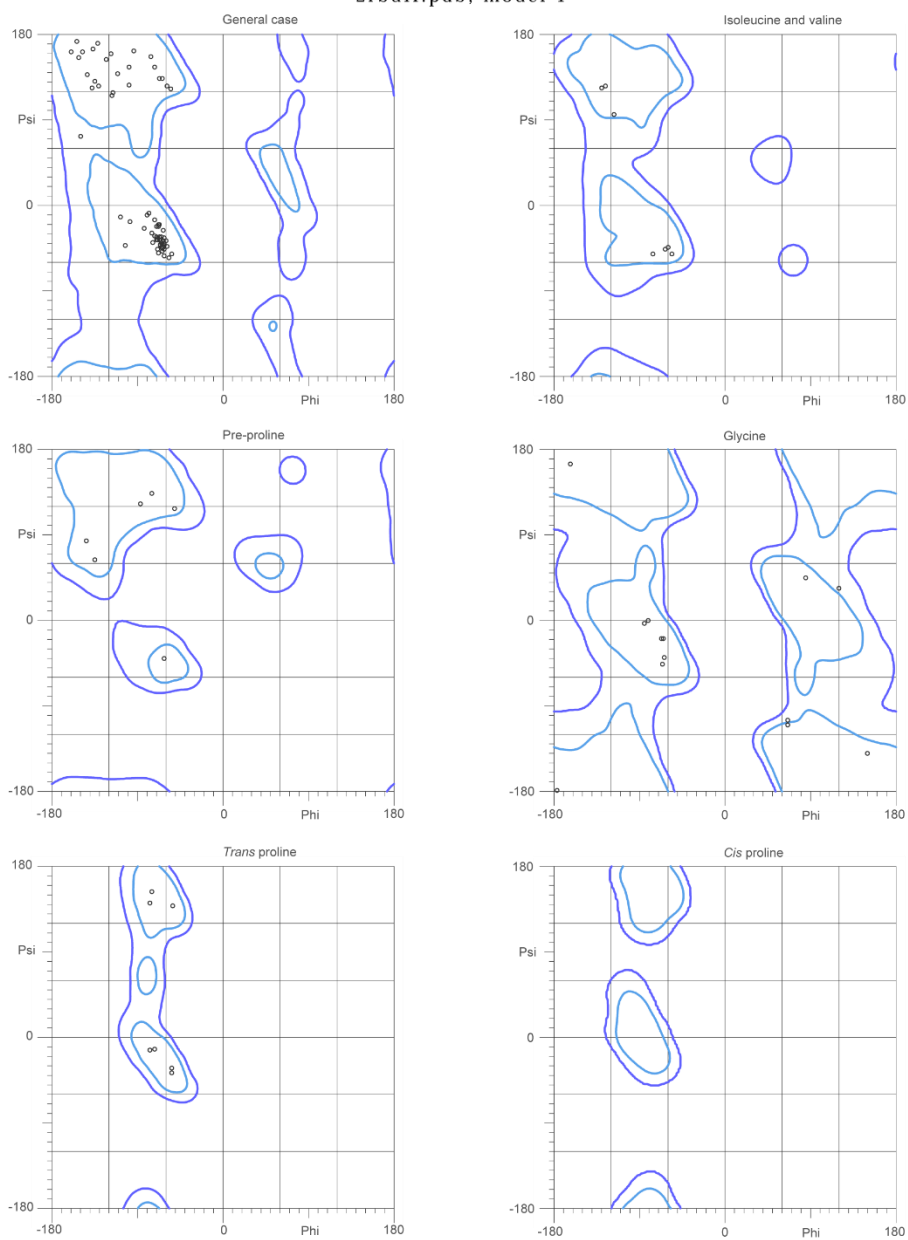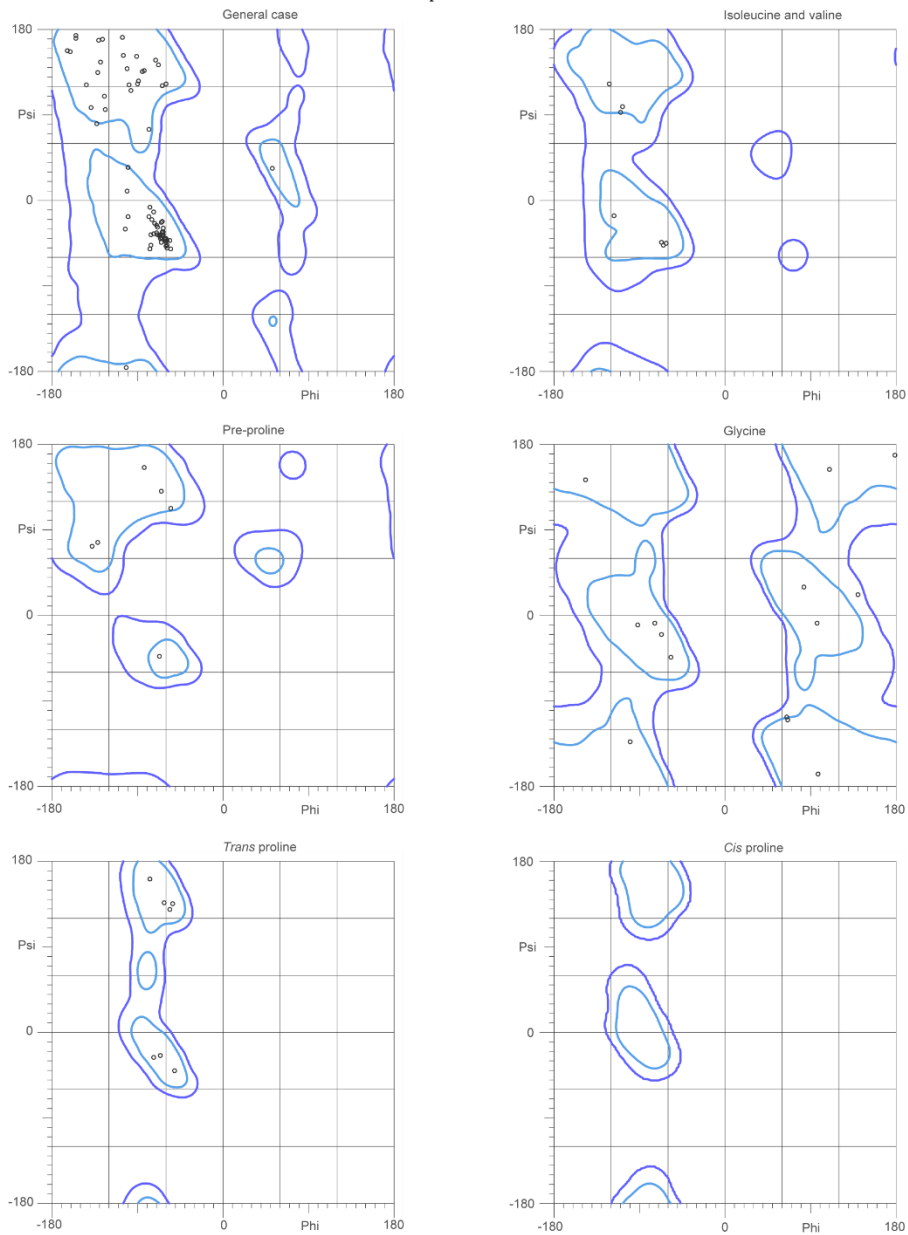
MolProbity Ramachandran analysis

2rbdH.pdb, model 2

98.1% (104/106) of all residues were in favored (98%) regions.
100.0% (106/106) of all residues were in allowed (>99.8%) regions.

There were no outliers.

MolProbity Ramachandran analysis

2rbdH.pdb, model 3
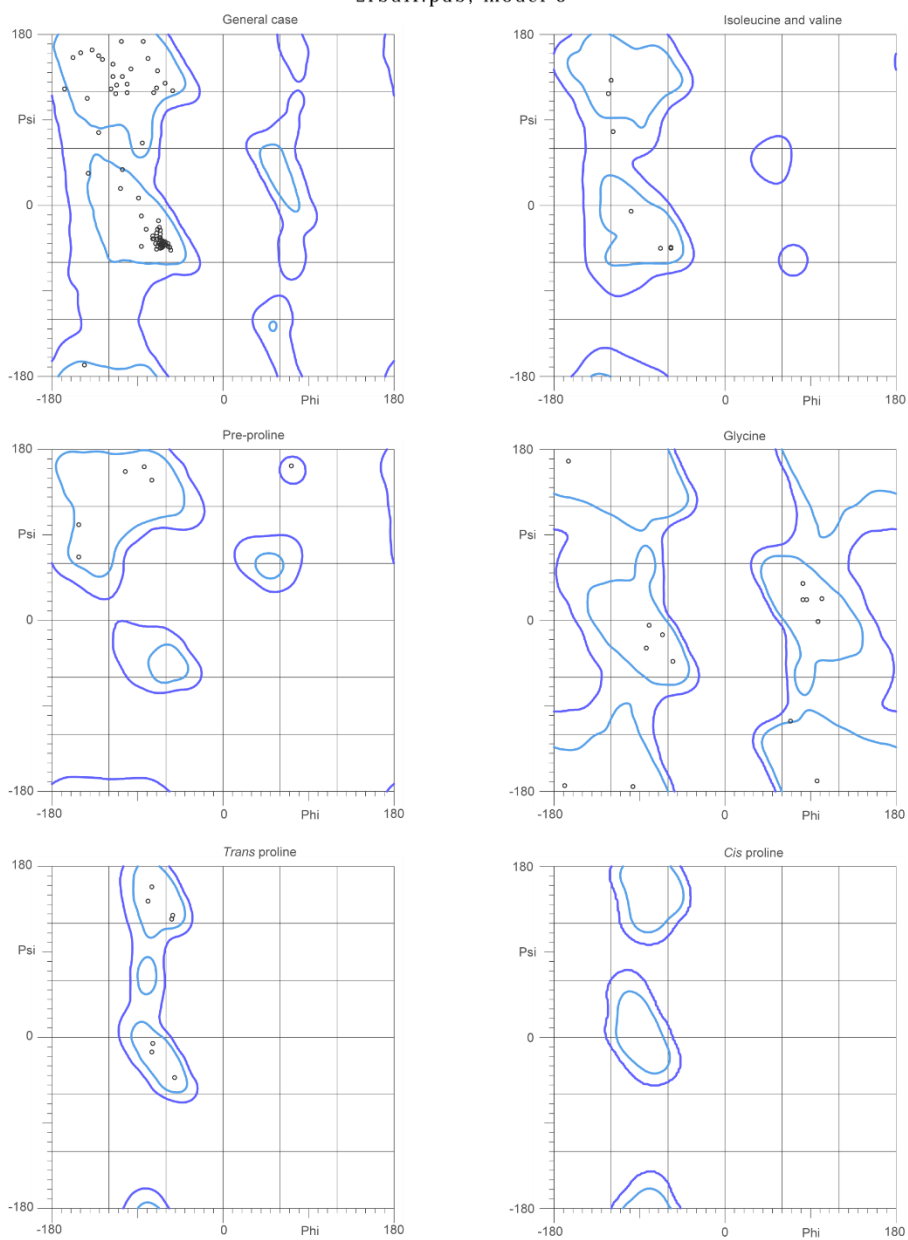
94.3% (100/106) of all residues were in favored (98%) regions.
100.0% (106/106) of all residues were in allowed (>99.8%) regions.

There were no outliers.

http://kinemage.biochem.duke.edu   Lovell, Davis, et al. Proteins 50:437 (2003)

MolProbity Ramachandran analysis

2rbdH.pdb, model 4
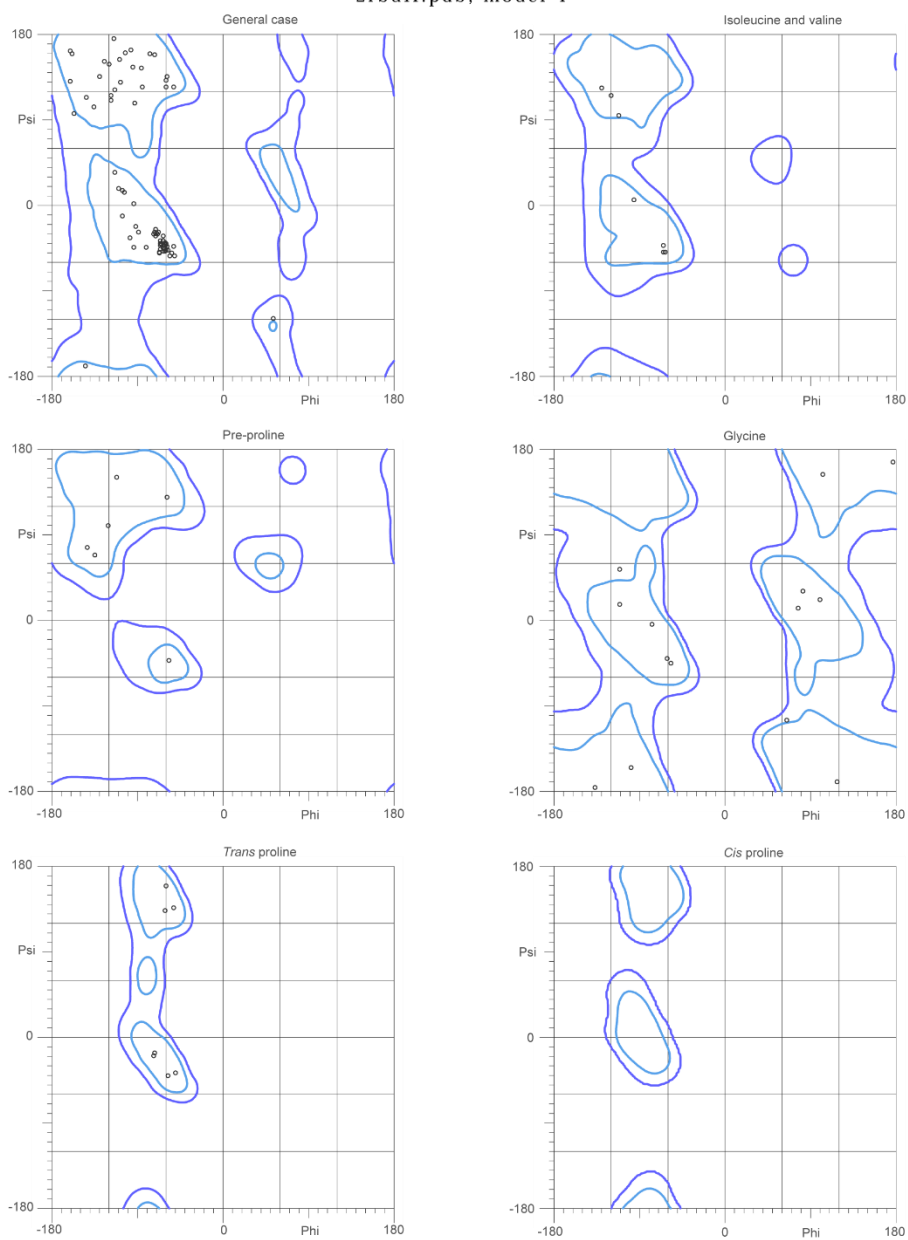
96.2% (102/106) of all residues were in favored (98%) regions.
100.0% (106/106) of all residues were in allowed (>99.8%) regions.

There were no outliers.

http://kinemage.biochem.duke.edu   Lovell, Davis, et al. Proteins 50:437 (2003)
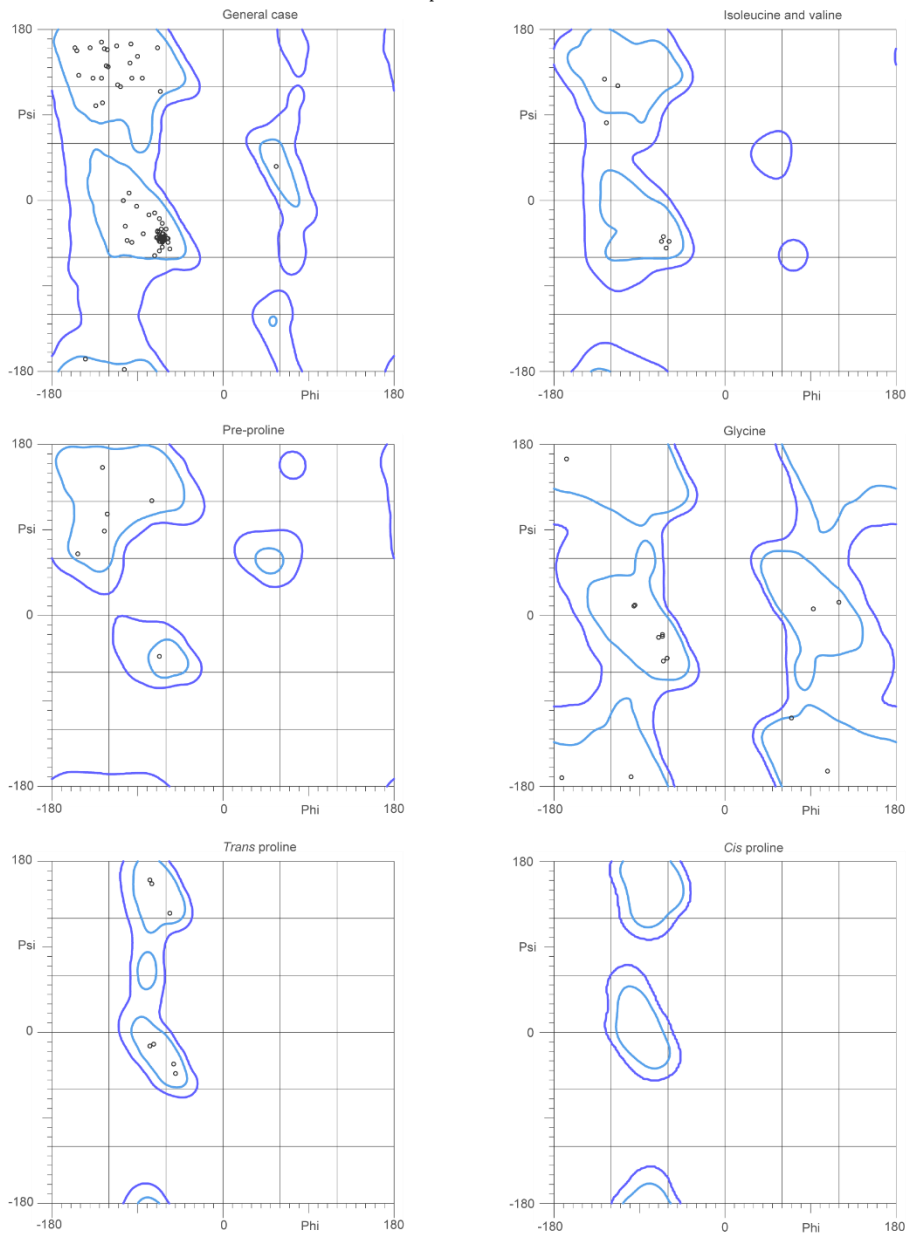
MolProbity Ramachandran analysis

2rbdH.pdb, model 5

99.1% (105/106) of all residues were in favored (98%) regions.
100.0% (106/106) of all residues were in allowed (>99.8%) regions.

There were no outliers.

MolProbity Ramachandran analysis

2rbdH.pdb, model 6
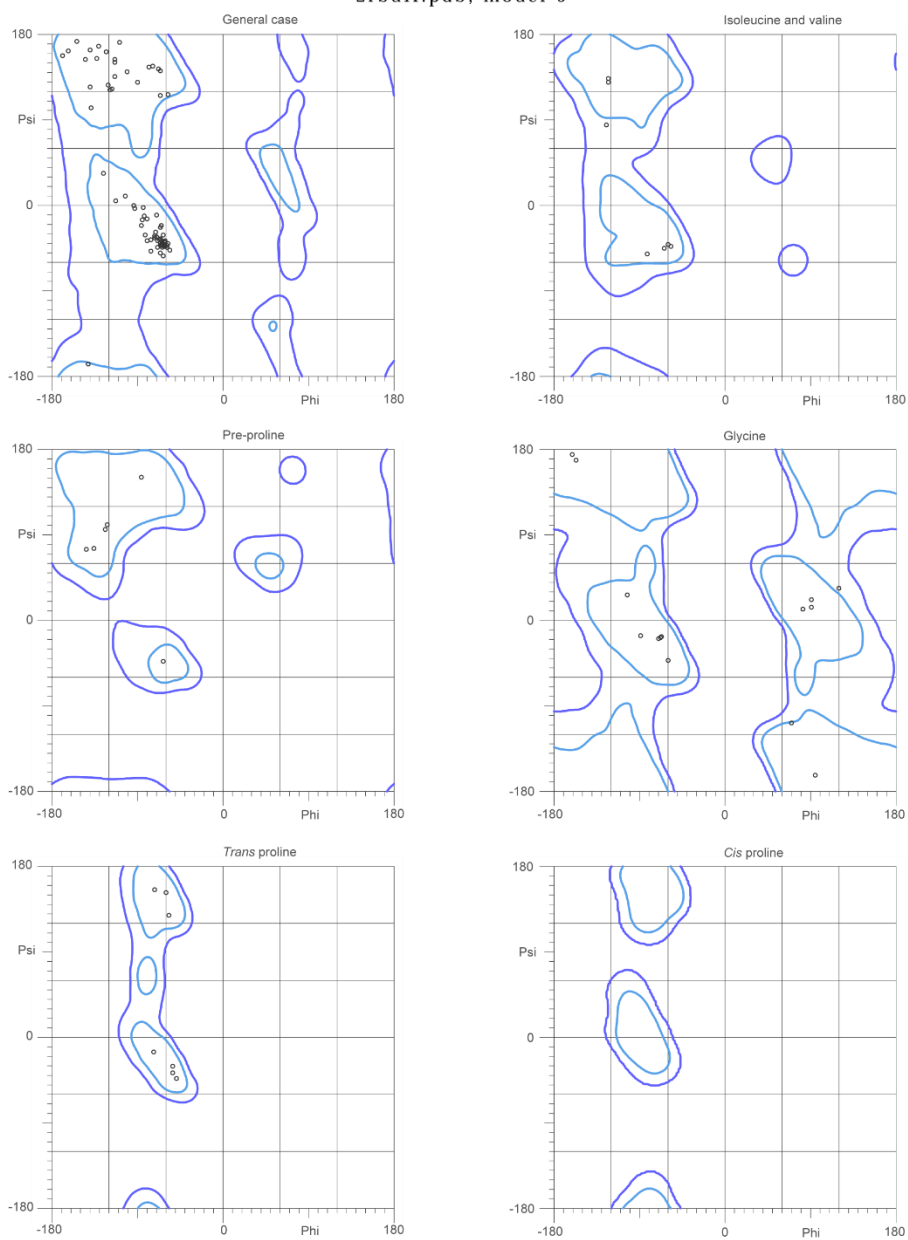
98.1% (104/106) of all residues were in favored (98%) regions.
100.0% (106/106) of all residues were in allowed (>99.8%) regions.

There were no outliers.
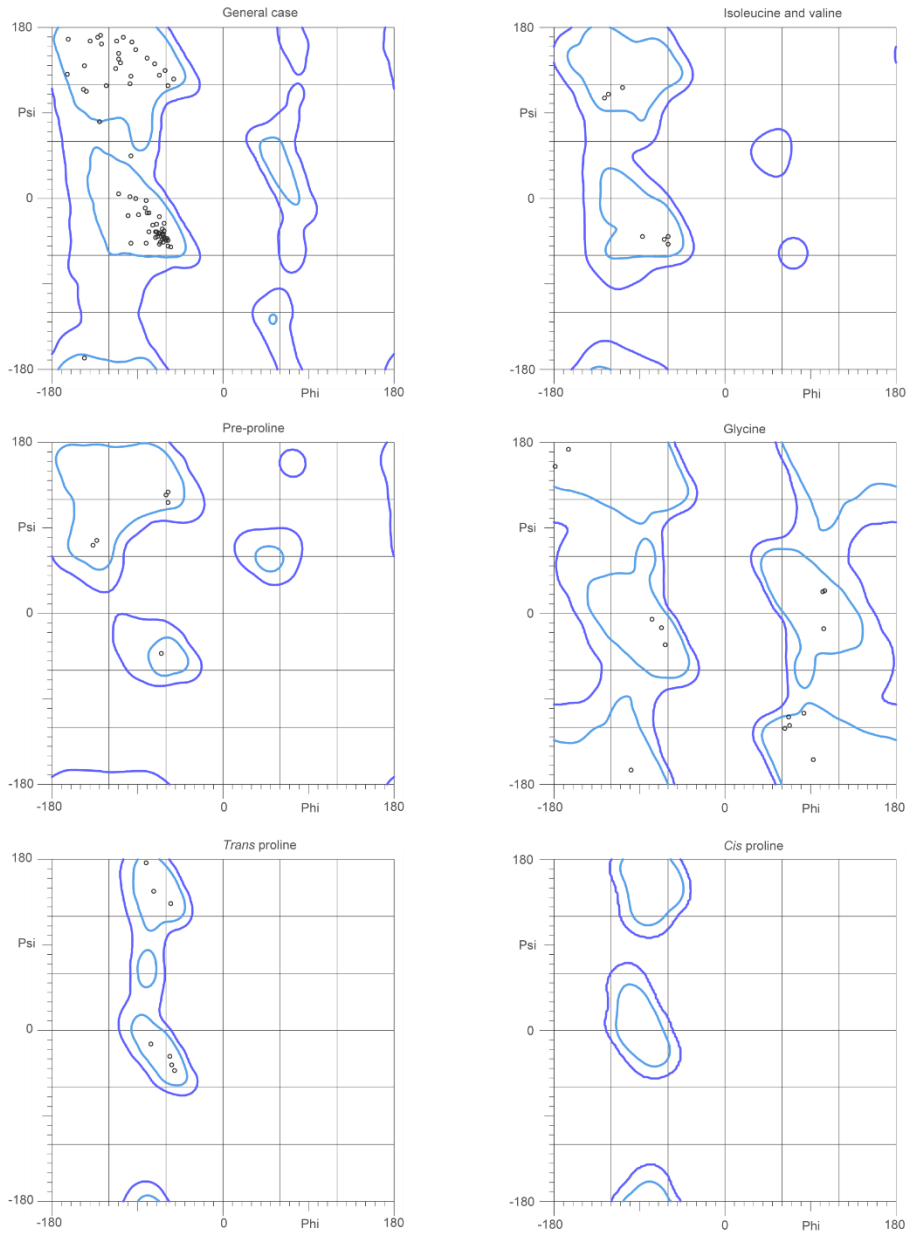
MolProbity Ramachandran analysis

2rbdH.pdb, model 7

99.1% (105/106) of all residues were in favored (98%) regions.
100.0% (106/106) of all residues were in allowed (>99.8%) regions.

There were no outliers.

MolProbity Ramachandran analysis

2rbdH.pdb, model 8

100.0% (106/106) of all residues were in favored (98%) regions.
100.0% (106/106) of all residues were in allowed (>99.8%) regions.

There were no outliers.

http://kinemage.biochem.duke.edu   Lovell, Davis, et al. Proteins 50:437 (2003)
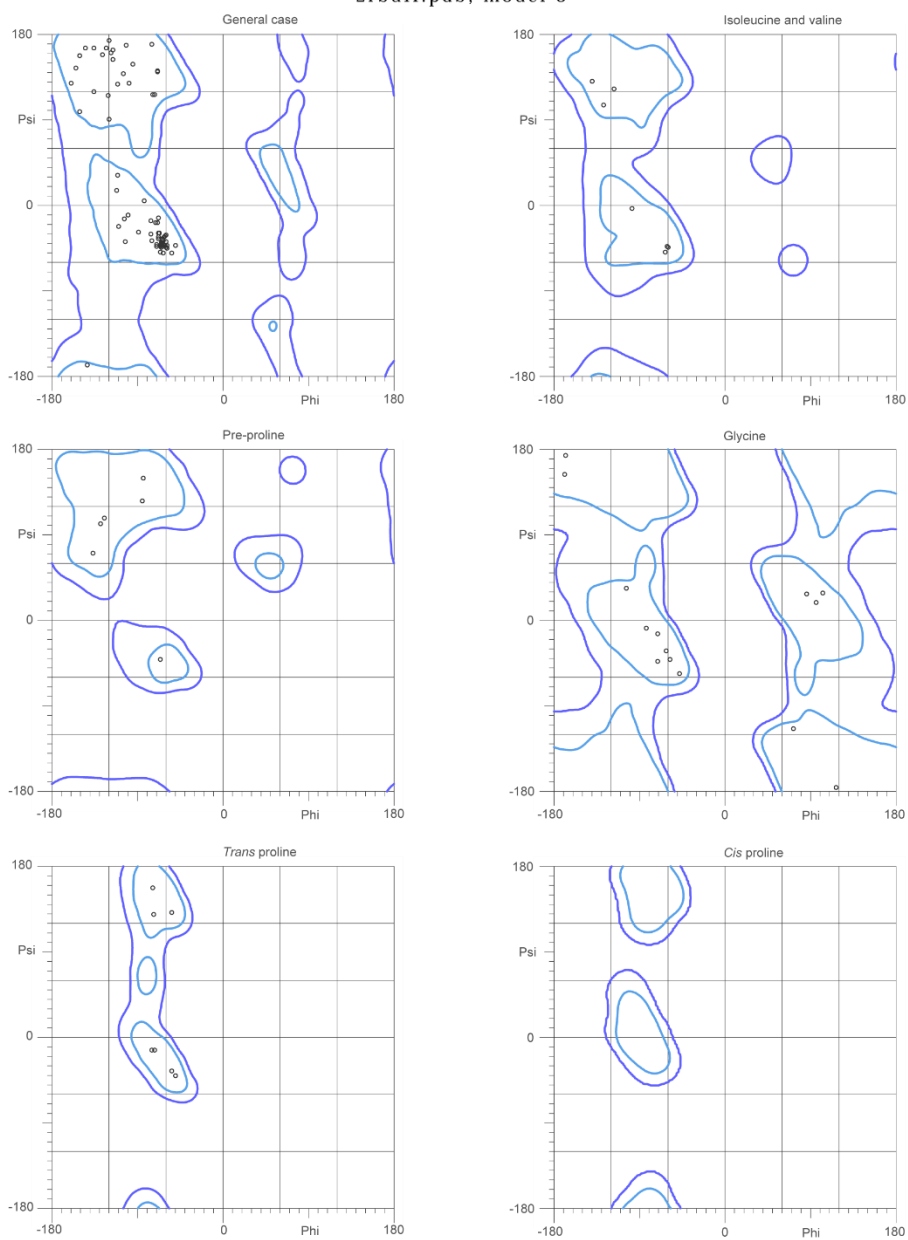
MolProbity Ramachandran analysis

2rbdH.pdb, model 9
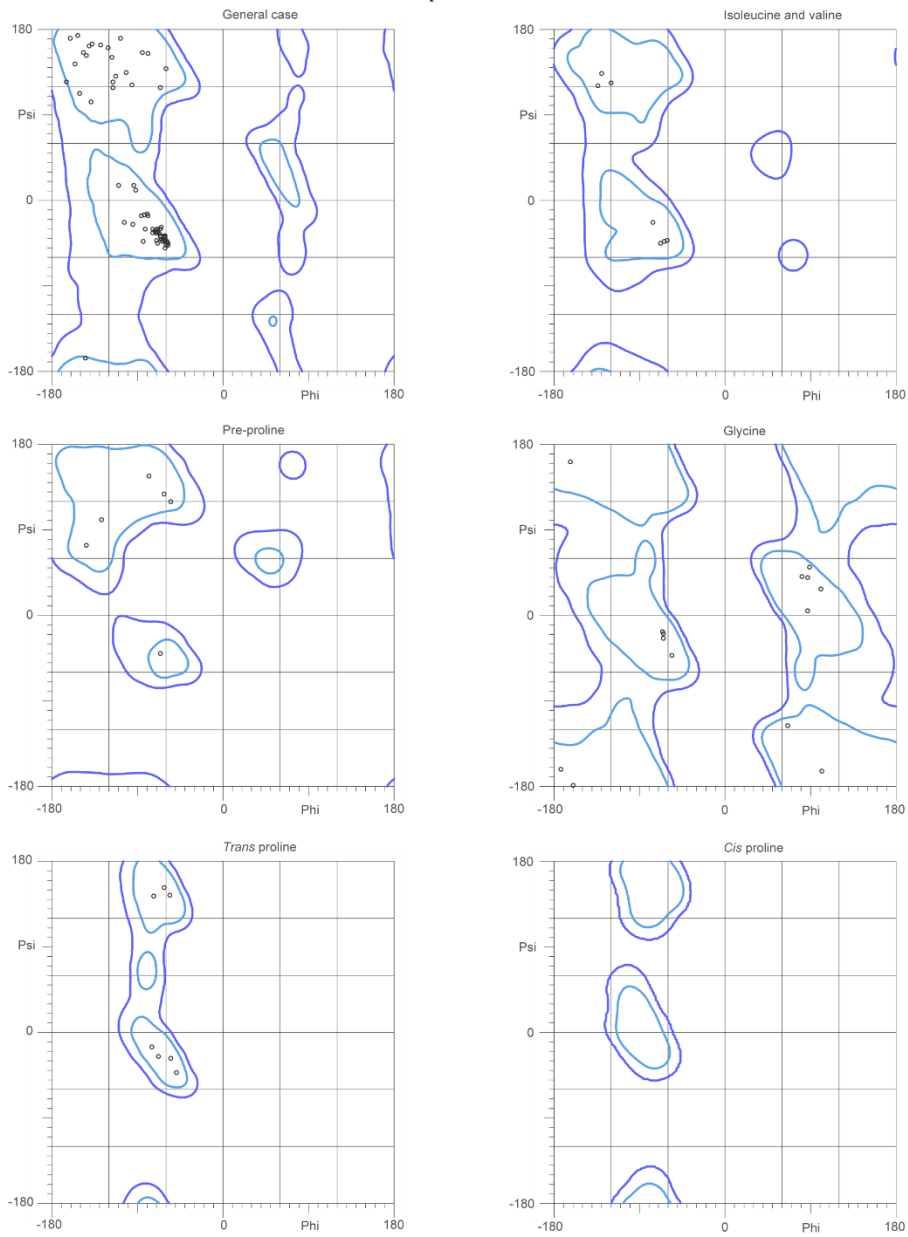
99.1% (105/106) of all residues were in favored (98%) regions.
100.0% (106/106) of all residues were in allowed (>99.8%) regions.

There were no outliers.

MolProbity Ramachandran analysis

2rbdH.pdb, model 10
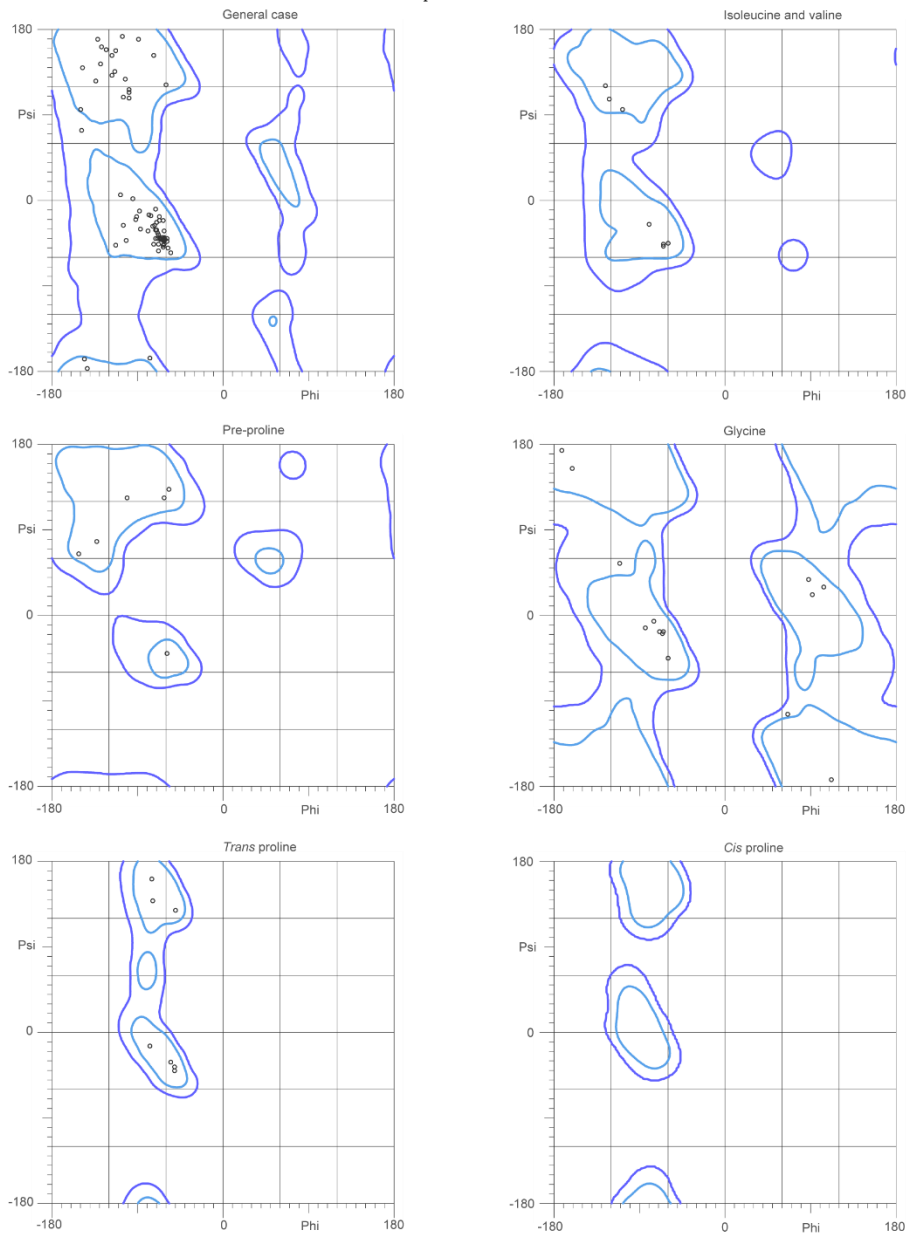
96.2% (102/106) of all residues were in favored (98%) regions.
100.0% (106/106) of all residues were in allowed (>99.8%) regions.

There were no outliers.

http://kinemage.biochem.duke.edu   Lovell, Davis, et al. Proteins 50:437 (2003)

Appendix 3 Supporting Tables and Figures

Supporting Tables

Table A.1: Nuclear spin relaxation data for TRBP2-dsRBD1 recorded at 600 MHz and 750 MHz NMR spectrometer

Residue Number	600 MHz						750 MHz					
	R_1 (Hz)		R_2 (Hz)		NOE		R_1 (Hz)		R_2 (Hz)		NOE	
	Value	Error	Value	Error	Value	Error	Value	Error	Value	Error	Value	Error
2	1.33	0.04	1.72	0.06	-0.94	0.02	1.64	0.08	1.93	0.38	-0.42	0.02
3	1.53	0.05	2.00	0.17	-0.55	0.02	1.79	0.08	1.95	0.38	-0.11	0.02
5	1.54	0.02	2.06	0.07	-0.48	0.02	1.65	0.07	2.19	0.21	0.11	0.02
7	1.51	0.04	2.27	0.15	-0.41	0.02	1.65	0.06	1.58	0.46	-0.12	0.02
8	1.49	0.05	2.27	0.04	-0.41	0.02	1.65	0.07	2.15	0.38	0.03	0.02
9	1.46	0.05	2.20	0.09	-0.40	0.02	1.65	0.07	2.10	0.40	-0.06	0.02
10	1.52	0.04	2.06	0.05	-0.30	0.02	1.64	0.08	1.74	0.42	-0.07	0.02
11	1.51	0.05	2.35	0.04	-0.45	0.02	1.74	0.07	2.27	0.42	-0.06	0.02
12	1.55	0.05	2.50	0.04	-0.33	0.02	1.75	0.06	2.48	0.41	-0.09	0.02
13	1.50	0.05	2.49	0.14	-0.28	0.02	1.62	0.07	2.33	0.37	-0.04	0.02
14	1.52	0.04	2.63	0.05	-0.23	0.02	1.66	0.06	2.63	0.46	0.06	0.02
15	1.50	0.05	2.92	0.16	-0.19	0.02	1.62	0.06	2.75	0.41	0.02	0.02
16	1.47	0.02	4.26	0.20	0.11	0.02	1.48	0.04	4.40	0.30	0.27	0.02
18	1.65	0.04	5.89	0.06	0.29	0.02	1.70	0.07	6.83	0.39	0.44	0.02
24	1.58	0.02	7.98	0.16	0.50	0.02	1.46	0.05	8.30	0.29	0.54	0.02
25	1.60	0.02	8.54	0.11	0.43	0.02	1.54	0.04	9.30	0.28	0.56	0.02
26	1.56	0.04	7.22	0.08	0.38	0.02	1.55	0.04	7.57	0.37	0.46	0.02
28	1.53	0.05	6.54	0.21	0.41	0.02	1.59	0.06	9.65	0.49	0.51	0.02
30	1.51	0.02	8.66	0.27	0.55	0.02	1.43	0.04	9.21	0.27	0.60	0.02
32	1.49	0.03	11.02	0.14	0.66	0.02	1.34	0.03	10.56	0.33	0.70	0.02
33	1.60	0.04	12.77	0.12	0.75	0.02	1.52	0.03	13.31	0.41	0.82	0.02
34	1.54	0.03	9.83	0.45	0.73	0.02	1.41	0.03	9.33	1.03	0.78	0.02
35	1.67	0.03	7.54	0.07	0.47	0.02	1.62	0.08	7.96	0.19	0.59	0.02
36	1.59	0.03	11.03	0.26	0.65	0.02	1.35	0.06	11.02	1.11	0.72	0.02
39	1.49	0.02	12.15	0.06	0.73	0.02	1.39	0.04	12.93	0.29	0.79	0.02
40	1.59	0.03	12.21	0.13	0.74	0.02	1.43	0.03	12.87	0.32	0.76	0.02
41	1.53	0.02	11.03	0.11	0.72	0.02	1.34	0.04	11.05	0.29	0.75	0.02
42	1.39	0.01	10.94	0.33	0.71	0.02	1.31	0.03	13.22	0.50	0.77	0.02
43	1.58	0.02	10.06	0.34	0.72	0.02	1.45	0.04	10.53	0.15	0.79	0.02
44	1.54	0.02	6.51	0.11	0.50	0.02	1.47	0.06	7.32	0.19	0.60	0.02
45	1.24	0.02	7.35	0.05	0.47	0.02	1.24	0.02	8.05	0.24	0.47	0.02
48	1.51	0.02	10.41	0.11	0.74	0.02	1.28	0.06	11.51	0.19	0.78	0.02
49	1.48	0.02	10.19	0.23	0.74	0.02	1.24	0.06	10.28	0.29	0.73	0.02
50	1.49	0.02	10.14	0.12	0.74	0.02	1.25	0.08	11.25	0.34	0.75	0.02
51	1.55	0.02	11.73	0.12	0.73	0.02	1.42	0.04	12.71	0.47	0.81	0.02
53	1.50	0.04	7.91	0.16	0.50	0.02	1.48	0.05	8.76	0.43	0.55	0.02
54	1.44	0.02	7.12	0.14	0.38	0.02	1.45	0.04	7.06	0.33	0.42	0.02
56	1.52	0.04	5.53	0.06	0.24	0.02	1.61	0.05	5.75	0.43	0.35	0.02
57	1.48	0.05	5.92	0.13	0.26	0.02	1.69	0.06	5.94	0.52	0.28	0.02

Residue Number	600 MHz						750 MHz					
	R_1 (Hz)		R_2 (Hz)		NOE		R_1 (Hz)		R_2 (Hz)		NOE	
	Value	Error	Value	Error	Value	Error	Value	Error	Value	Error	Value	Error
61	1.46	0.03	9.17	0.06	0.50	0.02	1.45	0.04	9.48	0.22	0.55	0.02
62	1.44	0.02	10.40	0.25	0.69	0.02	1.31	0.09	9.93	0.16	0.74	0.02
63	1.42	0.03	10.76	0.09	0.75	0.02	1.47	0.09	11.04	0.31	0.83	0.02
64	1.55	0.03	10.10	0.21	0.74	0.02	1.25	0.11	11.80	0.27	0.77	0.02
65	1.49	0.02	10.30	0.09	0.74	0.02	1.34	0.06	10.30	0.32	0.78	0.02
66	1.64	0.04	10.36	0.41	0.72	0.02	1.34	0.06	12.01	0.31	0.70	0.02
67	1.55	0.02	10.34	0.17	0.73	0.02	1.41	0.03	10.09	0.59	0.75	0.02
68	1.54	0.03	9.81	0.23	0.72	0.02	1.27	0.03	11.02	0.38	0.71	0.02
69	1.53	0.03	10.38	0.07	0.69	0.02	1.40	0.06	11.15	0.31	0.78	0.02
70	1.38	0.05	10.54	0.14	0.65	0.02	1.28	0.09	11.19	0.54	0.67	0.02
71	1.51	0.05	10.40	0.11	0.69	0.02	1.39	0.04	10.97	0.44	0.71	0.02
72	1.57	0.03	9.63	0.09	0.68	0.02	1.51	0.06	10.02	0.33	0.78	0.02
73	1.58	0.02	10.36	0.09	0.72	0.02	1.49	0.05	10.65	0.21	0.80	0.02
74	1.50	0.02	9.65	0.35	0.69	0.02	1.34	0.04	6.94	0.35	0.66	0.02
75	1.57	0.02	11.58	0.11	0.72	0.02	1.42	0.04	12.67	0.44	0.74	0.02
77	1.50	0.01	11.83	0.04	0.68	0.02	1.31	0.07	12.04	0.16	0.74	0.02
80	1.72	0.04	8.31	0.13	0.42	0.02	1.69	0.06	8.99	0.44	0.50	0.02
82	1.50	0.02	12.42	0.48	0.70	0.02	1.28	0.04	14.79	1.72	0.83	0.02
88	1.32	0.03	14.71	0.22	0.75	0.02	1.21	0.04	18.20	0.49	0.84	0.02
89	1.39	0.01	14.30	0.23	0.77	0.02	1.09	0.04	15.16	0.18	0.79	0.02
90	1.48	0.03	9.02	0.14	0.71	0.02	1.47	0.06	9.97	0.68	1.15	0.02
91	1.45	0.02	11.89	0.36	0.70	0.02	1.35	0.03	11.63	0.42	0.85	0.02
94	1.70	0.04	7.89	0.08	0.55	0.02	1.54	0.06	7.79	0.39	0.62	0.02
95	1.51	0.01	7.69	0.17	0.55	0.02	1.40	0.08	7.47	0.25	0.58	0.02
97	1.64	0.04	9.07	0.12	0.47	0.02	1.56	0.06	9.26	0.49	0.54	0.02
98	1.73	0.05	4.74	0.24	0.42	0.02	1.69	0.07	6.41	0.45	0.48	0.02
99	1.69	0.05	4.86	0.05	0.33	0.02	1.73	0.05	5.25	0.39	0.40	0.02
101	1.65	0.03	3.90	0.17	0.14	0.02	1.67	0.06	4.63	0.51	0.24	0.02
104	1.32	0.02	2.34	0.26	-0.65	0.02	1.49	0.03	0.46	0.58	-0.22	0.02
105	0.88	0.01	1.73	0.11	-0.72	0.02	0.87	0.03	1.39	0.09	-0.71	0.02

Table A.2: Nuclear spin relaxation data for dADAR-dsRBD1 recorded at 600 MHz and 750 MHz NMR spectrometer

Residue Number	600 MHz						750 MHz					
	R_1 (Hz)		R_2 (Hz)		NOE		R_1 (Hz)		R_2 (Hz)		NOE	
	Value	Error	Value	Error	Value	Error	Value	Error	Value	Error	Value	Error
59	1.44	0.05	10.10	0.44	0.37	0.02	1.37	0.07	8.84	0.84	0.49	0.04
65	1.38	0.06	17.28	0.32	0.79	0.02	1.21	0.09	17.98	1.25	0.71	0.04
66	1.33	0.05	12.34	0.34	0.81	0.02	1.26	0.07	11.17	0.48	0.90	0.04
67	1.39	0.04	13.17	0.30	0.77	0.02	1.32	0.04	11.65	0.57	0.68	0.04
68	1.29	0.04	12.86	0.29	0.74	0.02	1.15	0.04	12.57	0.60	0.65	0.04
69	1.32	0.03	13.49	0.24	0.82	0.02	1.19	0.03	12.15	0.48	0.84	0.04
70	1.39	0.04	13.51	0.19	0.75	0.02	1.20	0.05	13.74	0.64	0.78	0.04
72	1.28	0.03	13.41	0.14	0.75	0.02	1.14	0.03	14.55	0.73	0.76	0.04
73	1.29	0.04	10.18	0.34	0.64	0.02	1.19	0.05	9.47	0.49	0.73	0.04
75	1.33	0.09	8.40	0.45	0.50	0.02	1.29	0.12	7.20	0.95	0.50	0.04
76	1.33	0.04	9.90	0.37	0.63	0.02	1.20	0.05	9.06	0.72	0.70	0.04
77	1.22	0.03	10.43	0.15	0.69	0.02	1.16	0.04	10.43	0.36	0.66	0.04
78	1.34	0.03	11.85	0.19	0.64	0.02	1.17	0.04	12.34	0.36	0.76	0.04
80	1.38	0.04	10.75	0.40	0.74	0.02	1.23	0.06	11.17	0.72	0.82	0.04
81	1.32	0.04	13.59	0.26	0.77	0.02	1.15	0.05	13.98	0.93	0.77	0.04
82	1.28	0.06	13.67	0.28	0.69	0.02	1.20	0.06	13.86	0.73	0.77	0.04
84	1.26	0.04	12.51	0.26	0.65	0.02	1.17	0.06	13.40	0.70	0.69	0.04
85	1.25	0.06	11.39	0.25	0.60	0.02	1.19	0.08	10.43	0.68	0.62	0.04
89	1.27	0.03	10.01	0.24	0.36	0.02	1.18	0.05	12.65	0.54	0.49	0.04
91	1.23	0.03	11.40	0.18	0.55	0.02	1.12	0.05	11.71	0.60	0.55	0.04
92	1.34	0.04	14.90	0.26	0.69	0.02	1.12	0.05	16.10	0.41	0.79	0.04
93	1.26	0.04	12.73	0.27	0.68	0.02	1.08	0.06	13.33	0.71	0.78	0.04
94	1.36	0.04	13.42	0.19	0.73	0.02	1.23	0.07	13.72	0.62	0.79	0.04
95	1.40	0.05	13.10	0.27	0.71	0.02	1.25	0.04	13.25	0.45	0.78	0.04
96	1.40	0.04	12.89	0.21	0.72	0.02	1.29	0.04	14.32	0.55	0.78	0.04
97	1.36	0.02	13.14	0.20	0.73	0.02	1.19	0.04	13.37	0.41	0.76	0.04
98	1.32	0.03	11.50	0.37	0.66	0.02	1.11	0.04	12.29	0.40	0.88	0.04
99	1.48	0.04	13.08	0.21	0.78	0.02	1.36	0.07	12.86	0.78	0.72	0.04
100	1.36	0.03	12.55	0.29	0.73	0.02	1.20	0.05	12.36	0.46	0.77	0.04
101	1.30	0.03	12.61	0.26	0.68	0.02	1.21	0.04	12.71	0.39	0.75	0.04
102	1.40	0.11	2.68	0.21	-0.19	0.02	1.43	0.14	2.45	0.87	0.08	0.04
103	1.35	0.03	16.87	0.54	0.73	0.02	1.24	0.04	19.62	0.55	0.76	0.04
104	1.34	0.03	11.88	0.09	0.72	0.02	1.16	0.04	12.21	0.37	0.83	0.04
105	1.34	0.03	13.83	0.22	0.72	0.02	1.12	0.05	12.60	0.43	0.82	0.04
106	1.29	0.03	13.17	0.24	0.75	0.02	1.16	0.04	13.80	0.55	0.79	0.04
107	1.33	0.03	14.54	0.28	0.71	0.02	1.17	0.04	14.05	0.55	0.75	0.04
108	1.31	0.06	12.75	0.36	0.75	0.02	1.16	0.08	12.66	1.24	0.79	0.04
109	1.32	0.06	12.94	0.45	0.74	0.02	1.24	0.07	11.58	1.14	0.79	0.04
112	1.27	0.05	13.87	0.24	0.75	0.02	1.18	0.06	13.82	0.79	0.77	0.04
113	1.36	0.03	10.34	0.42	0.66	0.02	1.15	0.05	10.00	0.97	0.86	0.04
114	1.36	0.03	13.76	0.22	0.73	0.02	1.17	0.04	14.90	0.46	0.81	0.04

Residue Number	600 MHz						750 MHz					
	R_1 (Hz)		R_2 (Hz)		NOE		R_1 (Hz)		R_2 (Hz)		NOE	
	Value	Error	Value	Error	Value	Error	Value	Error	Value	Error	Value	Error
115	1.28	0.03	13.40	0.22	0.73	0.02	1.13	0.04	13.69	0.38	0.76	0.04
116	1.33	0.04	14.45	0.35	0.76	0.02	1.22	0.03	14.72	0.52	0.85	0.04
117	1.39	0.04	13.42	0.28	0.81	0.02	1.21	0.04	15.53	0.68	0.94	0.04
120	1.23	0.06	14.10	0.77	0.76	0.02	1.23	0.07	14.76	1.15	0.87	0.04
122	1.30	0.04	15.94	0.35	0.74	0.02	1.19	0.04	16.76	0.57	0.74	0.04
123	1.24	0.05	13.96	0.20	0.76	0.02	1.13	0.05	15.20	0.69	0.86	0.04
124	1.32	0.06	13.13	0.34	0.71	0.02	1.23	0.05	12.80	0.60	0.78	0.04
125	1.35	0.04	14.71	0.36	0.64	0.02	1.27	0.05	15.06	1.06	0.84	0.04
126	1.40	0.04	12.48	0.29	0.56	0.02	1.29	0.04	10.25	0.45	0.67	0.04
129	1.51	0.06	10.45	0.29	0.42	0.02	1.43	0.08	9.45	0.80	0.54	0.04
131	1.49	0.09	8.88	0.47	0.19	0.02	1.46	0.10	10.76	0.99	0.35	0.04
132	1.55	0.08	4.58	0.15	0.11	0.02	1.51	0.10	4.14	0.78	0.37	0.04
133	1.44	0.03	4.63	0.12	0.05	0.02	1.34	0.05	5.31	0.39	0.22	0.04
134	1.48	0.05	7.81	0.36	-0.03	0.02	1.44	0.06	9.51	0.54	0.14	0.04
135	1.44	0.08	4.17	0.21	0.00	0.02	1.47	0.10	5.02	0.74	0.17	0.04
137	1.44	0.04	4.05	0.08	-0.23	0.02	1.48	0.07	3.82	0.40	0.01	0.04
140	0.99	0.00	1.84	0.07	-1.29	0.02	0.95	0.01	1.76	0.04	-0.60	0.04

Table A.3: R_{2eff} values measured at different CPMG frequencies from CPMG relaxation dispersion experiment for TRBP2-dsRBD1 at 600 MHz NMR spectrometer

Residue Number	R_{2eff} at CPMG frequency (Hz)											
	25		50		100		200		350		500	
	value	error	value	error	value	error	value	error	value	error	value	error
1	15.38	0.81	14.18	0.91	14.32	1.02	14.19	1.24	14.84	1.15	14.46	1.00
2	16.89	0.08	16.19	0.10	16.25	0.11	16.43	0.13	16.20	0.12	16.17	0.10
3	12.85	0.05	12.75	0.06	13.17	0.07	13.34	0.08	12.90	0.07	12.75	0.06
5	8.77	0.03	8.76	0.04	9.38	0.05	8.81	0.06	8.68	0.05	8.67	0.04
8	27.96	0.22	28.18	0.25	28.12	0.28	28.11	0.35	27.78	0.31	27.65	0.27
9	27.42	0.32	27.21	0.37	28.00	0.43	28.99	0.54	27.29	0.46	27.53	0.41
10	21.39	0.15	21.18	0.18	21.51	0.20	21.59	0.24	21.20	0.22	21.18	0.19
11	32.32	0.50	32.33	0.58	31.63	0.63	32.22	0.79	32.21	0.71	31.98	0.62
12	28.52	0.35	28.55	0.41	28.22	0.45	28.52	0.55	28.03	0.49	28.25	0.44
13	31.54	0.63	31.31	0.73	31.34	0.81	32.07	1.02	30.85	0.88	31.15	0.79
14	37.56	0.86	37.30	1.00	36.44	1.08	36.71	1.33	37.06	1.22	36.90	1.07
15	32.54	0.82	31.36	0.92	32.75	1.08	32.73	1.32	32.10	1.16	32.16	1.03
16	16.17	0.27	15.85	0.31	16.18	0.35	15.87	0.42	15.72	0.38	15.20	0.33
18	27.98	0.51	28.44	0.61	28.07	0.67	27.68	0.80	27.92	0.74	27.97	0.65
24	25.74	0.92	25.69	1.08	25.13	1.18	24.60	1.40	25.27	1.31	24.43	1.12
25	26.43	1.05	26.79	1.25	25.46	1.33	25.58	1.62	24.98	1.43	25.04	1.27
26	28.47	0.86	27.50	0.97	27.71	1.09	26.48	1.26	26.28	1.13	27.12	1.04
28	37.55	1.67	38.15	2.00	37.70	2.20	38.16	2.73	37.79	2.43	36.80	2.07
30	31.10	0.66	31.08	0.77	30.58	0.85	30.77	1.04	29.69	0.90	29.55	0.79
32	34.93	2.90	33.76	3.24	36.20	4.00	37.20	5.05	32.21	3.75	32.38	3.34
33	34.07	0.82	33.97	0.96	34.21	1.09	33.36	1.28	33.36	1.16	34.06	1.05
34	36.65	2.03	36.65	2.38	37.04	2.71	38.49	3.49	34.45	2.69	34.88	2.42
35	23.95	0.28	23.56	0.33	23.78	0.37	23.31	0.44	22.83	0.39	23.14	0.35
36	33.68	0.62	32.72	0.69	33.10	0.79	33.16	0.96	32.53	0.85	32.42	0.75
39	35.82	1.05	35.86	1.23	38.04	1.51	35.24	1.63	36.17	1.54	35.22	1.31
41	33.53	0.88	31.87	0.96	32.93	1.12	31.78	1.30	30.56	1.12	31.87	1.05
42	34.44	1.69	34.48	1.98	35.30	2.29	36.79	2.96	34.98	2.49	34.13	2.13
43	32.88	0.80	32.20	0.91	31.54	0.99	32.26	1.24	30.76	1.06	31.03	0.95
44	26.48	0.83	25.96	0.95	25.23	1.03	24.26	1.21	24.75	1.12	24.91	0.99
45	24.26	0.29	24.07	0.34	23.47	0.37	23.94	0.46	23.62	0.41	23.58	0.36
47	36.07	3.22	34.35	3.52	35.43	4.12	34.31	4.78	32.30	3.99	33.56	3.72
48	34.95	1.38	32.90	1.49	34.04	1.75	33.13	2.05	34.58	1.97	30.65	1.49
49	33.45	0.86	33.72	1.02	32.72	1.10	31.91	1.29	31.78	1.16	31.77	1.03
50	34.87	1.67	34.63	1.93	35.68	2.26	34.93	2.66	34.09	2.33	32.43	1.93
51	37.20	2.65	37.48	3.14	38.90	3.72	41.16	4.95	38.72	4.07	34.71	3.06
53	31.46	1.39	29.84	1.53	30.42	1.75	30.22	2.11	32.08	2.06	28.69	1.59
54	25.02	0.27	24.81	0.31	25.15	0.36	23.82	0.41	23.36	0.37	23.43	0.32
56	30.78	0.38	30.62	0.44	29.75	0.48	30.04	0.59	29.79	0.53	29.81	0.46
57	41.28	2.57	42.11	3.11	41.62	3.41	41.43	4.11	40.50	3.59	39.06	3.00
61	28.96	0.50	27.23	0.54	27.39	0.61	27.26	0.74	27.17	0.67	27.32	0.59
62	34.61	1.24	34.95	1.47	33.83	1.58	33.55	1.89	32.87	1.67	33.30	1.50

Residue Number	R_{2eff} at CPMG frequency (Hz)											
	25		50		100		200		350		500	
	value	error	value	error	value	error	value	error	value	error	value	error
63	33.97	1.00	33.49	1.14	33.12	1.26	33.54	1.56	33.48	1.41	32.87	1.22
64	34.30	1.50	34.26	1.76	36.37	2.14	36.48	2.61	35.03	2.23	33.12	1.83
65	36.00	1.50	35.37	1.71	35.52	1.93	35.91	2.38	34.29	2.02	34.18	1.78
66	36.44	3.08	35.91	3.54	37.44	4.21	35.70	4.77	36.27	4.42	33.36	3.48
67	36.71	1.46	37.34	1.76	38.38	2.05	36.25	2.29	33.28	1.84	34.11	1.68
68	32.15	2.14	32.56	2.55	34.93	3.14	33.43	3.59	34.40	3.38	29.12	2.42
69	33.86	0.80	33.24	0.91	33.91	1.05	33.74	1.26	33.29	1.12	32.45	0.96
70	47.90	2.18	49.94	2.78	51.23	3.27	47.88	3.48	48.54	3.23	47.44	2.74
71	28.92	0.45	28.61	0.53	27.99	0.57	28.53	0.71	27.96	0.63	27.72	0.55
72	30.79	0.56	30.96	0.66	31.69	0.76	29.66	0.85	29.12	0.75	29.13	0.67
73	33.14	0.79	32.39	0.90	33.16	1.04	32.47	1.23	32.83	1.13	32.58	0.99
74	30.67	0.83	30.78	0.98	32.12	1.15	33.06	1.45	29.60	1.15	29.70	1.02
75	32.93	1.02	34.54	1.27	36.02	1.51	35.29	1.79	37.31	1.75	33.16	1.31
77	32.85	0.70	32.72	0.81	34.48	0.98	33.63	1.15	35.92	1.14	33.69	0.92
80	34.26	2.28	33.27	2.56	35.18	3.10	32.89	3.43	30.81	2.86	29.56	2.41
82	35.27	1.30	35.90	1.56	36.60	1.79	36.21	2.14	35.28	1.87	34.97	1.63
88	36.36	1.90	36.37	2.23	35.46	2.40	35.87	2.97	35.34	2.63	33.85	2.19
89	39.52	1.03	38.76	1.17	37.18	1.23	37.48	1.51	37.26	1.36	37.68	1.22
91	36.15	1.78	37.28	2.19	37.18	2.44	37.07	2.95	34.50	2.41	33.00	2.01
94	29.33	0.45	29.08	0.52	28.53	0.57	29.31	0.71	28.72	0.63	28.80	0.56
95	20.43	0.51	20.76	0.61	19.30	0.64	19.74	0.79	18.85	0.69	18.85	0.61
97	31.15	0.77	30.19	0.86	33.19	1.09	31.77	1.25	32.29	1.16	29.44	0.91
98	26.49	0.40	25.24	0.45	25.51	0.51	26.59	0.64	25.60	0.56	25.30	0.49
99	32.10	0.58	31.87	0.68	31.81	0.76	31.80	0.92	31.37	0.82	31.83	0.74
101	16.47	0.29	15.94	0.33	15.71	0.37	15.69	0.44	15.16	0.39	15.28	0.35
104	8.41	0.12	8.60	0.14	8.85	0.16	9.45	0.20	8.32	0.18	8.42	0.16
105	5.46	0.09	4.77	0.10	5.65	0.12	5.24	0.14	6.36	0.14	4.65	0.11

Table A.3: R_{2eff} values measured at different CPMG frequencies from CPMG relaxation dispersion experiment for TRBP2-dsRBD1 at 600 MHz NMR spectrometer (Continued)

Residue Number	R_{2eff} at CPMG frequency (Hz)									
	650		800		1000		50 (Repeat)		650 (Repeat)	
	value	error	value	error	value	error	value	error	value	error
1	14.54	1.05	14.50	1.14	14.51	1.13	15.02	0.98	14.67	1.05
2	16.56	0.11	16.09	0.12	16.09	0.12	16.50	0.10	16.29	0.11
3	13.22	0.07	13.13	0.07	13.46	0.07	12.98	0.06	12.92	0.07
5	9.03	0.05	8.81	0.05	9.04	0.05	8.88	0.04	8.76	0.05
8	28.04	0.29	27.57	0.31	27.64	0.31	28.45	0.27	27.83	0.28
9	27.94	0.44	27.70	0.47	28.07	0.47	27.39	0.39	27.67	0.43
10	21.43	0.20	50.51	0.71	21.47	0.22	21.37	0.18	21.45	0.20
11	32.30	0.66	22.80	0.49	31.63	0.69	32.62	0.61	31.85	0.65
12	28.32	0.46	43.89	0.93	28.26	0.49	28.97	0.43	28.00	0.45
13	32.08	0.86	39.04	1.23	32.13	0.92	31.46	0.76	31.75	0.84
14	37.09	1.13	36.75	1.22	37.16	1.22	37.46	1.05	37.30	1.13
15	32.73	1.11	-9.86	0.22	33.00	1.20	32.03	0.98	32.27	1.08
16	16.02	0.36	15.86	0.39	16.06	0.39	15.92	0.33	15.55	0.35
18	28.46	0.70	27.60	0.73	27.56	0.72	28.69	0.64	27.67	0.67
24	24.92	1.20	24.50	1.28	24.98	1.28	25.87	1.13	25.67	1.22
25	25.75	1.37	25.84	1.50	25.61	1.46	27.20	1.32	25.08	1.32
26	27.40	1.10	27.00	1.18	26.51	1.14	27.39	1.00	26.29	1.04
28	37.13	2.20	37.84	2.46	37.27	2.37	38.74	2.14	37.45	2.21
30	29.87	0.84	29.46	0.90	30.20	0.92	31.05	0.81	29.39	0.82
32	33.99	3.73	34.19	4.10	32.91	3.83	35.48	3.61	32.51	3.49
33	34.38	1.12	33.59	1.18	34.13	1.18	34.29	1.01	33.86	1.08
34	35.97	2.65	36.05	2.89	34.87	2.71	35.70	2.39	35.18	2.55
35	23.31	0.37	23.35	0.40	23.08	0.39	23.59	0.34	23.05	0.36
36	32.62	0.79	32.49	0.86	33.11	0.86	33.49	0.75	33.19	0.80
39	34.50	1.33	33.41	1.39	34.55	1.43	36.55	1.32	34.72	1.33
41	32.01	1.10	31.02	1.15	32.06	1.18	32.37	1.02	30.99	1.05
42	35.48	2.36	34.31	2.45	34.16	2.39	34.88	2.10	33.32	2.14
43	31.60	1.02	31.55	1.10	31.87	1.10	32.55	0.96	31.72	1.01
44	25.42	1.06	25.09	1.14	25.14	1.13	25.35	0.97	25.02	1.04
45	23.98	0.39	23.61	0.41	23.60	0.41	24.23	0.36	23.55	0.38
47	32.34	3.71	31.98	3.98	32.10	3.93	35.90	3.90	35.56	4.19
48	30.82	1.57	31.75	1.77	31.25	1.71	33.98	1.62	29.69	1.49
49	32.16	1.10	32.13	1.19	32.30	1.18	33.77	1.06	32.07	1.08
50	32.00	1.99	32.81	2.23	33.23	2.23	35.10	2.05	32.84	2.04
51	34.33	3.16	32.61	3.21	33.29	3.25	36.64	3.16	36.82	3.47
53	28.38	1.65	29.34	1.86	30.07	1.89	30.45	1.63	26.98	1.55
54	23.81	0.35	23.82	0.38	23.70	0.37	25.30	0.33	23.72	0.34
56	30.25	0.50	29.75	0.53	29.61	0.52	30.87	0.46	29.85	0.48
57	40.15	3.28	40.23	3.58	41.13	3.65	41.19	3.12	39.59	3.18
61	27.75	0.63	27.31	0.68	27.01	0.66	27.61	0.57	26.95	0.61
62	33.86	1.61	33.55	1.73	34.07	1.74	36.48	1.63	32.43	1.51

Residue Number	R_{2eff} at CPMG frequency (Hz)									
	650		800		1000		50 (Repeat)		650 (Repeat)	
	value	error	value	error	value	error	value	error	value	error
63	33.67	1.32	33.17	1.41	32.85	1.37	33.94	1.21	33.37	1.29
64	34.00	1.99	34.45	2.20	34.24	2.15	34.67	1.86	32.82	1.88
65	35.47	1.97	34.78	2.08	34.34	2.01	36.31	1.85	35.34	1.94
66	32.68	3.55	34.74	4.20	34.92	4.16	32.83	3.25	34.06	3.72
67	34.10	1.76	35.11	2.00	34.27	1.90	36.56	1.77	34.65	1.79
68	31.47	2.79	30.47	2.92	31.17	2.95	32.66	2.67	31.14	2.73
69	33.45	1.05	32.63	1.10	32.71	1.09	33.68	0.96	32.61	1.00
70	46.27	2.74	45.73	2.92	45.63	2.86	49.58	2.85	46.96	2.79
71	28.20	0.59	27.73	0.63	27.58	0.62	28.97	0.56	27.88	0.58
72	29.47	0.71	29.63	0.77	29.51	0.76	30.79	0.68	29.28	0.70
73	32.73	1.05	32.13	1.11	32.41	1.11	32.84	0.96	32.95	1.05
74	29.84	1.07	30.00	1.18	29.99	1.16	31.28	1.04	29.82	1.06
75	33.07	1.37	32.57	1.46	32.45	1.43	34.19	1.31	32.75	1.34
77	33.10	0.94	32.83	1.01	33.24	1.02	33.00	0.86	33.38	0.95
80	32.45	2.83	31.77	3.00	32.84	3.08	32.64	2.60	32.57	2.82
82	35.19	1.73	35.67	1.92	35.94	1.91	36.10	1.63	34.72	1.68
88	34.33	2.34	34.32	2.55	34.09	2.49	36.11	2.29	34.47	2.34
89	37.89	1.29	36.75	1.34	36.49	1.31	38.93	1.23	37.32	1.25
91	34.61	2.24	35.75	2.56	36.85	2.63	37.24	2.27	34.06	2.18
94	29.03	0.59	28.67	0.63	28.72	0.62	29.45	0.55	28.60	0.58
95	19.07	0.65	18.64	0.69	18.60	0.68	20.76	0.63	18.60	0.63
97	29.66	0.97	29.05	1.02	30.01	1.05	30.58	0.91	29.31	0.94
98	26.37	0.53	25.41	0.56	25.51	0.55	25.45	0.47	25.56	0.51
99	32.30	0.79	31.90	0.84	31.74	0.82	32.12	0.71	31.80	0.76
101	15.45	0.37	15.42	0.40	15.68	0.40	15.98	0.34	15.34	0.37
104	8.82	0.17	8.89	0.18	9.07	0.18	8.67	0.15	8.49	0.16
105	5.39	0.12	5.60	0.13	5.38	0.13	4.77	0.11	4.97	0.12

Table A.4: R_{2eff} values measured at different CPMG frequencies from CPMG relaxation dispersion experiment for TRBP2-dsRBD1 at 750 MHz NMR spectrometer

Residue Number	R_{2eff} at CPMG frequency (Hz)											
	25		50		100		200		350		500	
	value	error	value	error	value	error	value	error	value	error	value	error
2	44.12	1.30	45.57	0.98	45.11	0.88	44.39	1.78	44.39	1.88	44.36	1.90
3	30.00	0.32	28.84	0.22	29.98	0.21	30.54	0.45	29.56	0.45	29.73	0.46
5	14.41	0.09	14.20	0.06	14.72	0.06	14.46	0.12	14.13	0.12	14.47	0.12
8	53.12	6.03	50.94	3.92	57.40	4.65	52.24	7.89	57.22	10.13	55.17	9.46
10	54.19	3.63	52.47	2.41	56.54	2.59	56.26	5.35	57.00	5.79	57.30	5.94
11	33.76	3.74	34.72	2.76	35.29	2.59	33.17	4.95	37.76	6.26	33.72	5.40
16	35.06	1.60	33.91	1.08	34.34	1.01	34.91	2.16	34.91	2.27	33.51	2.17
18	51.36	5.49	50.83	3.82	52.82	3.79	55.56	8.81	54.68	8.94	51.22	7.89
24	31.34	2.75	31.93	2.00	28.74	1.61	30.42	3.60	28.01	3.43	29.84	3.75
25	37.69	4.94	34.96	3.14	31.48	2.51	32.75	5.49	34.28	6.14	30.68	5.39
26	41.74	6.55	43.45	4.98	43.05	4.49	42.46	9.13	44.24	10.31	45.93	11.18
30	36.25	2.03	37.00	1.49	28.77	0.98	34.46	2.57	33.83	2.63	35.77	2.88
32	34.76	7.66	35.49	5.60	3.65	1.44	34.90	10.43	34.98	11.01	31.78	9.82
33	38.57	2.05	37.44	1.39	73.38	5.36	37.85	2.70	38.75	2.94	38.45	2.94
35	29.36	0.81	44.68	1.07	51.63	1.29	28.51	1.07	28.40	1.12	28.28	1.13
36	35.73	1.48	43.00	1.41	61.99	2.76	36.80	2.10	34.39	2.00	36.67	2.22
39	37.40	2.00	33.91	1.24	16.43	0.56	40.26	3.04	38.52	2.98	38.43	3.01
41	36.53	1.79	49.90	2.17	31.17	0.94	34.64	2.25	35.30	2.43	35.45	2.47
42	41.23	3.43	17.31	0.93	35.39	1.76	36.12	3.78	38.40	4.36	37.75	4.31
43	35.88	1.40	46.00	1.49	42.65	1.20	37.01	1.99	35.44	1.97	33.03	1.81
44	29.36	2.11	30.75	1.58	40.61	2.15	27.41	2.64	27.85	2.83	28.26	2.91
48	33.32	2.36	25.61	1.23	19.96	0.90	36.72	3.67	35.30	3.64	34.25	3.54
49	34.34	1.70	57.37	3.03	43.71	1.60	35.03	2.36	31.51	2.16	32.38	2.27
50	38.38	4.39	35.88	2.82	14.33	1.09	39.53	6.22	44.56	8.00	40.43	6.88
51	38.80	4.89	44.20	4.31	35.26	2.76	37.76	6.36	40.05	7.33	36.81	6.53
54	30.47	0.70	78.54	3.42	87.66	4.52	30.68	0.96	28.54	0.93	29.72	0.99
56	56.42	4.55	16.13	0.65	9.31	0.45	55.74	6.01	57.30	6.72	55.21	6.27
61	31.97	0.92	50.10	1.35	70.65	2.82	30.84	1.19	31.14	1.27	30.71	1.27
62	37.20	2.12	31.79	1.21	16.26	0.60	37.15	2.87	35.74	2.85	34.59	2.76
63	32.94	1.58	49.37	2.16	39.91	1.36	36.94	2.51	36.55	2.60	35.75	2.55
64	36.83	3.16	33.55	1.97	21.62	1.12	35.70	4.09	38.33	4.78	34.59	4.17
65	38.44	2.83	54.67	3.85	45.92	2.48	35.70	3.44	36.70	3.76	38.16	4.04
66	41.29	7.02	29.49	3.11	19.15	1.88	39.10	8.71	37.46	8.58	32.05	7.00
68	33.19	3.96	19.61	1.63	48.27	4.71	33.01	5.33	36.43	6.43	33.92	5.89
69	40.78	2.35	18.52	0.69	58.58	3.12	38.65	2.93	40.43	3.30	38.80	3.14
71	32.15	1.03	35.09	0.82	52.23	1.49	30.34	1.29	30.37	1.36	30.53	1.39
72	33.86	1.18	40.87	1.11	29.21	0.64	33.35	1.57	32.89	1.62	32.50	1.61
73	33.23	1.50	28.10	0.86	28.96	0.82	32.23	1.95	33.20	2.13	34.11	2.24
74	30.77	1.29	36.03	1.13	36.23	1.05	32.20	1.85	32.61	1.98	30.02	1.81
75	31.04	1.64	27.06	0.99	26.44	0.89	39.79	3.15	38.08	3.10	37.28	3.04
77	37.83	1.50	66.28	3.31	43.11	1.20	37.82	2.03	39.17	2.25	38.60	2.23

Residue Number	R_{2eff} at CPMG frequency (Hz)											
	25		50		100		200		350		500	
	value	error	value	error	value	error	value	error	value	error	value	error
82	41.10	3.21	37.45	1.97	37.81	1.83	36.82	3.67	40.03	4.39	39.46	4.35
88	37.44	4.07	33.32	2.45	38.08	2.71	37.85	5.61	37.21	5.75	36.13	5.58
89	37.48	1.68	35.96	1.12	36.09	1.03	36.24	2.17	36.04	2.26	35.23	2.22
90	24.22	4.87	24.14	3.45	29.18	3.86	27.55	7.54	28.70	8.30	26.61	7.74
91	34.87	3.19	35.66	2.34	37.31	2.29	40.37	5.40	36.32	4.83	32.07	4.13
94	42.59	2.22	42.42	1.56	40.72	1.34	42.40	2.98	42.07	3.10	42.64	3.21
95	25.20	1.78	25.34	1.27	25.67	1.18	24.01	2.31	23.74	2.40	23.35	2.39
97	41.82	4.20	45.58	3.46	45.16	3.12	45.94	6.70	45.05	6.81	44.67	6.79
98	46.87	4.18	45.93	2.86	49.19	2.98	46.88	5.67	49.99	6.75	46.81	6.03
104	44.14	0.99	12.88	0.20	15.02	0.20	13.73	0.40	14.31	0.43	12.89	0.41
105	5.67	0.14	4.82	0.10	6.82	0.10	6.06	0.20	8.63	0.23	5.45	0.21

Table A.4: R_{2eff} values measured at different CPMG frequencies from CPMG relaxation dispersion experiment for TRBP2-dsRBD1 at 750 MHz NMR spectrometer (Continued)

Residue Number	R_{2eff} at CPMG frequency (Hz)									
	650		800		1000		50 (Repeat)		650 (Repeat)	
	value	error	value	error	value	error	value	error	value	error
2	43.93	1.25	43.47	1.77	45.55	1.01	45.93	1.51	44.14	0.88
3	29.85	0.31	29.61	0.45	30.03	0.24	28.87	0.33	30.16	0.22
5	14.66	0.08	14.52	0.12	14.58	0.06	14.11	0.09	14.64	0.06
8	55.19	6.32	53.54	8.55	53.19	4.42	53.99	6.74	56.46	4.65
10	59.48	4.33	58.44	6.00	56.92	2.96	53.94	3.88	54.76	2.50
11	32.19	3.39	31.11	4.69	32.74	2.63	32.79	3.89	32.46	2.39
16	32.82	1.41	33.80	2.12	34.80	1.16	34.96	1.72	33.52	1.01
18	55.01	6.13	49.42	7.09	56.97	5.03	46.29	4.84	57.28	4.69
24	30.52	2.57	30.56	3.72	30.93	1.98	31.64	3.01	30.09	1.76
25	34.42	4.18	31.54	5.39	32.18	2.90	35.05	4.80	29.99	2.45
26	41.67	6.30	41.35	8.99	43.12	5.06	49.97	9.82	42.53	4.56
30	34.15	1.81	34.75	2.67	35.57	1.45	36.35	2.21	35.45	1.33
32	34.12	7.20	33.61	10.20	28.80	4.41	32.70	7.61	32.92	4.79
33	37.52	1.89	37.83	2.77	37.69	1.45	37.60	2.13	37.96	1.35
35	28.19	0.75	28.85	1.11	28.69	0.58	28.80	0.86	29.03	0.54
36	35.53	1.42	36.42	2.13	36.05	1.10	36.21	1.63	35.93	1.01
39	39.27	2.08	36.35	2.68	35.99	1.38	36.43	2.08	38.28	1.40
41	34.57	1.59	34.49	2.30	36.46	1.30	36.50	1.93	35.32	1.15
42	39.53	3.09	37.64	4.14	37.94	2.20	35.74	2.97	40.21	2.22
43	34.23	1.27	34.75	1.87	34.63	0.98	34.77	1.45	34.40	0.89
44	29.46	2.04	30.05	3.02	31.23	1.66	28.96	2.24	27.53	1.32
48	32.54	2.21	31.88	3.11	33.06	1.71	32.50	2.47	33.81	1.62
49	34.18	1.63	33.02	2.24	34.10	1.23	34.47	1.84	33.04	1.09
50	35.94	3.84	38.99	6.27	36.89	3.02	37.90	4.64	38.47	2.97
51	37.96	4.56	33.58	5.54	34.42	3.00	35.19	4.57	36.29	2.98
53	43.34	5.83	46.07	9.40	42.97	4.35	48.05	7.87	41.60	3.80
54	29.59	0.66	30.12	0.97	29.50	0.50	30.75	0.77	29.51	0.46
56	57.63	4.61	55.20	6.05	52.10	2.80	57.76	5.19	55.38	2.94
61	30.88	0.85	31.84	1.28	32.22	0.68	31.89	0.99	31.49	0.61
62	35.78	1.93	34.87	2.69	36.31	1.50	36.08	2.19	36.15	1.37
63	35.06	1.66	36.34	2.52	36.52	1.33	34.12	1.78	34.74	1.14
64	34.58	2.79	35.84	4.23	36.55	2.28	36.10	3.31	34.63	1.95
65	36.52	2.53	38.23	3.91	37.22	1.97	38.45	3.06	36.41	1.76
66	33.70	5.00	32.94	7.01	32.20	3.57	35.55	6.02	35.09	3.69
68	32.94	3.79	33.57	5.61	36.21	3.27	35.38	4.67	30.62	2.41
69	39.00	2.11	38.50	2.99	39.39	1.63	40.14	2.47	40.17	1.55
71	30.83	0.94	30.28	1.33	30.25	0.69	30.10	1.02	30.72	0.65
72	32.56	1.08	32.96	1.59	33.55	0.85	32.89	1.23	33.20	0.77
73	34.30	1.51	33.16	2.08	33.36	1.10	33.71	1.65	33.37	1.01
74	31.70	1.29	30.72	1.80	32.03	0.99	29.50	1.33	31.05	0.88
75	36.56	1.97	33.61	2.53	35.79	1.45	30.79	1.75	34.83	1.29

Residue Number	R_{2eff} at CPMG frequency (Hz)									
	650		800		1000		50 (Repeat)		650 (Repeat)	
	value	error	value	error	value	error	value	error	value	error
77	35.49	1.31	33.11	1.73	35.49	1.00	35.45	1.47	36.64	0.96
82	39.40	2.90	39.29	4.17	39.48	2.20	39.40	3.24	40.20	2.09
88	38.03	4.02	33.89	4.92	37.57	2.99	35.93	4.14	37.05	2.70
89	36.76	1.58	35.23	2.14	35.29	1.13	36.28	1.73	36.86	1.10
90	25.58	4.96	24.34	6.82	25.64	3.77	24.77	5.37	26.48	3.59
91	33.41	2.91	34.93	4.47	35.63	2.41	36.45	3.67	36.19	2.27
94	40.99	2.01	41.07	2.91	41.47	1.55	40.89	2.24	42.10	1.47
95	23.96	1.64	23.99	2.37	23.33	1.21	24.36	1.86	24.45	1.17
97	39.65	3.71	42.25	5.95	43.03	3.22	44.33	5.01	42.31	2.88
98	47.21	4.09	46.81	5.82	46.65	3.03	48.27	4.78	45.75	2.70
104	14.04	0.29	13.88	0.41	14.53	0.22	13.27	0.31	14.12	0.20
105	5.61	0.14	5.57	0.20	6.92	0.11	4.82	0.15	5.66	0.10

Table A.5: R_{2eff} values measured at different CPMG frequencies from CPMG relaxation dispersion experiment for dADAR-dsRBD1 at 600 MHz NMR spectrometer

Residue Number	R_{2eff} at CPMG frequency (Hz)											
	50		100		150		200		300		450	
	value	error	value	error	value	error	value	error	value	error	value	error
59	44.20	0.55	42.23	0.52	41.17	0.51	39.16	0.53	39.18	0.50	36.09	0.47
65	62.73	1.40	63.18	1.38	59.33	1.27	62.99	1.49	58.34	1.28	53.81	1.18
66	39.47	1.85	40.69	1.85	39.81	1.81	40.63	2.00	38.71	1.82	39.65	1.87
67	40.63	1.38	42.77	1.41	42.48	1.40	39.37	1.42	40.82	1.38	38.04	1.32
68	41.61	1.80	41.83	1.76	41.12	1.73	38.59	1.78	38.71	1.69	40.85	1.78
69	45.46	1.05	44.27	1.00	44.65	1.00	45.64	1.11	43.23	1.00	44.16	1.02
70	42.14	0.53	41.14	0.51	40.51	0.50	40.66	0.54	39.47	0.50	39.96	0.51
72	42.61	1.11	42.23	1.07	42.20	1.07	42.80	1.17	40.56	1.06	41.35	1.09
73	33.82	0.46	34.67	0.46	33.97	0.45	34.36	0.49	32.42	0.45	33.14	0.46
75	53.39	1.33	50.55	1.23	53.90	1.31	51.12	1.34	52.15	1.29	48.86	1.22
76	35.28	0.49	34.57	0.47	33.59	0.46	33.85	0.50	33.71	0.47	32.86	0.46
77	39.00	0.71	36.72	0.66	37.04	0.66	38.17	0.73	37.81	0.69	37.25	0.68
78	38.59	0.71	41.68	0.74	40.25	0.71	41.53	0.80	42.34	0.76	37.87	0.70
79	43.81	6.04	39.64	5.41	41.28	5.57	42.76	6.22	32.24	4.76	31.13	4.70
80	40.72	0.78	41.90	0.77	40.52	0.75	42.77	0.85	39.10	0.75	36.78	0.72
81	45.60	1.06	45.34	1.03	47.70	1.08	48.63	1.19	49.65	1.15	55.55	1.30
82	40.93	0.55	40.96	0.54	37.72	0.50	48.05	0.67	39.19	0.53	38.57	0.53
84	38.16	0.53	40.00	0.54	38.53	0.52	38.42	0.56	37.11	0.52	37.16	0.52
85	35.43	0.53	36.56	0.53	33.33	0.50	42.19	0.64	34.22	0.52	34.63	0.53
87	44.08	0.81	43.62	0.78	44.97	0.80	45.50	0.88	44.37	0.81	45.12	0.83
89	30.61	0.74	29.41	0.70	32.82	0.75	32.21	0.80	30.55	0.73	29.71	0.73
91	34.69	0.45	33.64	0.43	32.65	0.42	33.00	0.46	32.77	0.43	32.65	0.44
92	49.83	1.23	50.60	1.21	49.68	1.19	54.23	1.41	47.33	1.16	44.87	1.12
93	40.35	0.73	41.45	0.72	40.98	0.72	40.03	0.76	40.51	0.73	40.95	0.74
94	41.61	1.19	43.38	1.20	45.93	1.26	44.84	1.33	44.31	1.25	52.64	1.49
95	41.75	0.73	42.00	0.71	41.73	0.71	41.24	0.76	40.60	0.71	40.50	0.71
96	43.33	1.58	43.81	1.55	42.58	1.51	42.45	1.63	42.12	1.53	40.41	1.49
97	40.68	0.59	44.05	0.62	47.96	0.66	40.91	0.63	48.70	0.69	40.03	0.59
98	42.12	1.46	44.19	1.48	43.79	1.46	43.52	1.58	41.60	1.44	38.42	1.36
99	42.35	0.60	43.67	0.60	46.05	0.62	45.69	0.67	47.87	0.66	53.15	0.74
100	35.48	0.48	40.39	0.52	37.87	0.49	41.57	0.57	37.41	0.50	50.38	0.65
101	34.49	0.37	35.48	0.37	34.32	0.36	35.03	0.40	34.45	0.37	34.66	0.38
102	29.26	0.25	30.11	0.25	32.18	0.26	30.18	0.27	30.45	0.26	31.45	0.26
103	62.74	2.01	64.37	2.02	62.33	1.93	59.67	1.99	57.87	1.81	51.20	1.60
104	40.06	0.95	39.95	0.92	39.49	0.91	39.02	0.98	39.55	0.93	37.61	0.91
105	42.45	0.83	41.65	0.80	39.11	0.76	47.79	0.98	40.51	0.80	41.72	0.82
106	39.81	0.57	38.50	0.54	38.79	0.54	38.33	0.58	38.24	0.55	38.42	0.56
107	43.23	0.70	42.27	0.67	48.38	0.75	45.60	0.77	45.70	0.73	50.78	0.82
108	55.74	1.74	51.25	1.55	50.20	1.51	52.76	1.73	49.32	1.52	48.92	1.52
109	39.12	0.46	37.73	0.44	40.74	0.46	37.90	0.47	39.15	0.46	35.99	0.43
112	41.85	1.18	43.43	1.18	42.82	1.16	41.95	1.24	41.72	1.17	42.75	1.20

Residue Number	R_{2eff} at CPMG frequency (Hz)											
	50		100		150		200		300		450	
	value	error	value	error	value	error	value	error	value	error	value	error
113	38.70	0.99	38.56	0.96	39.58	0.98	39.58	1.06	38.45	0.98	37.02	0.96
114	42.09	0.58	42.78	0.58	41.64	0.56	42.27	0.62	40.80	0.57	40.47	0.57
115	45.35	1.00	46.06	0.99	43.51	0.94	43.58	1.02	44.31	0.98	43.53	0.97
116	44.18	0.68	45.68	0.68	45.62	0.68	44.66	0.72	43.66	0.67	42.82	0.66
117	45.12	1.48	42.80	1.38	41.65	1.34	47.23	1.63	42.02	1.38	41.59	1.39
119	22.32	0.60	22.12	0.58	21.80	0.58	22.25	0.63	22.21	0.60	21.85	0.60
120	52.33	1.08	49.60	1.00	50.52	1.02	49.30	1.08	47.82	0.99	45.87	0.96
121	41.09	1.19	43.77	1.23	42.28	1.19	42.60	1.30	40.00	1.16	37.66	1.12
122	52.29	1.32	48.76	1.20	49.40	1.21	47.57	1.27	47.33	1.19	46.13	1.17
123	42.62	1.28	43.03	1.25	42.38	1.23	42.97	1.35	42.97	1.28	41.85	1.26
124	41.84	0.60	41.66	0.58	41.05	0.58	41.50	0.63	40.07	0.58	38.87	0.57
125	47.46	0.78	46.80	0.75	45.86	0.74	45.23	0.79	42.24	0.70	42.42	0.71
126	38.86	1.10	38.18	1.06	38.36	1.06	38.00	1.14	37.04	1.06	36.05	1.05
129	37.52	0.65	36.18	0.61	36.40	0.61	36.74	0.67	32.68	0.58	33.04	0.59
131	38.49	0.35	40.56	0.35	38.39	0.34	40.58	0.38	33.34	0.31	30.08	0.29
132	15.47	0.25	16.29	0.25	17.89	0.26	16.68	0.27	16.38	0.26	17.08	0.26
133	15.77	0.25	15.35	0.24	15.03	0.24	15.61	0.27	14.81	0.25	14.23	0.25
134	30.84	0.49	31.01	0.48	28.91	0.46	33.77	0.54	25.67	0.44	23.46	0.42
135	18.10	0.16	17.32	0.16	17.08	0.16	17.65	0.17	17.28	0.16	16.86	0.16
137	15.42	0.20	15.10	0.19	14.69	0.19	15.38	0.21	14.72	0.19	13.44	0.19
140	5.30	0.12	5.52	0.11	8.50	0.12	7.26	0.13	10.21	0.13	14.38	0.14

Table A.5: R_{2eff} values measured at different CPMG frequencies from CPMG relaxation dispersion experiment for dADAR-dsRBD1 at 600 MHz NMR spectrometer (Continued)

Residue Number	R_{2eff} at CPMG frequency (Hz)									
	600		800		1000		150		600	
	value	error	value	error	value	error	value	error	value	error
59	33.22	0.43	31.38	0.43	29.24	0.41	42.43	0.54	34.05	0.43
65	54.64	1.17	49.94	1.10	48.57	1.06	58.98	1.33	51.62	1.08
66	39.60	1.82	40.32	1.90	39.51	1.85	40.87	1.94	39.39	1.77
67	38.71	1.30	40.46	1.39	39.54	1.35	41.54	1.44	37.69	1.25
68	39.20	1.68	39.99	1.75	39.72	1.73	42.73	1.87	40.05	1.67
69	43.84	0.99	43.75	1.02	42.46	0.98	44.73	1.05	43.89	0.97
70	39.87	0.50	39.30	0.50	38.81	0.50	41.21	0.53	39.61	0.48
72	41.81	1.07	39.93	1.06	40.13	1.06	42.36	1.13	40.21	1.02
73	33.93	0.45	34.38	0.47	33.84	0.46	34.14	0.48	33.88	0.45
75	51.23	1.25	51.35	1.29	51.40	1.28	52.81	1.34	51.36	1.23
76	33.64	0.46	32.79	0.47	32.78	0.46	34.22	0.49	32.94	0.44
77	36.12	0.65	37.02	0.68	36.45	0.67	37.09	0.69	37.15	0.65
78	36.43	0.67	35.02	0.67	38.95	0.72	40.74	0.76	35.07	0.64
79	32.83	4.74	41.90	5.86	36.40	5.20	43.01	6.06	41.00	5.48
80	38.79	0.73	40.72	0.78	41.06	0.78	41.74	0.81	38.74	0.72
81	45.51	1.04	44.61	1.05	45.15	1.05	49.09	1.16	44.93	1.01
82	41.47	0.55	40.56	0.55	40.60	0.55	38.30	0.54	40.50	0.53
84	37.73	0.52	37.20	0.53	36.73	0.52	39.03	0.55	36.49	0.49
85	37.82	0.55	35.79	0.54	35.98	0.54	33.42	0.52	36.96	0.53
87	45.26	0.81	44.18	0.82	45.12	0.83	44.85	0.84	45.25	0.80
89	30.01	0.71	31.12	0.75	31.91	0.76	32.48	0.78	28.92	0.68
91	33.69	0.44	32.53	0.44	32.29	0.43	32.82	0.45	32.50	0.42
92	47.71	1.15	45.62	1.14	43.38	1.08	49.51	1.24	46.30	1.10
93	41.08	0.72	39.81	0.73	39.06	0.71	41.35	0.76	40.15	0.70
94	41.96	1.17	39.14	1.14	39.25	1.13	45.15	1.30	39.54	1.09
95	42.58	0.72	41.75	0.73	42.53	0.74	41.18	0.73	42.16	0.70
96	42.68	1.52	41.19	1.52	40.42	1.48	42.69	1.59	40.27	1.42
97	36.52	0.53	38.45	0.57	40.76	0.59	48.28	0.70	35.92	0.52
98	39.51	1.36	42.24	1.47	40.11	1.40	43.77	1.54	38.42	1.30
99	42.69	0.59	41.84	0.59	41.61	0.59	46.38	0.66	41.74	0.56
100	36.60	0.48	33.56	0.47	39.97	0.53	37.76	0.52	35.58	0.46
101	35.29	0.37	35.15	0.38	35.27	0.38	35.05	0.39	35.01	0.36
102	31.06	0.25	30.86	0.26	31.10	0.26	32.35	0.27	30.94	0.25
103	49.27	1.50	46.85	1.47	46.73	1.45	60.05	1.94	49.24	1.47
104	36.61	0.87	39.10	0.94	36.54	0.88	39.73	0.96	37.76	0.87
105	43.35	0.83	40.76	0.81	42.84	0.84	38.36	0.78	41.91	0.79
106	37.92	0.54	36.85	0.54	37.09	0.54	39.12	0.57	37.74	0.53
107	42.20	0.67	39.99	0.66	41.02	0.67	49.53	0.81	41.65	0.65
108	51.63	1.57	52.46	1.64	50.14	1.55	49.93	1.58	49.72	1.48
109	37.11	0.43	37.61	0.45	39.23	0.46	40.76	0.49	36.55	0.42
112	41.83	1.15	40.66	1.16	41.29	1.16	44.30	1.26	42.18	1.14

Residue Number	R_{2eff} at CPMG frequency (Hz)									
	600		800		1000		150		600	
	value	error	value	error	value	error	value	error	value	error
113	38.15	0.96	37.03	0.97	38.50	0.99	40.90	1.06	38.38	0.95
114	41.00	0.56	39.80	0.56	39.34	0.55	43.00	0.61	41.13	0.55
115	44.12	0.96	43.39	0.97	44.82	0.99	44.89	1.01	43.66	0.93
116	43.73	0.66	43.23	0.67	44.11	0.68	45.45	0.71	43.77	0.64
117	45.02	1.45	44.69	1.48	39.69	1.33	42.83	1.44	42.74	1.36
119	22.51	0.59	21.82	0.60	21.46	0.59	22.03	0.61	21.58	0.57
120	44.25	0.90	42.94	0.91	42.76	0.89	50.72	1.07	43.18	0.87
121	39.39	1.13	40.02	1.18	42.73	1.23	42.41	1.25	38.31	1.08
122	44.91	1.12	42.61	1.10	43.05	1.10	47.89	1.23	43.70	1.07
123	42.34	1.24	40.57	1.24	41.23	1.24	42.73	1.31	41.54	1.20
124	39.28	0.56	38.71	0.57	38.93	0.57	41.04	0.61	39.24	0.55
125	42.59	0.70	40.35	0.69	40.08	0.68	46.35	0.78	41.50	0.67
126	36.85	1.04	34.59	1.02	36.01	1.04	40.31	1.16	36.95	1.02
129	32.20	0.57	30.12	0.56	29.99	0.56	36.53	0.65	31.86	0.55
131	31.24	0.29	28.81	0.29	27.02	0.28	38.86	0.36	30.14	0.28
132	16.84	0.25	16.45	0.26	16.92	0.26	18.20	0.27	16.34	0.25
133	15.44	0.25	14.57	0.25	14.89	0.25	15.66	0.26	14.67	0.24
134	23.96	0.42	22.09	0.41	20.94	0.40	28.82	0.48	23.24	0.40
135	17.51	0.16	16.44	0.16	16.19	0.16	17.73	0.17	16.67	0.15
137	13.62	0.19	12.55	0.19	12.54	0.19	15.41	0.20	13.31	0.18
140	7.04	0.12	8.16	0.12	7.61	0.12	8.98	0.13	6.32	0.11

Table A.6: R_{2eff} values measured at different CPMG frequencies from CPMG relaxation dispersion experiment for dADAR-dsRBD1 at 750 MHz NMR spectrometer

Residue Number	R_{2eff} at CPMG frequency (Hz)											
	50		100		150		200		300		450	
	value	error	value	error	value	error	value	error	value	error	value	error
59	41.89	0.89	46.87	0.97	43.01	0.91	45.55	0.96	38.50	0.83	41.33	0.84
65	69.77	2.67	74.01	2.87	60.16	2.20	68.44	2.62	75.32	2.98	62.50	2.22
66	46.43	3.56	42.94	3.28	39.75	3.11	49.66	3.83	37.30	2.97	47.82	3.52
67	44.65	2.61	41.31	2.41	42.79	2.51	51.83	3.03	37.47	2.26	45.69	2.56
68	40.95	3.12	41.87	3.14	43.08	3.25	37.68	2.95	32.59	2.64	40.67	2.98
69	45.70	1.55	43.18	1.46	46.96	1.59	46.95	1.61	46.38	1.58	40.38	1.34
70	38.33	0.83	38.50	0.82	41.95	0.89	40.74	0.88	37.59	0.82	39.47	0.81
72	44.09	1.72	44.01	1.70	41.87	1.65	43.15	1.71	45.87	1.79	40.35	1.54
73	38.87	0.90	33.79	0.80	38.69	0.89	39.25	0.91	35.16	0.83	37.05	0.83
75	60.22	2.66	62.79	2.77	60.30	2.66	54.94	2.42	55.11	2.40	62.21	2.66
76	34.55	0.86	42.37	0.99	36.42	0.89	35.59	0.89	33.70	0.85	34.70	0.83
77	33.66	1.00	42.74	1.18	35.86	1.04	35.30	1.04	37.74	1.08	37.25	1.03
78	43.35	1.40	39.07	1.26	46.61	1.49	48.20	1.55	55.33	1.77	43.60	1.35
80	41.69	1.53	45.81	1.64	37.76	1.41	43.54	1.60	56.31	2.05	36.91	1.33
81	48.02	1.84	45.50	1.72	58.82	2.28	50.45	1.95	62.26	2.44	73.51	2.94
82	38.93	0.82	40.24	0.83	45.65	0.94	42.28	0.89	46.40	0.95	39.44	0.80
84	34.36	0.79	44.09	0.95	42.87	0.94	37.26	0.85	35.54	0.81	38.49	0.83
85	35.97	0.94	38.16	0.97	45.72	1.14	36.94	0.97	42.39	1.07	35.88	0.90
87	56.50	2.28	50.56	2.00	56.71	2.29	56.54	2.30	58.10	2.36	49.11	1.89
89	27.66	1.13	42.50	1.50	34.35	1.29	35.86	1.35	30.23	1.19	33.73	1.23
91	35.01	0.72	38.19	0.76	33.50	0.70	32.65	0.70	39.42	0.79	33.84	0.68
92	53.55	2.12	56.61	2.22	57.74	2.29	51.74	2.06	70.86	2.99	50.53	1.91
93	37.27	1.15	44.74	1.31	43.16	1.29	38.95	1.20	38.00	1.16	39.86	1.16
94	47.88	2.41	43.05	2.16	50.38	2.53	49.17	2.50	59.84	3.06	66.05	3.33
95	43.00	1.21	39.99	1.12	43.64	1.22	43.26	1.22	37.36	1.08	43.83	1.18
96	41.35	2.55	40.43	2.47	40.95	2.52	41.19	2.56	44.25	2.70	40.94	2.43
97	42.18	1.06	45.03	1.11	53.00	1.32	51.51	1.29	53.96	1.34	51.12	1.22
98	46.48	2.67	44.69	2.54	41.50	2.41	54.32	3.15	53.09	3.05	41.46	2.32
99	41.37	1.10	46.55	1.21	66.12	1.81	52.34	1.39	55.50	1.47	63.40	1.65
100	33.97	0.85	41.75	0.98	49.67	1.16	40.73	0.98	38.85	0.93	50.25	1.13
101	38.28	0.67	34.14	0.61	37.86	0.67	38.60	0.68	32.82	0.60	38.73	0.65
102	33.48	0.62	36.90	0.65	47.33	0.81	39.07	0.70	36.64	0.66	34.12	0.60
103	71.15	3.76	61.88	3.08	60.42	3.03	76.84	4.25	70.19	3.69	55.37	2.63
104	41.62	1.51	53.45	1.89	38.00	1.40	43.74	1.59	46.57	1.67	38.06	1.35
105	42.86	1.29	47.29	1.39	48.26	1.44	38.89	1.20	46.03	1.38	38.10	1.13
106	39.89	0.90	40.25	0.89	37.34	0.85	37.00	0.85	41.83	0.93	39.12	0.85
107	38.78	0.97	38.95	0.96	47.52	1.15	65.24	1.66	51.29	1.24	52.98	1.23
108	56.88	3.24	61.52	3.51	60.56	3.48	53.66	3.06	58.44	3.34	53.47	2.91
109	39.09	0.74	41.63	0.77	42.16	0.79	38.06	0.73	37.48	0.72	39.83	0.72
112	40.94	1.71	40.96	1.69	44.44	1.83	42.73	1.78	44.09	1.82	42.06	1.68
113	38.09	1.66	49.18	2.04	40.35	1.73	45.08	1.92	38.68	1.68	42.46	1.74

Residue Number	R_{2eff} at CPMG frequency (Hz)											
	50		100		150		200		300		450	
	value	error	value	error	value	error	value	error	value	error	value	error
114	41.56	0.97	47.09	1.07	46.31	1.07	41.52	0.98	39.51	0.93	42.14	0.95
115	41.00	1.35	51.18	1.64	45.46	1.47	46.76	1.53	43.04	1.41	45.09	1.41
116	50.01	1.21	43.57	1.05	50.77	1.22	49.83	1.21	44.10	1.07	47.54	1.10
117	39.12	2.22	58.91	3.26	50.64	2.79	48.79	2.72	56.68	3.16	46.71	2.48
119	23.36	1.14	32.54	1.35	27.80	1.24	26.51	1.22	24.48	1.16	25.23	1.14
120	48.34	1.59	45.37	1.47	53.40	1.75	55.25	1.84	48.49	1.59	47.21	1.49
121	19.73	1.03	20.33	1.03	15.25	0.94	31.05	1.31	28.89	1.24	15.84	0.92
122	53.01	2.15	48.68	1.94	48.07	1.94	45.38	1.86	49.15	1.99	46.08	1.80
123	40.05	2.14	37.56	2.01	44.53	2.34	46.66	2.47	40.19	2.15	37.46	1.95
124	42.05	0.94	41.21	0.92	49.69	1.10	47.26	1.06	38.62	0.88	48.42	1.03
125	51.87	1.38	47.19	1.24	51.82	1.38	50.08	1.35	46.59	1.25	43.85	1.13
126	41.67	1.98	37.42	1.79	42.49	2.00	43.17	2.05	43.73	2.06	35.78	1.69
129	43.80	1.36	37.82	1.19	39.38	1.24	41.89	1.32	39.25	1.24	31.51	1.02
131	40.76	0.74	36.10	0.67	39.62	0.72	43.59	0.79	39.39	0.72	44.32	0.76
132	15.37	0.54	17.75	0.56	27.69	0.69	22.31	0.63	17.50	0.57	16.15	0.53
133	14.66	0.50	20.88	0.56	15.86	0.51	14.57	0.50	18.96	0.54	15.44	0.49
134	30.74	1.03	30.62	1.01	32.36	1.06	32.42	1.07	47.51	1.44	26.42	0.90
135	19.97	0.38	17.42	0.36	18.72	0.37	19.58	0.38	19.10	0.38	18.43	0.36
137	16.00	0.37	22.69	0.42	16.09	0.37	20.54	0.41	13.53	0.35	20.19	0.39
140	8.65	0.29	5.53	0.26	24.02	0.39	16.00	0.33	17.84	0.34	26.09	0.39

Table A.6: R_{2eff} values measured at different CPMG frequencies from CPMG relaxation dispersion experiment for dADAR-dsRBD1 at 750 MHz NMR spectrometer (Continued)

Residue Number	R_{2eff} at CPMG frequency (Hz)									
	600		800		1000		150		600	
	value	error	value	error	value	error	value	error	value	error
59	39.86	0.83	33.07	0.73	35.15	0.76	43.40	0.88	36.12	0.76
65	66.12	2.41	58.71	2.09	56.76	2.01	64.05	2.29	63.88	2.29
66	45.61	3.40	44.96	3.39	45.46	3.42	45.68	3.38	37.27	2.86
67	40.26	2.32	42.78	2.46	40.24	2.34	45.18	2.53	42.35	2.40
68	33.12	2.59	39.48	2.97	37.92	2.88	39.95	2.95	37.95	2.84
69	44.52	1.47	41.47	1.40	40.74	1.38	49.66	1.62	43.02	1.42
70	37.57	0.79	37.81	0.80	38.33	0.81	41.98	0.86	38.09	0.80
72	39.72	1.53	40.03	1.56	40.03	1.56	40.61	1.55	41.11	1.57
73	35.54	0.82	35.05	0.81	32.77	0.78	39.89	0.88	34.43	0.79
75	62.20	2.69	61.43	2.67	63.37	2.78	57.54	2.43	62.70	2.70
76	34.46	0.83	34.81	0.85	33.19	0.82	37.55	0.88	34.85	0.84
77	35.02	0.99	37.13	1.04	37.30	1.05	35.03	0.98	38.37	1.06
78	39.83	1.26	43.94	1.38	39.83	1.27	48.66	1.49	38.73	1.23
80	39.94	1.43	44.14	1.57	43.93	1.57	39.45	1.41	39.71	1.42
81	48.72	1.81	45.32	1.70	49.69	1.86	61.08	2.30	49.48	1.83
82	43.29	0.87	47.05	0.95	46.76	0.94	47.12	0.93	41.81	0.84
84	35.54	0.79	35.60	0.80	37.77	0.83	41.34	0.88	35.82	0.79
85	36.22	0.92	45.23	1.11	42.90	1.06	46.67	1.12	35.18	0.89
87	60.19	2.39	55.51	2.19	52.80	2.08	59.36	2.33	56.46	2.20
89	30.70	1.17	34.63	1.28	35.08	1.29	32.98	1.21	29.07	1.13
91	35.45	0.71	35.72	0.72	33.29	0.69	36.11	0.71	34.68	0.70
92	44.99	1.73	47.81	1.85	46.08	1.78	56.04	2.14	42.99	1.65
93	38.73	1.15	38.26	1.14	39.73	1.18	42.34	1.22	38.62	1.14
94	45.01	2.21	44.20	2.19	42.25	2.11	55.10	2.68	43.21	2.12
95	41.75	1.14	40.05	1.11	41.82	1.15	44.23	1.19	41.31	1.13
96	40.18	2.42	41.92	2.52	42.24	2.54	44.03	2.59	39.80	2.39
97	40.45	1.00	36.82	0.93	39.91	0.99	58.18	1.41	38.70	0.96
98	43.00	2.42	40.98	2.34	42.46	2.41	40.68	2.29	43.07	2.41
99	45.16	1.16	45.42	1.17	45.74	1.18	67.42	1.79	44.04	1.13
100	39.03	0.91	36.33	0.87	38.70	0.91	50.11	1.13	38.72	0.90
101	36.24	0.63	36.40	0.64	35.50	0.62	40.94	0.68	34.90	0.61
102	39.19	0.67	39.19	0.68	40.88	0.70	46.76	0.78	39.22	0.67
103	61.00	2.98	49.47	2.39	49.90	2.41	60.53	2.93	57.61	2.77
104	42.32	1.49	43.51	1.54	36.71	1.34	43.10	1.50	45.56	1.58
105	39.57	1.18	49.68	1.45	45.88	1.35	48.89	1.40	39.93	1.18
106	40.30	0.88	39.10	0.87	37.97	0.85	39.68	0.86	38.91	0.85
107	46.34	1.09	49.85	1.18	50.14	1.19	51.92	1.21	43.09	1.02
108	60.23	3.36	57.37	3.20	50.04	2.77	57.94	3.18	52.49	2.87
109	43.18	0.78	44.31	0.81	46.28	0.84	41.50	0.75	44.42	0.80
112	41.84	1.69	42.12	1.71	42.06	1.71	42.34	1.69	41.50	1.67
113	40.40	1.69	41.13	1.73	37.27	1.60	45.09	1.84	40.98	1.70

Residue Number	R_{2eff} at CPMG frequency (Hz)									
	600		800		1000		150		600	
	value	error	value	error	value	error	value	error	value	error
114	40.14	0.92	41.01	0.94	41.93	0.96	43.93	0.98	38.90	0.89
115	43.09	1.37	42.19	1.36	43.43	1.39	45.81	1.43	44.11	1.39
116	45.16	1.06	45.05	1.07	44.43	1.06	49.74	1.15	45.47	1.06
117	43.74	2.36	40.90	2.25	44.13	2.40	47.91	2.55	41.96	2.27
119	25.88	1.16	25.49	1.16	23.88	1.13	29.49	1.24	25.44	1.15
120	44.46	1.42	44.19	1.43	44.42	1.44	51.60	1.63	45.59	1.45
121	23.98	1.09	20.94	1.04	22.75	1.08	16.75	0.94	22.01	1.05
122	47.59	1.87	46.64	1.85	42.86	1.72	45.94	1.80	47.98	1.88
123	39.33	2.05	37.75	2.00	39.25	2.06	42.07	2.15	38.13	1.99
124	41.97	0.92	41.84	0.92	41.20	0.91	51.06	1.09	41.77	0.91
125	45.25	1.18	42.20	1.12	41.77	1.11	54.39	1.40	44.42	1.15
126	42.18	1.94	38.51	1.82	36.33	1.74	46.19	2.08	42.60	1.94
129	37.48	1.16	34.34	1.10	32.68	1.06	44.59	1.33	36.60	1.13
131	41.41	0.73	35.02	0.65	36.42	0.66	39.68	0.70	41.67	0.73
132	21.03	0.59	20.30	0.59	22.13	0.61	28.49	0.68	20.56	0.58
133	16.63	0.50	16.14	0.50	14.08	0.48	17.31	0.51	16.75	0.50
134	23.98	0.87	29.88	0.99	24.24	0.88	32.20	1.02	24.05	0.87
135	17.27	0.35	17.80	0.36	18.19	0.36	18.73	0.36	17.84	0.35
137	18.65	0.38	15.51	0.36	15.30	0.36	18.13	0.37	15.99	0.36
140	8.88	0.28	13.03	0.30	12.92	0.30	25.83	0.39	7.83	0.27

Table A.7: $R_{1\rho}$ relaxation rates measured using HSn pulses (n=1,2,4,6,8) from HARD experiment for TRBP2-dsRBD1 at 600 MHz NMR spectrometer

Residue Number	$R_{1\rho}$ (Hz)									
	HS1		HS2		HS4		HS6		HS8	
	value	error	value	error	value	error	value	error	value	error
1	2.61	0.42	2.22	0.15	2.33	0.24	2.20	0.48	1.99	0.36
2	1.69	0.09	1.84	0.02	1.86	0.05	1.90	0.08	1.84	0.05
3	1.66	0.09	1.86	0.04	1.85	0.05	1.96	0.04	1.91	0.06
5	1.71	0.07	1.77	0.06	1.92	0.01	2.02	0.09	2.03	0.02
7	2.04	0.11	2.12	0.04	2.18	0.03	2.32	0.08	2.21	0.03
8	1.75	0.02	2.43	0.15	2.27	0.11	2.33	0.13	2.49	0.07
9	1.91	0.10	2.20	0.08	2.19	0.07	2.39	0.14	2.56	0.09
10	2.08	0.08	2.17	0.04	2.35	0.05	2.50	0.07	2.33	0.06
11	1.71	0.23	2.42	0.44	2.31	0.35	2.56	0.37	2.75	0.31
12	2.09	0.04	2.72	0.16	2.31	0.13	2.76	0.13	2.94	0.13
13	2.22	0.13	2.26	0.19	2.34	0.19	2.08	0.19	1.98	0.10
14	2.92	0.20	3.14	0.17	3.92	0.35	5.25	1.13	3.23	0.34
15	2.06	0.20	2.49	0.26	2.53	0.23	2.92	0.25	2.67	0.29
16	1.91	0.08	2.62	0.09	2.83	0.11	3.18	0.13	3.33	0.10
18	2.45	0.10	3.42	0.22	4.14	0.14	4.68	0.16	4.77	0.16
24	2.30	0.24	3.80	0.10	4.58	0.16	4.91	0.34	5.83	0.28
25	2.52	0.28	3.88	0.10	4.59	0.35	5.39	0.19	5.18	0.36
26	2.77	0.09	3.81	0.23	4.26	0.21	5.23	0.11	5.34	0.18
28	3.00	0.34	4.28	0.26	4.83	0.29	5.40	0.24	5.81	0.22
30	2.48	0.12	3.84	0.11	5.11	0.11	5.41	0.11	5.88	0.15
32	2.55	0.39	3.97	0.35	5.80	0.34	6.48	0.88	6.40	0.43
33	2.93	0.11	4.61	0.08	6.16	0.19	6.72	0.09	6.89	0.15
34	2.49	0.18	4.83	0.15	6.12	0.30	7.36	0.46	7.48	0.36
35	2.50	0.14	3.60	0.08	4.37	0.07	4.88	0.11	5.05	0.08
36	2.84	0.15	4.54	0.12	5.75	0.08	6.54	0.08	6.70	0.06
39	3.18	0.19	5.03	0.04	6.24	0.12	7.02	0.16	7.37	0.13
41	3.04	0.08	4.56	0.12	6.15	0.16	6.79	0.28	7.36	0.12
42	2.95	0.36	4.02	0.22	6.18	0.13	7.31	0.34	6.99	0.31
43	2.60	0.06	4.37	0.11	5.62	0.04	6.58	0.20	6.91	0.12
44	2.41	0.22	3.86	0.35	4.48	0.48	5.69	0.50	5.41	0.26
45	1.98	0.07	3.36	0.22	4.29	0.02	4.73	0.16	4.76	0.15
47	3.10	0.50	3.94	0.37	5.21	0.48	5.58	0.57	6.23	0.48
48	2.39	0.21	4.04	0.15	5.23	0.08	6.27	0.16	6.52	0.36
49	2.69	0.10	4.32	0.15	5.52	0.14	6.16	0.09	6.56	0.12
50	2.59	0.20	4.06	0.22	5.39	0.12	6.47	0.13	6.66	0.09
51	2.90	0.42	4.52	0.21	6.37	0.29	6.56	0.45	6.38	0.39
53	2.61	0.17	3.90	0.32	5.35	0.23	5.66	0.28	5.76	0.29
54	2.35	0.09	3.51	0.13	4.23	0.10	4.84	0.13	4.96	0.11
56	2.33	0.16	3.78	0.11	3.75	0.09	4.40	0.08	4.77	0.11
61	2.65	0.07	3.79	0.12	5.02	0.11	5.49	0.10	5.90	0.13
62	3.00	0.16	4.20	0.18	6.09	0.13	6.66	0.22	7.06	0.09

Residue Number	$R_{1\rho}$ (Hz)									
	HS1		HS2		HS4		HS6		HS8	
	value	error	value	error	value	error	value	error	value	error
63	2.70	0.07	4.42	0.22	5.72	0.17	6.32	0.14	7.00	0.18
64	2.74	0.33	4.59	0.14	6.04	0.30	6.33	0.27	6.81	0.11
65	3.06	0.29	4.45	0.10	5.82	0.13	6.47	0.24	7.10	0.15
66	3.41	0.20	4.92	0.78	5.42	0.45	6.39	0.77	6.66	0.45
67	3.06	0.10	4.39	0.29	5.99	0.21	6.79	0.16	6.73	0.25
68	3.25	0.33	4.38	0.30	5.46	0.12	6.11	0.34	6.49	0.41
69	2.80	0.09	4.30	0.09	5.64	0.09	6.34	0.05	6.55	0.17
70	3.27	0.14	4.86	0.18	6.27	0.55	6.31	0.86	6.69	0.28
71	2.63	0.11	4.14	0.11	5.32	0.08	6.05	0.09	6.28	0.07
72	2.94	0.08	4.15	0.11	5.39	0.07	5.82	0.18	6.44	0.13
73	2.90	0.25	4.40	0.15	5.88	0.20	6.43	0.18	6.58	0.11
74	2.92	0.09	4.14	0.12	5.59	0.14	6.13	0.17	6.56	0.19
75	2.98	0.09	4.26	0.26	5.87	0.14	6.53	0.19	6.54	0.09
77	2.92	0.14	4.58	0.07	5.84	0.03	6.85	0.21	6.88	0.10
80	2.61	0.52	3.89	0.62	4.95	0.43	4.46	0.51	5.76	0.13
82	3.06	0.46	4.88	0.33	7.00	0.32	7.16	0.47	8.04	0.20
88	3.26	0.24	4.63	0.17	6.16	0.11	7.16	0.28	7.70	0.40
89	2.58	0.17	4.83	0.12	6.52	0.15	7.44	0.13	8.00	0.09
90	3.29	0.27	4.80	0.27	6.27	0.30	7.10	0.22	7.06	0.52
91	2.85	0.22	4.95	0.21	5.91	0.40	6.58	0.30	7.49	0.36
94	2.94	0.06	3.95	0.10	5.07	0.11	5.60	0.11	6.14	0.08
95	2.03	0.21	2.84	0.21	3.08	0.25	3.29	0.33	3.56	0.06
97	2.92	0.20	4.37	0.07	5.34	0.07	5.77	0.10	5.69	0.21
98	2.51	0.12	3.41	0.07	3.92	0.11	4.22	0.14	4.76	0.11
99	2.30	0.18	3.27	0.23	3.54	0.34	4.18	0.29	4.26	0.27
101	2.21	0.07	2.53	0.08	3.14	0.10	3.26	0.16	3.50	0.17
104	1.38	0.05	1.63	0.07	1.75	0.03	1.88	0.07	1.88	0.03
105	0.81	0.05	0.97	0.05	1.02	0.04	1.10	0.05	1.08	0.04

Table A.8: $R_{2\rho}$ relaxation rates measured using HSn pulses (n=1,2,4,6,8) from HARD experiment for TRBP2-dsRBD1 at 600 MHz NMR spectrometer

Residue Number	$R_{2\rho}$ (Hz)									
	HS1		HS2		HS4		HS6		HS8	
	value	error	value	error	value	error	value	error	value	error
1	5.94	0.50	4.58	0.51	4.22	0.41	4.37	0.85	3.50	0.26
2	4.16	0.17	4.15	0.25	4.04	0.27	3.12	0.27	2.93	0.17
3	3.52	0.11	3.62	0.19	3.49	0.25	2.66	0.12	2.88	0.02
5	3.08	0.19	3.16	0.33	3.25	0.38	2.28	0.09	2.55	0.06
7	5.08	0.14	4.83	0.13	4.48	0.09	3.71	0.16	3.69	0.29
8	6.70	0.39	6.78	0.48	6.43	0.55	5.03	0.09	5.44	0.17
9	6.31	0.24	6.19	0.17	5.85	0.29	4.46	0.38	4.65	0.33
10	5.46	0.17	5.29	0.20	4.83	0.25	3.93	0.23	3.93	0.10
11	7.51	0.43	7.93	0.74	7.22	0.85	5.12	0.52	5.41	0.78
12	6.78	0.42	7.00	0.64	6.14	0.62	5.13	0.23	5.40	0.13
13	7.94	0.46	7.71	0.20	6.74	0.45	5.82	1.07	5.51	0.61
14	7.79	0.33	7.88	0.28	7.65	0.98	5.88	0.17	6.19	0.60
15	7.25	0.28	7.54	0.12	6.32	0.94	5.12	0.84	4.59	0.90
16	5.94	0.44	5.86	0.51	5.78	0.63	4.51	0.81	4.78	0.20
18	7.99	0.15	8.13	0.09	7.69	0.54	6.75	0.50	6.78	0.26
24	9.44	0.14	9.31	0.32	9.27	0.27	7.61	0.53	7.99	0.31
25	9.83	0.50	9.35	0.43	10.38	1.31	7.96	0.46	8.25	0.32
26	8.97	0.98	9.30	1.10	9.23	1.08	8.80	1.43	8.09	0.80
28	10.02	0.31	10.01	0.28	9.59	0.49	8.25	0.39	9.18	0.12
30	11.43	0.18	10.47	0.17	10.20	0.62	8.48	0.35	8.92	0.32
32	14.65	1.56	13.33	1.18	11.56	0.68	14.33	2.50	9.98	0.32
33	12.52	0.24	12.15	0.29	11.41	0.57	10.84	1.02	10.29	0.10
34	13.16	0.56	11.99	0.41	10.65	0.63	8.81	0.87	9.40	0.64
35	7.80	0.13	7.53	0.26	7.31	0.26	6.68	0.11	6.77	0.34
36	12.45	0.31	11.75	0.32	11.10	0.32	8.96	0.25	9.73	0.24
39	13.80	0.25	12.89	0.25	11.83	0.20	10.78	0.32	10.69	0.04
41	13.04	0.44	12.84	0.48	11.90	0.69	10.30	0.85	11.01	0.31
42	13.86	0.36	13.49	0.34	11.46	0.91	11.79	0.93	10.63	0.46
43	11.86	0.17	11.23	0.28	10.54	0.18	9.13	0.12	9.43	0.27
44	9.56	0.85	9.67	1.21	9.74	1.52	9.72	2.30	10.21	1.66
45	8.65	0.32	8.34	0.47	8.24	0.73	6.61	0.55	7.42	0.29
47	11.80	0.78	10.61	1.04	10.26	0.63	6.90	1.17	7.66	1.13
48	12.45	0.10	11.69	0.59	10.44	0.44	9.44	0.63	9.93	0.50
49	11.39	0.19	10.84	0.22	10.29	0.39	9.76	0.37	9.27	0.10
50	13.03	0.85	11.97	0.30	10.92	0.47	11.18	0.52	10.44	0.51
51	12.48	0.58	10.90	0.44	10.40	0.46	10.03	1.15	10.89	0.53
53	11.26	0.33	9.76	0.58	9.89	0.28	8.95	0.88	8.89	0.41
54	9.33	0.40	9.02	0.57	8.72	0.95	7.99	0.45	8.47	0.56
56	8.95	0.33	8.93	0.43	8.25	0.45	7.48	0.20	6.96	0.28
61	9.91	0.26	9.48	0.28	9.21	0.40	8.24	0.40	8.03	0.12
62	12.29	0.16	11.72	0.26	10.57	0.32	9.60	0.19	9.92	0.08

Residue Number	$R_{2\rho}$ (Hz)									
	HS1		HS2		HS4		HS6		HS8	
	value	error	value	error	value	error	value	error	value	error
63	12.33	0.26	11.93	0.27	11.00	0.48	9.56	0.44	9.84	0.31
64	12.67	0.36	11.95	0.21	11.11	0.95	8.63	0.28	9.62	0.15
65	11.96	0.29	10.87	0.37	10.64	0.59	9.97	0.33	9.78	0.20
66	11.76	0.59	12.17	0.48	10.74	0.99	9.64	0.54	10.49	0.39
67	12.51	0.30	11.19	0.23	10.94	0.10	9.67	0.82	10.29	0.30
68	11.37	0.44	11.35	0.53	10.48	0.60	9.60	1.06	10.02	0.64
69	12.00	0.37	11.48	0.32	10.95	0.13	9.80	0.42	9.79	0.32
70	15.31	0.65	14.55	0.31	14.43	0.78	12.23	0.54	12.42	0.63
71	10.64	0.04	10.56	0.19	9.68	0.30	9.38	0.46	8.81	0.17
72	10.81	0.16	10.37	0.18	9.58	0.20	8.26	0.12	8.62	0.13
73	11.53	0.23	10.80	0.13	10.10	0.09	9.33	0.25	9.10	0.21
74	12.79	0.09	11.61	0.41	10.61	0.52	9.28	0.82	8.83	0.79
75	12.48	0.36	11.92	0.20	11.45	0.62	9.45	0.46	10.80	0.21
77	13.36	0.31	12.21	0.23	11.59	0.37	10.88	0.37	10.57	0.29
80	12.39	1.60	9.21	0.28	8.74	1.12	7.83	0.63	7.57	0.45
82	16.38	0.96	14.93	0.70	14.30	1.11	11.70	1.02	13.20	0.78
88	13.19	0.28	13.34	0.84	11.96	0.44	11.16	0.53	11.11	0.34
89	13.41	0.27	12.99	0.36	11.97	0.44	11.38	0.23	11.37	0.24
90	6.34	1.75	5.97	1.35	5.63	1.18	2.51	1.63	5.42	1.61
91	14.32	0.94	12.71	0.64	11.37	0.71	8.30	0.80	10.34	2.29
94	10.92	0.26	9.69	0.22	9.36	0.34	8.77	0.29	8.62	0.42
95	5.89	0.38	5.81	0.39	5.26	0.36	3.34	0.53	4.52	0.17
97	10.49	0.27	10.67	0.22	9.54	0.45	8.82	0.25	8.81	0.44
98	8.22	0.29	8.27	0.31	7.65	0.33	6.42	0.43	6.43	0.45
99	9.09	0.60	8.45	0.29	8.57	0.90	7.52	1.09	6.67	0.17
101	5.69	0.42	5.80	0.33	5.75	0.68	4.99	0.45	5.16	0.17
104	2.84	0.16	3.00	0.30	3.10	0.29	2.49	0.26	2.52	0.19
105	1.52	0.12	1.73	0.20	1.91	0.29	1.13	0.16	1.55	0.13

Table A.9: $R_{1\rho}$ relaxation rates measured using HSn pulses (n=1,2,4,6,8) from HARD experiment for dADAR-dsRBD1 at 600 MHz NMR spectrometer

Residue Number	$R_{1\rho}$ (Hz)									
	HS1		HS2		HS4		HS6		HS8	
	value	error	value	error	value	error	value	error	value	error
59	3.13	0.23	4.17	0.32	4.05	0.30	5.13	0.12	5.57	0.46
65	3.61	0.39	6.04	0.33	6.63	0.54	7.74	0.12	8.46	0.59
66	3.40	0.92	6.68	1.18	6.52	0.69	7.46	0.25	9.10	0.96
67	3.81	0.41	5.79	0.32	6.21	0.75	7.84	0.14	8.41	1.11
68	3.91	0.33	6.12	0.52	6.28	0.58	6.64	0.39	8.25	0.96
69	3.81	0.36	6.66	0.76	6.02	0.63	7.80	0.24	8.47	0.78
70	3.87	0.24	6.13	0.41	6.67	0.26	7.69	0.17	8.53	0.41
72	3.46	0.25	6.10	0.39	6.30	0.39	7.14	0.36	7.91	0.31
73	3.33	0.40	5.29	0.48	5.90	0.44	6.86	0.22	7.33	0.66
75	3.74	0.88	3.49	0.83	5.90	0.27	7.51	0.52	8.32	0.47
76	3.04	0.41	5.15	0.27	5.82	0.21	6.64	0.16	7.64	0.42
77	3.20	0.34	5.32	0.47	5.06	0.38	5.78	0.24	7.07	0.52
78	3.38	0.48	5.11	0.33	5.62	0.43	6.48	0.29	7.57	0.53
79	2.26	1.68	3.42	1.29	6.58	1.43	7.17	1.98	7.99	1.69
80	3.54	0.51	4.88	0.40	5.23	0.41	6.98	0.21	7.65	0.78
81	3.74	0.38	5.90	0.67	6.60	0.42	6.74	0.13	8.23	0.56
82	3.59	0.45	5.87	0.35	6.05	0.42	7.06	0.16	8.18	0.60
84	3.33	0.32	5.58	0.39	6.24	0.30	7.06	0.12	8.13	0.49
85	3.05	0.40	4.83	0.30	5.16	0.28	6.26	0.22	7.11	0.71
87	2.48	0.94	0.00	0.00	3.70	0.74	4.27	0.44	4.25	1.11
88	2.47	0.31	3.26	0.21	3.03	0.15	3.59	0.16	3.90	0.41
89	3.40	0.34	4.81	0.41	5.40	0.18	6.12	0.31	6.54	0.54
91	3.18	0.23	4.97	0.22	5.75	0.20	6.95	0.10	7.62	0.60
92	3.45	0.56	6.22	0.53	6.51	0.47	7.27	0.13	8.26	0.53
93	3.34	0.49	5.83	0.10	6.22	0.34	7.11	0.21	7.92	0.69
94	3.37	0.51	6.14	0.47	5.25	0.59	6.71	0.42	8.47	0.88
95	3.75	0.30	6.30	0.51	6.69	0.43	7.37	0.17	8.36	0.47
96	3.95	0.54	6.20	0.70	6.02	0.84	7.72	0.30	8.43	0.52
97	3.48	0.21	5.74	0.47	6.38	0.24	7.29	0.33	7.83	0.46
98	3.60	0.19	6.05	0.53	6.09	0.25	6.76	0.53	7.48	0.55
99	3.71	0.46	5.88	0.32	6.30	0.28	7.25	0.31	8.28	0.62
100	3.23	0.46	5.49	0.30	5.78	0.21	7.07	0.36	8.00	0.74
101	3.45	0.38	5.91	0.28	6.06	0.17	7.33	0.15	8.12	0.59
102	2.11	0.68	0.00	0.00	2.66	0.52	3.67	0.45	3.21	0.82
103	3.94	0.22	6.54	0.98	4.77	0.89	6.01	0.41	7.79	0.63
104	3.83	0.18	6.37	0.67	6.73	0.19	7.59	0.49	8.42	0.19
105	3.19	0.32	5.57	0.55	6.07	0.20	6.87	0.27	7.92	0.49
106	3.48	0.29	5.74	0.39	6.08	0.16	7.13	0.04	7.74	0.41
107	3.69	0.29	6.52	0.70	6.22	0.46	7.61	0.06	8.26	0.51
108	3.42	0.20	5.33	0.59	7.35	0.13	7.80	0.18	8.60	0.61
109	3.58	0.32	5.84	0.18	6.61	0.28	7.77	0.21	8.61	0.49

Residue Number	$R_{1\rho}$ (Hz)									
	HS1		HS2		HS4		HS6		HS8	
	value	error	value	error	value	error	value	error	value	error
112	3.32	0.22	6.18	0.80	7.40	0.47	7.79	0.14	9.11	0.51
113	3.44	0.26	6.64	1.21	5.47	0.65	6.68	0.13	7.46	0.52
114	3.55	0.35	6.27	0.50	6.75	0.25	7.53	0.07	8.72	0.48
115	3.19	0.37	6.31	0.55	7.00	0.31	7.69	0.20	8.97	0.43
116	4.05	0.25	7.04	0.53	7.06	0.42	8.00	0.14	9.08	0.31
117	4.01	0.16	6.35	0.53	7.06	0.36	7.66	0.44	8.85	0.66
119	2.82	0.26	4.60	0.35	3.39	0.35	4.69	0.29	5.21	0.74
120	3.50	0.41	6.40	0.75	5.80	0.68	7.08	0.24	8.45	0.76
121	3.77	0.45	6.57	0.68	6.90	0.65	7.87	0.26	8.93	0.58
122	3.91	0.24	7.39	0.58	6.61	0.44	8.01	0.17	8.51	0.36
123	3.74	0.42	6.21	0.67	6.45	0.46	6.96	0.25	8.48	0.66
124	3.67	0.30	6.05	0.51	5.97	0.31	7.39	0.20	7.97	0.50
125	3.83	0.32	6.31	0.42	5.94	0.51	7.66	0.12	8.67	0.78
126	3.62	0.58	5.50	0.48	5.79	0.48	6.44	0.10	7.38	0.26
129	3.51	0.41	4.49	0.28	4.06	0.34	5.21	0.24	6.01	0.74
131	2.61	0.46	2.71	0.37	2.87	0.28	3.65	0.19	4.19	0.69
132	2.30	0.50	2.07	0.52	3.12	0.14	3.67	0.21	3.62	0.41
133	1.96	0.41	2.25	0.35	2.56	0.21	3.23	0.21	3.36	0.46
134	2.39	0.53	2.70	0.25	2.59	0.20	3.54	0.37	3.67	0.67
135	2.26	0.56	1.63	0.71	2.43	0.17	3.47	0.29	3.44	0.69
137	1.99	0.57	1.99	0.33	1.72	0.19	2.44	0.20	2.60	0.67
140	1.06	0.31	0.91	0.34	0.69	0.12	1.34	0.18	1.39	0.43

Table A.10: $R_{2\rho}$ relaxation rates measured using HSn pulses (n=1,2,4,6,8) from HARD experiment for dADAR-dsRBD1 at 600 MHz NMR spectrometer

Residue Number	$R_{2\rho}$ (Hz)									
	HS1		HS2		HS4		HS6		HS8	
	value	error	value	error	value	error	value	error	value	error
59	16.87	0.52	15.03	0.23	13.22	0.35	12.93	0.17	11.31	0.30
65	24.43	0.42	21.20	0.18	18.68	0.25	18.17	0.32	17.23	0.18
66	14.82	0.34	13.03	0.16	11.47	0.52	12.63	0.92	10.66	0.32
67	15.73	0.42	14.66	0.20	13.09	0.23	12.93	0.42	12.25	0.32
68	14.27	0.79	14.75	0.23	12.71	0.46	14.15	1.18	11.66	0.43
69	15.49	0.54	14.01	0.40	13.11	0.90	14.69	0.94	13.30	0.91
70	15.50	0.11	14.21	0.16	12.97	0.11	13.49	0.30	11.64	0.09
72	15.57	0.31	14.61	0.40	14.01	0.15	12.91	0.39	12.11	0.41
73	13.20	0.09	11.90	0.24	11.26	0.26	11.51	0.45	10.58	0.32
75	13.69	0.56	12.95	0.80	11.93	0.40	10.86	0.44	11.26	0.11
76	13.19	0.13	11.76	0.09	10.84	0.18	10.92	0.16	9.96	0.13
77	13.60	0.31	12.32	0.22	11.35	0.08	11.10	0.45	9.90	0.18
78	13.67	0.09	12.39	0.18	11.81	0.26	11.65	0.32	10.26	0.16
79	12.85	1.49	13.15	2.06	12.07	1.34	11.81	1.73	10.70	1.58
80	13.75	0.45	12.63	0.10	11.75	0.20	11.44	0.21	10.37	0.23
81	15.40	0.78	14.47	0.26	13.57	0.17	14.14	0.31	12.24	0.25
82	15.23	0.13	14.03	0.13	13.37	0.28	12.95	0.30	11.71	0.13
84	14.48	0.18	13.18	0.19	12.13	0.15	12.09	0.41	11.34	0.08
85	13.28	0.14	11.68	0.18	10.96	0.10	10.99	0.26	10.36	0.31
87	7.61	0.35	7.23	0.42	6.94	0.38	4.38	0.95	7.68	0.97
88	6.50	0.07	5.92	0.10	5.48	0.10	5.56	0.07	4.88	0.11
89	12.09	0.22	11.08	0.15	10.39	0.20	10.34	0.14	9.04	0.49
91	12.65	0.11	11.82	0.15	11.02	0.19	10.96	0.43	10.37	0.26
92	18.55	0.14	17.22	0.29	15.43	0.44	15.91	0.36	14.47	0.26
93	14.36	0.13	13.12	0.24	11.91	0.16	12.47	0.32	10.78	0.29
94	15.57	0.61	13.27	0.45	12.79	0.44	13.52	0.72	11.96	0.18
95	14.80	0.31	13.60	0.14	12.23	0.12	12.47	0.33	11.54	0.14
96	15.10	0.44	14.11	0.55	12.76	0.45	13.26	0.54	12.18	0.36
97	15.33	0.12	14.00	0.25	12.98	0.14	13.07	0.31	11.95	0.26
98	15.41	0.31	14.42	0.46	13.02	0.44	13.14	0.32	11.97	0.18
99	15.14	0.12	13.79	0.07	13.08	0.21	12.95	0.15	12.08	0.12
100	13.64	0.17	12.85	0.19	12.30	0.09	12.02	0.20	11.34	0.25
101	13.92	0.11	12.62	0.13	11.73	0.19	11.72	0.31	10.79	0.10
102	5.32	0.28	5.06	0.13	4.87	0.10	2.75	0.94	4.87	0.25
103	22.72	0.54	20.78	0.40	18.20	0.13	18.09	0.60	15.79	0.11
104	14.88	0.47	13.76	0.21	12.67	0.29	12.70	0.35	10.52	0.20
105	14.97	0.25	13.50	0.22	12.62	0.23	13.05	0.39	11.42	0.09
106	14.85	0.09	13.58	0.13	12.61	0.23	12.73	0.49	11.41	0.09
107	16.30	0.12	15.18	0.24	14.05	0.30	13.98	0.38	12.53	0.15
108	15.83	0.17	14.84	0.11	13.49	0.44	12.82	0.47	12.89	0.10
109	15.43	0.14	14.08	0.09	13.36	0.07	12.99	0.15	12.01	0.14

Residue Number	$R_{2\rho}$ (Hz)									
	HS1		HS2		HS4		HS6		HS8	
	value	error	value	error	value	error	value	error	value	error
112	16.19	0.40	14.49	0.29	14.02	0.25	14.14	0.44	12.09	0.37
113	14.17	0.15	12.85	0.23	12.06	0.26	12.45	0.34	11.05	0.31
114	15.88	0.25	14.56	0.08	13.38	0.11	13.82	0.58	12.05	0.16
115	15.76	0.17	14.60	0.26	13.80	0.28	13.87	0.34	11.94	0.10
116	17.23	0.25	16.00	0.13	14.26	0.18	14.68	0.70	13.31	0.14
117	16.57	0.80	14.89	0.55	13.86	0.28	13.43	0.37	12.06	0.34
119	7.87	0.31	7.36	0.02	7.31	0.21	7.59	0.37	7.07	0.20
120	19.34	0.55	17.91	0.43	15.76	0.47	17.09	1.31	14.89	0.59
121	16.11	0.34	14.73	0.31	13.75	0.47	13.40	0.58	12.73	0.31
122	19.67	0.29	16.85	0.27	15.89	0.34	15.58	0.47	13.91	0.30
123	16.27	0.07	14.40	0.61	13.80	0.18	14.29	0.62	12.27	0.16
124	15.87	0.17	14.35	0.26	13.00	0.21	13.49	0.44	11.81	0.13
125	18.32	0.18	16.41	0.25	14.86	0.17	15.17	0.22	13.07	0.20
126	14.87	0.14	13.87	0.31	12.44	0.05	13.05	0.32	10.77	0.28
129	14.41	0.09	12.70	0.09	11.52	0.15	11.94	0.38	9.98	0.13
131	14.41	0.06	12.88	0.21	11.40	0.16	10.70	0.13	9.87	0.11
132	5.83	0.17	5.12	0.10	5.27	0.20	4.43	0.30	4.67	0.13
133	5.37	0.16	5.06	0.15	4.80	0.08	4.71	0.07	4.53	0.12
134	11.92	0.06	11.07	0.17	9.73	0.19	9.08	0.17	8.40	0.07
135	5.62	0.06	5.12	0.14	4.78	0.11	4.20	0.29	4.55	0.09
137	5.41	0.14	4.88	0.08	4.59	0.12	4.46	0.15	3.89	0.12
140	1.68	0.07	1.62	0.06	1.73	0.09	1.67	0.10	1.58	0.05

Table A.11: Dynamics parameters extracted from HARD experimental data from geoHARD method for TRBP2-dsRBD1

Residue Number	k_{ex} (s⁻¹)		Δω (Hz)		p_A	
	value	error	value	error	value	error
1	29861	318	189	81	75.9	11.9
2	434	136	943	222	99.7	0.2
3	271	118	298	262	98.9	1.3
5	166	21	432	401	94.8	9.1
7	153	16	711	391	99.2	0.1
8	228	66	978	39	99.2	0.3
9	134	15	937	292	98.3	0.3
10	29455	294	210	44	85.9	9.0
11	375	36	773	263	99.0	0.1
12	368	128	906	212	99.4	0.3
13	17971	342	290	230	82.0	13.8
14	43266	609	348	201	84.5	10.6
15	352	159	366	295	98.3	1.2
16	163	24	175	191	98.9	0.8
18	112	9	660	174	99.1	0.1
24	240	64	512	407	99.4	0.2
25	61477	2320	552	298	88.6	12.4
26	77732	60493	455	98	81.8	13.0
28	141	17	730	30	99.1	0.2
30	316	106	116	43	96.4	3.4
32	835	155	34	3	61.8	7.2
33	178	43	835	253	99.3	0.2
34	654	123	36	6	75.4	9.4
35	93748	4826	328	84	76.0	10.9
36	63624	3927	345	261	73.8	13.6
39	387	165	540	351	99.4	0.5
41	172	19	638	287	99.5	0.1
42	214	44	297	108	98.6	0.7
43	178	38	264	135	99.0	0.6
44	733	354	5	2	94.7	3.2
45	583	154	235	394	86.2	14.9
47	169	24	802	126	98.9	0.4
48	1375	946	357	322	94.3	6.0
49	210	65	454	285	99.3	0.3
50	153	16	823	192	99.0	0.2
51	38572	30538	612	323	83.8	15.1
53	222	48	126	36	98.3	1.3
54	71920	2655	305	86	77.0	13.1
56	327	99	891	240	99.4	0.3
61	56783	3024	266	72	75.7	12.0
62	171	35	434	278	99.2	0.5
63	166	36	507	167	99.3	0.2

Residue Number	k_{ex} (s^{-1})		$\Delta\omega$ (Hz)		p_A	
	value	error	value	error	value	error
64	61490	2347	419	215	81.5	10.5
65	137	12	773	237	99.3	0.1
66	46110	1190	314	56	76.6	11.3
67	73723	3105	525	205	88.6	8.3
68	60054	2401	470	265	82.2	12.4
69	225	57	826	19	99.2	0.3
70	216	43	1107	167	98.8	0.4
71	231	85	502	233	99.5	0.3
72	220	61	454	314	99.6	0.3
73	21686	16498	857	263	98.5	1.7
74	237	98	389	328	94.1	7.9
75	145	20	765	257	99.1	0.2
77	410	184	836	258	99.5	0.3
80	372	121	114	101	89.9	9.5
82	70229	1927	398	134	74.9	12.8
88	149	30	634	180	99.2	0.3
89	247	45	78	35	95.7	2.9
90	3651	2985	234	413	95.4	5.4
91	386	120	56	38	80.9	14.4
94	8721	576	62	39	76.0	13.3
95	13739	18332	375	454	89.9	10.5
97	173	23	714	422	99.5	0.2
98	235	99	687	245	99.2	0.3
99	274	93	184	49	98.5	0.8
101	323	116	126	188	90.0	9.0
104	39519	30481	139	370	86.2	14.0
105	298	84	122	248	85.5	10.8

Table A.12: Dynamics parameters extracted from HARD experimental data from geo HARD method for dADAR-dsRBD1

Residue Number	k_{ex} (s^{-1})		$\Delta\omega$ (Hz)		p_A	
	value	error	value	error	value	error
59	21247	1	647	355	90.5	10.2
65	24407	5	608	340	88.6	10.0
66	89667	9	374	79	70.8	9.8
67	52735	5	553	304	84.0	12.2
68	54873	1	564	264	84.2	12.8
69	119	0	653	29	98.8	0.1
70	62783	3	572	272	83.0	12.4
72	195	0	692	401	98.8	0.3
73	179	0	705	337	99.5	0.1
75	181	0	511	162	99.1	0.2
76	59950	6	403	210	81.2	9.4
77	42845	1	429	195	82.4	12.3
78	44850	7	445	216	84.5	13.1
80	39052	4	606	346	85.7	16.1
81	2329	6	1051	57	98.8	0.3
82	29061	39	477	298	82.6	14.6
84	57533	3	541	287	81.4	14.8
85	343	0	643	339	99.1	0.5
89	61114	5	446	241	78.4	13.8
91	71271	6	406	105	80.9	10.2
92	248	0	349	260	97.5	1.3
93	66127	3	444	135	81.9	9.5
94	378	0	825	322	99.2	0.3
95	77920	3	461	150	73.9	14.6
96	59039	5	581	323	79.7	16.0
97	3299	8	577	253	97.5	2.6
98	40459	7	569	239	89.4	11.2
99	306	0	757	348	99.3	0.3
100	182	0	960	359	99.2	0.2
101	71491	5	482	269	79.5	12.3
103	21325	2	775	416	88.6	13.0
104	132518	7	556	112	78.2	10.0
105	319	0	450	417	98.7	0.6
106	46020	4	606	328	86.1	13.4
107	44315	3	523	243	88.4	8.1
108	229	0	720	315	99.1	0.4
109	422	1	693	423	99.2	0.3
112	169	0	210	30	98.7	0.4
113	189	0	691	342	99.1	0.3
114	49029	6	503	298	78.5	15.7
115	59525	5	498	259	81.3	10.6
116	57321	3	597	256	85.0	12.1

Residue Number	k_{ex} (s^{-1})		$\Delta\omega$ (Hz)		p_A	
	value	error	value	error	value	error
117	67330	4	530	178	83.3	10.8
119	206	0	762	264	99.6	0.1
120	497	0	624	281	98.7	0.7
121	62372	3	467	156	78.4	13.8
122	40264	3	432	261	77.1	11.9
123	43880	3	678	400	85.0	14.4
124	44193	3	524	285	86.8	8.2
125	36593	2	596	270	90.3	6.9
126	36698	9	469	218	88.1	7.2
129	26751	2	646	297	92.3	12.2
131	286	0	99	8	86.8	6.8
132	207	0	96	139	91.8	6.9
133	353	0	388	299	99.5	0.4
134	395	0	120	35	90.5	7.5
135	229	0	49	33	82.7	8.9
137	189	0	73	21	88.0	9.3
140	222	0	392	356	99.4	0.4

Table A.13: Thermodynamic parameters calculated for dsRBD-dsRNA interaction calculated from fitting of Isothermal Titration Calorimetry data to one-set of sites binding model

RNA sequences	TRBP2-dsRBD1	dADAR-dsRBD1
k_d (µM)		
miR-16-1	0.89 ± 0.21	0.27 ± 0.05
miR-16-1-D	0.50 ± 0.04	0.43 ± 0.10
miR-16-1-M	2.12 ± 0.22	0.78 ± 0.24
miR-16-1-B	0.69 ± 0.13	0.27 ± 0.07
D10-RNA	2.21 ± 0.51	0.21 ± 0.10
Number of Binding sites		
miR-16-1	3.9 ± 0.1	4.3 ± 0.1
miR-16-1-D	5.2 ± 0.1	4.4 ± 0.1
miR-16-1-M	1.5 ± 0.0	1.6 ± 0.1
miR-16-1-B	3.0 ± 0.1	3.6 ± 0.1
D10-RNA	2.5 ± 0.1	2.4 ± 0.1
ΔH (kcal.mol^{-1})		
miR-16-1	-20.6 ± 1.1	-69.0 ± 1.8
miR-16-1-D	-34.8 ± 0.6	-80.9 ± 3.2
miR-16-1-M	-9.4 ± 0.2	-24.6 ± 1.1
miR-16-1-B	-19.8 ± 0.7	-61.8 ± 2.0
D10-RNA	-20.9±1.6	-44.0 ± 2.2
$T\Delta S$ (kcal.mol^{-1})		
miR-16-1	-12.4 ± 1.0	-59.9 ± 1.8
miR-16-1-D	-26.2 ± 0.6	-72.1 ± 3.1
miR-16-1-M	-1.6 ± 0.2	-16.3 ± 0.9
miR-16-1-B	-11.4 ± 0.6	-52.8 ± 1.9
D10-RNA	-13.2 ± 1.4	-34.9 ± 2.0

Table A.14: Nuclear spin relaxation data for TRBP2-dsRBD1 recorded at 950 MHz

Residue Number	950 MHz					
	R_1 (Hz)		R_2 (Hz)		NOE	
	Value	Error	Value	Error	Value	Error
1	1.09	0.12	1.46	0.71	-0.43	0.02
2	1.31	0.14	2.22	0.70	0.07	0.02
3	1.51	0.11	2.18	0.63	0.27	0.02
5	1.47	0.06	2.45	0.31	0.23	0.02
8	1.37	0.14	2.38	0.78	0.25	0.02
9	1.36	0.15	2.27	0.81	0.26	0.02
10	1.42	0.14	2.24	0.75	0.28	0.02
11	1.46	0.13	2.83	0.79	0.22	0.02
12	1.47	0.12	2.73	0.79	0.24	0.02
13	1.35	0.15	2.53	0.87	0.24	0.02
14	1.32	0.14	3.03	0.81	0.28	0.02
15	1.39	0.13	2.91	0.91	0.26	0.02
16	1.33	0.04	5.03	0.48	0.41	0.02
18	1.39	0.08	7.33	0.64	0.66	0.02
24	1.20	0.05	9.52	0.25	0.65	0.02
25	1.24	0.05	11.13	0.38	0.63	0.02
26	1.19	0.06	8.39	0.59	0.58	0.02
28	1.22	0.08	9.57	0.86	0.65	0.02
30	1.13	0.06	10.13	0.60	0.63	0.02
33	1.12	0.06	12.68	0.55	0.85	0.02
34	1.07	0.04	14.80	0.93	0.86	0.02
35	1.35	0.04	9.61	0.38	0.69	0.02
36	1.12	0.05	11.89	0.50	0.82	0.02
39	1.13	0.03	12.70	0.70	0.92	0.02
40	1.14	0.05	13.08	0.48	0.84	0.02
41	1.05	0.02	13.08	0.31	0.76	0.02
42	1.05	0.02	14.85	0.48	0.80	0.02
43	1.16	0.02	11.98	0.50	0.82	0.02
44	1.23	0.03	9.62	0.21	0.72	0.02
45	1.00	0.04	8.33	0.37	0.55	0.02
47	1.03	0.04	13.02	0.44	0.78	0.02
48	1.02	0.04	12.20	0.55	0.84	0.02
49	0.95	0.04	11.16	0.48	0.79	0.02
50	1.01	0.04	13.38	0.50	0.77	0.02
51	1.09	0.04	13.20	0.54	0.84	0.02
53	1.09	0.06	10.04	0.44	0.57	0.02
54	1.19	0.06	7.58	0.41	0.53	0.02
56	1.22	0.11	6.12	0.81	0.50	0.02
61	1.11	0.03	10.13	0.39	0.65	0.02
62	1.08	0.04	11.87	0.38	0.76	0.02
63	0.90	0.03	11.15	2.20	0.76	0.02
64	1.04	0.02	13.53	0.39	0.70	0.02

Residue Number	950 MHz					
	R_1 (Hz)		R_2 (Hz)		NOE	
	Value	Error	Value	Error	Value	Error
65	1.06	0.03	12.21	3.14	0.68	0.02
66	1.08	0.05	15.33	0.60	0.87	0.02
67	1.05	0.04	11.83	0.40	0.83	0.02
68	1.02	0.03	12.61	0.38	0.76	0.02
69	1.09	0.06	12.11	0.44	0.75	0.02
70	1.01	0.10	12.96	1.01	0.75	0.02
71	1.08	0.07	11.49	0.64	0.79	0.02
72	1.11	0.05	10.47	0.55	0.76	0.02
73	1.15	0.06	10.87	0.49	0.79	0.02
74	1.08	0.04	9.95	0.41	0.75	0.02
75	1.10	0.04	11.59	0.64	0.79	0.02
77	1.06	0.04	13.06	0.37	0.80	0.02
80	1.37	0.07	10.45	0.69	0.62	0.02
82	1.04	0.05	14.23	0.47	0.89	0.02
88	1.00	0.03	14.67	0.21	0.88	0.02
89	0.92	0.03	14.51	0.28	0.84	0.02
90	1.10	0.04	11.56	0.46	0.89	0.02
91	1.13	0.03	14.83	0.32	0.73	0.02
92	1.04	0.03	13.76	0.39	0.86	0.02
94	1.30	0.07	9.18	0.56	0.65	0.02
95	1.37	0.06	4.41	0.59	0.53	0.02
97	1.23	0.09	10.64	0.68	0.67	0.02
98	1.50	0.12	7.51	0.77	0.61	0.02
99	1.44	0.14	5.57	0.85	0.56	0.02
101	1.51	0.05	4.83	0.36	0.48	0.02
104	1.29	0.04	4.23	0.35	0.20	0.02
105	0.96	0.02	2.38	0.05	-0.47	0.02

Table A.15: Nuclear spin relaxation data for TRBP2-dsRBD1 in presence of miR-16-1 duplex recorded at 950 MHz

Residue Number	950 MHz					
	R_1 (Hz)		R_2 (Hz)		NOE	
	Value	Error	Value	Error	Value	Error
1	2.65	0.46	3.99	0.56		
2	2.97	0.52	4.50	0.55	-0.02	0.08
3	2.89	0.50	4.47	0.43	0.26	0.08
5	2.72	0.45	3.77	0.37	0.30	0.08
8	3.16	0.59	5.14	0.58	0.29	0.08
9	3.39	0.59	5.48	0.66	0.18	0.08
10	3.33	0.54	5.35	0.54	0.30	0.08
11	3.54	0.66	5.33	0.61	0.36	0.08
12	3.49	0.63	5.98	0.70	0.33	0.08
13	2.93	0.48	5.58	0.44	0.30	0.08
14	3.47	0.62	6.20	0.75	0.40	0.08
15	3.33	0.59	6.35	0.65	0.42	0.08
16	2.18	0.27	8.10	0.61	0.61	0.08
18	2.44	0.51	14.46	2.30	0.63	0.08
24	1.73	0.35				
25	1.52	0.50				
26	1.86	0.21			0.83	0.08
28					0.64	0.08
35	1.85	0.44	11.56	1.40	0.83	0.08
41	1.16	0.19				
43	1.44	0.30			0.89	0.08
44	1.47	0.33				
54					0.42	0.08
69	1.24	0.25				
71	1.51	0.26			0.85	0.08
72	1.61	0.26	11.51	1.88	0.69	0.08
74	1.10	0.15			0.54	0.08
77					0.90	0.08
94	1.93	0.31			0.67	0.08
97	1.94	0.37				
98	2.64	0.39	12.54	1.09	0.68	0.08
99	3.03	0.54			0.70	0.08
101	2.46	0.35	7.64	0.82	0.38	0.08
104	2.39	0.41	4.29	0.37	0.23	0.08
105	1.59	0.27	1.68	0.37	-1.10	0.08

Table A.16: Nuclear spin relaxation data for TRBP2-dsRBD1 in presence of miR-16-1-D duplex recorded at 950 MHz

Residue Number	950 MHz					
	R_1 (Hz)		R_2 (Hz)		NOE	
	Value	Error	Value	Value	Error	Value
1	2.47	0.39	3.92	0.46	-0.63	0.07
2	2.74	0.45	4.27	0.47	0.01	0.07
3	2.72	0.42	4.26	0.38	0.30	0.07
5	2.61	0.38	3.66	0.29	0.32	0.07
8	2.89	0.44	4.78	0.49	0.34	0.07
9	2.96	0.47	5.01	0.45	0.29	0.07
10	3.16	0.46	5.19	0.51	0.36	0.07
11	2.97	0.46	5.48	0.53	0.29	0.07
12	2.93	0.43	5.45	0.44	0.26	0.07
13	3.02	0.43	5.51	0.42	0.33	0.07
14	2.98	0.48	6.20	0.54	0.36	0.07
15	2.98	0.51	6.40	0.52	0.41	0.07
16	2.37	0.36	9.44	0.65	0.52	0.07
18	2.13	0.43			0.44	0.07
24	2.04	0.32				
25	1.87	0.48				
26	2.32	0.37			0.93	0.07
28	2.45	0.47			0.18	0.07
35	1.88	0.41			0.91	0.07
41	2.32	0.45				
43	1.53	0.36				
44	1.15	0.49				
45	1.76	0.41			0.30	0.07
54	2.63	0.32	5.29	1.47	0.62	0.07
56	2.04	0.34				
69	1.42	0.23			0.65	0.07
70	1.44	0.45				
71	1.83	0.41				
72	1.53	0.34	5.71	3.76	0.89	0.07
73	1.63	0.42			0.34	0.07
74	2.32	0.54				
77	1.57	0.48				
94					0.70	0.07
95	2.88	0.45	6.87	0.82	0.24	0.07
97	1.92	0.41			0.72	0.07
98	2.83	0.48	15.03	1.30	0.82	0.07
99	2.76	0.48	12.17	0.79	0.67	0.07
101	2.85	0.40	6.86	2.64	0.51	0.07
104	2.28	0.36	4.16	0.22	0.30	0.07
105	1.50	0.30	1.76	0.24	-1.08	0.07

Table A.17: Nuclear spin relaxation data for TRBP2-dsRBD1 in presence of miR-16-1-M duplex recorded at 950 MHz

Residue Number	950 MHz					
	R_1 (Hz)		R_2 (Hz)		NOE	
	Value	Error	Value	Value	Error	Value
1	2.60	0.40	2.43	0.49		
2	2.76	0.41	2.79	0.37	-0.04	0.10
3	2.73	0.43	2.83	0.27	0.29	0.10
5	2.60	0.40	2.70	0.22	0.33	0.10
8	3.04	0.47	3.36	0.39	0.36	0.10
9	3.00	0.48	3.06	0.40	0.35	0.10
10	3.36	0.53	3.43	0.47	0.46	0.10
11	3.06	0.49	3.67	0.45	0.36	0.10
12	3.18	0.53	4.34	0.36	0.41	0.10
13	3.21	0.50	3.88	0.53	0.49	0.10
14	3.10	0.48	4.47	0.68	0.18	0.10
15	3.25	0.46	4.15	0.61	0.40	0.10
16	2.45	0.39	6.15	0.62	0.46	0.10
18	2.49	0.44	10.87	1.61	0.75	0.10
24	2.04	0.26			0.72	0.10
25	2.30	0.29			0.82	0.10
26	2.51	0.47	12.68	1.76	0.63	0.10
28	2.58	0.46			0.65	0.10
30	2.07	0.32			0.72	0.10
33	2.19	0.36			0.68	0.10
35	2.09	0.35	10.87	1.22	0.75	0.10
39	1.28	0.33				
41	1.84	0.33			0.90	0.10
42	1.24	0.27				
43	1.87	0.31	15.74	2.86	0.76	0.10
44	1.94	0.34	11.05	1.87	0.73	0.10
45	1.63	0.29	11.15	1.42	0.98	0.10
48	1.23	0.27			0.87	0.10
49	0.86	0.21				
50	1.85	0.34			0.50	0.10
53	1.98	0.36				
54	1.98	0.39	8.57	0.64	0.27	0.10
56	2.59	0.46	11.75	1.63	0.79	0.10
61	1.77	0.35			0.91	0.10
63	1.36	0.26			0.83	0.10
64	1.97	0.31			0.90	0.10
65	1.82	0.28			0.83	0.10
68	1.70	0.31			0.38	0.10
69	1.61	0.29			0.82	0.10
70	2.28	0.40			0.55	0.10
71	1.71	0.28	16.65	1.82	0.97	0.10

| Residue Number | 950 MHz | | | | | |
| | R_1 (Hz) | | R_2 (Hz) | | NOE | |
	Value	Error	Value	Value	Error	Value
72	1.89	0.33	14.88	2.29	0.91	0.10
73	2.00	0.29			0.97	0.10
74	1.71	0.28				
75	2.10	0.35				
77	1.84	0.33				
82					0.61	0.10
89	1.72	0.35				
94	2.37	0.35			0.79	0.10
95	1.67	0.26	4.65	0.95		
97	2.25	0.37	12.14	1.95	0.75	0.10
98	3.19	0.51	9.29	0.71	0.66	0.10
99	3.01	0.48	7.45	0.75	0.76	0.10
101	2.86	0.46	5.94	0.47	0.57	0.10
104	2.34	0.37	3.26	0.22	0.29	0.10
105	1.54	0.29	1.39	0.34	-1.34	0.10

Table A.18: Nuclear spin relaxation data for TRBP2-dsRBD1 in presence of miR-16-1-B duplex recorded at 950 MHz

Residue Number	950 MHz					
	R_1 (Hz)		R_2 (Hz)		NOE	
	Value	Error	Value	Value	Error	Value
1	2.38	0.38	4.09	0.38	-0.17	0.06
2	2.67	0.41	4.43	0.42	-0.01	0.06
3	2.69	0.41	4.32	0.34	0.33	0.06
5	2.52	0.35	3.84	0.27	0.30	0.06
8	2.91	0.45	4.93	0.49	0.33	0.06
9	2.84	0.46	5.19	0.46	0.27	0.06
10	3.10	0.45	5.44	0.47	0.37	0.06
11	2.90	0.45	5.36	0.56	0.32	0.06
12	2.92	0.46	6.06	0.50	0.34	0.06
13	3.01	0.46	6.04	0.50	0.40	0.06
14	3.03	0.48	6.24	0.61	0.38	0.06
15	2.75	0.44	6.65	0.57	0.36	0.06
16	2.33	0.34	9.91	0.82	0.62	0.06
18	2.17	0.41			0.96	0.06
24	1.72	0.27				
25	2.04	0.64				
26	2.02	0.35			0.50	0.06
28	1.30	0.39				
35	1.86	0.35	12.54	3.03	0.84	0.06
41	1.74	0.37				
43	1.63	0.39				
44	1.41	0.27				
45	1.54	0.26			0.34	0.06
54	2.39	0.35			0.35	0.06
56	1.88	0.36				
69	1.12	0.32				
71	1.46	0.38			0.60	0.06
72	1.51	0.31				
73	2.09	0.37				
74	2.31	0.37				
95	2.54	0.28	7.88	1.53		
97	2.11	0.35			0.67	0.06
98	2.81	0.43	13.57	1.52	0.79	0.06
99	2.61	0.49	11.37	0.85	0.63	0.06
101	2.55	0.42	8.37	0.56	0.46	0.06
104	2.25	0.35	4.32	0.28	0.20	0.06
105	1.47	0.28	1.75	0.23	-1.22	0.06

Table A.19: Nuclear spin relaxation data for TRBP2-dsRBD1 in presence of D10-RNA recorded at 600 MHz

Residue Number	600 MHz					
	R_1 (Hz)		R_2 (Hz)		NOE	
	Value	Error	Value	Error	Value	Error
2	1.35	0.06	1.74	0.21	-0.65	0.11
3	1.53	0.04	1.96	0.21	-0.12	0.11
5	1.56	0.03	2.15	0.20	-0.06	0.11
8	1.46	0.07	2.13	0.28	-0.08	0.11
9	1.48	0.07	2.07	0.29	-0.15	0.11
10	1.49	0.07	2.10	0.25	-0.29	0.11
11	1.52	0.07	2.48	0.34	-0.14	0.11
12	1.55	0.08	2.51	0.31	-0.08	0.11
13	1.52	0.07	2.50	0.29	-0.11	0.11
16	1.47	0.04	3.70	0.30	0.03	0.11
18	1.58	0.05	6.17	0.65	0.34	0.11
24	1.50	0.04	7.40	0.72	0.39	0.11
25	1.47	0.05	8.82	0.86	0.53	0.11
26	1.41	0.05	6.88	0.68	0.40	0.11
28	1.40	0.06	6.23	0.82	0.45	0.11
30	1.34	0.04	8.76	0.81	0.57	0.11
33	1.38	0.03	11.04	1.15	0.75	0.11
34	1.27	0.05	11.15	1.19	0.64	0.11
36	1.41	0.04	9.87	1.11	0.76	0.11
39	1.31	0.04	12.81	1.37	0.82	0.11
41	1.33	0.03	10.56	0.95	0.71	0.11
42	1.23	0.04	10.79	1.24	0.74	0.11
43	1.38	0.04	9.54	0.89	0.71	0.11
44	1.57	0.03	5.11	0.52	0.33	0.11
48	1.30	0.03	10.67	1.02	0.91	0.11
49	1.28	0.04	9.28	0.92	0.79	0.11
50	1.35	0.04	9.94	1.20	0.65	0.11
51	1.32	0.06	10.80	1.42	0.76	0.11
53	1.34	0.04	8.53	0.87	0.50	0.11
54	1.32	0.04	6.02	0.60	0.41	0.11
56	1.46	0.06	5.14	0.48	0.32	0.11
61	1.33	0.03	8.15	0.78	0.55	0.11
62	1.24	0.04	9.92	1.05	0.73	0.11
63	1.24	0.03	9.89	1.14	0.74	0.11
64	1.36	0.04	10.04	0.97	0.75	0.11
65	1.34	0.05	9.64	0.96	1.10	0.11
66	1.38	0.09	10.52	1.31	0.84	0.11
67	1.38	0.05	8.98	0.93	0.51	0.11
68	1.30	0.09	9.93	0.97	0.87	0.11
69	1.34	0.04	9.82	1.02	0.79	0.11
70	1.25	0.06	10.16	1.05	0.67	0.11

| Residue Number | 600 MHz | | | | | |
| | R_1 (Hz) | | R_2 (Hz) | | NOE | |
	Value	Error	Value	Error	Value	Error
71	1.32	0.05	9.44	0.94	0.66	0.11
73	1.36	0.04	9.31	1.04	0.71	0.11
75	1.30	0.04	12.31	1.37	0.72	0.11
77	1.32	0.02	12.16	1.31	0.84	0.11
80	1.55	0.05	7.82	0.90	0.65	0.11
82	1.32	0.07	11.22	1.31	0.73	0.11
88	1.37	0.07	14.06	1.49	0.50	0.11
89	1.23	0.03	12.59	1.44	0.60	0.11
90	1.43	0.06	9.88	1.36	-0.47	0.11
94	1.56	0.04	7.46	0.76	0.48	0.11
95	1.60	0.04	2.99	0.34	0.07	0.11
97	1.52	0.04	9.22	0.99	0.49	0.11
98	1.63	0.07	6.18	0.60	0.46	0.11
99	1.58	0.07	5.00	0.52	0.40	0.11
101	1.60	0.03	4.07	0.41	-0.21	0.11
104	1.31	0.03	1.96	0.19	-0.67	0.11
105	0.98	0.01	2.25	0.19	-0.69	0.11

Table A.20: R_{2eff} values measured at different CPMG frequencies from CPMG relaxation dispersion experiment for TRBP2-dsRBD1 in presence of D10-RNA at 600 MHz NMR spectrometer

Residue Number	R_{2eff} at CPMG frequency (Hz)											
	25		50		100		200		350		500	
	value	error	value	error	value	error	value	error	value	error	value	error
1	9.48	1.04	8.95	0.87	8.82	0.88	9.02	0.82	7.80	0.39	8.35	0.33
2	8.66	0.20	8.47	0.17	8.19	0.17	8.53	0.16	8.01	0.08	8.24	0.07
3	7.99	0.18	8.12	0.15	8.17	0.15	8.29	0.14	8.35	0.07	8.75	0.06
5	7.63	0.16	7.70	0.14	8.13	0.14	7.65	0.13	7.42	0.06	7.86	0.05
8	12.48	0.28	12.66	0.24	12.52	0.24	12.75	0.23	12.26	0.11	12.19	0.09
9	12.08	0.34	12.30	0.29	12.87	0.30	13.37	0.28	12.24	0.13	12.70	0.11
10	10.09	0.28	10.11	0.24	10.36	0.25	10.51	0.23	10.45	0.11	10.30	0.09
11	14.33	0.44	14.07	0.37	13.86	0.37	14.24	0.35	13.87	0.17	14.15	0.14
12	13.78	0.39	13.87	0.34	13.53	0.34	13.65	0.31	13.59	0.16	13.65	0.13
13	14.68	0.51	14.07	0.42	14.02	0.43	14.81	0.41	13.98	0.20	14.41	0.17
16	12.81	0.65	12.69	0.55	12.94	0.56	13.07	0.53	12.93	0.26	13.44	0.22
18	24.58	1.29	25.12	1.12	24.86	1.13	24.59	1.03	22.09	0.46	23.09	0.40
24	26.69	4.02	25.85	3.31	25.23	3.28	25.44	3.06	22.86	1.37	24.11	1.20
25	26.73	4.29	26.08	3.56	27.04	3.75	27.05	3.48	24.94	1.59	25.75	1.36
26	24.31	1.88	23.40	1.55	23.29	1.56	23.72	1.47	22.54	0.70	23.56	0.60
28	28.02	2.45	27.41	2.04	28.33	2.14	26.95	1.88	26.98	0.93	27.86	0.80
30	32.58	3.04	31.90	2.52	29.79	2.35	31.56	2.34	29.37	1.06	30.62	0.93
33	36.71	3.86	36.04	3.21	37.22	3.40	37.07	3.14	35.20	1.44	34.47	1.17
34	31.28	5.32	33.04	4.87	36.26	5.61	34.45	4.84	38.53	2.82	35.10	2.05
36	34.86	2.63	35.36	2.29	34.65	2.26	35.18	2.14	32.24	0.94	32.80	0.80
39	37.68	4.88	36.46	3.97	35.99	3.94	37.01	3.81	38.41	2.00	34.33	1.41
41	30.81	4.46	32.16	4.01	34.45	4.46	29.16	3.35	33.33	1.96	34.97	1.74
42	24.71	4.33	27.26	4.09	29.42	4.52	30.29	4.34	32.08	2.31	36.61	2.30
43	32.15	3.10	31.84	2.61	29.97	2.46	30.82	2.36	30.95	1.17	30.50	0.96
44	21.91	1.18	19.09	0.90	20.11	0.95	18.99	0.84	17.68	0.40	18.42	0.34
48	37.76	6.17	35.87	4.88	37.09	5.19	38.99	5.19	32.69	2.00	31.98	1.62
49	31.45	3.33	32.32	2.95	31.23	2.86	32.34	2.77	31.77	1.34	31.21	1.09
50	38.73	7.79	34.78	5.68	44.21	8.38	37.07	5.84	32.57	2.42	29.70	1.80
51	40.38	11.42	44.60	11.53	44.70	11.73	49.98	13.43	42.04	4.85	38.21	3.46
53	29.49	5.78	28.61	4.76	26.84	4.49	26.47	4.10	26.87	2.07	25.48	1.63
54	22.49	1.04	22.34	0.88	22.55	0.90	21.20	0.79	21.62	0.40	21.57	0.33
56	21.24	0.70	20.97	0.59	20.42	0.59	20.69	0.55	19.02	0.25	19.83	0.22
61	27.92	1.82	27.62	1.54	26.73	1.50	28.09	1.47	26.89	0.69	25.97	0.56
62	32.47	4.75	32.70	4.09	32.73	4.15	33.16	3.91	32.41	1.88	31.43	1.51
63	40.25	5.53	39.45	4.57	38.03	4.38	40.25	4.44	33.18	1.66	35.23	1.50
64	32.30	5.66	32.71	4.91	30.11	4.48	33.09	4.68	34.07	2.41	32.02	1.85
65	38.17	9.57	34.05	6.93	35.79	7.52	32.71	6.17	33.77	3.19	33.89	2.67
66	24.79	8.18	29.01	8.26	31.63	9.29	28.54	7.62	36.58	5.21	34.19	3.94
69	33.32	3.25	33.53	2.80	33.88	2.87	34.70	2.75	32.13	1.23	31.94	1.02
70	38.51	3.63	36.44	2.85	39.20	3.22	36.85	2.72	36.36	1.32	35.10	1.05
71	29.12	1.96	28.85	1.66	28.99	1.69	28.59	1.54	28.18	0.75	26.95	0.60

Residue Number	R_{2eff} at CPMG frequency (Hz)											
	25		50		100		200		350		500	
	value	error	value	error	value	error	value	error	value	error	value	error
73	30.31	2.72	30.36	2.33	31.23	2.44	31.13	2.26	30.86	1.11	30.50	0.91
75	33.76	4.20	34.74	3.72	33.99	3.66	36.79	3.80	37.80	1.96	34.35	1.42
77	33.44	3.31	33.51	2.83	35.04	3.04	34.47	2.76	35.34	1.42	34.75	1.15
82	48.42	11.58	48.54	9.93	48.80	10.16	45.36	8.21	37.33	2.95	36.22	2.35
88	41.89	14.22	46.04	14.33	40.03	11.41	44.28	12.54	35.21	4.33	34.15	3.45
89	44.82	4.66	44.77	3.97	43.02	3.75	42.23	3.37	36.92	1.35	40.82	1.31
94	27.96	1.62	28.12	1.39	26.52	1.32	26.62	1.23	25.21	0.58	25.78	0.49
95	17.46	2.71	17.18	2.28	16.93	2.29	14.47	1.93	9.48	0.78	9.09	0.64
97	27.25	2.55	26.39	2.10	27.82	2.26	28.29	2.13	28.63	1.07	25.33	0.78
98	22.54	1.26	21.06	1.01	21.55	1.05	22.34	1.00	19.53	0.44	20.26	0.38
99	20.68	0.91	20.49	0.77	20.51	0.78	20.43	0.72	20.44	0.36	20.97	0.30
101	16.20	1.08	15.83	0.91	15.30	0.90	15.35	0.84	14.93	0.41	15.00	0.34
104	8.16	0.67	8.59	0.58	8.57	0.59	8.81	0.55	7.14	0.25	7.98	0.22
105	5.04	0.42	4.57	0.35	5.15	0.37	4.92	0.34	6.32	0.18	4.92	0.14

Table A.20: R_{2eff} values measured at different CPMG frequencies from CPMG relaxation dispersion experiment for TRBP2-dsRBD1 at 600 MHz NMR spectrometer (Continued)

Residue Number	R_{2eff} at CPMG frequency (Hz)									
	650		800		1000		50 (Repeat)		650 (Repeat)	
	value	error	value	error	value	error	value	error	value	error
1	8.63	0.42	7.67	0.39	8.02	0.41	8.12	0.41	8.30	0.39
2	8.35	0.08	7.91	0.08	8.02	0.08	8.18	0.08	8.03	0.08
3	8.77	0.07	8.67	0.07	9.07	0.08	8.44	0.07	8.61	0.07
5	7.96	0.07	7.81	0.07	7.93	0.07	7.73	0.07	7.73	0.06
8	12.43	0.12	11.87	0.11	11.80	0.11	12.06	0.11	11.95	0.11
9	13.03	0.14	12.93	0.14	13.29	0.15	12.20	0.14	12.65	0.14
10	10.61	0.12	10.45	0.12	10.63	0.12	10.26	0.12	10.59	0.11
11	14.27	0.18	14.10	0.18	13.92	0.18	14.31	0.18	13.63	0.17
12	13.83	0.16	13.59	0.16	13.22	0.16	13.82	0.16	13.13	0.15
13	14.41	0.21	14.02	0.20	14.53	0.21	13.52	0.20	14.11	0.20
16	13.51	0.28	13.35	0.27	13.38	0.28	13.14	0.27	12.79	0.25
18	22.33	0.49	22.12	0.47	22.41	0.49	22.36	0.48	22.26	0.46
24	24.58	1.53	24.06	1.47	25.37	1.58	24.62	1.52	24.46	1.44
25	26.44	1.76	26.06	1.69	24.94	1.66	27.90	1.85	24.18	1.52
26	22.66	0.73	23.11	0.73	22.73	0.73	22.83	0.73	22.12	0.68
28	27.03	0.98	28.12	1.00	27.93	1.01	29.12	1.05	26.80	0.92
30	29.53	1.12	30.07	1.12	30.16	1.15	30.56	1.15	29.45	1.05
33	35.32	1.51	34.16	1.41	34.57	1.47	34.25	1.44	35.35	1.44
34	35.19	2.58	36.73	2.69	35.38	2.60	41.38	3.28	38.18	2.76
36	32.90	1.01	33.34	1.01	32.55	1.00	33.70	1.03	32.95	0.96
39	33.96	1.74	34.20	1.72	35.03	1.82	35.57	1.85	33.58	1.63
41	35.09	2.19	34.37	2.09	34.95	2.18	37.07	2.36	33.44	1.95
42	31.26	2.33	32.18	2.37	31.58	2.37	33.95	2.58	30.65	2.16
43	30.77	1.22	33.18	1.31	32.85	1.32	31.52	1.24	30.87	1.16
44	18.81	0.43	17.89	0.41	17.79	0.42	18.98	0.43	17.49	0.39
48	31.01	1.95	30.43	1.87	30.79	1.94	33.49	2.14	30.15	1.79
49	32.30	1.43	33.06	1.44	32.40	1.44	34.22	1.53	32.03	1.34
50	29.92	2.27	28.75	2.12	29.49	2.24	33.07	2.56	32.08	2.35
51	35.67	3.92	33.19	3.48	33.60	3.61	35.28	3.83	32.49	3.27
53	24.37	1.95	23.31	1.83	23.96	1.92	26.08	2.07	26.11	1.98
54	21.70	0.42	22.55	0.42	21.72	0.42	22.64	0.43	21.76	0.40
56	19.44	0.27	18.84	0.26	19.28	0.27	19.42	0.27	18.37	0.25
61	27.12	0.73	26.19	0.69	26.70	0.72	26.15	0.70	26.95	0.69
62	32.48	1.97	33.73	2.03	34.54	2.14	35.04	2.17	31.29	1.78
63	33.58	1.76	31.72	1.60	34.74	1.84	33.02	1.71	34.02	1.70
64	30.46	2.18	33.47	2.41	35.37	2.66	32.97	2.39	34.60	2.44
65	32.36	3.14	33.35	3.20	34.90	3.49	35.01	3.47	35.60	3.39
66	34.49	4.99	37.74	5.57	34.46	5.00	39.32	6.02	35.74	4.98
69	33.25	1.34	31.44	1.22	32.33	1.30	33.10	1.33	33.07	1.27
70	34.66	1.29	36.32	1.35	35.22	1.32	37.53	1.44	34.79	1.23
71	27.38	0.76	27.48	0.75	27.05	0.75	29.59	0.82	27.72	0.73

| Residue Number | R_{2eff} at CPMG frequency (Hz) | | | | | | | | | |
| | 650 | | 800 | | 1000 | | 50 (Repeat) | | 650 (Repeat) | |
	value	error	value	error	value	error	value	error	value	error
73	31.50	1.18	31.34	1.15	31.72	1.20	33.10	1.25	31.57	1.13
75	33.43	1.72	32.79	1.64	35.16	1.84	34.33	1.77	34.03	1.67
77	34.45	1.43	33.05	1.32	33.49	1.37	33.54	1.37	32.78	1.27
82	36.40	2.97	33.50	2.59	33.88	2.69	36.14	2.92	37.64	2.96
88	33.49	4.21	36.10	4.58	34.94	4.47	38.94	5.20	34.58	4.17
89	39.01	1.53	38.86	1.49	39.51	1.56	39.14	1.53	36.29	1.30
94	26.20	0.62	26.27	0.61	25.19	0.60	26.30	0.62	25.25	0.57
95	10.51	0.85	10.09	0.82	10.80	0.86	11.52	0.88	10.16	0.79
97	27.49	1.07	27.17	1.03	25.96	1.01	26.93	1.04	26.58	0.98
98	21.02	0.49	20.50	0.47	20.63	0.48	19.86	0.47	20.17	0.45
99	21.11	0.38	21.13	0.38	20.54	0.38	20.78	0.38	20.88	0.36
101	15.01	0.43	15.31	0.42	15.46	0.44	15.38	0.43	14.77	0.40
104	7.36	0.27	7.46	0.26	7.71	0.27	7.24	0.26	7.32	0.25
105	5.26	0.18	5.17	0.17	5.53	0.18	4.64	0.17	4.79	0.16

Table A.21: $R_{1\rho}$ relaxation rates measured using HSn pulses (n=1,2,4,6,8) from HARD experiment for TRBP2-dsRBD1 in presence of D10-RNA at 600 MHz NMR spectrometer

Residue Number	$R_{1\rho}$ (Hz)									
	HS1		HS2		HS4		HS6		HS8	
	value	error	value	error	value	error	value	error	value	error
1	2.08	0.28	1.80	0.46	1.16	0.16	1.69	0.05	1.84	0.24
2	1.64	0.06	1.88	0.09	1.40	0.09	2.13	0.12	1.97	0.10
3	1.78	0.07	1.96	0.07	1.56	0.11	2.45	0.08	2.12	0.10
5	1.93	0.10	2.13	0.02	1.75	0.07	2.35	0.04	2.15	0.13
8	1.72	0.08	2.22	0.14	1.76	0.09	2.64	0.21	2.50	0.18
9	2.00	0.02	2.21	0.11	1.84	0.05	2.40	0.02	2.31	0.17
10	2.18	0.03	2.15	0.09	1.75	0.07	2.45	0.10	2.36	0.05
11	1.97	0.09	2.38	0.18	1.92	0.30	2.90	0.06	2.88	0.08
12	2.04	0.15	2.37	0.06	1.88	0.17	2.93	0.15	2.60	0.28
13	1.96	0.09	2.34	0.09	1.90	0.11	2.89	0.20	2.77	0.32
16	1.64	0.04	2.51	0.21	2.35	0.04	3.37	0.12	3.28	0.03
18	2.35	0.13	3.89	0.38	3.94	0.24	4.58	0.04	4.82	0.19
24	2.62	0.20	3.01	0.42	4.43	0.18	5.39	0.68	5.96	0.80
25	3.39	0.48	4.15	0.06	4.68	0.59	5.30	0.92	5.70	1.07
26	2.74	0.37	3.42	0.21	3.88	0.30	4.54	0.18	4.72	0.24
28	2.88	0.20	3.79	0.17	4.56	0.24	5.49	0.17	5.36	0.45
30	2.16	0.29	4.30	0.37	4.80	0.56	6.05	0.04	5.65	0.24
33	2.49	0.11	4.77	0.39	5.50	0.44	6.31	0.65	7.04	0.29
34	3.03	0.13	3.89	0.63	5.87	0.12	7.59	0.58	7.73	0.38
36	2.79	0.16	4.71	0.20	5.76	0.17	5.86	0.54	6.06	0.28
39	3.16	0.25	4.98	0.30	6.09	0.11	6.93	0.55	7.24	0.49
41	2.64	0.42	5.80	0.33	5.40	0.63	5.95	0.40	6.70	1.10
42	2.41	0.68	4.71	1.18	6.31	0.70	7.32	0.73	6.69	0.72
43	2.65	0.41	4.65	0.17	5.52	0.16	7.25	0.25	7.04	0.26
44	2.56	0.12	3.56	0.17	3.78	0.19	4.78	0.11	3.94	0.42
47	5.04	1.58	4.08	1.03	6.27	0.74	6.77	0.51	5.43	2.25
48	3.04	0.71	4.38	0.05	5.08	0.07	5.64	0.17	5.93	0.34
49	2.31	0.16	3.57	0.21	4.56	0.40	6.50	0.37	6.82	0.46
50	2.82	0.45	4.21	1.25	4.78	0.60	5.52	0.85	7.71	0.51
51	3.89	0.30	3.31	0.44	5.96	0.43	6.68	0.31	8.49	0.26
53	2.43	0.44	3.11	0.56	4.94	1.19	5.48	0.03	4.83	0.40
54	2.33	0.20	3.30	0.11	3.71	0.10	4.66	0.07	4.60	0.43
56	1.79	0.17	2.93	0.06	2.94	0.20	4.23	0.12	3.80	0.41
61	2.56	0.20	3.93	0.23	4.42	0.05	5.45	0.12	5.40	0.24
62	3.08	0.37	4.87	0.23	4.94	0.27	6.70	0.08	7.20	0.16
63	3.09	0.21	4.65	0.22	5.01	0.76	6.48	0.40	6.76	0.27
64	2.55	0.46	5.04	0.45	6.52	0.29	6.41	0.97	5.98	0.14
65	2.77	0.85	3.18	0.63	5.32	1.07	8.17	0.58	6.19	0.88
66	3.83	0.70	4.66	0.38	3.86	0.20	7.69	0.86	5.84	2.02
67	2.01	0.76	4.36	0.46	6.26	0.20	6.66	0.62	6.78	0.81
68	3.30	0.65	4.14	0.54	6.47	0.09	5.61	0.91	5.62	0.52

Residue Number	$R_{1\rho}$ (Hz)									
	HS1		HS2		HS4		HS6		HS8	
	value	error	value	error	value	error	value	error	value	error
69	2.94	0.45	3.55	0.08	5.27	0.50	5.46	0.21	6.69	0.15
70	2.85	0.18	5.17	0.40	5.56	0.30	6.50	0.39	7.07	0.26
71	2.93	0.25	4.60	0.27	5.03	0.25	6.30	0.18	6.40	0.32
73	2.47	0.15	4.81	0.05	5.18	0.56	6.51	0.52	6.31	0.23
75	3.58	0.30	5.20	0.26	5.48	0.07	6.76	0.40	6.63	0.23
77	2.71	0.33	4.73	0.35	5.78	0.24	6.51	0.32	6.93	0.59
80	3.52	1.01	3.64	0.40	4.49	0.75	6.32	0.65	6.08	0.09
82	3.50	0.61	5.15	0.29	6.82	0.56	6.65	1.01	6.76	0.88
88	2.70	0.69	5.85	0.74	6.28	0.69	6.41	0.46	7.36	0.52
89	3.19	1.12	4.74	0.41	6.71	0.58	6.99	0.85	7.93	0.15
90	5.40	0.94	4.89	0.89	7.24	0.86	5.92	0.40	5.75	0.22
94	2.84	0.08	4.15	0.23	4.34	0.27	4.98	0.39	5.10	0.08
95	2.05	1.18	2.72	0.73	1.79	0.57	1.96	0.70	3.50	0.54
97	2.33	0.30	4.09	0.14	4.63	0.34	5.41	0.33	5.90	0.23
98	2.38	0.07	3.22	0.03	3.60	0.17	4.24	0.23	3.88	0.19
99	2.37	0.19	3.24	0.24	3.15	0.15	4.49	0.16	4.40	0.22
101	2.24	0.05	2.89	0.20	2.60	0.13	3.78	0.40	3.73	0.54
104	1.86	0.20	2.16	0.28	1.40	0.16	2.25	0.14	2.12	0.05
105	1.13	0.14	1.45	0.08	0.87	0.16	1.50	0.06	1.22	0.14

Table A.22: $R_{2\rho}$ relaxation rates measured using HSn pulses (n=1,2,4,6,8) from HARD experiment for TRBP2-dsRBD1 in presence of D10-RNA at 600 MHz NMR spectrometer

Residue Number	$R_{2\rho}$ (Hz)									
	HS1		HS2		HS4		HS6		HS8	
	value	error	value	error	value	error	value	error	value	error
1	2.17	0.41	1.27	0.18	1.90	0.12	2.48	0.19	2.10	0.22
2	2.94	0.03	2.01	0.08	2.02	0.23	2.44	0.10	2.26	0.21
3	3.05	0.08	2.31	0.08	2.09	0.37	2.73	0.10	2.41	0.07
5	3.16	0.07	2.43	0.04	2.26	0.23	2.87	0.24	2.64	0.16
8	3.82	0.26	2.58	0.20	3.34	0.02	3.33	0.11	3.35	0.13
9	3.81	0.16	2.58	0.12	2.81	0.19	3.17	0.15	3.07	0.10
10	3.76	0.24	2.36	0.06	2.58	0.38	3.02	0.22	2.86	0.10
11	3.73	0.38	3.76	0.17	1.74	0.99	3.66	0.65	2.86	0.18
12	4.29	0.32	3.28	0.17	2.73	0.50	3.33	0.34	3.12	0.25
13	4.24	0.15	3.44	0.02	3.11	0.20	3.45	0.34	2.77	0.24
16	5.19	0.15	4.34	0.13	4.18	0.34	4.47	0.49	3.77	0.38
18	8.06	0.03	7.89	0.15	6.58	0.33	7.08	0.04	6.61	0.06
24	9.38	0.78	8.18	0.42	8.73	0.98	7.57	0.82	7.21	0.54
25	10.64	0.26	8.49	0.46	7.87	1.15	9.58	0.50	8.44	0.63
26	8.84	0.60	7.54	0.17	7.72	0.21	7.03	0.23	7.14	0.10
28	8.78	0.94	8.73	0.26	7.83	0.58	8.88	0.69	7.96	0.86
30	10.86	0.25	9.00	0.22	8.76	0.31	9.57	0.57	8.71	0.48
33	13.78	0.30	11.36	0.64	11.20	0.63	11.66	0.26	9.91	0.30
34	15.88	1.52	14.16	1.34	10.65	0.38	10.77	1.26	8.46	0.55
36	11.85	0.44	11.29	0.47	10.70	0.23	10.18	0.23	9.74	0.09
39	13.70	0.85	12.46	0.28	11.34	0.22	11.43	0.66	11.16	0.45
41	12.62	0.48	11.15	0.87	9.09	0.57	11.44	0.57	10.62	0.77
42	12.34	1.40	11.51	0.84	10.69	0.76	9.96	0.66	11.52	0.37
43	11.75	0.66	11.17	0.11	10.45	0.55	10.69	0.43	9.51	0.15
44	7.88	0.40	6.32	0.47	6.76	0.25	6.42	0.42	6.16	0.91
47	14.95	2.05	13.85	1.20	12.35	1.21	8.97	1.48	10.02	1.17
48	12.41	1.15	11.09	0.26	11.36	0.16	9.40	0.72	10.13	0.26
49	12.01	0.29	10.90	0.47	9.91	0.79	10.35	0.48	9.12	0.11
50	12.30	1.11	11.18	0.94	10.17	1.13	10.52	0.93	9.11	0.47
51	16.26	1.29	13.92	0.73	10.79	0.20	12.11	0.77	8.95	1.08
53	9.30	0.32	9.68	0.58	7.46	0.42	6.70	0.38	9.25	0.41
54	8.53	0.24	7.18	0.19	6.91	0.07	7.05	0.22	6.58	0.23
56	7.67	0.13	5.75	0.22	5.17	0.34	6.11	0.18	5.77	0.30
61	10.40	0.36	8.66	0.43	8.36	0.16	8.63	0.23	8.09	0.10
62	13.37	0.61	11.33	0.26	10.48	0.36	10.55	0.97	9.49	0.79
63	12.38	0.53	11.06	0.20	9.44	0.39	10.22	0.25	10.36	0.39
64	11.72	0.40	11.08	0.22	10.79	1.13	11.48	0.84	9.68	0.41
65	16.49	1.96	11.63	0.63	9.92	1.50	11.80	1.49	9.72	0.34
66	12.45	1.59	10.64	0.59	11.98	0.98	9.68	2.79	11.20	1.87
67	12.64	0.96	11.52	0.85	10.91	0.85	11.83	0.64	9.34	0.65
68	9.23	0.99	11.69	0.95	9.25	1.29	9.22	0.80	9.71	0.82

Residue Number	$R_{2\rho}$ (Hz)									
	HS1		HS2		HS4		HS6		HS8	
	value	error	value	error	value	error	value	error	value	error
69	12.93	0.12	10.74	0.36	10.15	0.27	9.86	0.38	9.63	0.56
70	12.90	0.33	11.48	0.20	11.44	0.50	11.39	0.18	10.51	0.54
71	12.02	0.45	10.95	0.24	9.37	0.11	9.80	0.45	9.22	0.34
73	13.05	0.46	10.55	0.56	10.12	0.80	10.07	0.37	9.09	0.33
75	14.23	1.22	11.02	0.43	10.35	0.75	11.32	0.38	10.98	0.43
77	13.31	0.43	12.21	0.49	11.22	0.70	11.13	0.15	10.66	0.53
80	10.32	0.79	8.50	0.65	8.33	0.30	9.35	0.76	6.63	1.29
82	11.98	1.70	13.34	1.12	12.75	0.91	11.36	0.37	11.89	0.50
88	12.34	0.49	13.86	1.11	12.91	0.43	12.46	0.83	13.02	0.68
89	13.85	0.47	11.85	0.77	12.45	2.26	13.73	2.21	13.10	2.32
90	15.22	1.12	13.42	0.37	12.54	0.83	11.81	0.60	10.20	1.23
94	9.42	0.16	7.85	0.19	8.15	0.26	7.46	0.32	7.38	0.21
95	4.45	1.20	4.37	0.64	4.66	1.26	3.16	0.77	3.01	0.68
97	9.88	0.59	9.53	0.55	8.04	0.52	8.48	0.25	8.32	0.83
98	7.02	0.06	5.95	0.15	5.54	0.19	6.45	0.13	5.90	0.40
99	6.67	0.16	5.91	0.19	5.27	0.20	5.91	0.35	5.71	0.17
101	5.65	0.71	4.54	0.05	4.68	0.38	4.88	0.22	4.62	0.34
104	3.01	0.21	1.87	0.17	2.29	0.04	2.86	0.07	2.77	0.13
105	1.59	0.07	1.44	0.05	1.52	0.02	1.84	0.16	1.75	0.04

Table A.23: Dynamics parameters extracted from HARD experimental data from geoHARD method for TRBP2-dsRBD1 in presence of D10-RNA

Residue Number	k_{ex} (s^{-1})		$\Delta\omega$ (Hz)		p_A	
	value	error	value	error	value	error
1	696	1	154	297	96.5	2.2
2	13272	32	324	335	78.1	17.1
3	17151	37	400	250	90.6	11.6
5	62073	7	254	190	79.0	15.8
8	219	0	295	345	99.4	0.7
9	21456	46	434	252	88.0	14.0
10	9081	25	456	222	92.1	10.4
11	766	0	16	22	98.0	1.9
12	45246	4	220	104	84.1	13.5
13	49240	2	261	216	83.7	9.5
16	4087	1	38	21	82.4	9.5
18	216	0	327	357	97.6	3.1
24	206	0	49	20	86.9	6.9
25	644	2	635	228	99.5	0.6
26	193	0	861	270	99.4	0.3
28	4663	12	643	369	92.3	13.7
30	188	0	426	305	99.3	0.3
33	296	0	186	27	98.5	0.9
34	52751	5	425	140	85.4	10.4
36	4967	14	930	298	96.0	7.1
39	48007	5	365	161	78.6	11.4
41	12318	37	540	169	90.2	11.1
42	134	0	809	124	99.0	0.1
43	159	0	265	382	87.8	12.7
44	56141	26	414	320	81.5	12.9
47	93377	5	452	160	73.7	13.1
48	234	0	743	351	99.1	0.4
49	487	0	37	9	78.5	10.2
50	320	0	46	21	87.3	9.6
51	39961	2	705	372	91.0	10.2
53	9933	25	591	391	90.2	13.4
54	1365	3	414	320	98.6	2.1
56	7420	1	83	66	82.5	14.8
61	165	0	771	105	99.2	0.3
62	54050	2	504	264	84.8	11.3
63	15556	37	641	266	89.4	12.6
64	169	0	858	266	99.2	0.2
65	7322	1	72	10	74.2	10.9
66	1021	2	1113	227	98.4	1.1
67	944	0	35	5	79.4	7.2
68	130	0	253	362	83.7	16.4
69	6846	1	72	19	77.7	9.5

| Residue Number	k_{ex} (s^{-1})		$\Delta\omega$ (Hz)		p_A	
	value	error	value	error	value	error
70	154	0	757	379	99.3	0.2
71	60339	6	352	102	79.1	10.7
73	4772	1	48	13	78.6	12.4
75	137	0	783	164	99.2	0.2
77	228	0	423	272	98.9	0.6
80	241	0	235	297	99.0	0.8
82	157	0	799	241	99.3	0.2
88	105	0	604	15	98.7	0.1
89	207	0	769	280	99.6	0.2
90	34739	2	726	373	90.4	11.2
94	70987	3	297	67	68.5	12.1
95	681	1	134	294	85.2	14.5
97	381	0	183	274	94.5	7.3
98	207	0	792	225	99.7	0.2
99	206	0	121	112	97.7	2.3
101	2871	9	506	284	97.9	4.3
104	450	1	229	294	85.0	15.8
105	192	0	214	243	99.6	0.3

Supporting Figure
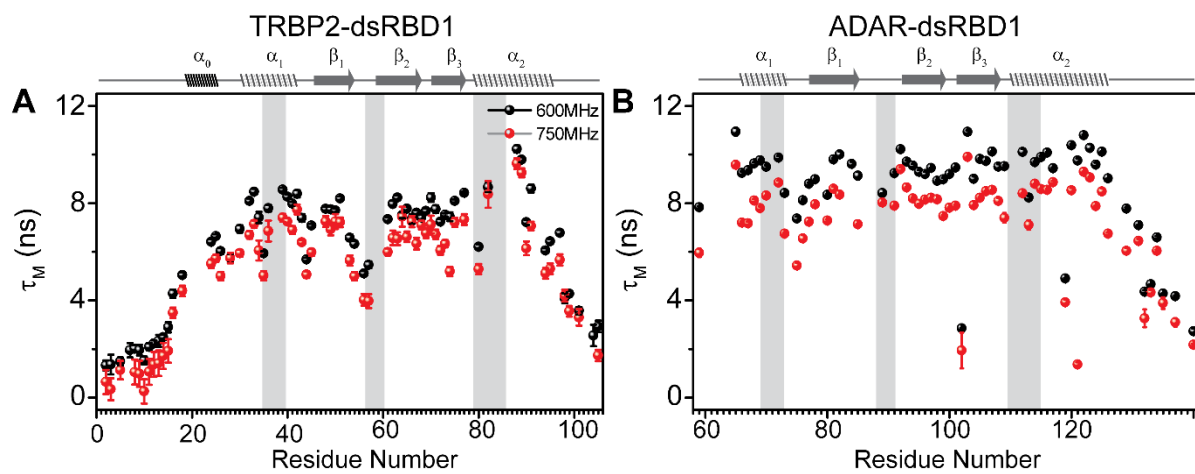
Figure A.1: Residue wise plot of local correlation time (τ_M) for (A) TRBP2-dsRBD1 and (B) dADAR-dsRBD1.
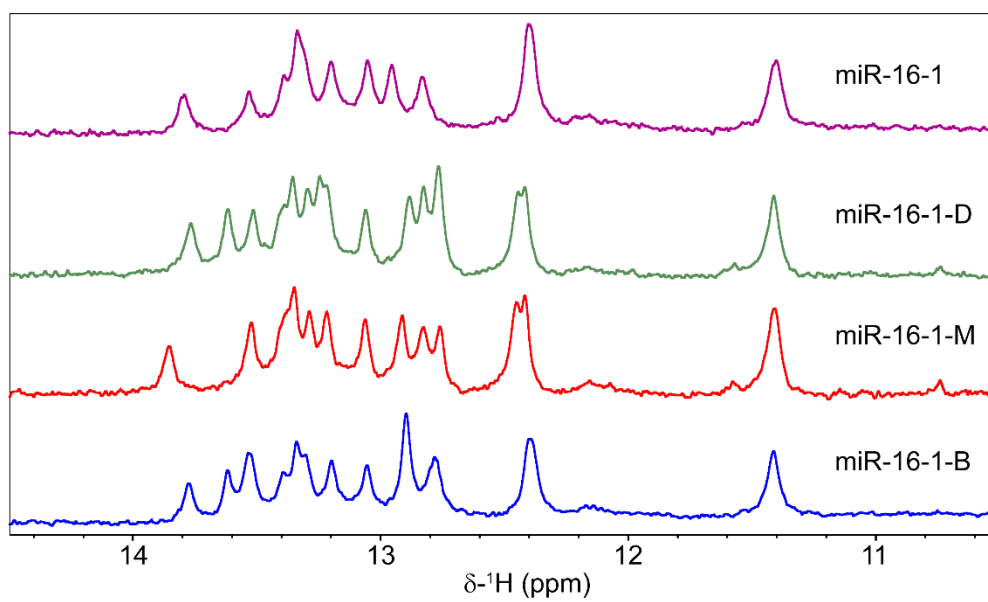
Figure A.2: ^{1}H-NMR spectra of the imine-region of the annealed RNAs indicating the formation of RNA duplexes.

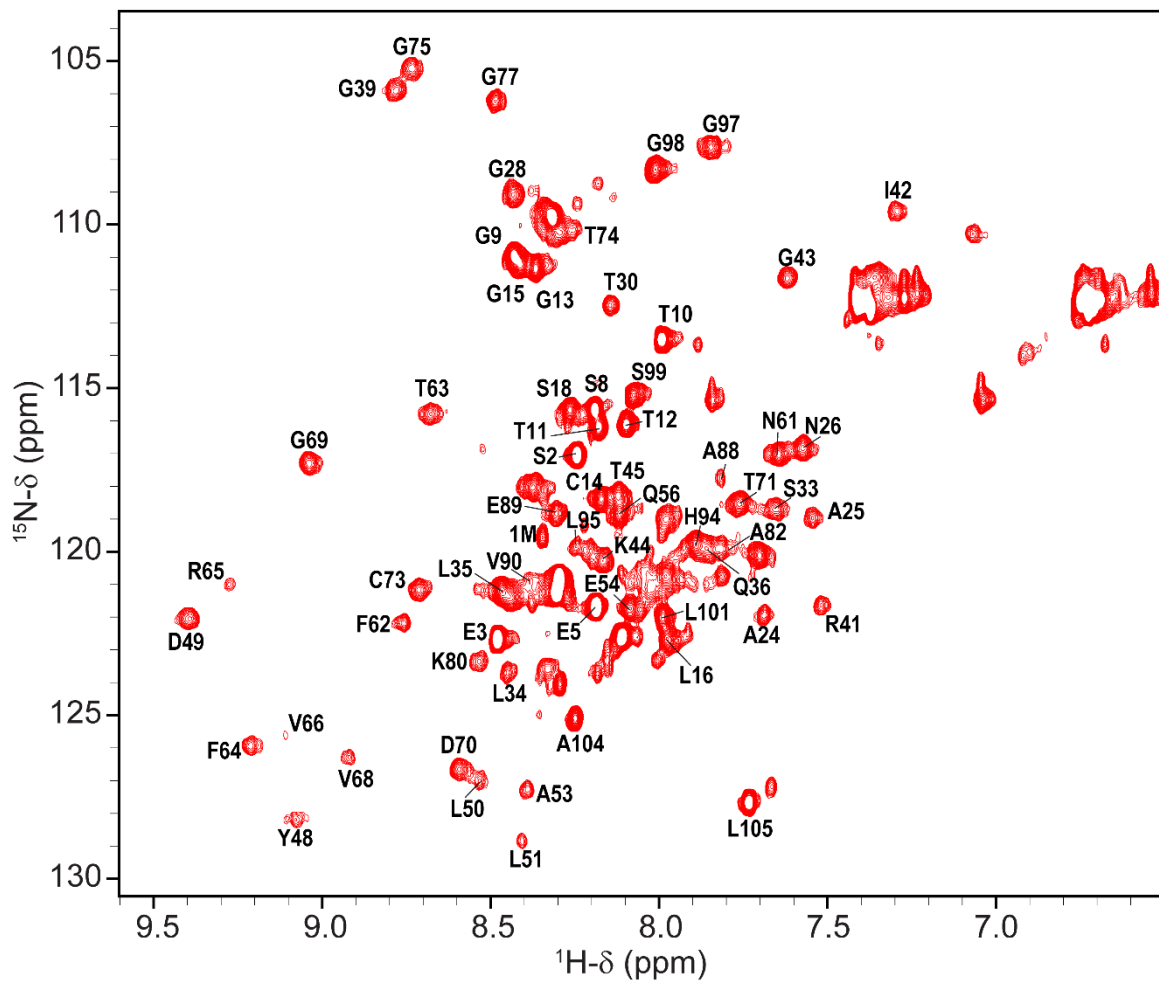**Figure A.3**: ^{1}H-^{15}N-HSQC spectrum of TRBP2-dsRBD1 in presence of 0.5 equivalents of D10-RNA.